MODELING, SIMULATION, AND OPTIMIZATION OF

LARGE-SCALE COMMERCIAL DESALINATION PLANTS

by

Khawla AbdulMohsen Al-Shayji

Dissertation submitted to the Faculty of the
Virginia Polytechnic Institute and State University
in partial fulfillment of the requirements for the degree of

Doctor of Philosophy
in
Chemical Engineering

Approved by:

_____
Dr. Y.A. Liu, Chairman

_____ _____
Dr. William L. Conger (ChE) Dr. Willam H. Velander (ChE)

_____ _____
Dr. Hanif D. Sherali (ISE) Dr. Hugh F. Vanlandingham (ECE)

Key words: Neural Network, Artificial Intelligence, Desalination, Multistage Flash, Reverse Osmosis, Modeling, Simulation, Optimization, Linearization.

April, 17, 1998
Blacksburg, Virginia

Modeling, Simulation, and Optimization of
Large-Scale Commercial Desalination Plants

by

Khawla A. Al-Shayji
Dissertation Committee Chairman
Dr. Y.A. Liu
Chemical Engineering

(ABSTRACT)

This dissertation introduces desalination processes in general and multistage flash (MSF) and reverse osmosis (RO) in particular. It presents the fundamental and practical aspects of neural networks and provides an overview of their structures, topology, strengths, and limitations. This study includes the neural network applications to prediction problems of large-scale commercial MSF and RO desalination plants in conjunction with statistical techniques to identify the major independent variables to optimize the process performance.

In contrast to several recent studies, this work utilizes *actual operating data (not simulated)* from a large-scale commercial MSF desalination plant (48 million gallons per day capacity, MGPD) and RO plant (15 MGPD) located in Kuwait and the Kingdom of Saudi Arabia, respectively. We apply Neural Works Professional II/Plus (NeuralWare, 1993) and SAS (SAS Institute Inc., 1996) software to accomplish this task.

This dissertation demonstrates how to apply modular and equation-solving approaches for steady-state and dynamic simulations of large-scale commercial MSF desalination plants using ASPEN PLUS (Advanced System for Process Engineering PLUS) and SPEEDUP (Simulation Program for Evaluation and Evolutionary Design of Unsteady Processes) marketed by Aspen Technology, Cambridge, MA.

This work illustrates the development of an optimal operating envelope for achieving a stable operation of a commercial MSF desalination plant using the SPEEDUP model. We then discuss model linearization around nominal operating conditions and arrive at pairing schemes for manipulated and controlled variables by interaction analysis. Finally, this dissertation describes our experience in applying a commercial software, DynaPLUS, for combined steady-state and dynamic simulations of a commercial MSF desalination plant.

This dissertation is unique and significant in that it reports the first comprehensive study of predictive modeling, simulation, and optimization of large-scale commercial desalination plants. It is the first detailed and comparative study of commercial

desalination plants using both artificial intelligence and computer-aided design techniques.
The resulting models are able to reproduce accurately the actual operating data and to predict the optimal operating conditions of commercial desalination plants.

To the memory of my dearest friend Dr. Layla Al-Zaid, and

TO ALL I LOVE

this dissertation is affectionately dedicated

Acknowledgments

There are many who have contributed of their time, energy, and often their heartfelt sympathy to my efforts. First, I am greatly indebted to my advisor and chair of my dissertation committee, Professor Y.A. Liu, without whom I would never have completed this work. Also I am indebted to Kuwait University for their support and sponsorship.

It is a pleasure also to thank a number of very special persons and organizations who contributed to the completion of this research.

I am greatly indebted to Dr. Al-Gobaisi, D., the director of the International Center for Water and Energy Systems in Adu Dhabi, United Arab Emirates, Dr. A. Woldai, and Dr. A. Husain, of the same center. Dr. Darwish with his invaluable constructive and perceptive comments and suggestions as well his kind support which was of immense assistance to me in accomplishing this work, made it possible for me to design this research project.

Dr. Woldai responded graciously to every phone call I made and to every question I had, and provide swift and thoughtful reviews of earlier versions of some chapters. Dr. Husain contributed valuable suggestions and comments.

Dr. W. Velander from the Chemical Engineering Department at Virginia Tech, has been a source of inspiration for this work with his foresight, continuous encouragement, and cooperation. I thank him for his confidence in my ability to meet higher standard of scholarly research and writing. I express my appreciation to all the members of my committee who each made special and unique contributions to the improvement of this work.

In order to complete this project, the support and help extended by many parties within the Ministry of Electricity and Water in Kuwait have been vital and greatly appreciated. I would like especially to convey my appreciation to Engineer Tareq Shemshar, the Chemical Laboratory Section Head at AZ-ZOUR South Station, and Engineer Rami Goushah from Water Resources Development Center for their invaluable assistance, co-operation, efficiency and prompt responsiveness to my ceaseless requests for information on AZ-ZOUR South Station.

I would like to express my appreciation to Mr. Abdullah Al-Azaz at Saline Water Conversion Corporation (SWCC) in the Kingdom of Saudi Arabia and Mr. Abdulmajeed Al-Awadhi at Ministry of Electricity and Water in Bahrain for providing me with the critical data necessary for the successful completion of my research.

I wish to thank Aspen Technology, Inc., Cambridge, MA, and its Neural Net Business Unit (formerly, NeuralWare, Inc.) in Pittsburgh, PA, for providing free use of their PC-based software tools, inclusing Professional II/Plus, ASPEN PLUS, SPEEDUP, and DynaPLUS for use in our case studies.
I thank Mr. Rily Chan and my colleague James Mann who offered invaluable computer technical support.

I would also like to personally thank my friends and family for their encouragement during this period of my life.

Specifically, I want to thank Dr. Mona Hassuna and Ms. NingLing Wang for their emotional support, interest in my work, and companionship.

Shirly Murphy, my first Blacksburg friend, provides me with her love and valuable friendship.

Meeting Salwa Jawhar and her family was one of the best things that happened to me in Blacksburg. I want to thank them for their love, support, and letting me be a part of their family.

Though they live on the other side of the world, I acknowledge the indispensable contribution of my parents, whose inspiration shines through every page of this work. To my sisters Najat and Huda, and my brothers, Yousef, Mohammad, Abdullah, and Raed, their love and patience both stretch beyond what any reasonable person would tolerate.

Special thanks and appreciation to my dearest brother in law, Mohammad Al-Roshood, who is as dear to me as my real brother, and to my friend Muneera Al-Manaie who always provides me with her love and friendship.

Words are not adequate to describe how thankful I am to have had and to continue to have the love and support of my family and friends. I greatly appreciate their unconditional love and support all the time, especially during this period in my life.

Above all, I am in debt to ALLAH who has given me the health, strength and patience to succeed in my work and persevere during this critical stage of my life.

TABLE OF CONTENTS

Chapter 4: Neural Networks for Predictive Modeling and Optimization of Large-Scale Commercial Water Desalination Plants

List of Figures

List of Tables

CHAPTER 1

INTRODUCTION

This chapter describes the water crisis in Arab counties and the need for water desalination, which provides the motivation for this research. We summarize the goals, significance and uniqueness of our research on modeling, simulation and optimization of large-scale commercial desalination plants. Lastly, we give an overview of two approaches (data-based and model-based) used in this research, as well as the organization and interrelationship (Figure 1.1) of various chapters of this dissertation.

1.1 Water Crisis in Arab Countries

Many arid and semi-arid countries face shortages of portable water available from natural sources. The Arab World is representative of such countries. Arab countries pay increasing attention and interest in water resources because they are situated in the driest area in the world as well as because of increasing demand on water access for agricultural, industrial and house purposes. These Arab countries continuously exert effort for the development of their resources and provision of large amounts of water supplies to urban centers, villages, farms and other users. However, the limited water resources and the need to balance economic and social development resulted in the emergence of an imbalance between the available water resources and demand.

Undoubtedly, the Arab World suffers from severe pressure on its available water resources. It represents 10% of the world's area and 5% of the world's consumption. However, it has only 0.5% of the world's regenerated fresh-water resources. The situation becomes more difficult because water consumption in Arab countries is

increasing at a high rate due to continuous increased population growth and current economic and social changes. Hence, there is an urgent need to increase the rate of development of water resources in the Arab World in particular and in developing countries in general.

In reviewing the alternative water resources available in other arid and semi-arid zone countries when appraising water sectors for providing aid for development, it becomes increasingly evident that there will be a great demand for desalination by the turn of the century.

Desalination of seawater is fast becoming a major source of potable water for long-term human survival in many parts of the world. Among all the seawater desalination processes, the multistage flash (MSF) process produces potable water much more successfully than any other processes. In spite of its relatively high cost, the modular structure of a MSF plant is an obvious asset for a facility which must satisfy a variety of production demands. Additionally, the capability of coupling the MSF plant to a power-generation plant as the heat source makes the process increasingly important for future drinking water and power production.

Thus, the importance of desalination plants is due to their major role in obtaining fresh water and for life support on our planet. The MSF process, in particular, needs immediate efforts to ensure design improvement and to control costs.

1.2 Research Motivation

The importance of desalinated water will no doubt increase as natural water resources are depleted and the need for diversification of national income increases. Desalination is at the threshold of becoming an acceptable alternative to conventional water resources. Its improvement and advancement is in the hands of those who benefit most from it. The

Arabian Gulf region is in the position to lead a crusade for promoting the production of desalinated water, not only for its own economic development but also for the rest of the world.

Attempting to reduce the cost of desalination, we need to consider two aspects: first, the technology and secondary, the management of, the production and conversation of desalinated water. Technological efforts must concentrate on reducing the capital, operation, maintenance, and above all, the energy costs. The capital cost of a desalination plant is directly related to its life span. Technological improvements in plant design, heat-transfer technology, corrosion protection, and chemical selection have lead to extended life spans and reduced operation and maintenance costs, so that the life span of some MSF desalination units may exceed 15 years.

However, desalination plants are large and complex. They are also energy-and cost-intensive and above all, crucial to life support in several regions of the world. Consequently, desalination plant must meet high standards of performance, including optimality, cost effectiveness, reliability, and safety. Many of these criteria can be satisfied by improved design and control. This can be studied by using modern computer-based simulation techniques.

Water being the essence of life for any society, the development of large-scale desalination plants for satisfying the needs of citizens of arid lands such as the Middle East countries is, therefore, vitally important.

1.3 Research Aims and Significance

This research investigates the following:

A. Neural networks for predictive modeling of a large-scale commercial water desalination plants.
B. Steady-state and dynamic simulations of a large-scale commercial multistage flash (MSF) desalination plant.
C. Performance optimization of a large-scale commercial multistage flash (MSF) desalination plant.

A. The Significance of Neural Networks for Modeling of Large-Scale Commercial Desalination Plants.

Artificial intelligence, which can be applied to the design, operation, control, and performance optimization of desalination plants, will result in better design, improved process efficiency, and enhanced operational safety. Desalination processes make good candidates for neural network modeling due to their process complexity, nonlinear behavior with many degrees of freedom, and the presence of uncertainty in the control environment. The nonlinearity of desalination processes is mainly due to the dependence of physical properties of the streams upon temperature, pressure, and salinity. The considerable amounts of mass and heat transfer could also contribute to the nonlinearity of the model in thermal desalination processes.

Artificial intelligence techniques (i.e., expert system, neural network, and fuzzy logic) could be introduced into water desalination plants in many ways. In particular, neural networks could be applied to desalination plants in the following areas:

1. Prediction and optimization of plant performance
2. Process control and operational management
3. Plant diagnosis: fault detection, alarm processing and feature categorization
4. Load forecasting

The results of these applications would be better design, improved efficiency, and increased operational safety. Neural networks provide a good alternative model for a model MSF desalination plant.

B. The Significance of Steady-State and Dynamic Simulations of a Large-Scale Commercial Multistage Flash (MSF) Desalination Plant.

The goals of modeling and simulation in the process industry include improving and optimizing designs, and developing better insight into the working of the process, ultimately leading to the optimal operation and control of the process.

A steady-state model consists primarily of algebraic equations, and it is mainly applicable for design purposes as well as for parametric studies of existing plants to evaluate their performance and to adjust or optimize operating conditions.

A dynamic model consists of algebraic and differential equations that describe the time-dependent behavior of the process when introducing any kind of disturbances. Dynamic

models are suitable for simulating transient behavior, studying control strategies, investigating stability problems, identifying process interactions, performing process troubleshooting, and examining reliability, start-up, and shut-down conditions.

The dynamic simulation model could be used for off-line simulation as well as on-line simulation. In the off-line simulation, the plant is simulated without connection with the actual plant. The dynamic simulation can be used for training operating personnel and investigating plant behavior under dynamic situations, which helps to predict the dynamic conditions of the plant in order to study potential operating modes and control behavior. In addition, dynamic simulation could work as an off-line simulator consultant to help the operator check an action before its implementation on the real plant. We can use on-line dynamic simulation to assist the plant's control system, to detect plant failure, and to diagnose faults.

The motivation for the simulation is that any improvement in plant efficiency could significantly reduce operating costs and/or increase water production.

C. The Significance of Performance Optimization of a Large-Scale Commercial Multistage Flash (MSF) Desalination Plant.

Optimization can improve a chemical process at various stages of its life cycle, spanning various phases of conceptualization, design, construction, operation, and control of a plant.

For MSF desalination plants, optimization can be quite useful at the planning, design, and operation phases. Optimization of planning and design phases is well established, while

optimization in the operation phase has not received much attention. The goals of MSF process optimization are to :

- minimize energy consumption: this means high performance ratio, which is defined as the ratio of distillate production rate to the steam condensate rate.
- achieve stable operation: this means reasonable brine levels in flashing stages.
- avoid equipment fouling: which limit the top brine temperature and tube-side velocities.
- reduce chemical consumption (e.g., for antiscaling and antifoaming in process operation).

1.4 Uniqueness of the Research

This work drives its uniqueness from the following:

- Development of neural networks, in conjunction with engineering knowhow and statistical techniques, for predictive modeling of large-scale commercial water desalination plants. In contrast to several previous studies, our work utilizes *actual operating data* collected during summer and winter operations (*not simulated data*) from a large-scale commercial multistage flash (MSF) desalination plant and a large-scale commercial reverse osmosis (RO) plant.

- Development of steady-state and dynamic simulations using advanced commercial software tools, such as ASPEN PLUS and SPEEDUP marketed by Aspen Technology, Cambridge, MA.

To our knowledge, this research represents the first comprehensive study of predictive modeling and simulation of large-scale commercial water desalination plants using artificial intelligence techniques and Aspen Tech advanced simulation software tools.

1.5 Research Setting

We have used two different approaches to predict the plant performance. The first approach is data-based using a neural network in conjunction with engineering knowhow and statistical technique to predict the operating variables of large-scale desalination plants. We apply NeuralWorks Professional II/Plus (NeuralWare, 1993) and a statistical regression software, SAS (Statistical Analysis System, SAS, 1997) in this research. The second approach is model-based utilizing a mathematical model derived from physical principles to describe the steady-state and dynamic behavior of an MSF plant. The second approach incorporates both a modular approach using ASPEN PLUS software, as well as an equation-solving approach, using SPEEDUP. We apply Aspen Technology advanced commercial software tools, specifically, ASPEN PLUS, SPEEDUP, and DynaPLUS packages.

The work is based on a comprehensive study of a large 24-stage multistage flash (MSF) desalination plant (48 Million Gallons Per Day capacity, MGPD), which is currently operating in Kuwait and a reverse osmosis (RO) desalination plant (15 MGPD) located in the Kingdom of Saudi Arabia.

The overall objective of this research is to understand the process and to investigate with the aid of modeling and simulation, the possibilities for enhancing the performance, efficiency, and operational safety of desalination plants.

1.6 Dissertation Organization

This dissertation has been organized into nine chapters and supporting appendices. Figure 1.1 shows the research layout in the development of the two approaches used to predict the performance of large-scale commercial desalination plants.

This chapter outlines the scope of our research which is further detailed in subsequent chapters.

Chapter 2 gives a concise description of the desalination processes, specifically, Multistage Flash (MSF) and Reverse Osmosis (RO) processes, which are the objective of present study.

Chapter 3 briefly introduces a brief introduction to computing with neural networks, while Chapter 4 demonstrates the accuracy and efficiency of the neural networks in conjunction with engineering knowhow and statistical techniques to predict the operating variables of large-scale commercial desalination plants. This work utilizes actual operating data from a multistage flash (MSF) desalination plant (48 Million Gallons Per Day capacity, MGPD) and reverse osmosis (RO) plant (15 MGPD) located in Kuwait and the Kingdom of Saudi Arabia, respectively. We apply Neural Works Professional II/Plus (NeuralWare, 1993) and SAS (SAS Institute Inc., 1996) software to accomplish this task.

Chapter 5 presents the development of steady-state and dynamic simulation models of a large-scale commercial MSF desalination plant based on the physical principles. It is simulated on a commercially available flowsheet simulator (ASPEN, Advanced System

for Process Engineering) PLUS and SPEEDUP (Simulation Program for Evaluation and Evolutionary Design of Unsteady Process) marketed by Aspen Technology, Cambridge, MA. The model is tuned with the help of measured data on 24-stage plant in operation (AZ-ZOUR-Kuwait).

Chapter 6 discusses the performance optimization of a large-scale commercial MSF desalination plant. This is based on a case-study approach made on different operating conditions, in which the major operating variables are recirculating brine flowrate and the top brine temperature. The objectives of the study are to maximize either the product rate or the performance ratio.

Chapter 7, discusses model linearization around certain nominal operative conditions of a commercial MSF desalination plant and development the control structure using an interaction analysis called relative gain array (RGA).

Chapter 8, illustrates our experience in applying a commercial software for combine steady-state and dynamic simulations of a commercial MSF desalination plant.

Chapter 9 concludes the thesis by pointing out directions for future research.

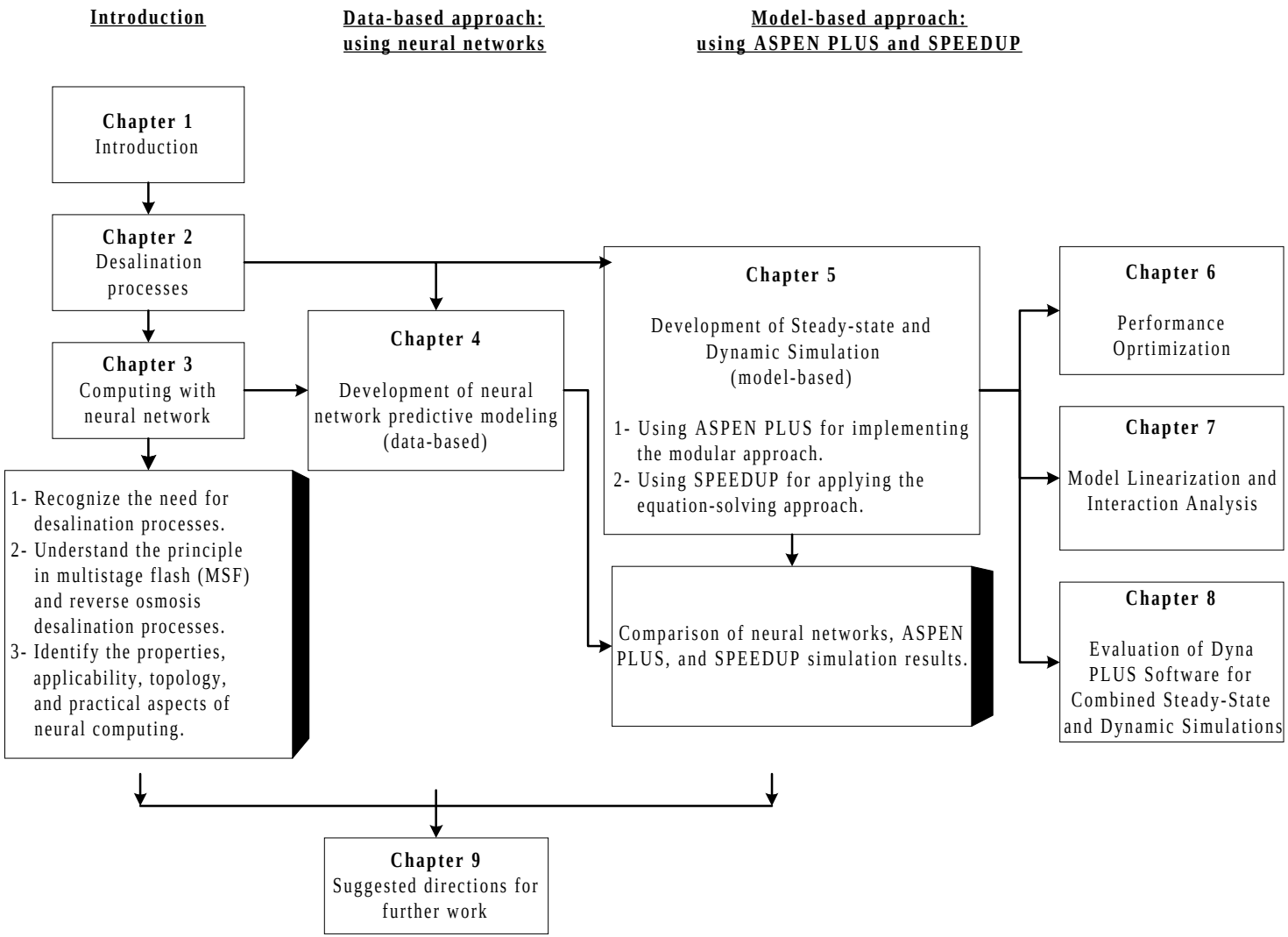

Figure 1.1: Research profile in developing simulation models for large-scale commercial desalination plants.

CHAPTER 2

DESALINATION PROCESSES

This chapter introduces desalination processes starting with the history of desalination and its needs and moving on to the classifications of desalination processes. We next illustrate the principle and operational variables in multistage flash and reverse osmosis desalination plants.

2.1 Need for Desalination

Water is an important resource for use of mankind. It is essential for agricultural and industrial growth, as well as for supporting growing populations who require a safe drinking water supply. We find 97% of all water in oceans, 2% in glaciers and ice caps, and the rest in lakes, rivers and underground. Natural resources cannot satisfy the growing demand for low-salinity water with industrial development, together with the increasing worldwide demand for supplies of safe drinking water. This has forced mankind to search for another source of water. In addition, the rapid reduction of subterranean aquifers and the increasing salinity of these non-renewable sources will continue to exacerbate the international water shortage problems in many areas of the world. Desalination techniques are capable of providing the solution (Temperely, 1995). "Desalination" or "Desalinization" refers to water treatment processes that remove salts from saline water.

Desalination has already become an acceptable solution for shortages in conventional water resources. This is now acknowledged by reputable institutions such as the World Bank (Dabbagh, 1995).

2.2 History of Desalination

Desalination as a natural phenomenon has occurred on earth for millions of years. The natural distillation cycle of water evaporating from the sea and then condensing to form pure rain water is probably the most obvious example of this phenomenon. Aristotle describes the natural water cycle as follows (Hanbury, 1993):

> *The sun, moving, as it does, sets up processes of change and by its agency, the finest and sweetest water is every day carried up and is dissolved into vapor and rises to the upper region, where it is condensed again by cold and so water is formed, which falls down again to earth. Salt water evaporated forms fresh, and the vapor does not when it condenses, condense into seawater again.*

The other desalination phenomenon that occurs in nature is the freezing of seawater near the polar region. The ice crystals formed are pure water, the salt being excluded from participation in the crystal growth.

Desalination has been practiced in the form of distillation for over 2000 years. It is not until the eighteen century A.D, for people to recognize that the distillation process could be enhanced by cooling the condensing surface. In the eighteen century A.D., Jaber Ibn Hayyan, an Arabic scientist, wrote a major treatise on distillation (in the context of perfumery) which contained the first reference to water-cooled condensation. However, there appears no evidence of the idea being applied to seawater distillation for another thousand years (Hanbury, 1993).

Since the turn of the century, necessity has driven scientists and engineers to utilize desalination technology of varying effectiveness to produce pure water from saline water. With the development of temperature and pressure measurements, together with an understanding of the properties of gases, land desalination began to play an important role from the early 1950's. The expansion of oil discoveries in the Arabian Gulf countries, USA, Caribbean Island, and a few others, where drinking water is rare, also affected desalination development.

The first commercial land-based seawater desalination plant was installed by the Ottomans in Jeddah, Saudi Arabia. This crude distillation unit was a boiler working under atmospheric pressure, but this unit suffered from severe scale deposits and corrosion problems. It is now part of a historical monument on Jeddah Corniche.

With the improvement in submerged-tube technology, the first evaporators with a total capacity in excess of 45,000 m3/d were built in Kuwait Curacao in the early 1950's. But it was not until the development of the multistage flash distillation method by Professor Robert Silver in the 1950's, when the research and development of saline water conversion was promoted, that desalination became a practical solution to the shortage of drinking water.

The historical turning point in the history of desalination is the introduction of multistage flash desalination (MSF) in Kuwait in 1957. The Kuwait Department of Electricity and Water placed an order with Westinghouse for four 0.5-million-gallon-per-day (MGD), evaporator units each with four stages, designed by Rowland Colte. Their success encouraged the authority in Kuwait to go for larger and more efficient desalination units, and to accept an offer from G and J Weir to supply a new desalination concept known as the "*Multistage Flash*".

The innovator of the multistage flash system was Professor Robert Silver. Although he held patents on the process both in Europe and the USA, he never received any financial rewarded for his work.

With this success, companies all over the world, especially in the USA and the UK, undertake extensive research and development on large flash-type evaporator units to achieve lower production cost.

The installation of similar evaporators manufactured by other contractors followed the great success of flash evaporation. Subsequently, Sasakura installed the first 5 million-gallon-per-day MSF units at Shuwaikh in Kuwait. Similar units were then installed in the new Kuwait plants located at Shuiabah. The success of these large units, proving that the MSF process could produce water economically and with greater reliability than previous systems, set the stage for the great advances in desalination capacity that were to follow in the 1970-1980's (Temperly, 1995).

Kuwait continues to lead the field of desalination. It has gained wide experience in the design, commission, operation, and maintenance of MSF distillation plants.

Distillation was the only method available at that time. In the later 1960's, membrane processes began to take a place in the market.

In 1953, Reid, C. E. and Breton, E. J. at the University of Florida proposed a research program to the Office of Saline Water (OSW). They developed a membrane that was made of a cellular acetate material and had the ability to reject salt. However, the water flux through the dense membrane was too low to have commercial significance.

The major breakthrough in membrane development came in a parallel research program, from 1958 to 1960, at the University of California at Los Angeles (UCLA) where S.

Leob, and S. Sourirajan were credited with making the first high-performance membranes by creating an asymmetric cellulose acetate structure with improved salt rejection and water flux.

In 1965, the UCLA team installed the first municipal reverse osmosis plant in Coalinga, California. The plant was desalting water containing 2,500 ppm salts, and producing 5,000 GPD with a tubular cellular acetate membrane. The development of the tubular, spiral-wound, and hollow-fine-fiber modules together with the development of the polyamide membranes takes place from 1965-1970.

Through the 1980s, improvements were made to these membranes to increase water flux and salt rejection with both brackish water and seawater. Brackish water is water that contains dissolved matter at an approximate concentration range from 1,000-35,000 mg/l.

2.3 Classification of Desalination Processes

Desalination means the removal of fresh water from saline water. Many methods have been proposed for desalting saline water, but few were commercially used. Figure 2.1, shows the major desalting processes.
The two most popular methods for classifying the well-known desalination processes are as follows:

- Processes in which desalination taking place involves phase change. There are three main methods:
    - Multieffect (ME) distillation
    - Multistage flash (MSF) distillation
    - Vapor-compression (VC) distillation.

- Processes in which desalination takes place without any phase change. These include the following two main methods:
    - Reverse osmosis (RO)
    - Electrodialysis (ED)

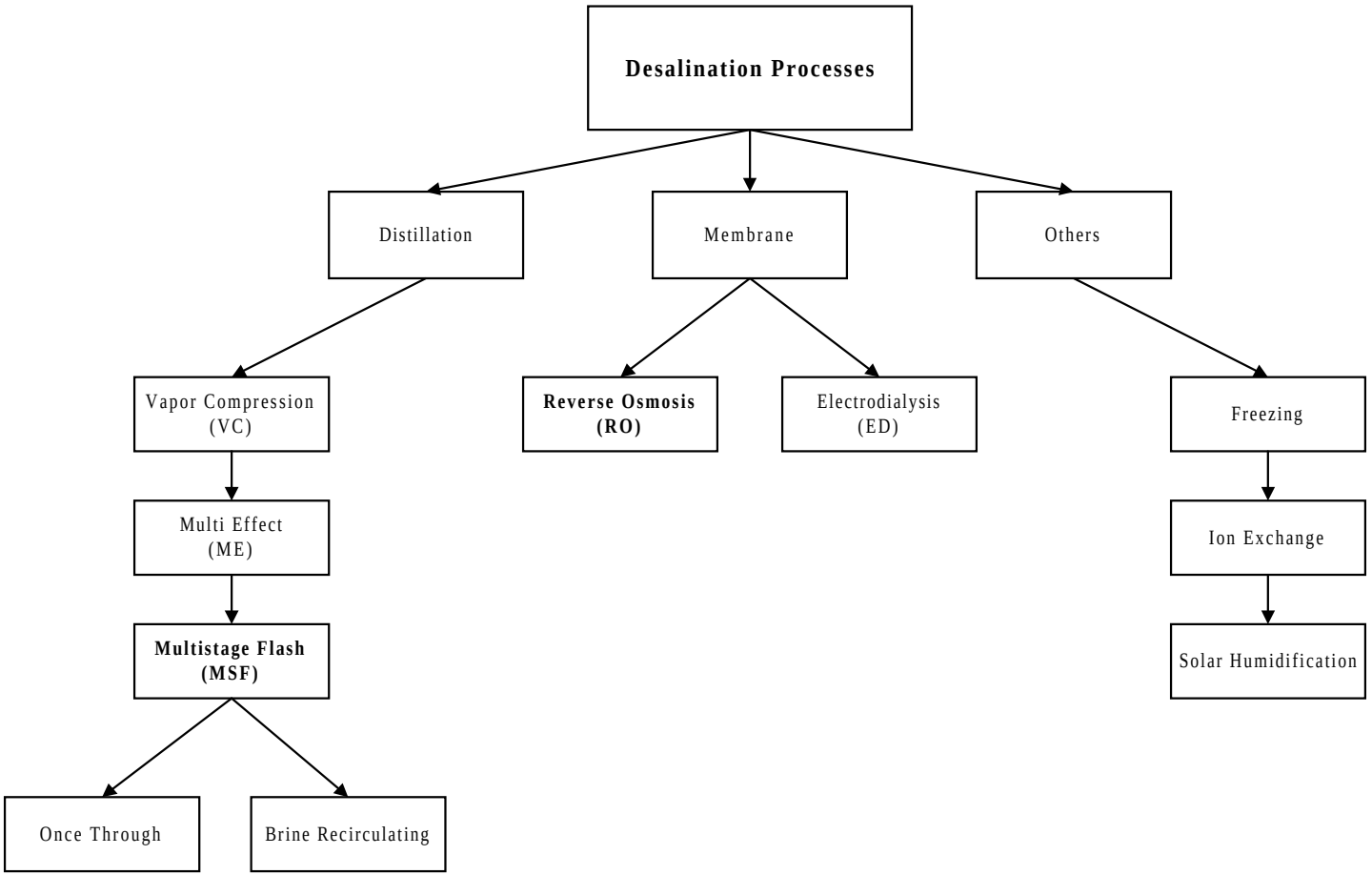

Figure 2.1: Classification of desalting processes.

The applicability of any process depends on the salt concentration in the feed water and on its water unit cost. Distillation is the oldest and most commonly-used desalting techniques. In this process, evaporation of the saline water and condensation of the generated vapor occur to obtain fresh water. This process produces freshwater with a better quality as compared with crystallization and membrane processes.

A. Distillation: Thermal Processes

Distillation is one of the oldest and most commonly used desalting techniques. In this process, the water evaporation and vapor condensation occur to obtain distillate at the end.

1. Vapor Compression (VC).

Vapor-compression distillation uses mechanical energy rather than thermal energy. It is based on a simple principle. Saline water is sprayed over an evaporator tube bundle. The vapor formed at some temperature and pressure is then compressed either thermally in a steam ejector, or mechanically (high and low pressure) in a compressor, causing the condensation temperature and pressure to increase and the volume to decrease. Compressed vapor is passed through the evaporator bundle, where it condenses and forms distilled water. The heat of condensation could be recycled to evaporate more brine.

Most vapor-compression plants have single effects, but a multieffect configuration could be used for a larger product capacity. Figure 2.2 illustrates the principle of vapor compression.

The vapor-compression process consumes a small amount of energy and has a low operating cost . However, its capacity is limited, and the quality of water produced and maintenance costs do not match those by other distillation processes.

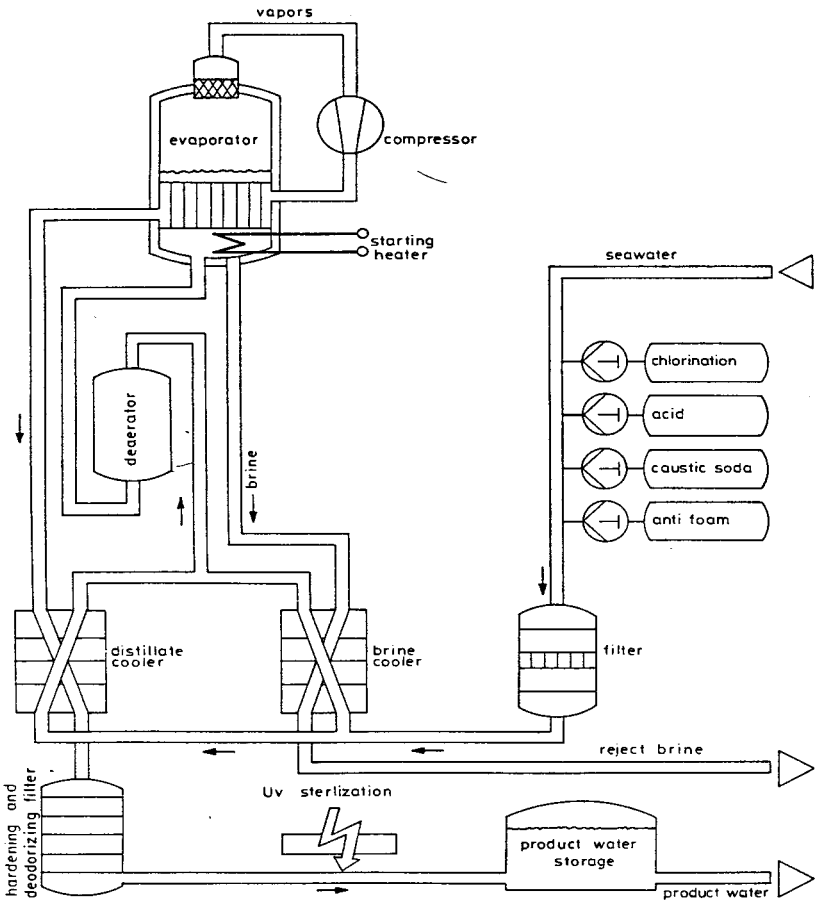

Figure 2.2: Principle of vapor compression (Khan, 1986).

2. Multieffect (ME) Distillation.

Multieffect (ME) distillation was the first process used to produce a significant amount of water from the sea. This process takes place in a series of effects (vessels) and uses the principle of reducing the ambient pressure in the various effects in order of their arrangement. This causes the feed water to undergo boiling in a series of effects without supplying additional heat after the first effect. Figure 2.3 illustrates the arrangement a ME distillation. Vapor generated in the first effect gives up heat to the second effect for evaporation and is condensed inside the tubes. This continues for several effects.

The seawater is either sprayed, or otherwise distributed onto the surface of evaporator tubes in a thin film to promote rapid boiling and evaporation. The condensate from the boiler steam is recycled to the boiler for reuse.
The larger the number of effects, the less heat that is required as heat sources. There are vertical- and horizontal-tube evaporation effects. The vertical tubes could be of the rising or the falling-film type. The formation of falling films of water on the inner surfaces of the heating tubes affects evaporation in the vertical-tube evaporators, so the falling films are heated by the steam passing outside the tubes.

However, with horizontal effects, evaporation takes place on the outer surfaces of the heating tubes, steam for heating being condensed inside the tubes.

ME distillation plants tend to come in a much greater variety of plant designs than do MSF processes. The designer could select a number of heat-transfer surface configurations and a number of flowsheet variations, thus leading to a larger number of possible combinations.

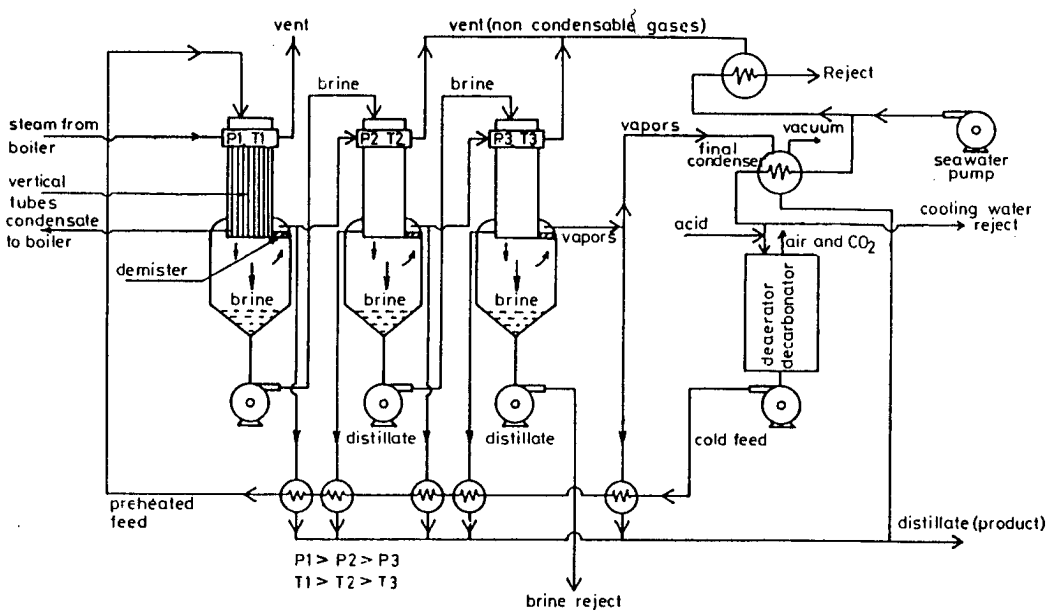

Figure 2.3: Schematic diagram of a multieffect distillation plant (Khan, 1986).

3. Multistage Flash (MSF) Distillation.

The multistage flash distillation processes work on the principle that seawater will evaporate as it is introduced into the first evaporator (flash chamber) with lower pressure than saturation pressure. It then condenses and cools down to a saturation temperature equivalent to chamber pressure.

The MSF plant consists of three sections: *heat-rejection, heat-recovery,* and *heat input (brine heater).* The heat-rejection and heat-recovery consist of a number of flash chambers (stages) connected to one another. Section 2.4 gives more details on this process.

B. Membrane Processes

1. Reverse Osmosis (RO).

Osmosis processes are of current technical interest in two widely separated fields: (1) in the biological science, because of the importance of selective transport through cell membranes to life processes: (2) and in chemical processing, including water and waste water treatment.

One of the great attractions of reverse osmosis is its conceptual simplicity. Basically, we can visualize reverse osmosis as a very fine filtration process using a membrane to filter the salt out from the solution. The only thing that makes it different from ordinary filtration is that there is a minimum driving pressure (osmotic pressure) difference below which the process will not work (Hanbury et al., 1993). Section 2.5 describes desalination by reverse osmosis.

Reverse-osmosis desalination efficiency usually depends on the type of membrane used, its ability for separation and its extent to resist chemical and environmental effects. Recent developments in membrane technology and construction material made reverse osmosis plant attractive for large desalting capacities.

2. Electrodialysis (ED)

Figure 2.4 illustrates an electrodialysis process. In electrodialysis (ED), two types of membranes are used. The cation membrane allows only cations (positive ions) to permeate, and the anion membrane allows only anions (negative ions) to permeate. These exchange membranes are alternately immersed in salty water in parallel, and an electric current is passed through the liquid. The cations will migrate to the cathode, and the anions will migrate to the anode. Therefore, water passing between membranes is split into two streams. One is pure water, and the other is concentrated brine. Because ED uses energy at a rate directly proportional to the quantity of salts to be removed, this process is more useful in desalting brackish water.

Reverse osmosis and electrodialysis are the two most important membrane processes. To affect salt separation, RO uses hydraulic pressure, whereas ED uses electric current.

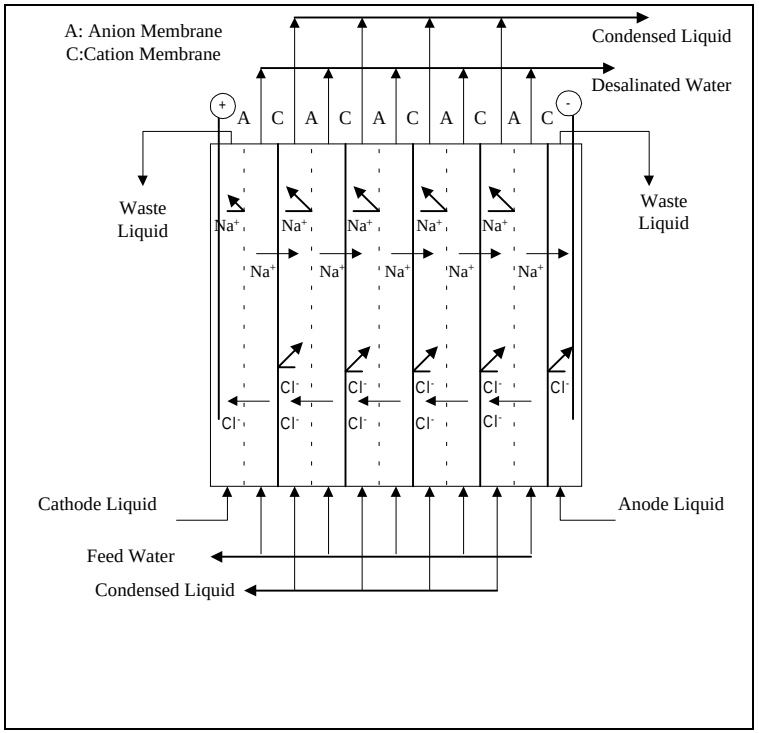

Figure 2.4: Principle of electrodialysis.

2.4 Multistage Flash (MSF) Distillation

A. Process Description

The multistage flash distillation process involves boiling seawater and condensing the vapor to produce distilled water. It works on the principle that seawater will evaporate as it is introduced into the first evaporator (flash chamber) with lower pressure than saturation pressure. It then condenses and cools down to a saturation temperature equivalent to the chamber pressure.

Figure 2.5 shows a schematic diagram of the MSF desalination plant. The MSF plant consists of three sections: *heat-rejection*, *heat-recovery*, and *heat input (brine heater).* The heat rejection and heat recovery consist of a number of flash chambers (stages) connected to one another.

Seawater enters through the heat-rejection section. This section uses the heat released during condensation to preheat the feed, and to reject energy into the supplementary cooling water. The recirculating brine, which is a formed by mixing part of the feed seawater (make-up) and a large mass of brine from the last stage, is circulated through heat-recovery tubes (water boxes). In the heat-recovery section, the brine gets heated as it passes through the tubes from one stage to another by exchanging the thermal energy from the flashing vapor in each stage. In another word, the heat released by condensation of vapor is used to heat the recirculating brine. Passing through the last stage, the water enters the brine heater, where its temperature is raised to a certain temperature which is equal to the saturation temperature (i.e., top brine temperature) for the system's pressure.

After heating the saturated brine to the top brine temperature in the brine heater by the saturated or supersaturated steam coming from the boiler, the saturated brine enters the first stage of the heat-recovery section through an orifice or weir. As the brine runs into the first stage, it will become superheated and flashed off to give pure vapor as a result of pressure reduction. The vapor then passes through the demisters, where the salt carried with the vapor is removed, condenses on the cooling tubes (water box) and is collected as distillate in the distillate tray. Figure 2.6 shows the cross section of a single stage. The process is then repeated all the way down the plant as both brine and distillate enter the next stage at a lower pressure. The distillate is finally collected, disinfected, and treated for pH and hardness before going to storage vessels.

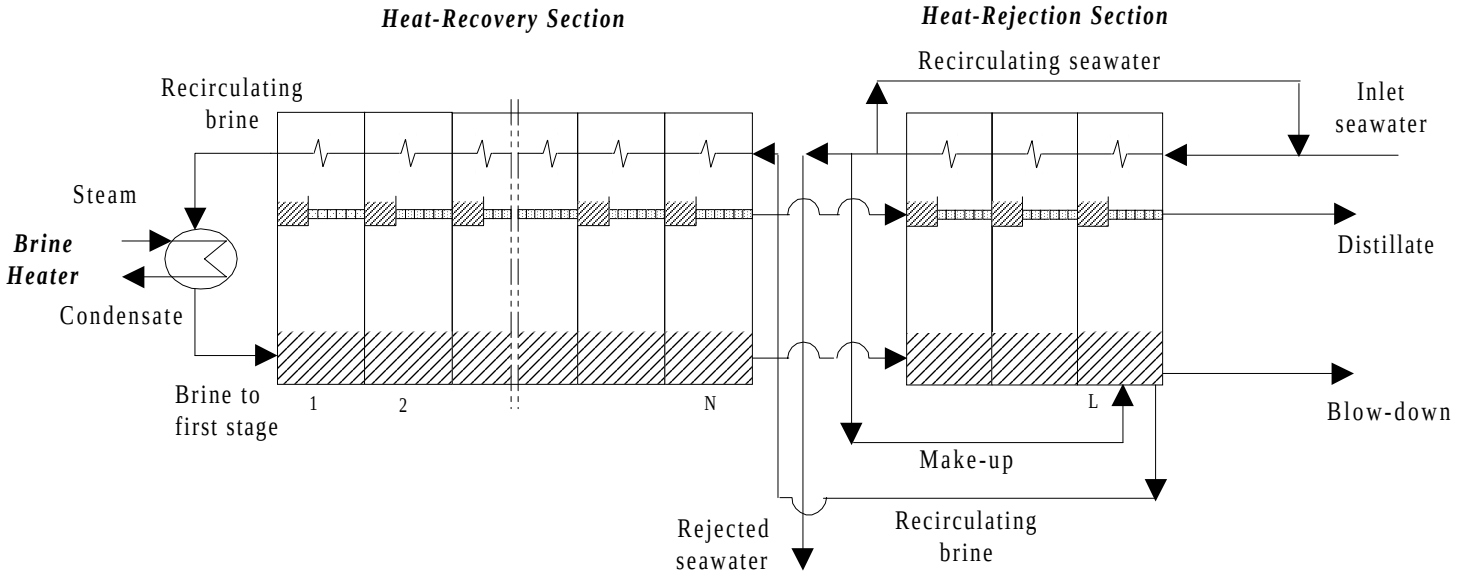

Figure 2.5: A recirculating-brine multistage flash (MSF) desalination plant.

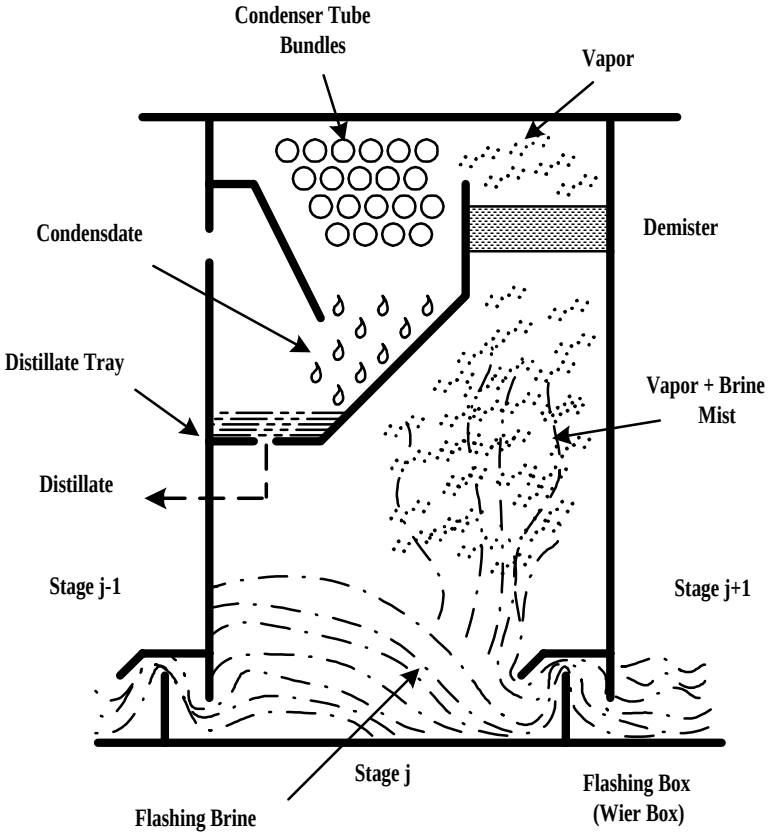

Figure 2.6: A single stage in a MSF desalination plant.

Finally, as mentioned above, part of the brine from the last stage is then recycled to the heat recovery tubes after adding make-up seawater to it . The brine gets heated as it passes through the tubes from one stage to another by exchanging the thermal energy from the flashing vapor in each stage, and the cycle is repeated a gain.

The flashing flow system in the MSF processes can be either a “once through“ or with a “recirculation”. We briefly describes the recirculating brine system above.

Figure 2.7 shows a “once through” MSF flowsheet. In this system, all the brine left in the last stage after flashing is then rejected to the sea. This means that no brine is circulated and there is no specific heat rejection section. The thermal rejection in this plant is achieved by virtue of the temperature difference between the in-coming feed stream and the out-going brine and distillate streams.

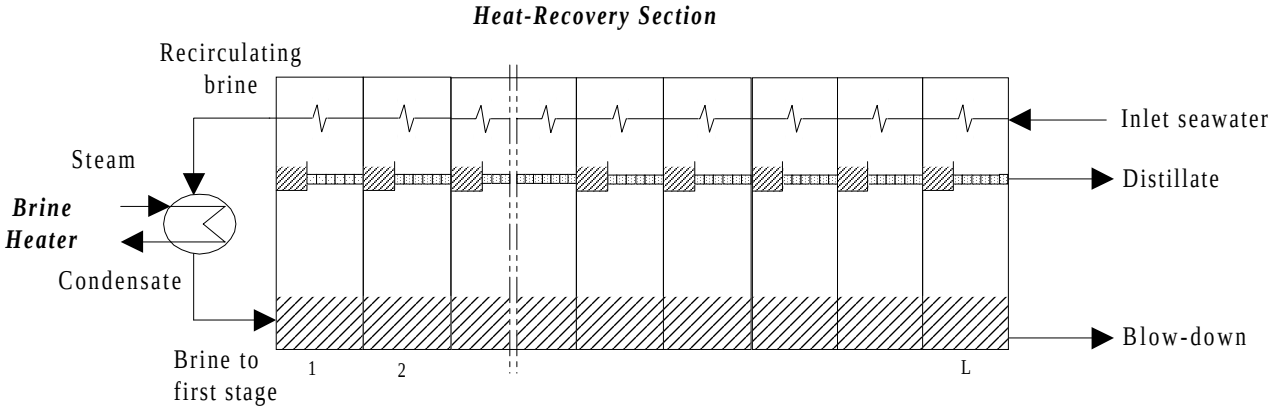

Figure 2.7: A once-through multistage flash desalination plant.

B. Operational Variables and Constraints

Figure 2.8 shows a schematic diagram of a MSF desalination plants, in which all key variables are labeled. We describe those variables as follows.

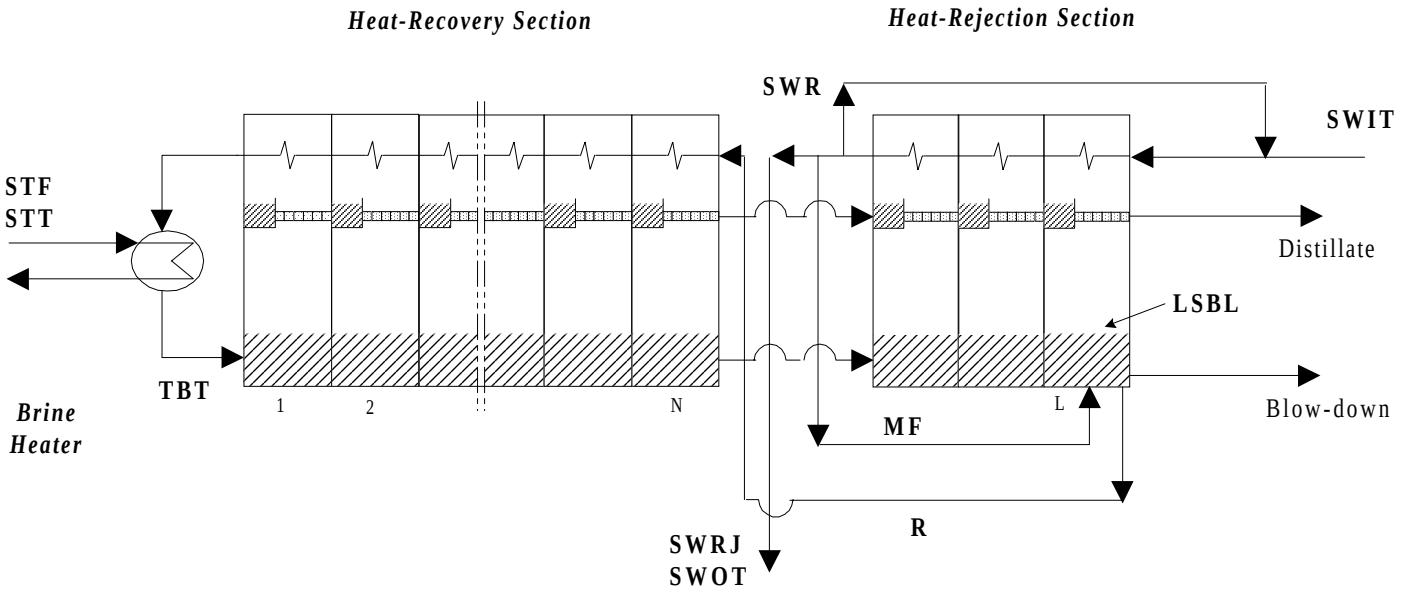

Figure 2.8 Schematic diagram of MSF desalination plants depicting operational variables.

1. Top Brine Temperature (TBT).

The top brine temperature plays a crucial role in determining the performance of a MSF plant. It is usually expressed in terms of a performance ratio (PR), which is the ratio the flowrate of the distillate produced to the steam flowrate supplied to the brine heater. TBT cannot be raised above a certain value due to scaling problems. The type of chemicals and the brine concentration determine the value of the upper limit. TBT depends on the type of feed treatment. With the use of a polyphosphate threshold treatment, the limit is about 90 °C. Some high-temperature additives can be used to increase TBT to 121 °C. However, they are generally used up to 110 °C only. With acid use, TBT can be increased to 118 °C. At this temperature, the scale deposition rate is accelerated. However, if TBT is reduced below a certain limit, the pressure difference to the vent condenser may become insufficient, causing an incomplete extraction of noncondensable gases, followed by instability and possible vapor-side corrosion problems. Evaporators normally work with fixed TBTs. If the last-stage brine temperature (bottom brine temperature) changes during operation, the interstage temperature differences, and therefore the pressure, will also vary. As a result, the brine flow through the interstage orifices will change. To restore to original conditions, the operator adjusts the orifices, which is a tedious operation.

Changing the brine flow would not be a solution because the evaporator output would also change and some modifications of the orifice settings would be needed to prevent high or low levels in some stages. The brine temperature in the heat-rejection section stages is a function of cooling seawater temperature, heat-transfer surface conditions, and ejector performance. These factors are subject only to very slow changes, except in plants where scale is formed and causes changes in the heat-transfer surface conditions, leading to a low bottom brine temperature.

Recirculating Brine Flowrate (RBF)

The recirculating brine flowrate is one of the most important operational variables that could affect the performance of the unit. Increasing the recirculating brine increases the distillate production, but adversely affects the performance ratio. Additionally, the recirculating brine flowrate determines the brine flow velocity inside the condenser tubes. This brine velocity plays an important role in scale formation, deposition, and removal.

Recirculating brine flowrate has a direct effect on unit production and thermal efficiency. It can also influence the degree of fouling occurring, as a reduced recirculating flowrate can increase the fouling by reducing the scouring of deposits from tube surfaces. All scaling processes are time-dependent, a fact not always adequately appreciated. Most scale-control additives extend the " induction period " during which precipitation is retarded, and any factor that increases the residence time increases the possibility of fouling. Thus, reduced recirculation rates may result in increased fouling.
However, when we change the brine flowrate we may need to adjust the transfer devices since operation is not at the design point. If the brine flow rate is low, sealing between stages may not be adequate. The plant will be unstable and operation will be inefficient. If the flow rate is high, the product will be contaminated because flooding can occur; once contaminated, it takes a long time for the product salinity to drop.

Therefore, the lower limit is fixed to avoid scaling problems caused by a low velocity of brine in the brine heater or brine boiling in the tubes. The upper limit should be controlled to avoid erosion and carry-over of brine to the distillate. Usually, we run the plant close to the upper limit of recirculating brine flowrate.

3. Steam Flowrate (STF) and Temperature (STT) to the Brine Heater.

Low-pressure steam is required in the brine heater and high-pressure steam is required for operating the ejector. The LP steam affects the top brine temperature (TBT) and distillate production (DP). For example, in case of scale precipitation, we increase the steam temperature and shell pressure to maintain the desired top brine temperature and distillate production. This will cause a high tube-wall temperature with localized overheating and an increase in scale thickness, resulting eventually in tube failure

4. Seawater Flowrates (SWR and SWRJ)

We reduce the seawater flow as the ambient temperature decreases, in order to maintain the requited seawater outlet temperature from the heat-rejection section. However, as flow is progressively reduced, a point is reached when it is not possible to maintain the required minimum velocity through the tubes. Therefore, scaling can occur. In such a situation, the operator pumps a part of the reject cooling water (SWRJ) from the heat-rejection section, called the recirculating seawater stream (SWR), into the seawater line before entry to the heat-rejection section. This ensures that the seawater meets the temperature and velocity requirements at entry to the heat-rejection section. Therefore, the lower limit corresponds to the requirement of specified rate of evaporation in the heat-rejection section. The upper limit is restricted by the maximum available pump flow of the seawater supply pump. Both limits are correspond to the limits on the velocities in the tubes.

For the specified seawater temperature, simulation indicates that the seawater flowrate has marginal effect on the performance ratio or the distillate produced.

5. Cooling-Seawater Inlet and Outlet Temperatures (SWIT and SWOT)

The seawater temperature in the Arabian Gulf, where most of the MSF plants are located, varies from 14 °C in the winter to 35 °C in the summer.

The efficiency of the MSF desalination plant depends on the flash range, which is the difference between the top brine temperature and the cooling-water inlet temperature to the heat-rejection section. At high seawater temperatures, the flash range will be the smallest. Therefore, the recirculating brine and the heat-transfer areas should be designed at these conditions. At low seawater temperatures, the thermodynamic situation of the whole evaporator changes. The evaporator pressure would decrease in accordance with the decrease in the saturation temperatures. This, in turn, affects the interstage brine flow because of pressure drop between the adjacent stages changes. Moreover, due to decrease in the vapor density with decreasing pressure, the vapor velocity increases.

In order to limit deviations from design conditions, the MSF plants operate during the winter with a recycle of cooling water in the heat-rejection section for raising the inlet seawater temperature. The recycled heated seawater flow may not be sufficient to keep the inlet seawater temperature constant throughout the year. Therefore, most plants operate with seawater temperature drop during winter operation. This will minimize the operation time of the recycle cooling-water system as well as the total electrical energy demand.

6. Make-up Flowrate (MF)

As the make-up flow increases, the salt concentration in brine stream decreases, which in turn will decrease the specific gravity of the brine and the boiling-point elevation. This lowers steam consumption and decreases the blowdown salt concentration.

Consequently, some increase in the performance ratio can be expected. The lower limit

of the make-up flowrate depends on the salt concentration of the recirculating brine flow, and its upper limit changes with the cooling seawater flowrate and seawater supply-pump discharge pressure. Usually, the MSF plant operates at a high make-up flowrate.

7. Interstage Brine-Transfer Arrangements (Orifice Height).

The interstage brine transfer through orifice plays a very crucial role. The aims of such a transfer should be to:

- produce a smooth brine flow downstream of the orifice;
- promote mixing of the brine by turbulence to minimize unsteady-state losses; and
- avoid brine splashing into the demisters to minimize liquid entrainment into the vapor.

Two strategies for designing the interstage brine-transfer mechanism are:

- to set orifice so as to provide optimum brine levels for *a nominal load operation*.
- set orifices so as to provide *a stable operation* over a wide range of partial loads.

The design philosophies of venders of MSF plants differ considerably. Figure 2.9 illustrates some interstage brine-transfer configurations. Instability in the operation may rise with improper brine-level settings in the transfer orifices. A under-sized orifice causes high brine levels upstream of the orifice, and the number of stages affected depends upon its location relative to the downstream stages with a level control.

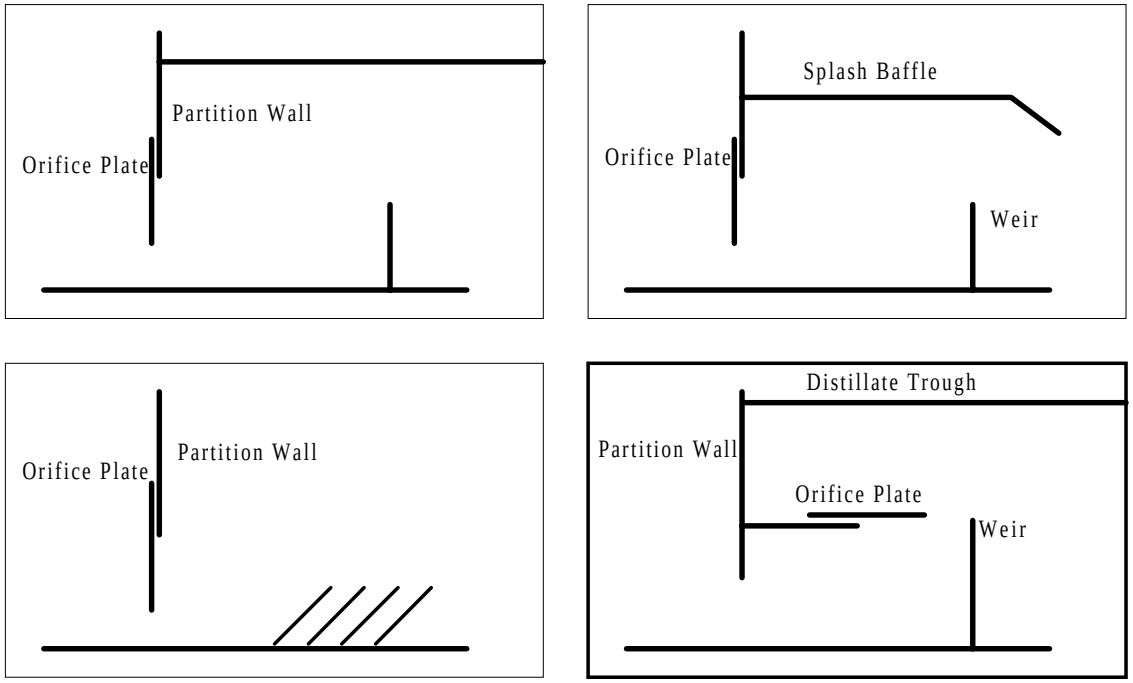

Figure 2.9: Interstage brine-transfer configurations.

Too high brine levels can result into excessive splashing and flooding of the demisters with corresponding thermal losses. Over-sized orifices can lead to vapor blowing-through into the subsequent stages.

8. Last-Stage Brine Level (LSBL)

As discussed in the previous section, the control of brine level in each stage is crucial in maintaining the stability of the process. Brine level through the plant must always be high enough to seal the interstage orifice and prevent blowing-through of vapor. At the same time, the brine should be low enough to ensure less equilibration losses. This can be done by maximizing interstage pressure drop or minimizing brine flow per unit width . The last-stage brine level is linked with the levels in all other stages, flowrates (blowdown, recirculating brine, distillate, etc.), and the top brine temperature.

C. Water Unit Cost

Cogeneration power/desalination plants offer economic advantages over single-purpose plants. These advantages are derived from more efficient utilization of fuel and saving in capital investment costs of common components (Al-Zubadi, 1989). Table 2.1 illustrates the capital investment costs of cogeneration plants which consist of direct and indirect costs.

Table 2.1: Summary of capital investment cost allocations (AL-Zubaidi, 1989)

Capital cost item	**Water production 1000$**
Direct Cost:	
Dredging of intake channel and offshore work	13,107
Site preparation	5,570
Boilers and auxiliary systems	620,94
Turbines and auxiliary systems	356,30
Civil work	997,20
Distillation plants	459,046
Total direst capital cost	675,167
Indirect Cost:	
Engineering consultants and power project cost	13,795
Distillation project cost	13,172
Supporting service costs	7,236
Total indirect cost	34,203
Total capital costs	709,370
Capital investment cost $/m^3/day	1,355

Based on Al-Zubaidi's cost study (Al-Zubaidi, 1998), Figure 2.10 shows the distribution water production unit cost among the different costing components at a power/water ratio of 2750 KW/1000m^3/day. The water unit cost is 3.132 $/m^3.

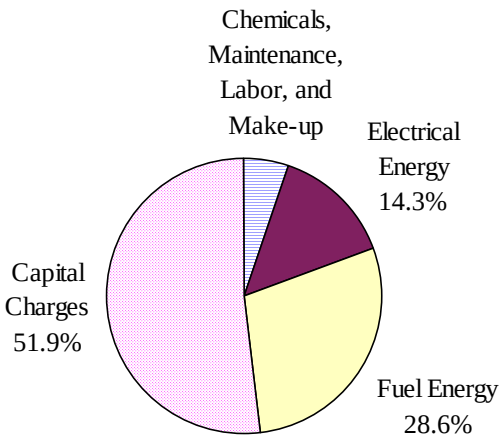

Figure 2.10: Water unit-cost distribution

2.5 Reverse Osmosis

A. Principle of Reverse Osmosis.

When we try to separate pure water and a salt solution through a semipermeable membrane, the pure water diffuses through the membrane and dilutes the salt solution. The membrane rejects most of the dissolved salts, while allowing the water to permeate. This phenomena is known as *natural osmosis* (Figure 2.11.a).

As water passes through the membrane, the pressure on the dilute side drops, and the pressure of the concentrated solution rises. The osmotic flux continues until an equilibrium is reached, where the net water flux through the membrane becomes zero (Figure 2.11.b).

At equilibrium, the liquid level in the saline water will be higher than that on the waterside. The amount of water passing in either direction will be equal. The hydrostatic pressure difference achieved is equal to the effective driving force causing the flow, called *osmotic pressure*. This pressure is a strong function of the solute concentration and the temperature, and depends on the type of ionic species present.

Applying a pressure in excess of the osmotic pressure to the saline water section slows down the osmotic flow, and forces the water to flow from the salt solution into the waterside. Therefore, the direction of flow is reversed, and that is why this separation process is called *reverse osmosis* (Figure 2.11.c).

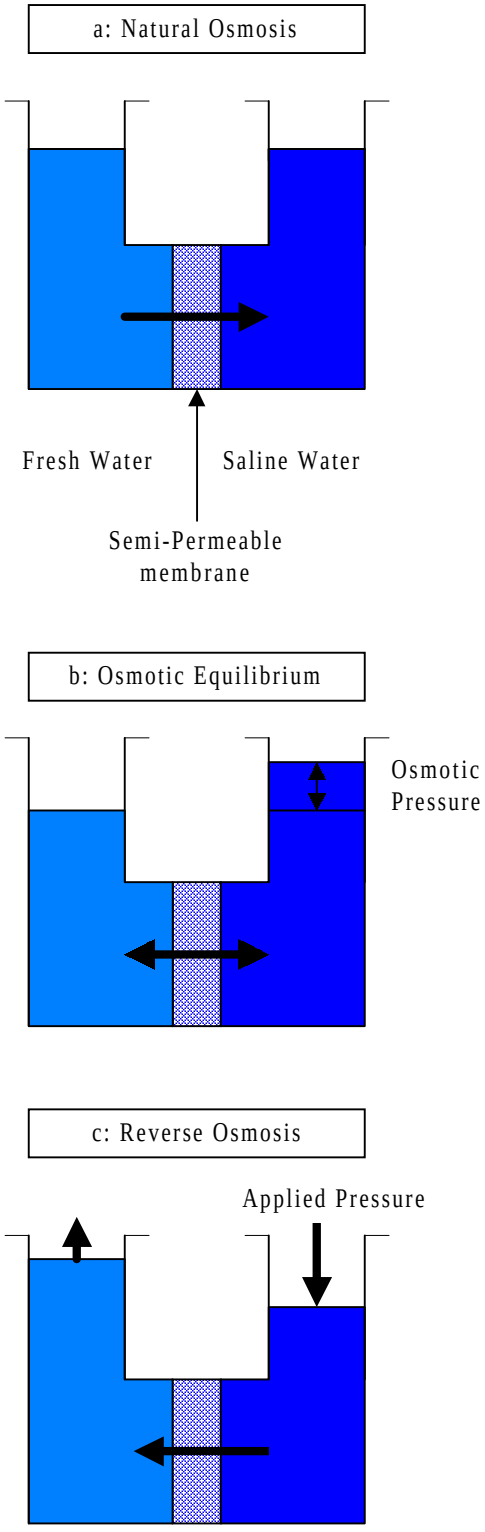

Figure 2.11: Principle of reverse osmosis.

B. Process Description and Terminology

A reverse osmosis system consists of four major components, shown in Figure 2.11. They are:

- pretreatment system
- high-pressure pump
- membrane assembly
- post-treatment system

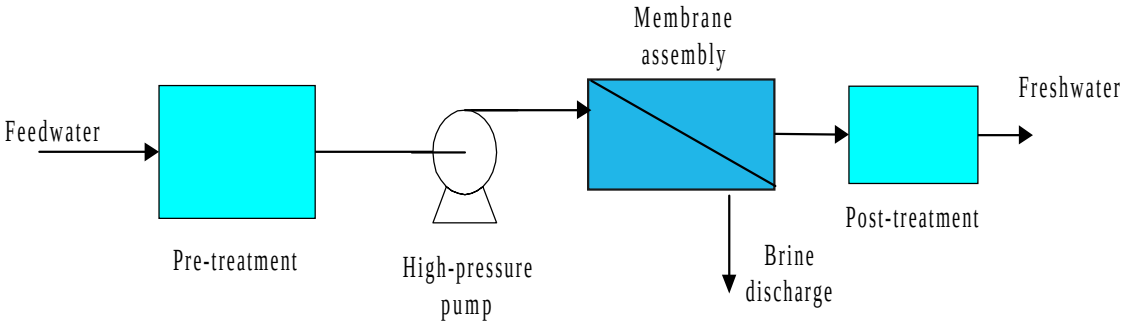

Figure 2.12: Flow diagram of a reverse osmosis system.

1. Pretreatment System

Feed pretreatment is necessary in all desalination methods, and reverse osmosis is no exception. The proper pretreatment of water before it reaches the membrane is the key to successful operation of a reverse osmosis plant. The need for pretreatment depends on the feedwater composition, the recovery of the RO system (see section 2.5C), and the solubility of the particular salt. Specifically, a pretreatment step has the following objectives:

- To remove excess turbidity and suspended solids. The tiny particles are usually removed by coagulation followed by filtration. Typical coagulants include alum, lime and polymers.
- To inhibit or control scaling and the formation of compounds, which upon precipitation, will plug the water passages or coat the membranes. Most scaling is due to calcium carbonate, sulfate and iron. The common way to minimize precipitation of dissolved substances is to lower the pH by adding acid, thereby increasing their solubility or reducing their concentration by conversion to a more soluble form.
- To disinfect and prevent biofouling (micro-organism growths) and equipment contamination.
- Chlorine has been the most frequently used disinfectant for reducing the presence of micro-organisms. The effectiveness of chlorine is dependent on the chlorine concentration, contact time, and pH of the water. A free residual chlorine of 1.0 mg/l prevents biological growth in the filtrate storage tank upstream of the RO system. Because membranes differ in their compatibility with chlorine, we must perform chlorination.

2. High-Pressure Pump

The function of this component is to raise the pressure of the pretreated feed water to the level appropriate for the membrane and for the feed water being used.

The pressure required depends on the concentration and temperature of the feed water. Osmotic pressure increases with increasing concentration, so that the operating pressure must exceed the osmotic pressure corresponding to the concentration of the rejected brine at the membrane outlet. It can be up to three times the osmotic pressure for seawater desalination. Brackish water requires 17-27 bar, whereas seawater operates in the range of 50-80 bar.

Figure 2.13 depicts the osmotic pressure of sodium nitrate, chloride and sulfate, and seawater as a function of salt content 25°C.

In addition, osmotic pressure increases with temperature, so that any increase in the temperature must be accompanied by an increase in the applied pressure.

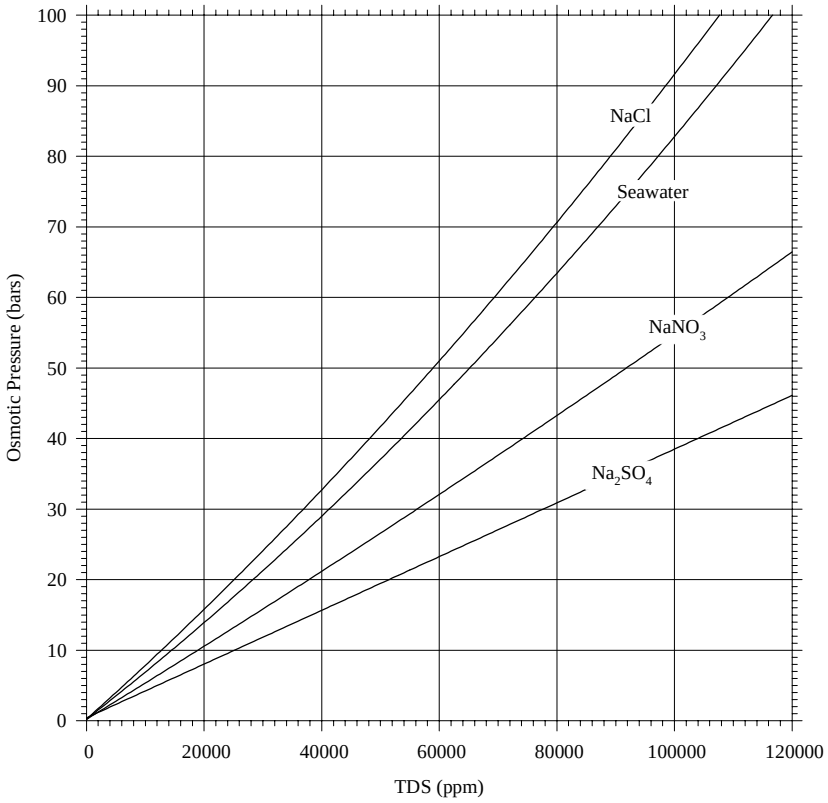

Figure 2.13: Osmotic pressures of sodium nitrate, chloride and sulfate, and seawater at 25 °C (Hanbury, et al., 1993).

3. Membrane Assembly

The original membranes were made from cellular acetate. Since then, RO processes use a variety of blends or derivatives of cellular acetate, polyamides. Plate-and-frame, tubular, spiral-wound and hollow-fine-fiber membranes are the most popular reverse osmosis devices.

An ideal membrane has the following characteristics:

- High salt rejection.
- High permeability to water.
- Resistant to high temperature.
- Resistant to oxidizing agents, especially chlorine.
- Resistant to all kind of fouling (inorganic, organic, colloidal, and microbiological fouling).
- Chemically, physically, and thermally stable in saline water.
- Capable of being formed to yield high membrane area-to-volume ratio (packing density).
- Resistance to creep deformation.
- Long and reliable life.
- Inexpensive.

Figure 2.14 shows the factors influencing the membrane performance.

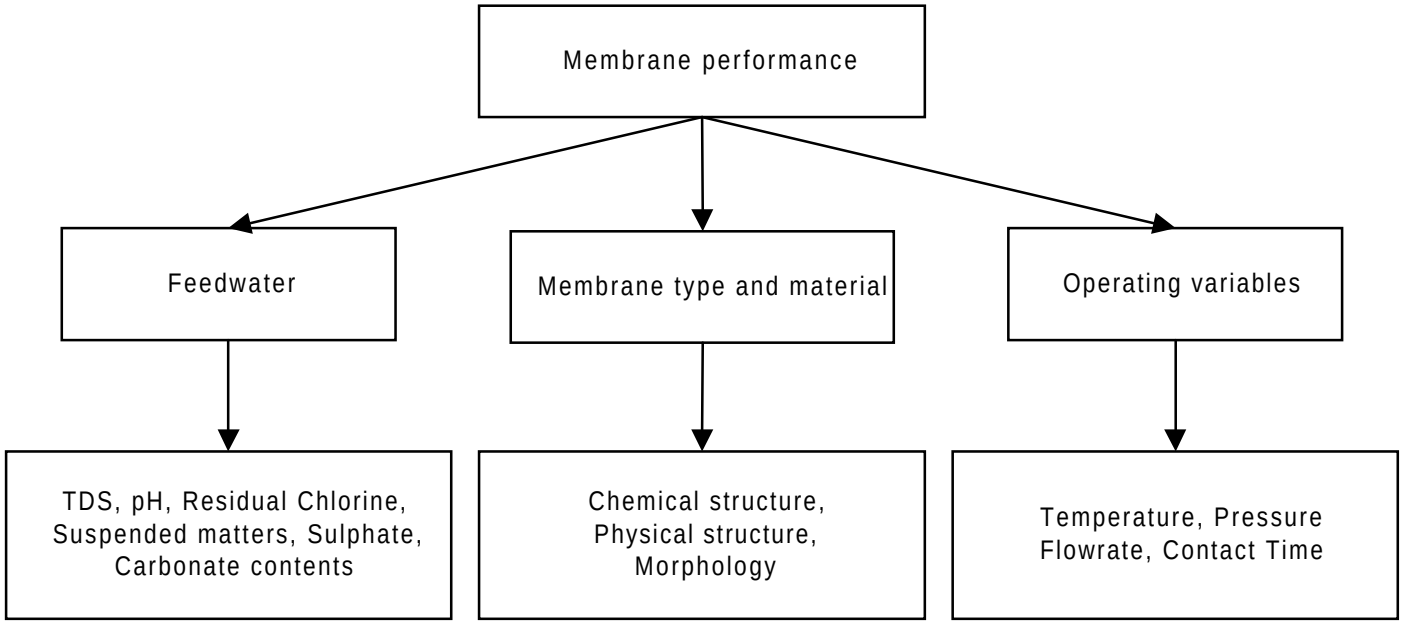

Figure 2.14: Factors influencing the membrane performance.

a. Spiral-Wound Systems

Spiral-wound membranes were originally developed in the mid-1960's at Gulf General Atomics through funding by the U.S. Department of Interior. They were commercially available in the late 1960's, and they rapidly displaced the tubular membranes for use in water production. They are characterized by their high packing densities of the order of 600 m^2/m^3 and can operate at pressures up to 80 bar.

Figure 2.15 shows the spiral-wound membrane assembly. It consists of two or more leaves (envelopes). Each leaf has two flat sheets of semipermeable membrane separated and supported by a porous backing material (i.e., a polyester tricot fabric), and sealed together at the edges by special epoxy or polyurethane adhesives. The edges of the membrane are sealed on three sides only to form a flexible envelope. The open end of the envelope is, in turn, sealed around a central product collection tube from which the permeate may flow. A flexible-spacing, plastic netting is placed on top of the sealed membrane sandwich and the whole roll material is wrapped around the central tube, to form a spiral wound unit. This unit is then inserted into a glass-fiber, pressure vessel for use.

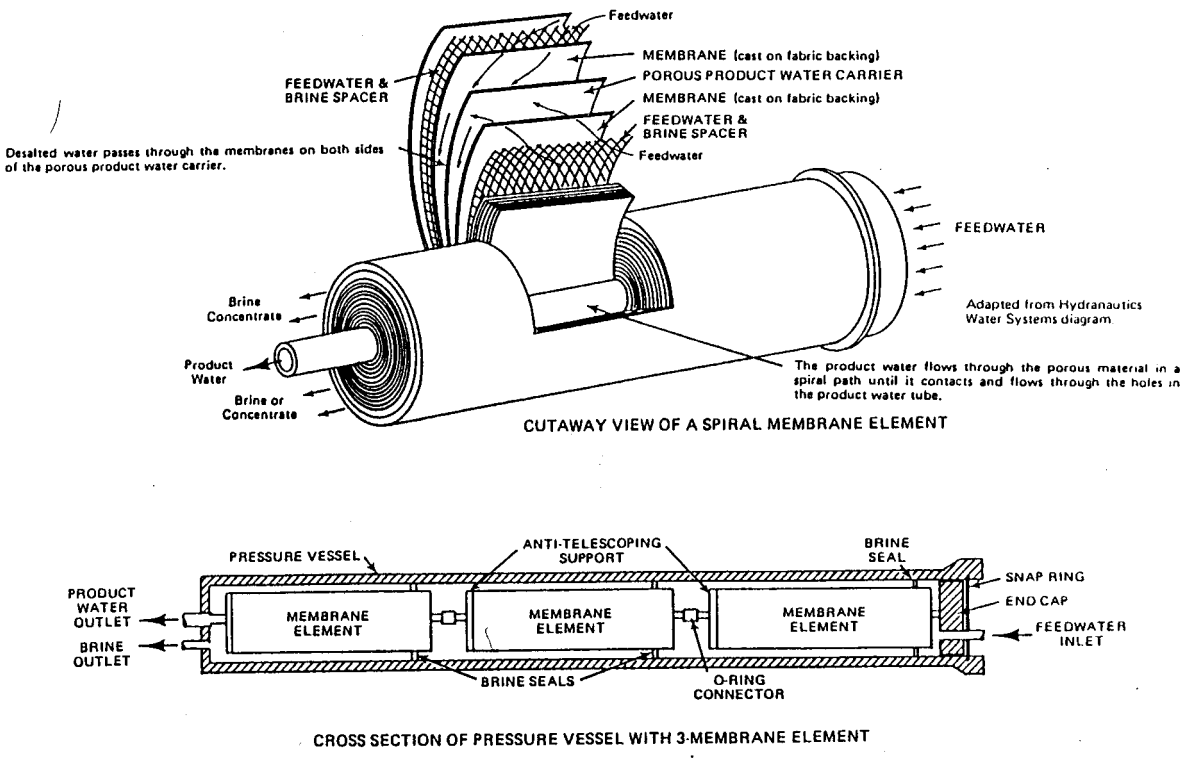

Figure 2.15: Spiral-wound membrane assembly (Khan, 1986).

a. Hollow-Fine-Fiber Membranes

Hollow-fine-fiber membrane configuration was first developed by Du Pont in the late 1960's, followed by Dow Chemical Company and Toyobo. They became commercially available in 1969. This configuration has the maximum area per unit volume (about 30,000 m^2/m^3). The membranes are designed as long capillary tubes with a diameter of about a human hair. The capillary tubes have an outside diameter of 80-200 microns, about twice the inside diameter of 40-100 microns, so they are relatively thick-walled tubes. An outside-to-inside diameter ratio of 2 to 1 gives the fibers the strength to resist the high pressure involved.

Figure 2.16 shows the hollow-fine fiber membrane configuration. Millions of membrane fibers are arranged and wound around a backing cloth as a bundle which is rolled up around a feed distribution pipe (with the fiber parallel to the pipe axis), and then assembled into a sealed cylindrical pressure vessel made of a glass-reinforced plastic. Each end of the fiber bundle is set into epoxy resin blocks so that the bores are exposed. One end remains sealed, while the other is then cut away to expose the open end. This arrangement is much like a shell-and-tube arrangement, with the fine tube open at one end.

Pressurized feedwater is enters through the distributor tube at one end and flows radially outwards through the fiber bundle. Flow of the permeate is from the outside into the bore of the fibers. The purified product is collected in the bore of the fibers and is removed from the open end of the fiber loop. The concentrated brine on the other side (feed end) is extracted. Table 2.2 summarizes the advantages and the disadvantages of the basic membrane configurations.

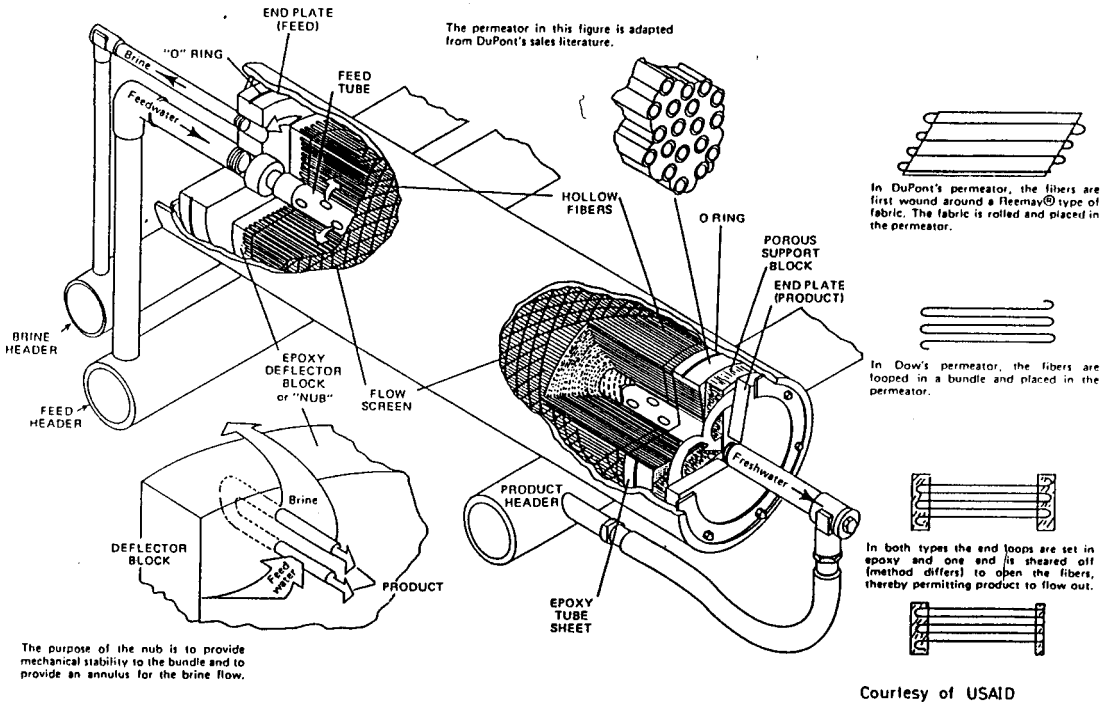

Figure 2.16: Hollow-fine fiber membrane assembly (Khan, 1986).

Table 2.2: Advantages and disadvantages of basic membrane configurations.

Membrane configuration	Advantages	Disadvantages
Spiral-wound	• Operates at a pressures up to 80 bar. • Good resistance to fouling . • Easy to clean. • Easy to change bundles in the field. • Available in a wide variety of materials and from several manufacturers.	• Moderate packing densities of the order of 600 m^2/m^3. • More susceptible to blocking due to the narrowness of their brine passages, which could lead to concentration polarization. • Difficult to troubleshoot individual elements in multiple-element tubes. • Membrane tends to hydrolyze and lose its rejection capacity at a temperature above 35 C or a pH outside the range of 3-8. • Difficult to achieve high recoveries in small systems, requires use of elements with several diameters.
Hollow-fine fiber	• Has extremely high membrane area-to-volume ratio (packing densities) of the order of 30,000 m^2/m^3. • High recovery in individual permeators. • Easy to change bundles in the field. • Easy to troubleshoot.	• Sensitive to fouling by colloidal and suspended materials due to the narrowness of their brine passages. It is therefore necessary to have extensive pretreatment even on relatively clean feedwater. • Immune to biological attack and does not hydrolyze in water • Limited number of manufacturers and membrane materials.
Tubular	• Large flow passages which allow high flow velocities. • Low tendency to foul. • Easy to clean, remove, and reforme. • Operates at a very high pressures (100 bar).	• Very low packing density of the order of 300 m^2/m^3. • Expensive • Minimal choice of membrane materials.
Plate and frame	• Low tendency to foul. • Easy disassembly for cleaning and membrane replacement. • Can use several membrane types. • Suitable for specialized applications producing high quality products such as pharmaceutical or food stuffs.	• Low packing density. • Potential for leaks between leaves. • Expensive.

4. Post-Treatment System

Product water from the RO plant requires treatment prior to storage and transmission to consumers. This is necessary as the product water can cause serious corrosion problems in the pipe transmission system.(Hanbury, 1993)

The product from the membrane usually requires pH adjustment. This is done by adding a base or by degasification (H_2S and CO_2). Since most RO membranes reject calcium in preference to sodium, this necessitates the addition of calcium salts (calcium carbonate or sodium carbonate/bicarbonate) to the product water.

Finally, product water requires disinfection to prevent bacterial growth before transferring the product water to the distribution system.

C. Basic Transport Equations in Reverse Osmosis

Once the RO system has been installed, both membranes assembly must be tested for fluxes, salt rejection, and recovery under various temperatures, pressures, and feed water salinities.

1. Water Flux

The following equation defines the water flux:

$$J_1 = K_1(\Delta P - \Delta \pi) \qquad (2.1)$$

$$K_1 = K_w \frac{A}{\tau} \quad (2.2)$$

$$\pi = 1.21\, T \sum Mi \quad (2.3)$$

where

J_1 = Water flux = [m^3/m^2/sec]

ΔP = Hydraulic pressure differential across the membrane = [atm]

$\Delta \pi$ = Osmotic pressure differential across the membrane = [atm]

K_1 = Pure water transport coefficient, i.e. the flux of water through the membrane per unit driving force, = [m^3/m^2/sec atm]

K_w = Membrane permeability coefficient for water.

A = Membrane area = [m]

τ = Membrane thickness = [m]

T = Feed water temperature =[K]

Mi = Molality of the i^{th} ionic or nonionic materials.

K_1 is given by the membrane manufacturer or may be found by solving the equation at the standard test conditions. It depends on the membrane properties, temperature of the system and the chemical composition of the salt solution.

2. Salt Flux

The salt flux is an indicator for the membrane effectiveness in removing salts from water. The salt flux is a function of the system temperature and the salt composition. Therefore, it is a property of the membrane itself and indirectly related to the feed pressure. It is

proportional to the salt concentration difference across the membrane, according to the following equations;

$$J_2 = K_2 \Delta C \quad (2.4)$$

$$\Delta C = Cf - Cp \quad (2.5)$$

where

J_2 =Salt flux = [Kg/m^2/sec]

K_2 =Salt transport coefficient = [m/sec]

Cf = Salt concentration in the feed = [Kg/m^3]

Cp = Salt concentration in the product = [Kg/m^3]

Since the water flux through the RO membrane is higher than that of salt, there is an accumulation of salt on the membrane surface on the pressurized side of a membrane. This phenomenon is called *concentration polarization*.

The increase in concentration polarization has two effects:

- Increases the osmotic pressure, and reducing the water flux across the membrane.
- Increases the driving force of the concentration difference across the membrane, which reduces the driving potential, increases the salt passage and gives poor product quality.

All these effects increase the capital cost and the power requirements per unit of potable water produced.

Salt Rejection

Salt rejection expresses the effectiveness of a membrane to remove salts from the water. It can be calculated from the following equation;

$$\%Salt\ rejection=(1-\frac{Product\ concentration}{Feed\ concentration})\acute{}100\% \qquad (2.6)$$

$$\%\ Salt\ rejection = (1-\frac{Product\ TDS}{Feed\ TDS})\acute{}100\%$$

$$\%\ Salt\ rejection = 1-\%\ Salt\ \ passage$$

The salt passage depends on the feedwater temperature and composition, operating pressure, membrane type and material, and pretreatment.
Salt passage and bundle pressure drop are the two indicators of membrane fouling.

4. Recovery

The recovery rate for an RO system is:

$$\text{Recovery(R)} = \frac{Qp}{Qf} * 100\% \qquad (2.7)$$

where

Qp = Product flow = [m^3/day]

Qf = Feed flow = [m^3/day]

The recovery is specified by the feedwater salinity. For example, seawater plant's recovery varies between 20-35%.

Increasing the recovery raises the brine concentration and the osmotic pressure, thus decreasing the permeate flux and increasing the total dissolved solid (TDS) in the product. We can increase the recovery by increasing the number of banks in the system.

The above transport equation lead to the following important conclusions;

- J_1 is proportional to ΔP .
- J_2 is proportional to ΔC and is independent of the applied pressure.
- The increase in the operating pressure increases the water flow without changing the salt flow.

D. Operational Variables

When a reverse-osmosis system is used on a commercial level, it is important to check its performance periodically. As time passes, the membrane performance deteriorate continuously due to pressure compaction and fouling. This causes its transport parameters to change, and the performance of the module to decline. Therefore, data monitoring is an important step in optimizing the performance of an RO plant. The important operating variables of a RO desalination process are as follows.

1. Permeate flux

At a given feed salinity, the feed flow rate affects the production rate of the plant, water recovery, and the number of modules. A low production rate, below design specifications, could be an indication of membrane fouling. Every stage in an RO plant is designed to operate at a certain recovery, which is the ratio of product flow to the feed flow. If the recovery is above the design specification, then the brine concentration and the osmotic pressure will increase, causing a decrease the permeate flux and an increase in dissolved solid content in the product.
Since the feed flow is maintained constant during operation, the product flow must be controlled to maintain a constant recovery during operation.

2. Permeate conductivity

The main objective of an RO process is to produce product of a low total dissolved solids content. However, since the TDS is not easily measured except under controlled conditions in laboratories, the plant operators use conductivity to estimate the quality of the water produced.

Monitoring the product conductivity is necessary to produce good water product. A gradual or rapid increase in the product conductivity is an indication of membrane fouling or mechanical damage in the membrane module, respectively.

Both permeate flux and conductivity are affected by :

- pH
- Temperature

- Pressure

a. pH

pH adjustment is a major steps in the pretreatment processes. The pH of the feed water must be monitored and controlled for the following reasons:

1. To prevent alkaline (calcium carbonate) scale precipitation.
2. To increase the life of a cellular acetate membranes by protecting them from degradation that result from hydrolysis. Hydrolysis is the reaction of cellular acetate with water to produce an alcohol and an acid. Hydrolysis depends on both pH and temperature. The minimum hydrolysis rate occurs at a pH of 4.5-5.
3. To optimize the membrane salt rejection.

b. Temperature

The feed temperature has a significant effect on the membrane performance for the following reasons:

1. The K_1 value in equation (2.1) depends on temperature of the system. An increase in the feed water temperature will cause an increase in water flux.
2. The feed water temperature affects the water flux in another way. If the RO plant is operating under an ideal condition with no fouling or scaling, water flux will decline with time, because of compaction phenomena. The compaction correction factor (CCF) is found from the following equation:

   $$CCF = t^m \qquad (2.8)$$

where

t = Operating time

m = A negative exponent whose value depends on the membrane, operating pressure, and temperature.

For a membrane under a certain operating pressure, the m value is higher at a higher temperature, which means more compaction loss, and less water flux.

c. Pressure

Equation (2.1) shows that the water flux though the membrane is directly proportional to the pressure drop across the membrane. Since the pressure at the product side is constant, it follows that the water flux is directly related to the feed pressure.

Additionally, the salt flux is a function of the system temperature and the chemical composition of the salt solution and is indirectly related to the feed pressure.
At low operating pressure, less water permeates the membrane while the salt flux stays the same. At higher operating pressures more water permeates the membrane at the same salt flux.

High feed pressure may cause a membrane compaction, which reduces the water flux after operating for a certain time as illustrated in Equation (2.1).

Summary

- Desalination means the removal of fresh water from saline water. Distillation is the oldest and most commonly-used desalting techniques. In this process, evaporation of the saline water and condensation of the generated vapor occur to obtain fresh water.
- The major desalting processes are: (1) multieffect; (2) multistage flash; (3) vapo-compression; (4) reverse osmosis; and (5) electrodialysis

- The multistage flash desalination processes work on the principle that seawater will evaporate as it is introduced into the first evaporator (flash chamber) with lower pressure than saturation pressure. It then condenses and cools down to a saturation temperature equivalent to chamber pressure.
- The MSF plant consists of three sections: *heat-rejection*, *heat-recovery*, and *heat input (brine heater)*. The heat-rejection and heat-recovery consist of a number of flash chambers (stages) connected to one another.

- There are two types of MSF plant configurations: (1) recirculating-brine; and (2) once-through.
- Reverse osmosis is pressure-driven processes, to allow water, not salt, to diffuse from a salty solution across a semipermeable membrane. The pressure difference across the membrane should be high enough to overcome the osmotic pressure and push reasonable water flux across the membrane.
- A reverse osmosis system consists of four major components: (1) pretreatment system; (2) high-pressure pump; (3)membrane assembly; and (4) post-treatment system.
- The proper pretreatment of water before it reaches the membrane is the key to successful operation of a reverse osmosis plant. A pretreatment steps has the

following objectives: (1) to remove excess turbidity and suspended solids; (2) to inhibit or control scaling and the formation of compounds; (3) to disinfect and prevent biofouling; and (4) to perform chlorination and dechlorination.

- The most popular reverse-osmosis membranes are: (1) plate-and-frame; (2) tubular; (3) spiral-wound; and (4) hollow-fine-fiber.
- Product water from the RO plant requires treatment prior to storage and transmission to consumers. This is necessary as the product water can cause serious corrosion and fouling problems in the pipe transmission system.
- Once the RO system has been installed, both membranes assembly must be tested for fluxes, salt rejection, and recovery under various temperatures, pressures, and feed water salinities.
- When a reverse-osmosis system is used on a commercial level, it is important to check its performance periodically. As time passes, the membrane performance deteriorate continuously due to pressure compaction and fouling.

2.7 Nomenclature

T	: Feed water temperature
ΔP	: Hydraulic pressure differential across the membrane
A	: Membrane area
K_w	: Membrane permeability coefficient for water.
τ	: Membrane thickness
Mi	: Molality of the i^{th} ionic or nonionic materials.
$\Delta\pi$	: Osmotic pressure differential across the membrane
Cf	: Salt concentration in the feed
Cp	: Salt concentration in the product
J_2	: Salt flux
K_2	: Salt transport coefficient

J_1 : Water flux

K_1 : Pure water transport coefficient, i.e. the flux of water through the membrane per unit driving force

DP : Distillate produced

LSBL : Last stage brine level

m : A negative exponent whose value depends on the membrane, operating pressure, and temperature.

MF : Make-p flowrate

Qf : Feed flow

Qp : Product flow

RBF : Recirculating brine flowrate

STF : Low pressure steam flowrate

STT : Low pressure steam temperature

SWIT : Seawater inlet temperature

SWOT : Seawater outlet temperature

SWRC : Seawater recirculating flowrate

SWRJ : Seawater reject flowrate

t : Operating time

TBT : Top brine temperature

2.8 References

Al-Zubaidi, A.A.J., "Technoeconomics of Power/Desalting Cogeneration Plants in Kuwait- A Preliminary Study", *Desalination*, **76**, 121 (1989).

Dabbagh, T.A., "The Role of Desalination in Sustaining Economic Growth in the Gulf", *Proceeding of the IDA World Congress on Desalination and Water Sciences*, Abu Dhabi Publishing Co., Abu Dhabi, United Arab Emirates, V.I, 213 (1995).

El-Saie, M.H., "The MSF Desalination Process and its Prospects for the Future", *Desalination*, **93**, 43 (1993).

Khan, A.H., *Desalination Processes and Multistage Flash Distillation Practice*, Elsevier Publishers, New York, N. Y. (1986).

Hanbury, W.T., T., Hodgkiess, and R., Morris, *Desalination Technology*, Intensive Course Manual, Porthan Ltd.- Easter Auchinloch, Glasgow, UK (1993).

Ho, Winston W. S. and K. K. Sirkar, *Membrane Handbook*, Van Nostrand Reinhold, New York, N. Y. (1992).

Lior, N., *Measurements and Control in Water Desalination*, ELSIVIER, New York, N. Y. (1986).

Seul, K.W. and S.L., Lee, "Effect of Liquid Level on Flow Behaviors Inside A Multistage Flash Evaporator: A Numerical Prediction", *Desalination*, **85**, 2, 161 (1992).

Temperely, T. G., "The Coming of Age of Desalination", *Proceeding of the IDA World Congress on Desalination and Water Sciences*, Abu Dhabi Publishing Co., Abu Dhabi, United Arab Emirates, V. I, 219 (1995).

CHAPTER 3

AN INTRODUCTION TO COMPUTING WITH NEURAL NETWORKS

Chapter 3 introduces neural networks, beginning with a discussion of neural network architecture, then moving to the properties and applicability of neural networks. We next illustrate what makes up a neural network, and present the topology of neural network. Finally, we discuss network training and the practical aspects of neural computing.

3.1 Introduction

The human brain is known for its ability to learn and classify. The inspiration of neural networks came from studies on the structure and function of the brain and nerve systems as well as the mechanism of learning and responding. Neural networks take their name from the simple processors in the brain, called neurons, which are interconnected by a network that transmits signals between them.

In order to understand the principle of "computational" neural networks, we must have some idea of its counterpart, "biological" neural networks.

3.2 Introduction to Neurons

A brain is made up of a large number of highly connected cells, called neurons, coupled to receptors and effectors. To understand the relationship between receptors and effectors, we must study a single neuron. Figure 3.1 shows the major components of a

typical nerve cell (neuron) in the central nervous system. The major structure of a typical nerve cell includes dendrites, cell body, and axon. Dendrites are the receptive zones which constitute the major part of the input surface of the neuron, and the axon is the transmission (output) line. Synapses are elementary structural and functional units that connect the axon of one neuron to various parts of other neurons.

When the input signals (nerve impulse) come into these synapses, this results in local changes in the input potential in the cell body of receiving neurons. These potentials are spread through the main body of the cell, and are weighted since some are stronger than others. The resulting inputs can be either excitatory or inhibitory. Excitatory inputs decrease the polarization of the cell, while inhibiting inputs increase the cell polarization. The input potentials are summed at the axon hillock. If the amount of depolarization at the axon hillock is equal to or greater than the threshold for the neuron, then an action potential (output) is generated and travels down the axon away from the main cell body. Figure 3.2 shows the block diagram of the nervous system.

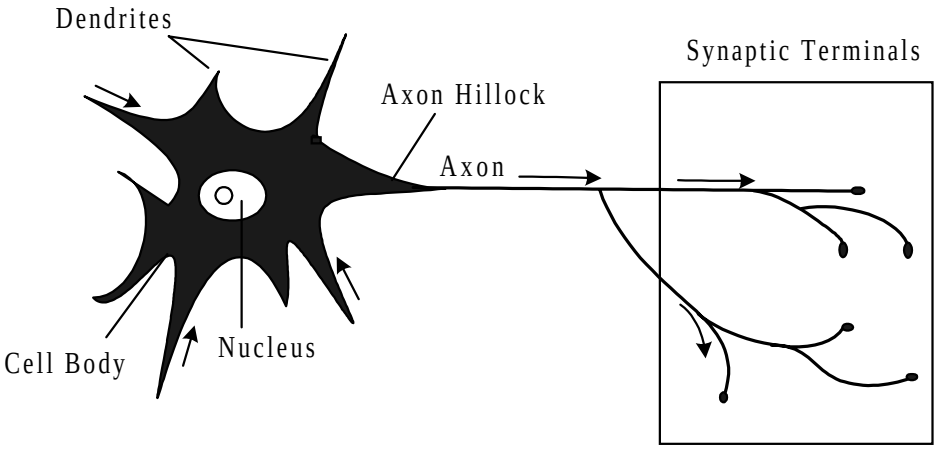

Figure 3.1: A simplified representation of a neuron

The ability of the nervous system to adjust to signals is a mechanism of learning, and the rate of firing an output (response) is altered by the activity in the nervous system.

Simply, a single neuron processes information by receiving signals from its dendrites, and produces an output signal which is then transmitted to other neurons.

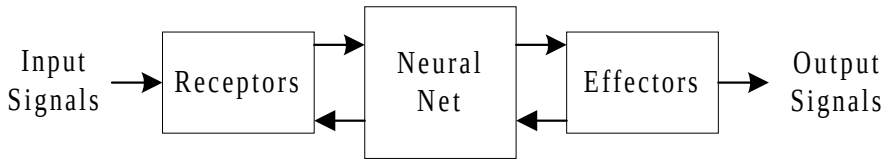

Figure 3.2: Block diagram of the nervous system.

3.3 Neural Network Architecture

Neural networks can be thought of as "black box" devices that accept inputs and produces outputs. Figure 3.3 shows a typical neural network structure.

- *Input Layer*: A layer of neurons that receives information from external sources, and passes this information to the network for processing. These may be either sensory inputs or signals from other systems outside the one being modeled.
- *Hidden Layer*: A layer of neurons that receives information from the input layer and processes them in a hidden way. It has no direct connections to the outside world (inputs or outputs). All connections from the hidden layer are to other layers within the system.

- *Output Layer*: A layer of neurons that receives processed information and sends output signals out of the system.
- *Bias*: Acts on a neuron like an offset. The function of the bias is to provide a threshold for the activation of neurons. The bias input is connected to each of the hidden and output neurons in a network

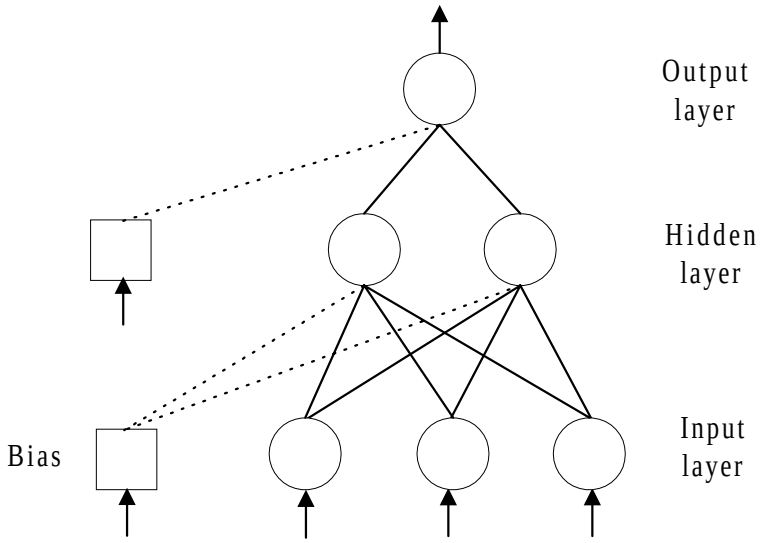

Figure 3.3: Structure of a typical multilayer neural network.

The number of input neurons corresponds to the number of input variables into the neural network, and the number of output neurons is the same as the number of desired output variables. The number of neurons in the hidden layer(s) depends on the application of the network.

As inputs enter the input layer from an external source, the input layer becomes "activated" and emits signals to its neighbors (hidden layer) without any modification. Neurons in the input layer act as distribution nodes and transfer input signals to neurons

in the hidden layer. The neighbors receive excitation from the input layer, and in turn emit an output to their neighbors (second hidden layer or output layer). Each input connection is associated to a quantity, called "*a weight factor*" or "*a connection strength*".

The strength of a connection between two neurons determines the relative effect that one neuron can have on another. The weight is positive if the associated connection is excitatory, and negative if the connection is inhibitory.

3.4 Properties of Neural Networks

A. Strengths of Neural Networks

Neural networks derive their computing power in solving complex problems through their parallel distributive structure, and their ability to learn and therefore generalize.

Table 3.1 summarizes some of the useful properties and capabilities of neural networks that give them advantages over conventional algorithmic techniques.

Table 3.1: Neural network properties and capabilities.

Strengths	**Remarks**
Input-Output Mapping.	The network learns (supervised learning) from the labeled training samples or task examples by identifying the input-output relationship for the problem at hand.
Adaptability.	The adaptive capability is a result of the self-discovery capability. A neural network trained to operate in a specific environment can be easily retrained to discover the new input-output relationship caused by changes in operating environmental conditions.
Nonlinearity.	Neural networks are inherently nonlinear, which enables them to model complex relationships.
Effectiveness for processing noisy, incomplete or inconsistent data.	The effect of noisy or incomplete data in any given node is minimized. Signals send to and from nodes are continuous functions, thus enabling the network to deduce proper conclusions.
Knowledge is distributed throughout the system.	Knowledge in a neural network is not stored in specific memory locations. This provides great flexibility to the system.
Potential for online use.	Training time may be long for some neural networks, but once trained, it takes less than a second to calculate results. This gives the network the potential to be used online in a control system.

Table 3.1: Neural network properties and capabilities (continued).

Strengths	Remarks
No programming.	An algorithm does not have to be explicitly known and programmed by an expert. A neural network can learn to program its own solution to a problem.
Knowledge indexing	The network can index and store a large amount of knowledge related to the interconnections between variables and access it easily.

B. Limitations of Neural Networks

Along with every strength comes weakness. In general, neural networks are inappropriate for applications that require number crunching, or for situations where an explanation of behavior is required. Table 3.2 illustrates a number of concerns that must be understood before deciding to use neural networks for a specific application.

Table 3.2: Limitations of neural networks

Limitations	**Remarks**
Long training time.	Training time may be long for some neural networks, depending on the complexity of the problem; however today's advanced computers may eliminate this problem.
Not good if precise answers are required.	Neural networks cannot justify the accuracy of computed answers. Most training techniques do not guarantee the proper operation of the network. Training may get trapped in "local minima" during iterations.
No guarantee of 100% reliability.	This is true with limited training data.
Difficult to select input variables.	The selection of outputs is straightforward and depends on the problem definition. However, informed input-variable selection is critical to achieving an efficient model performance. Selecting input variables properly affects the entire process of neural network development.
Large amount of training data.	We may reconsider the use of neural networks if little input-output data exist or when all the training data are very similar. Neural networks are best suited for problems with a large amount of training data.

3.5 Applicability of Neural Networks

Neural networks can deal with problems that are complex, nonlinear, and uncertain, due to the properties and capabilities listed in Table 3.2. Table 3.3 lists several typical neural network applications as provided by *Neural Computing* (NeuralWare, 1993).

Table 3.3: Potential applications of neural networks.

Application	Definition
Prediction	Uses input values to predict output; e.g., given temperature, humidity and wind velocity, predict evaporation rate.
Classification	Use input values to predict a categorical output; e.g., given symptoms and lab results, determine the most likely disease.
Data Association	Learn associations of error-free or ideal data, then classify or associate data that contain error; e.g., learn five ideal patterns and then recognize noisy input patterns as one of the five patterns.
Data Conceptualization	Analyze data and determine conceptual relationships; e.g., cluster data with many attributes so that grouping relationships can be inferred.
Data Filtering	Smooth an input signal; e.g., smooth a noisy electrocardiogram signal.
Optimization	Determine optimal value; e.g., determine the shortest-distance trip for a traveling salesperson.

3.6 Elements of Neural Networks

The basic component of a neural network is the neuron, also called “node”, or the “processing element, PE”. Nodes contain the mathematical processing elements which govern the operation of a neural network. Figure 3.4 illustrates a single node of a neural network.

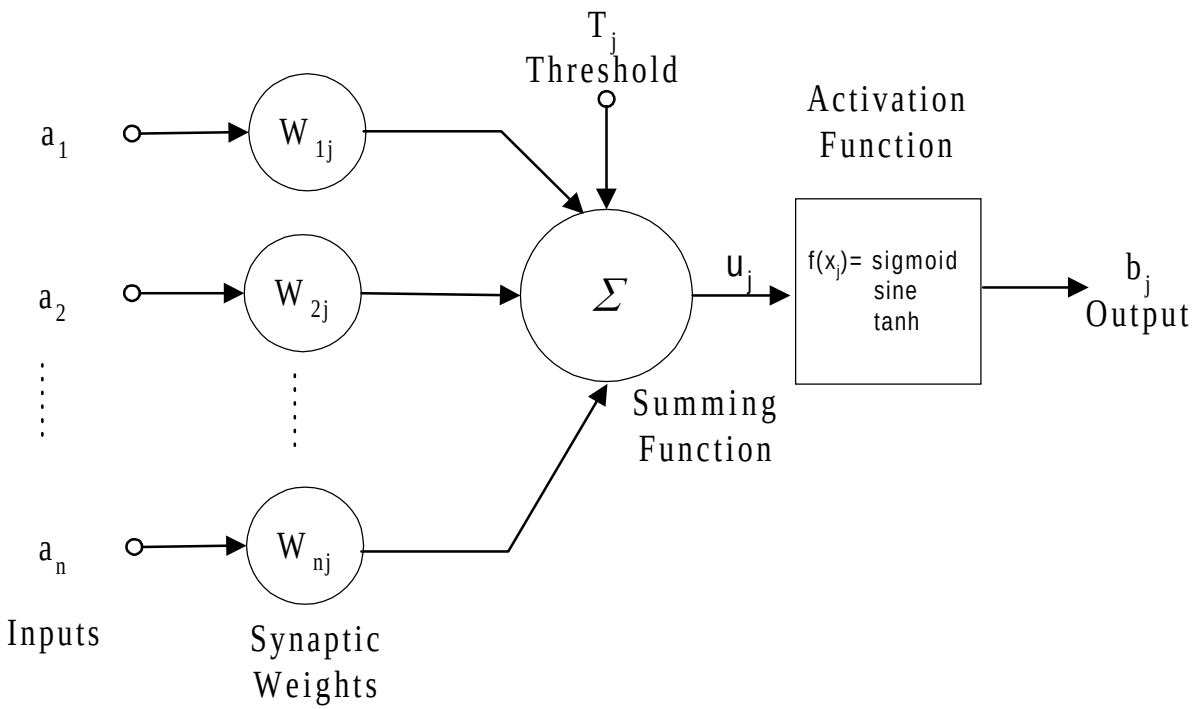

Figure 3.4: Single node anatomy.

A. Inputs and Outputs

We represent inputs by a_1, a_2 and a_n, and the output by b_j. Just as there are many inputs to a neuron, there should be many input signals to our PE. The PE manipulates these inputs to give a single output signal.

B. Weighting Factors

The values w_{1j}, w_{2j}, and w_{nj}, are weight factors associated with each input to the node. This is something like the varying synaptic strengths of biological neurons. Weights are adaptive coefficients within the network that determine the intensity of the input signal. Every input (a_1, a_2, …, a_n) is multiplied by its corresponding weight factor (w_{1j}, w_{2j}, …, w_{nj}), and the node uses this weighted input ($w_{1j}\ a_1$, $w_{2j}\ a_2$, …, $w_{nj}\ a_n$) to perform further calculations. If the weight factor is positive, then ($w_{ij}\ a_i$) tends to excites the node. If the weight factor is negative, then ($w_{ij}\ a_i$) inhibits the node.

In the initial setup of a neural network, we choose weight factors according to a specified statistical distribution. We then adjust the weight factors in the development of the network or "learning" process.

C. Internal Threshold

The other input to the node, T_j, is the node's internal threshold. This is a randomly chosen value that governs the "activation" or total input of the node through the following equation.

$$\text{Total Activation} = x_i = \sum_{i=1}^{n} \left(w_{ij} a_i \right) - T_j \qquad (3.1)$$

The total activation depends on the magnitude of the internal threshold T_j. If T_j is large or positive, the node has a high internal threshold, thus inhibiting node-firing. If T_j is zero or negative, the node has a low internal threshold, which excites node-firing. If no internal threshold is specified, we assume it to be zero.

D. Transfer Functions

We determine node's output using a mathematical operation on the total activation of the node. This operation is called *a transfer function*. The transfer function can transform the node's activation in a linear or nonlinear manner. Figure 3.5 shows several types of commonly used transfer functions.

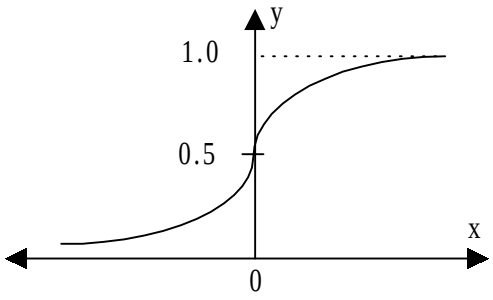

a- A sigmoidal transfer function

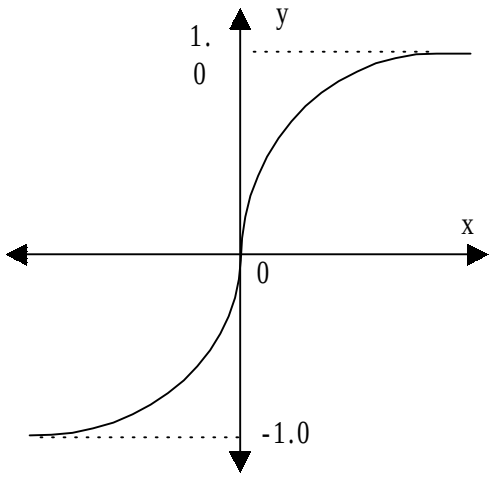

b- A hyperbolic tangent transfer function

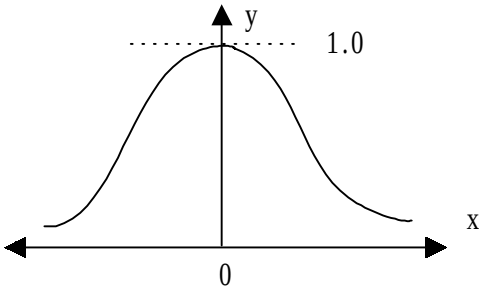

c- A Gaussian transfer function

Figure 3.5: Commonly used transfer functions.

The corresponding equations for the transfer functions are as follows:

- Sigmoid transfer function:

$$f(x) = \frac{1}{1+e^{-x}} \qquad 0 \leq f(x) \leq 1 \tag{3.2}$$

- Hyperbolic tangent transfer function:

$$f(x) = \tanh(x) = \frac{e^{x} - e^{-x}}{e^{x} + e^{-x}} \quad -1 \leq f(x) \leq 1 \tag{3.3}$$

- Gaussian transfer function:

$$f(x) = \exp\left(\frac{-x^{2}}{2}\right) \quad 0 \leq f(x) \leq 1 \tag{3.4}$$

The output, b_j, is found by performing one of these functions on the total activation, x_i.

3.7 Topology of a Neural Network

There are two different classification levels of neural networks structures. The first level is known as *the external structure*. The term "external" describes the overall, or macro, arrangement of and connections between inputs, outputs, and hidden layers that compose the network. The second level is *the internal structure*. It refers to the actual connections between individual nodes both within and between layers. The various arrangements incorporate both internal and external connections, depending upon the specific application of the network, the available data, and the ease of use.

A. External Neural Network Structure

There are several general external arrangements for neural networks: single-input and single-output (SISO), multiple-input and single-output (MISO), and multiple-input and multiple-output (MIMO). The fourth arrangement, single-input and multiple-output (SIMO), is not generally used, because data for a single input are not sufficient to predict the behavior of several output variables. Any of these arrangements may have one or multiple hidden layers.

The simplest external structure is the SISO network. As the name implies, this is a network that is designed to predict the behavior of one output variable based on data for one input variable. This type of network is only applicable to very simple systems, or in cases where there is a direct relationship between two variables. A disadvantage of this type of network is that it is unable to consider the interactions between input variables. Figure 3.6 illustrates a SISO network.

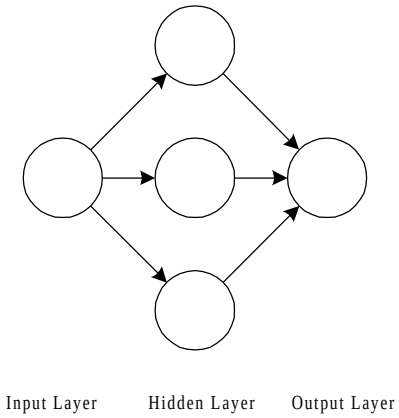

Figure 3.6: Example of a SISO arrangement with one hidden layer having three nodes.

The next simplest network arrangement is the MISO network. This type of network takes input data from many variables and uses them to predict the value of single output variable. We choose the MISO network, for instance, in soft-sensor applications where sensor data from many sources in a process are used to predict a single downstream variable such as product quality. Figure 3.7.shows an example of a MISO network.

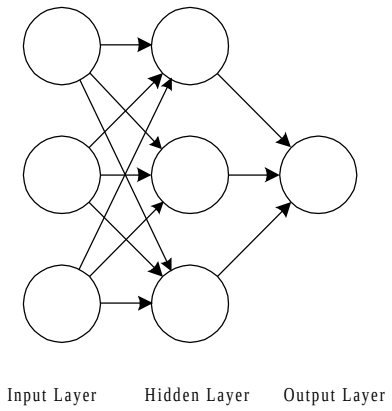

Figure 3.7: Example of a MISO network with 3 inputs and 1 hidden layer with 3 nodes.

The most complex network arrangement is the MIMO network. In this type of network, we use input data from multiple variables to predict the values for multiple output variables. The MIMO network is particularly convenient for on-line applications, as it can predict the values of several variables that may be of interest in the process with only a single pass of input data through the network. Figure 3.8 illustrates a MIMO network.

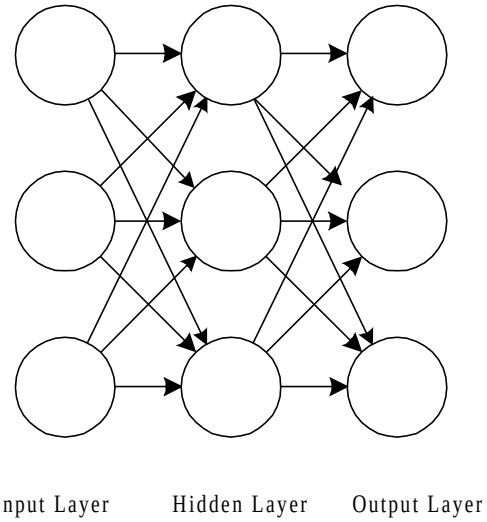

Figure 3.8: Example of a MIMO network with three inputs, three outputs, and one hidden layer with three nodes.

B. Internal Network Structure

The types of individual connections between the nodes compose the internal structure of a neural network. We can connect a node to any node in the network. The relative position of the origin to the endpoint of the connection defines the network's internal structure. There are three types of connections that are used: *interlayer*, *intralayer*, and *recurrent*. Figure 3.9 shows the three options for connecting nodes to one another. Layers K, H, and W could be any layer in the network.

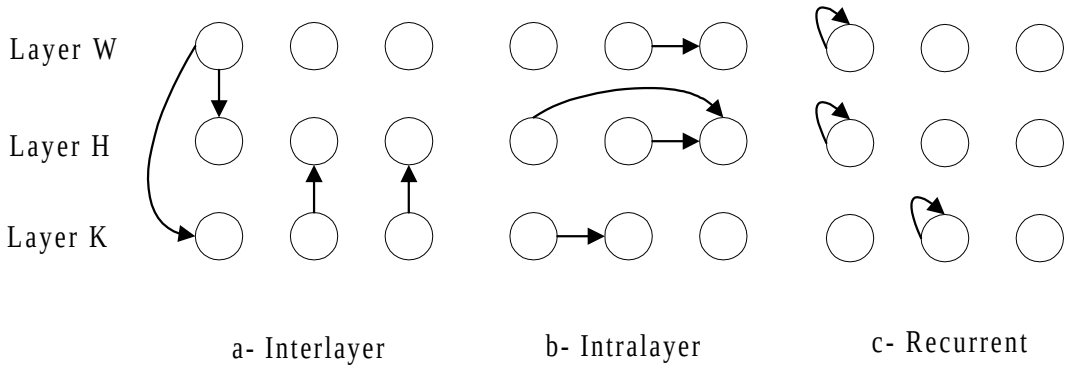

Figure 3.9: The connection options in a neural network.

- *Interlayer Connection*

  Outputs from nodes on one layer feed into nodes in a different layer.
- *Intralayer Connection*

  Outputs from nodes in one layer feed into nodes in that same layer.
- *Recurrent Connection*

  Outputs from a node feeds into itself as inputs.

Within the interlayer connection, we have two main network architectures: (1) *feedforward* and (2) *feedback* networks, shown in Figure 3.10.

In the feedforward network, the direction of signal flow is from the input layer, through each hidden layer, to the output layer. We frequently use feedforward networks in process modeling and in most engineering applications of neural networks. In a feedback network, signals flow from the input layers to the hidden layers. However, in a feedback network, the output from a hidden layer can return to the input layer.

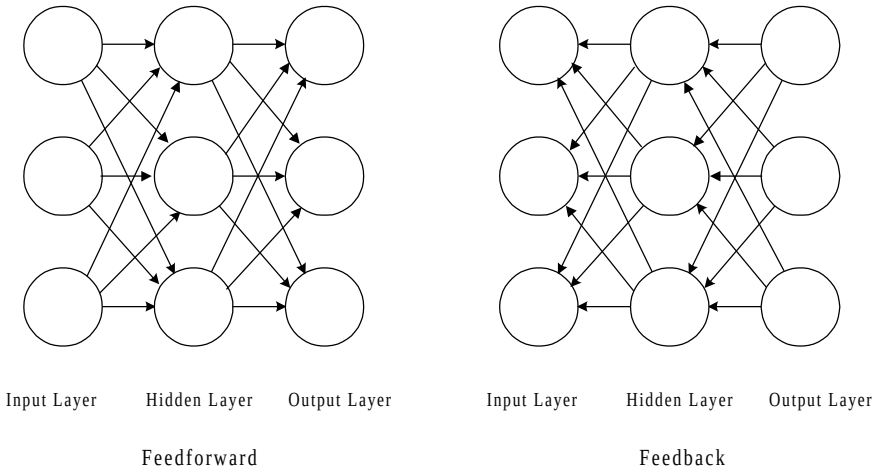

Figure 3.10: Feedforward and feedback networks.

C. Multilayer Networks

Most neural networks contain one to three hidden layers. The function of the hidden layer is to intervene between the external input and the network output. Multilayer networks are feedforward networks with one or more hidden layers between the input and output layers. These may be formed by cascading a group of single layers; the output of one layer provides the input to the subsequent layer. Figure 3.11 shows such a network with three hidden layers.

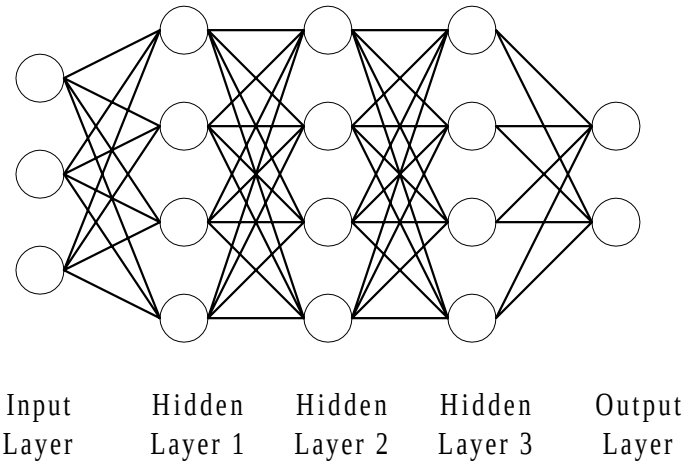

Figure 3.11: Feedforward network with three hidden layers.

Large, more complex networks generally offer greater computational capabilities. These multilayer networks have greater representational power than single-layer networks if nonlinearity is introduced.

Throughout this study, the network configuration refers to the number of nodes in each hidden layer. *For example, a 5:30:15:10 configuration designates that there are 5 nodes in the input layer, 30 nodes in hidden layer 1, 15 nodes in hidden layer 2, and 10 nodes in the output layer.*

3.8 Learning and Training with Neural Networks

Two subsets of data are used to build a model: a training set and a testing set. The training phase needs to produce a neural network that is both stable and convergent. Therefore, selecting what data to use for training a network is one of the most important steps in building a neural-network model.

Neural networks interpolate data very well, but they are less effective with extrapolation. Therefore, we should select the training set in such a way that it includes data from all regions of desirable operation.

A. Training the Network

Training is the process by which the neural network systematically adjusts the weights of interconnections between nodes so that the network can predict the correct outputs for a given set of inputs. For the best "learning" possible, we need a large and robust set of historical input/output data.

1. Learning Modes

There are a number of approaches to training neural networks. Most fall into one of two modes:

- *Supervised Learning*: Supervised learning requires an external teacher to control the learning and incorporates global information. The teacher may be a training set of data or an observer who grades the performance. Examples of supervised learning algorithms are *the least-mean-squire (LMS) algorithm* and its generalization, known as *the backpropagation algorithm*.
- *Unsupervised Learning*: When there is no external teacher, the system must organize itself by internal criteria and local information designed into the network. Unsupervised learning is sometimes referred to as *self-organizing learning*, learning to classify without being taught.

2. Fundamentals of Backpropagation Learning

There are many different types of training algorithms. One of the most common classes of training algorithms for feedforward interlayer networks is called *backpropagation*. In a backpropagation algorithm, a set of inputs is fed to the network and outputs are returned. Then, the network compares its output with the output of the actual data source. The network calculates the amount of error between its predicted output and the actual output. The network works backwards through the layers, adjusting the weight factors according to how much error it has calculated in its output. Once all of the weight factors have been adjusted, the network works in a forward path, taking the same input data to predict the output, based on the new weight factors. The network again calculates the error between the predicted and actual outputs. It adjusts the weight factors and the process continues, iteratively, until the error (i.e., sum-of-square errors) between the predicted and actual outputs has been minimized

To describe the basic concept of backpropagation learning algorithm, we first look at each of its elements and how they combine to form the backpropagation topology. Figure 3.12 illustrates a simple three-layer feedforward neural network.

- Input layer A: The input vector I is feeding into layer A. It has L nodes, a_i (I=1 to L), one node for each input variable.
- Hidden layer B: It has m nodes, b_j (j=1 to m).
- Output layer C: It has n nodes, c_k (k=1 to n), one node for each output variable: d_k is the desired output, and c_k is the calculated output.
- Interconnecting weight between the i^{th} node of layer A and the j^{th} node of layer B is denoted as v_{ij}.

- Interconnecting weight between the j^{th} node of layer B and the k^{th} node of layer C is denoted as w_{ij}.
- Internal threshold value for layer A is T_{Ai}, for layer B, T_{Bj}, and for layer C, T_{Ck}.

Note that each layer could have different numbers of nodes.

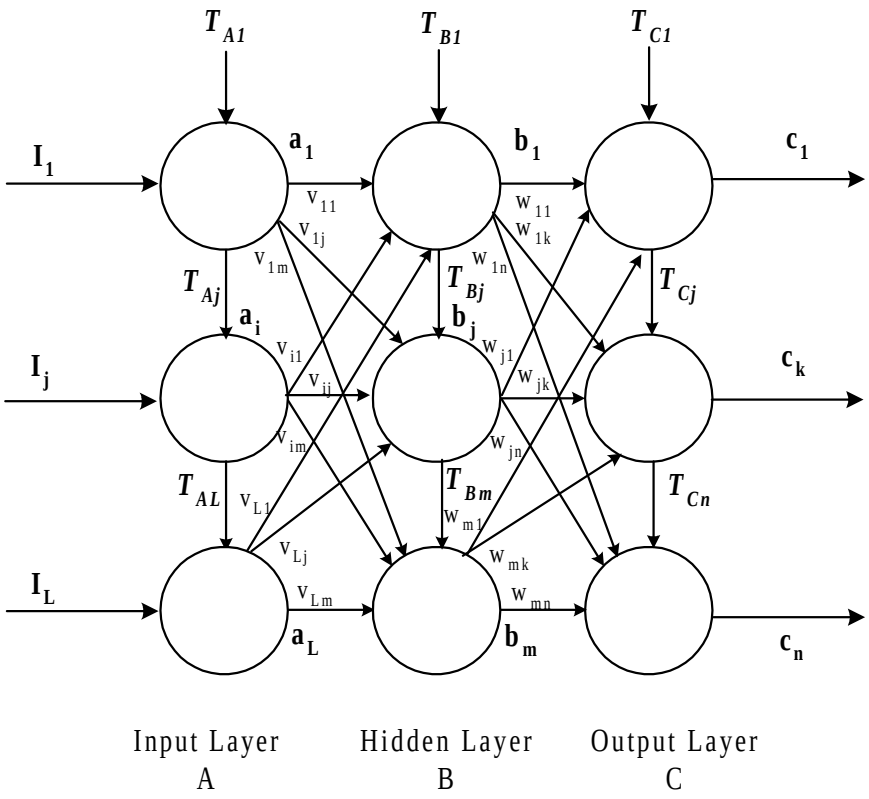

Figure 3.12: Three-layer feedforward neural network.

Backpropagation learning attempts to map given inputs with desired outputs by minimizing the sum-of-square errors, by adjusting both sets of weight factors, v_{ij} and w_{jk}, along with the internal thresholds.

The total mean-square errors function, E, is:

$$E = (\text{Output error})^2 = \sum_k \in_k^2 = \sum_k (d_k - c_k)^2 \qquad (3.5)$$

Figure 3.13 illustrates the step-by-step adjustment procedure as described below.

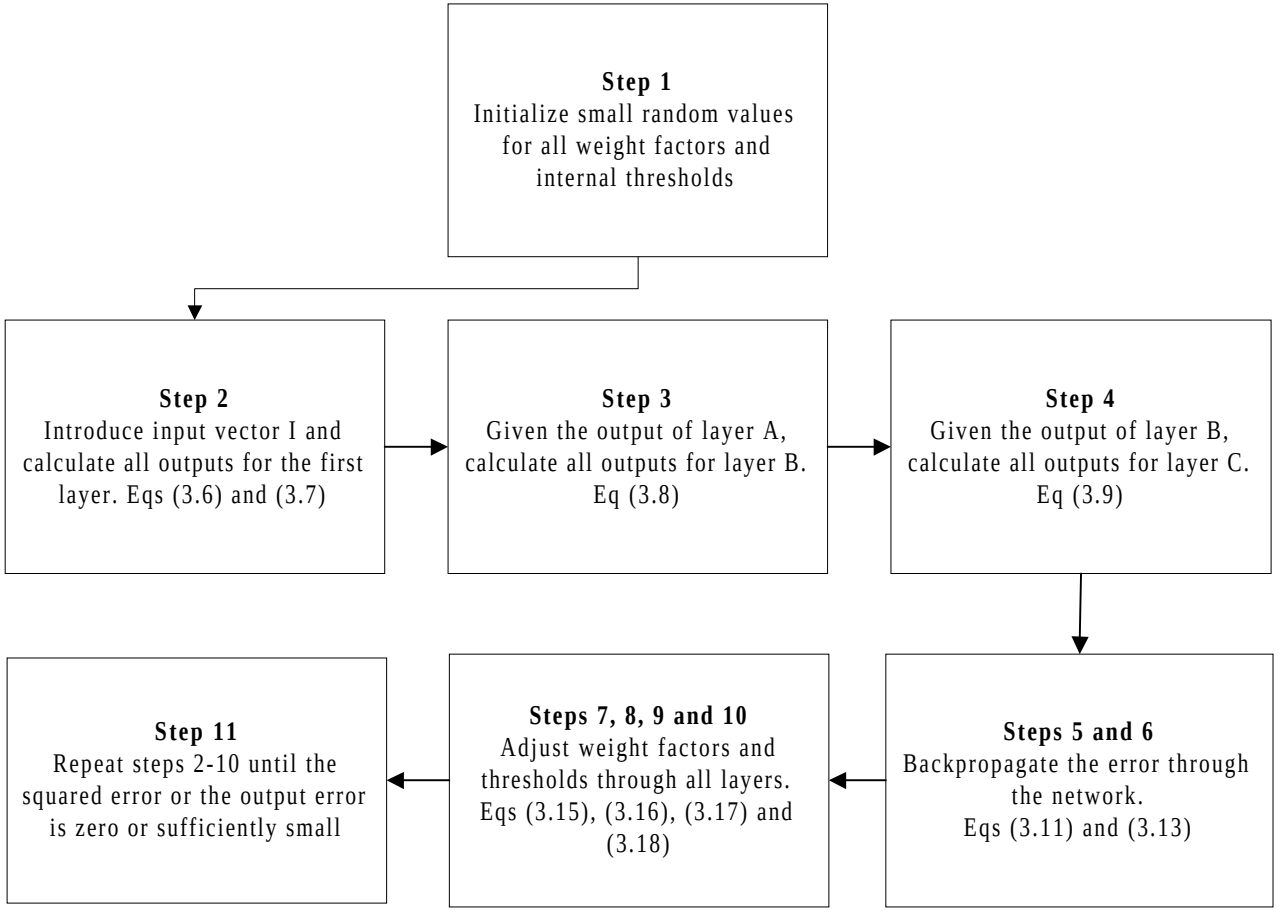

Figure 3.13: Backpropagation learning steps.

Step 1: Initialize weight factors (v_{ij}'s and w_{jk}'s) and threshold [T_{Ai}, T_{Bj}, T_{Ck}] to small random values within the interval [-1, +1].

Step 2: Present input vector I and calculate all desired outputs from the first layer, using the hyperbolic tangent transfer function introduced previously in Section 3.6.D.

$$x_i = I_i - T_{Ai} \tag{3.6}$$

$$f(x_i) = \frac{1}{1+e^{-x_i}} = a_i \tag{3.7}$$

where

I_i: normalized input into the i^{th} node on the input layer.

T_{Ai}: internal threshold for the i^{th} node.

x_i: total activation of the i^{th} node.

a_i: the output from the node.

Step 3: Given the output from layer A, calculate the output from layer B, using the equation:

$$b_j = f\left(\sum_{i=1}^{L}(v_{ij}a_j) - T_{Bj}\right) \tag{3.8}$$

Step 4: Given the output from layer B, calculate the output from layer C, using the equation:

$$c_k = f\left(\sum_{j=1}^{m}(w_{jk}b_j) - T_{Ck}\right) \tag{3.9}$$

The next few steps of the backpropagation algorithm represent the backward error flow in which we propagate the errors between the desired output d_k (k = 1 to 3) and the actual output c_k backward through the network, and try to find the best set of network parameters (v_{ij}, w_{jk}, T_{ij}) that minimize the total mean-square errors function:

$$E = \sum_k \in_k^2 = \sum_k (d_k - c_k)^2 \tag{3.10}$$

However, more efficient training methods, such as the vanilla backpropagation algorithm, slightly modify the output-error equation, $\in_k = d_k - c_k$, by introducing the least-mean-squares (LMS) output-error equation as described in step 5.

Step 5: Propagate backward the error through the network, starting at the output and moving backward toward the input. Calculate the k^{th} component of the output error, $\in_k$, for each node in layer C, according to the equation:

$$\in_k = c_k(1-c_k)(d_k - c_k) \tag{3.11}$$

The sigmoid transfer function of the output is:

$$f(x_k) = \frac{1}{1+ e^{-x_k}} = c_k \tag{3.12}$$

Step 6: Continue backpropagation, moving to layer B. Calculate the j^{th} component of the error vector, e_j, of layer B, relative to each $\in_k$, using the equation:

$$e_j = b_j(1-b_j)\left(\sum_{k=1}^{n}(w_{jk} \in_k)\right) \tag{3.13}$$

Step 7: Adjust weight factors, calculating the new w_{jk}, i.e., $w_{jk,new,}$ for the connections between layers 2 and 3 as:

$$\begin{bmatrix}\text{new weight}\\ \text{factor}\end{bmatrix} = \begin{bmatrix}\text{old weight}\\ \text{factor}\end{bmatrix} + \begin{bmatrix}\text{learning}\\ \text{rate}\end{bmatrix} \times \begin{bmatrix}\text{input}\\ \text{term}\end{bmatrix} \times \begin{bmatrix}\text{gradient - decent}\\ \text{correction term}\end{bmatrix} \tag{3.14}$$

$$w_{jk,new} = w_{jk} + \eta_c b_j \in_k \tag{3.15}$$

Step 8: Adjust the internal thresholds T_{Ck} (k=1 to n) in layer C, according to the equation:

$$T_{ck,new} = T_{ck} + \eta_c \in_k \tag{3.16}$$

Step 9: Adjust weight factors, calculating the new v_{jk}, i.e., $v_{jk,new,}$ for the connections between layers 1 and 2 as:

$$v_{ij,new} = v_{ij} + \eta_B a_i e_j \tag{3.17}$$

Step 10: Adjust the internal thresholds T_{Bj} (k=1 to n) in layer B, according to the equation:

$$T_{Bj,new} = T_{Bj} + \eta_B e_j \tag{3.18}$$

Step 11: Repeat steps 2-10 until the squared error, E, or the output error, $\in_k$, is zero or sufficiently small.

B. Testing the Network

An important aspect of developing neural networks is determining how well the network performs once training is complete. Checking the performance of a trained network involves two main criteria: (1) how well the neural network recalls the predicted response (output vector) from data sets used to train the network (called *the recall step*); and (2) how well the network predicts responses from data sets that were not used in training (called *the generalization step*).

In the recall step, we evaluate the network's performance in recalling (retrieving) specific initial input used in training. Thus, we introduce a previously used input pattern to the trained network. The network then attempts to predict the corresponding output. If the network has been trained sufficiently, the network output will differ only slightly from the actual output data. Note that in testing the network, the weight factors are not changed: they are frozen at their last values when training ceased. Recall testing is so named because it measures how well the network can recall what it has learned.
Generalization testing is conducted in the same manner as recall testing; however, now the network is given input data with which it was not trained. Generalization testing is so named because it measures how well the network can generalize what it has learned and form rules with which to make decisions about data it has not previously seen.

In the generalization step, we feed new input patterns (whose results are known for us, but not to the network) to the trained network. The network generalizes well when it sensibly interpolates these new patterns.
The error between the actual and predicted outputs is larger for generalization testing and recall testing. In theory, these two errors converge upon the same point corresponding to the best set of weight factors for the network. When we perform both types of testing at

various points during the learning process, and plot the errors versus the number of data samples in the testing set, the result is a learning curve.

3.9 Practical Aspects of Neural Computing

There are many neural network parameters that control the network's performance and prediction capability. We must control these parameters (presented in Figure 3.14) carefully if we are to develop effective neural network models.

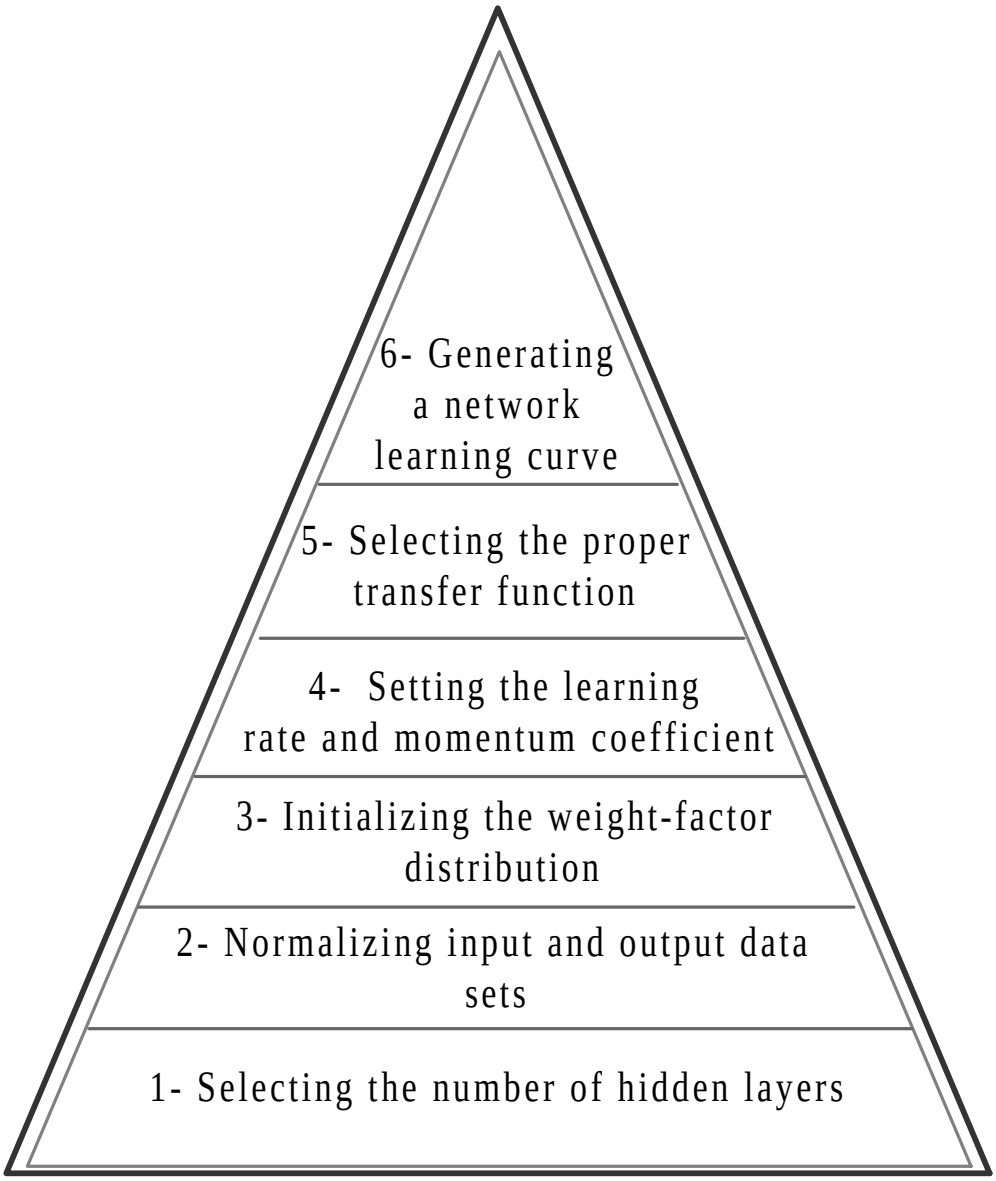

Figure 3.14: Neural network parameters that control the network's performance and prediction capability.

A. Selecting the Number of Hidden Layers

The number of input and output nodes corresponds to the number of network inputs and desired outputs, respectively. The choice of the number of hidden layers and the nodes in the hidden layer(s) depends on the network application. Determining the number of hidden layers is a critical part of designing a network and it is not straightforward as it is for input and output layers.

To determine the optimal number of hidden layers, and the optimal number of nodes in each layer, we train the network using various configurations, then select the configuration with the fewest number of layers and nodes that still yield the minimum *root-mean-squares (RMS) error* quickly and efficiently. Baugham and Liu (1995) find out that adding a second hidden layer significantly improves the network's prediction capability without having any detrimental effects on the generalization of the testing data set. However, adding a third hidden layer yields prediction capabilities similar to those of 2-hidden layer networks, but requires longer training times due to the more complex structures.

Therefore, Baugham and Liu (1995) recommend a 30:15 hidden-layer configuration as the initial architecture for most networks. The 30:15 hidden-layer configuration performs effectively for all prediction networks in this study, but it may not always be the optimal configuration.

Although using a single hidden layer is sufficient for solving many functional approximation problems, some problems may be easier to solve with a two-hidden-layer configuration.

B. Normalizing Input and Output Data Sets (Baugham and Liu, 1995).

Neural networks require that their input and output data are normalized to have the same order of magnitude. Normalization is very critical; if the input and the output variables are not of the same order of magnitude, some variables may appear to have more significance than they actually do. The training algorithm has to compensate for order-of-magnitude differences by adjusting the network weights, which is not very effective in many of the training algorithms (i.e., backpropagation algorithms). For example, if input variable 1 has a value of 10,000 and input variable 2 has a value of 10, the assigned weight for the second variable entering a node of hidden layer 1 must be much greater than that for the first in order for variable 2 to have any significance. In addition, typical transfer functions, such as a sigmoid function, or a hyperbolic tangent function, cannot distinguish between two values of x_i when both are very large, because both yield identical threshold output values of 1.0. Using the sigmoid function, when $x_i = 5$, $f(x_i) = 0.993$; when $x_i = 50$, $f(x_i) = 1.00$; and when $x_i = 500$, $f(x_i) = 1.00$.

To avoid such problems, we recommend normalizing all input and output variables. Often one can normalize input and output data in different ways for different runs. Figure 3.15 shows the three normalization methods.

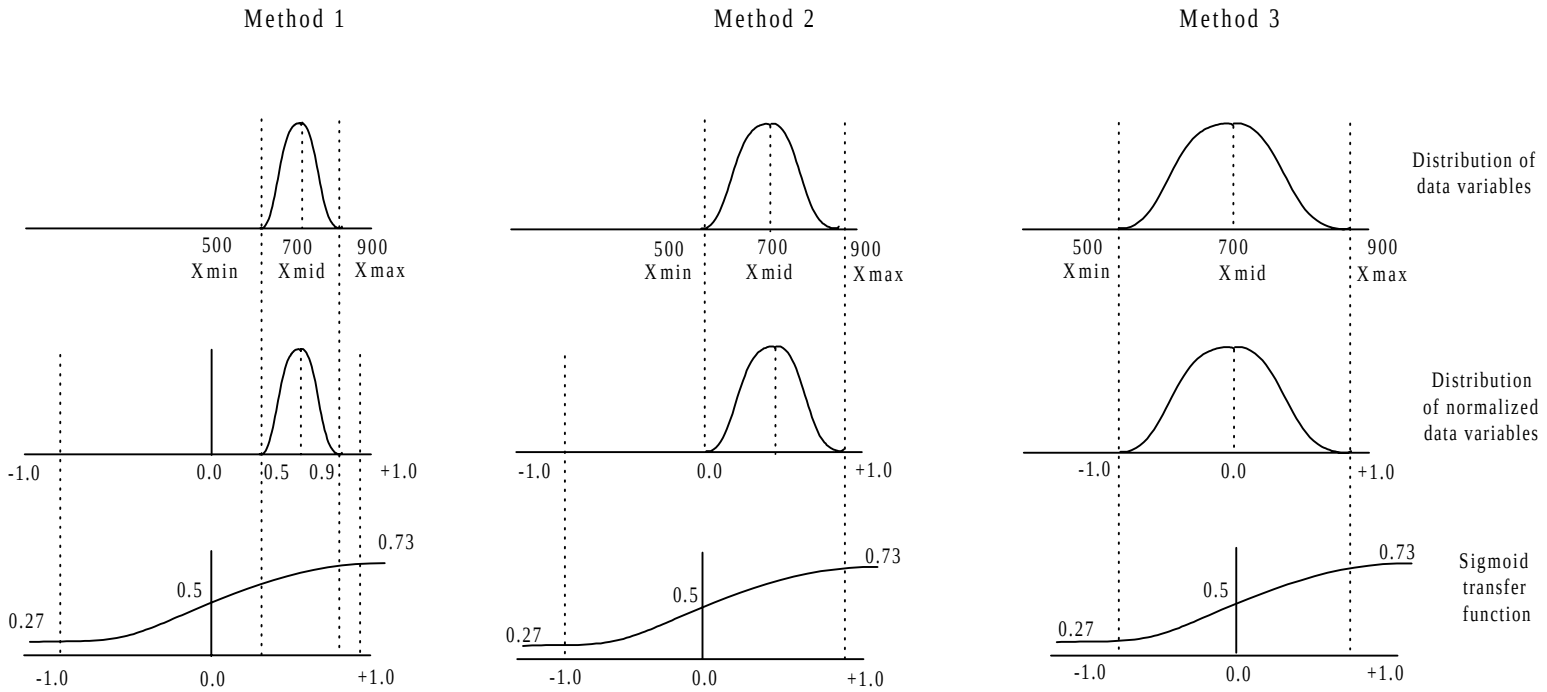

Figure 3.15: Three normalization techniques.

Method 1: Normalize each variable, x_i , in the data set to between 0 and 1. The normalized variable is calculated from:

$$x_i = \frac{x_i}{x_{i,\,max}} \tag{3.19}$$

For example, let us give variable x_i a normal distribution between 500 and 900 and assign a normalization factor of $x_{i,max} = 1000$. Using Equation 3.19, we transform the variable, x_i, to a normal distribution between 0.5 and 0.9. One limitation of this method is that it does not utilize the entire range of transfer function. Figure 3.15 shows that only a small portion of the transfer function corresponds to x_i values of 0.5 to 0.9 and -0.5 to -0.9. (Note that we include the negative range also, even though it is not represented in Figure 3.15, because the weight factors also have negative values.) The weight factors can broaden and shift this range to include a larger region of the transfer function. However, as the number of variables and weight factors increase, these adjustments become more difficult for training algorithms. As a result, this normalization method is adequate for many simple networks, but problems can arise as the network architecture becomes more complex. We have chosen to use this normalization technique for most data sets and to interpret results without more complex data transformations.

Method 2: Expand the normalization range so that the minimum value of the normalized variable, $x_{i,norm}$, is set at 0 and the maximum value, $x_{i,norm}$ is set at one. We define the normalized variable $x_{i,norm}$ by using the minimum and maximum values of the original variable, $x_{i,min}$ and $x_{i,max}$, respectively.

$$x_{i,\,norm} = \frac{x_i - x_{i,\,min}}{x_{i,\,max} - x_{i,\,min}} \tag{3.20}$$

This method significantly improves on the first method by using the entire range of the transfer function, as Figure 3.15 illustrates. Moreover, with this method, every input variable in the data set has a similar distribution range, which improves training efficiency.

Method 3: Normalize the data set between limits of -1 and +1, with the average value set to zero. We call this technique *the zero-mean normalization* and represent the normalization variable, $x_{i,norm}$ by:

$$x_{i,\,norm} = \frac{x_i - x_{i,\,avg}}{R_{i,\,max}} \tag{3.21}$$

and

$$R_{i,\,max} = \text{Maximum}[\,(x_{i,\,max} - x_{i,\,avg})\,,\,(x_{i,\,avg} - x_{i,\,min})] \tag{3.22}$$

where x_i is an input or output variable, $x_{i,avg}$ is the average value of the variable over the data set, $x_{i,min}$ is the minimum value of the variable, $x_{i,max}$ is the maximum value of the variable, and $R_{i,max}$ is the maximum range between the average value and either the minimum or the maximum value.

As in the second method, the zero-mean normalization method utilizes the entire range of the transfer function, and every input variable in the data set has a similar distribution range (Figure 3.15). This allows the weight factors to follow a more standard distribution, without requiring them to shift and broaden the input variables to match their respective output variables. This method gives some meaning to the values of the normalized variable; 0 represents the normal states (average) of the variable; -1 represents a very low level of the variable, and +1 represents a very high level of variable. In addition, by setting all of the normal states of the variables to zero, the network will have

a standard structure that makes training more efficient and consistent from one problem to the next. That is, all networks should normally predict output responses of approximately 0 (normal value) for a set of input variables at their normal values. Therefore, the network is essentially only training deviations in the output variable due to various deviations in the input variables. We use this zero-mean normalization method in the illustrative case throughout this research.

C. Initializing the Weight-Factor Distribution

Prior to training a neural network, initial values for the weight factors must be set, between the nodes of the hidden layers. Typically, the weight factors are set randomly using either a normal or Gaussian distribution. The objective is to adjust weights so that the error in the output layer is reduced. The wrong choice of initial weights can lead to a premature saturation phenomenon. The latter refers to a situation where the sum of square errors remains almost constant for some period during the learning process, and then decreases after this period is finished.

NeuralWare's NeuralWorks Professional II/Plus (1993) software package sets the initial weight-factor distribution to a fairly narrow range, and allows it to broaden using high learning rates and high momentum coefficients in the early stages of the training process. However, when using a very large data set or a complex network architecture, the weight-factor distribution must be set to coincide without normalized input and output variables. Table 3.4 illustrates Baugham and Liu's (1995) recommendation for effective initial weight-factor distributions used in training backpropagation networks based on number of input variables and total number of nodes in the hidden layer(s).

Table 3.4: A standard set of weight-factor distributions which identify the good initial Gaussian distributions for different number of nodes in the hidden layer(s) for neural networks with 1 to 3 hidden layers.

Number of input variables (nodes)	Total number of nodes in the hidden layer(s)		
	30	45	100
5	-0.70 to 0.70	-0.50 to 0.50	-0.35 to 0.35
10	-0.50 to 0.50	-0.40 to 0.40	-0.30 to 0.30
20	-0.45 to 0.45	-0.35 to 0.35	-0.30 to 0.30
30	-0.40 to 0.40	-0.30 to 0.30	-0.25 to 0.25
50	-0.30 to 0.30	-0.20 to 0.20	-0.20 to .020
100	-0.25 to 0.25	-0.20 to 0.20	-0.20 to 0.20

D. Setting the Learning Rate and Momentum Coefficient.

There are two very important parameters that are used in more complex backpropagation algorithms: *the learning rate* and *the momentum coefficient*. The use of more complex algorithm leads to significantly faster training times and also better results. Both the momentum coefficient and the learning rate are major points of interest in this study.

1. Learning Rate

The main purpose of the learning rate is to speed up the rate at which the network learns. This is also accomplished by multiplying the learning rate by the change in weight factor from the previous iteration in order to determine the new weight factors.

In general, the entire data set of inputs and outputs is divided into 4 or 5 sets. The network is then asked to train on the first set, then the first and second sets together, and

so on. This helps the network handle large amounts of information and also provides a means of generating a learning curve, which is discussed in the next section.

2. Momentum Coefficient

The momentum coefficient is a parameter of what has been termed "gradient-descent learning". In gradient-descent learning, we use the momentum coefficient to allow the network to avoid settling in local minima of the error (root-mean-squares error, RMS). Local minima in the RMS error do not represent the best set of weight factors and the global minimum does. Figure 3.16 illustrates the problems associated with network training

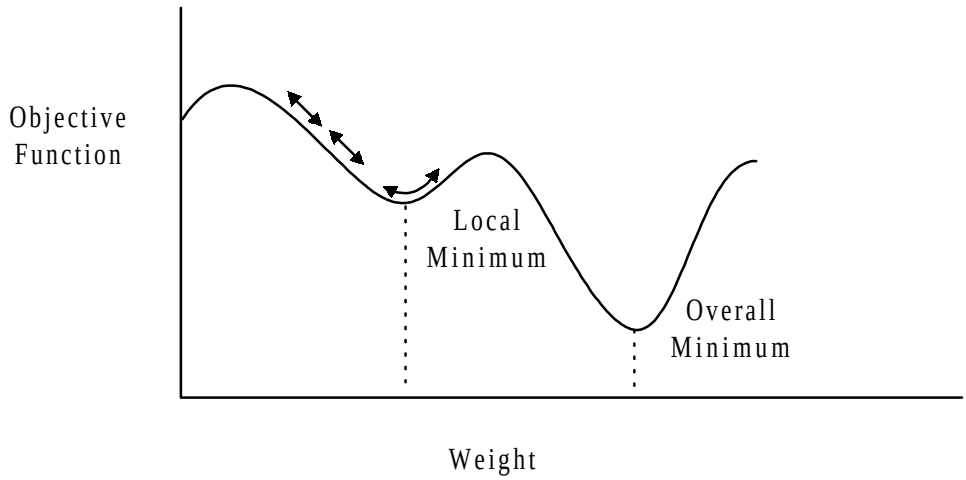

Figure 3.16: Problems associated with network training.

The momentum coefficient is used to determine new weight factors by multiplying by the change in the weight factor that was produced in the last iteration. Therefore, the change in weight factor for the current iteration is based on how fast the weight factor has been changing. When the RMS error approaches a local minimum, the momentum coefficient can then produce such a change in the weight factor that the solution is not "stuck". At the other extreme, a very high learning rate causes unstable training which results in oscillation across the overall minimum.

E. Selecting the Proper Transfer Function

We choose a transfer function based on the function of the network being used. The hyperbolic tangent and sigmoid functions are appropriate for most types of networks, especially prediction problems. The Gaussian function is only recommended for classification networks.

We prefer the hyperbolic tangent function over the sigmoid function for the following reasons:

1. The output varying from -1 to +1 for the hyperbolic tangent and only 0 to 1 for the sigmoid function. This means that the hyperbolic tangent function has a negative response for a negative input value and a positive response for a positive input value, while the sigmoid function always has a positive response.
2. The slope of the hyperbolic tangent is much greater than the slope of the sigmoid function. Which means the hyperbolic tangent function is more sensitive to small changes in input.

Baugham and Liu (1995) give further demonstration of the advantages of the hyperbolic tangent transfer function for prediction networks.

F. Generating a Network Learning Curve

To visualize how well a network performs recall and generalization, we often generate *a learning curve*, which represents the average error for both the recall of training data sets and the generalization of the testing sets as a function of the number of examples in the training data set (see Figure 3.17).

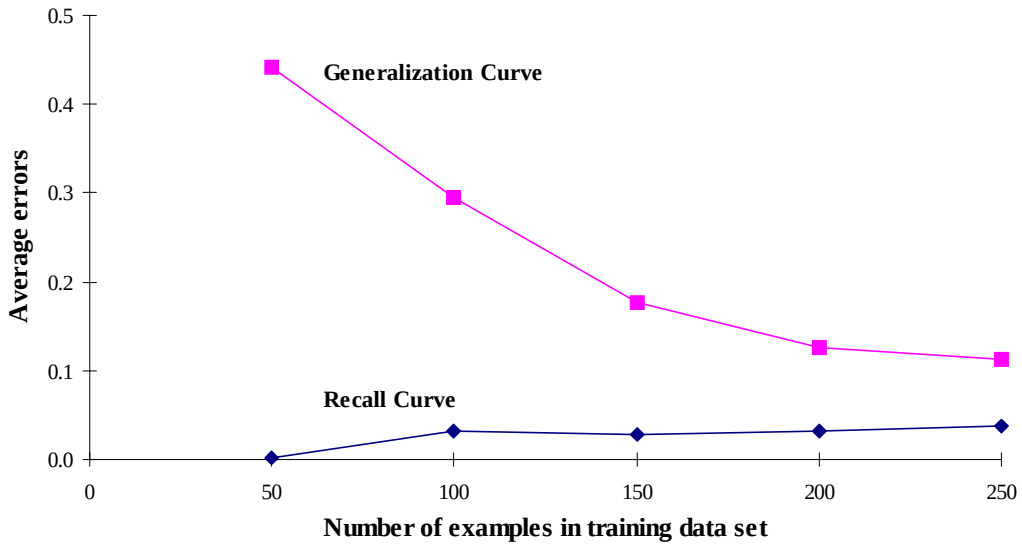

Figure 3.17: A sample learning curve.

The two main uses of a learning curve are (Baughman, and Liu, 1995):

- to find the number of training examples required to achieve a fixed average error
- to estimate the minimum average error attainable through adding data sets

Figure 3.17 shows low average error for recall with small training data sets; recall error increases slightly as more examples are included. In contrast, the generalization is very poor (high average error) for small training data sets and the error decreases as more examples are included. For a well-trained network, as it receives more information, the recall and generalization curves approach each other. Once the network has been tested as described, and it has reached appropriately low error, it is ready for use.

A well-trained network should be able to produce an output that deviates very little from the desired value.

3.10 Summary

- The inspiration of neural networks came from studies on the structure and function of the brain and nerve systems as well as the mechanism of learning and responding.
- The basic component of a neural network is the neuron, also called "*node*", or the "*processing element, PE*", which contains the mathematical processing element that governs the operation of a neural network.
- The number of *input neurons* corresponds to the number of input variables into the neural network, and the number of *output neurons* is the same as the number of desired output variables. The number of neurons in the *hidden layer(s)* depends on the application of the network.
- Every input entering a node is multiplied by its *weight factor*, w_{ij}, which are adjusted in the network training algorithm, store the pattern behavior of the system.
- The node's *internal threshold*, T_j, is a randomly chosen value that governs the "activation" or total input of the node.
- The input of a node goes through *a transfer function*, the most common being the sigmoid, hyperbolic tangent, and Gaussian functions.

- There are two different classification levels of neural networks structures: (1) *external structure*, which describes the overall, or macro, arrangement of and connections between inputs, outputs, and hidden layers that compose the network; and (2) *internal structure*, which refers to the actual connections between individual nodes both within and between layers.
- Two subsets of data are used to build a model: (1) *training set*; and (2) *testing set*. The training phase needs to produce a neural network that is both stable and convergent.
- Training is the process by which the neural network systematically adjusts the weights of interconnections between nodes so that the network can predict the correct outputs for a given set of inputs.
- There are a number of approaches to training neural networks: (1) *Supervised Learning*, which has an external teacher to control the learning and incorporates global information, and (2) *Unsupervised Learning*, which has no external teacher; instead the system organizes itself by internal criteria and local information designed into the network.
- There are many different types of training algorithms. One of the most common classes of training algorithms for feedforward interlayer networks is called *backpropagation.* In a backpropagation algorithm, a set of inputs is fed to the network and outputs are returned. Backpropagation learning attempts to map given inputs with desired outputs by minimizing the sum-of-square errors.
- A learning curve provides a good method to visualize how well a network performs. The learning curve (Figure 3.17) represents the average error for both the recall of training data sets and the generalization of the testing sets as a function of the number of examples in the training data set.

3.11Nomenclature

a	: input vector entering a node.
a_i	: the i^{th} component of an input vector entering a node.
b	: output vector.
b_j	: calculated output for the j^{th} node.
c_k	: calculated output from the k^{th} node
d_k	: desired output for the k^{th} node.
e_j	: output error of j^{th} node of layer B relative to each $\in$k in the three-layer network.
E	: total squared error on the output layer.
f( )	: transfer function.
I	: input vector entering a neural network.
I_i	: the i^{th} component of the input vector entering a neural network.
L	: number of nodes in layer A of three-layer network.
m	: number of nodes in layer B of three-layer network.
n	: number of nodes in layer C of three-layer network.
$R_{i,max}$	: maximum range between the average value $x_{i,avg}$ and either the minimum value $x_{i,min}$ or maximum value $x_{i,max}$.
T_j	: internal threshold for j^{th} node.
T_{Ai}	: internal threshold for i^{th} node (layer A) of three-layer network.
T_{Bj}	: internal threshold for j^{th} node (layer B) of three-layer network.
T_{Ck}	: internal threshold for k^{th} node (layer C) of three-layer network.

t : time

w_j : weight-factor vector for the j^{th} nodes

w_{ij} : weight-factor vector for between i^{th} and j^{th} nodes.

$w_{ij,new}$: newly adjusted weight factor between the i^{th} and j^{th} nodes during network training.

W_{jk} : weight-factor vector for between j^{th} (layer B) and k^{th} (layer C) nodes in the three-layer network.

$w_{jk,new}$: newly adjusted weight factor between the j^{th} (layer B) and k^{th} (layer C) nodes in the three-layer network.

v_{ij} : weight factor between i^{th} (layer A) and j^{th} (layer B) nodes in the three-layer network.

$v_{ij,new}$: newly adjusted weight factor between i^{th} (layer A) and j^{th} (layer B) nodes in the three-layer network.

x_i : an input or output variable in a training or testing network

$x_{i,avg}$: average value of x_i.

$x_{i,min}$: minimum value of x_i.

$x_{i,max}$: maximum value of x_i.

$x_{i,norm}$: normalized value of x_i.

α : momentum coefficient.

$\in_k$: output error of the k^{th} node.

η_j : learning rate.

3.12 References

Baughman, D.R. and Y.A. Liu, *Neural Network in Bioprocessing and Chemical Engineering*, Academic Press, San Diego, CA (1995).

Chester, M., *Neural Networks A Tutorial*, PTR Prentice Hall, Englewood Cliffs, New Jersey (1993).

Eberhart, R.C. and R.W., Dobbins, *Neural Network PC Tools A Practical Guide*, Academic Press, San Diego, CA (1990).

Freeman, J.A. and D.M., Skapura, *Neural Networks Algorithms, Applications, and Programming Techniques*, Addison-Wesley, Reading, Massachusetts (1992).

Haykin, S., *Neural Networks: A Comprehensive Foundation*, Macmillan College Co., New York, N. Y. (1994).

Mehra, P. and B.W. Wah, *Artificial Neural Networks: Concepts and Theories*, IEEE Press, Los Alamitos, CA (1992).

Nelson, M. M. and W. T. Illingworth, *A Practical Guide to Neural Nets*, Addison-Wesley, Reading, Massachusetts (1991).

NeuralWare, Inc., *Neural Computing: A Technical Handbook for Professional II/Plus and NeuralWorks Explorer*, Pittsburgh, PA (1993).

Simpson, P., *Artificial Neural Systems: Foundations, Paradigms, Applications, and Implementations*, Pergamon Press, New York, N. Y. (1990).

VerDuin, W., *Better Products Faster: A Practical Guide to Knowledge-Based Systems for Manufacturers*, Irwin, New York, N. Y. (1995).

Wasserman, P., *Neural Computing Theory and Practice*, Van Nostrand Reinhold, New York, N. Y. (1989).

CHAPTER 4

NEURAL NETWORKS FOR PREDICTIVE MODELING OF LARGE-SCALE COMMERCIAL WATER DESALINATION PLANTS

This chapter describes how to apply neural networks specifically to prediction problems of large-scale commercial multistage flash (MSF) and reverse osmosis (RO) desalination plants. We first introduce the desalination plants under study. We next demonstrate the use of neural-network predictors in conjunction with statistical techniques to identify the major independent variables to optimize the process performance. This study also compares the neural network model and the statistical model in predicting the performance variables of desalination plants.

4.1 Introduction

Artificial intelligence techniques (i.e., expert systems, neural networks, and fuzzy-logic systems) could be introduced into desalination processes such as multistage flash Distillation (MSF) and reverse osmosis (RO) in many ways. They could be involved in the design, operation, control, and performance optimization of desalination plants. The purpose is achieving better design, improving efficiency, and increasing operational safety (El-Hawary, 1993).

This work develops neural networks for predictive modeling of large-scale commercial water desalination plants. In developing a neural-network model, it is essential to determine what the neural network is expected to do. In order to develop an efficient neural-network model that maximizes the prediction performance, we need to do some extensive data analysis and preparation prior to training the neural network. For example,

analyzing the problem with an existing technique, such as statistical regression, can often aid in identifying the problem.

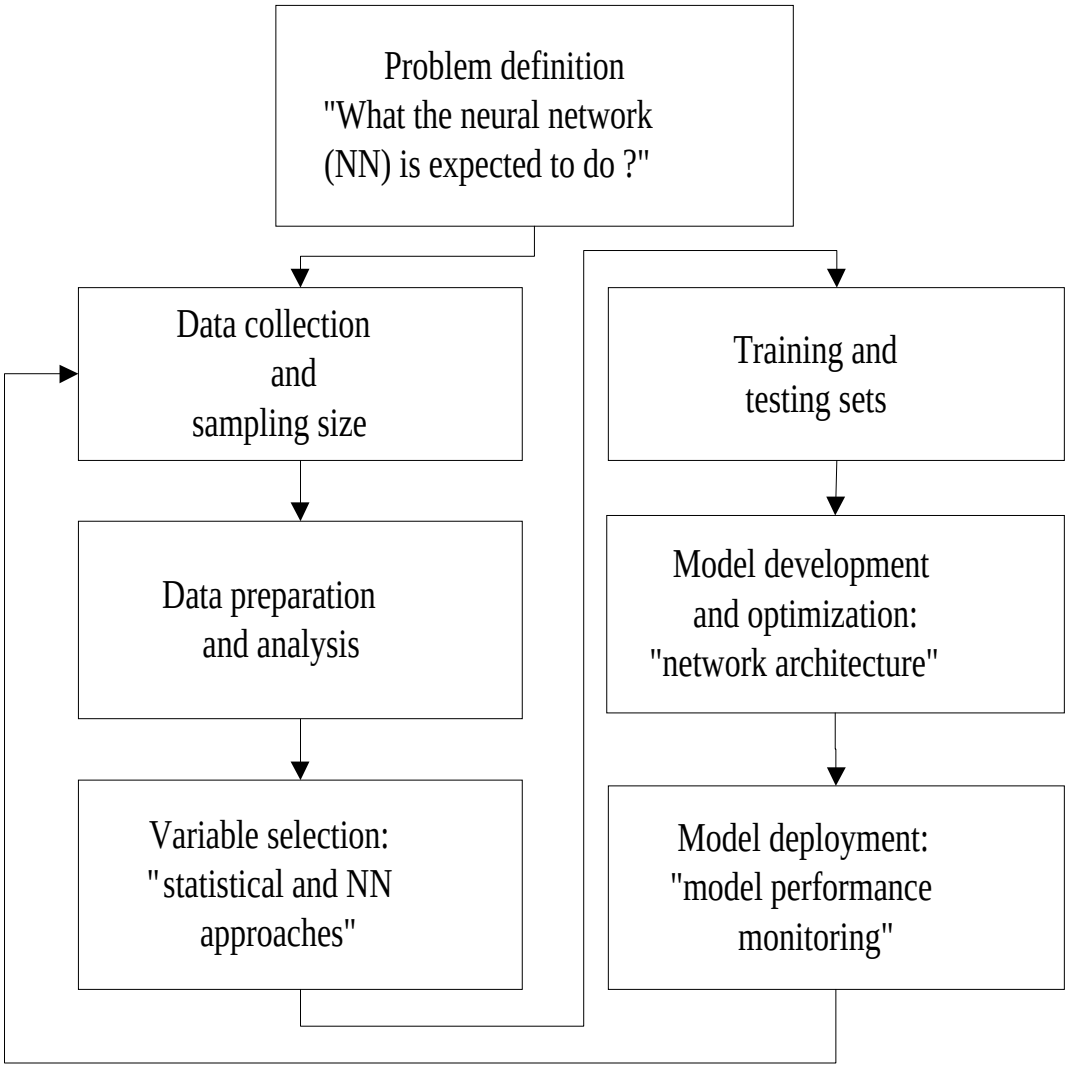

Figure 4.1: Methodology of neural network development.

Figure 4.1 illustrates the methodology used for developing a neural network model, based on the backpropagation algorithm (Baughman and Liu, 1995, pp. 32-66), for the prediction and optimization of process performance variables of large-scale desalination plants. In contrast to several recent studies (Abdulbary, 1995; Parenti, et al., 1995; Selvaraj and Deshpande, 1995), this work utilizes *actual operating data (not simulated data)* from a Multistage Flash (MSF) Distillation Plant (48 million gallons per day, MGPD, or 181,760 m^3/day) and a Reverse Osmosis (RO) Plant (15 MGPD, or 56,800 m^3/day), located in the State of Kuwait, and the Kingdom of Saudi Arabia, respectively. The application of neural computing to MSF and RO plants is necessary due to the computational complexity, nonlinear behavior, high degrees of freedom, and the presence of uncertainty in the control environment of desalination plants.

Quantitative optimization of operating variables could lead to an increase in production rates, higher product quality, and better plant performance with less energy consumption and lower operating costs. This optimization can also give the operator an early warning of any decline in unit performance.

This study demonstrates the use of neural-network predictors in conjunction with statistical techniques to determine the optimal operating conditions of commercial desalination processes. This study also compares the neural network model and the statistical model in predicting the performance variables of desalination plants.
To accomplish this work, we use NeuralWare Professional II/Plus (Neural Works, 1993) and SAS (SAS Institute Inc., 1996) software. Professional II/Plus is a package that integrates all the components needed to apply neural computing to a wide variety of problems. The SAS software is a complete data access, management, analysis and presentation system. SAS allows the easy storage and efficient retrieval of vast amounts of data from widely varying sources. It can then be used to collect and manipulate large

amounts of data, allowing data to be accessed in usable form. SAS can perform many statistical analyses on data and create time-based comparisons, trend analyses, and forecasts. SAS can also be used as an organized resource for decision support and data presentation. In this study, we use SAS primarily for its statistical analysis capabilities.

To our knowledge, this work represents by far the most comprehensive development and application of neural networks for large-scale commercial desalination process plants among all available reports in the literature.

4.2 Multistage Flash (MSF) Distillation Plant

A. AZ-ZOUR SOUTH Power Generation and Water Product Station

Table 4.1 shows the design information of the distillation unit used in this study. The unit, commissioned in late 1988, is located at AZ-ZOUR, approximately 100 km south of Kuwait City. The plant uses a cross-tube-type multistage flash (MSF) evaporator with recirculating brine. The multistage condensers for the evaporator have two sections: the heat-recovery section (21 stages) and the heat-rejection section (3 stages). The stage I distillation plant consists of eight multistage flash-type desalting units and their common facilities. Each of the eight units has a daily output of 6.0 MGPD distillate, for a total output of 48.0 MGPD. Each unit is also designed to produce 7.2 MGPD distillate during higher-temperature operation (e.g., 108-110 °C), for a total output of 57.6 MGPD. Anti-scaling chemical treatment is used to prevent scale formation inside the condenser tubes. Figure 4.2 shows the plant flow diagram. Table 4.2 summarizes the operational variables and their design values of the distillation units.

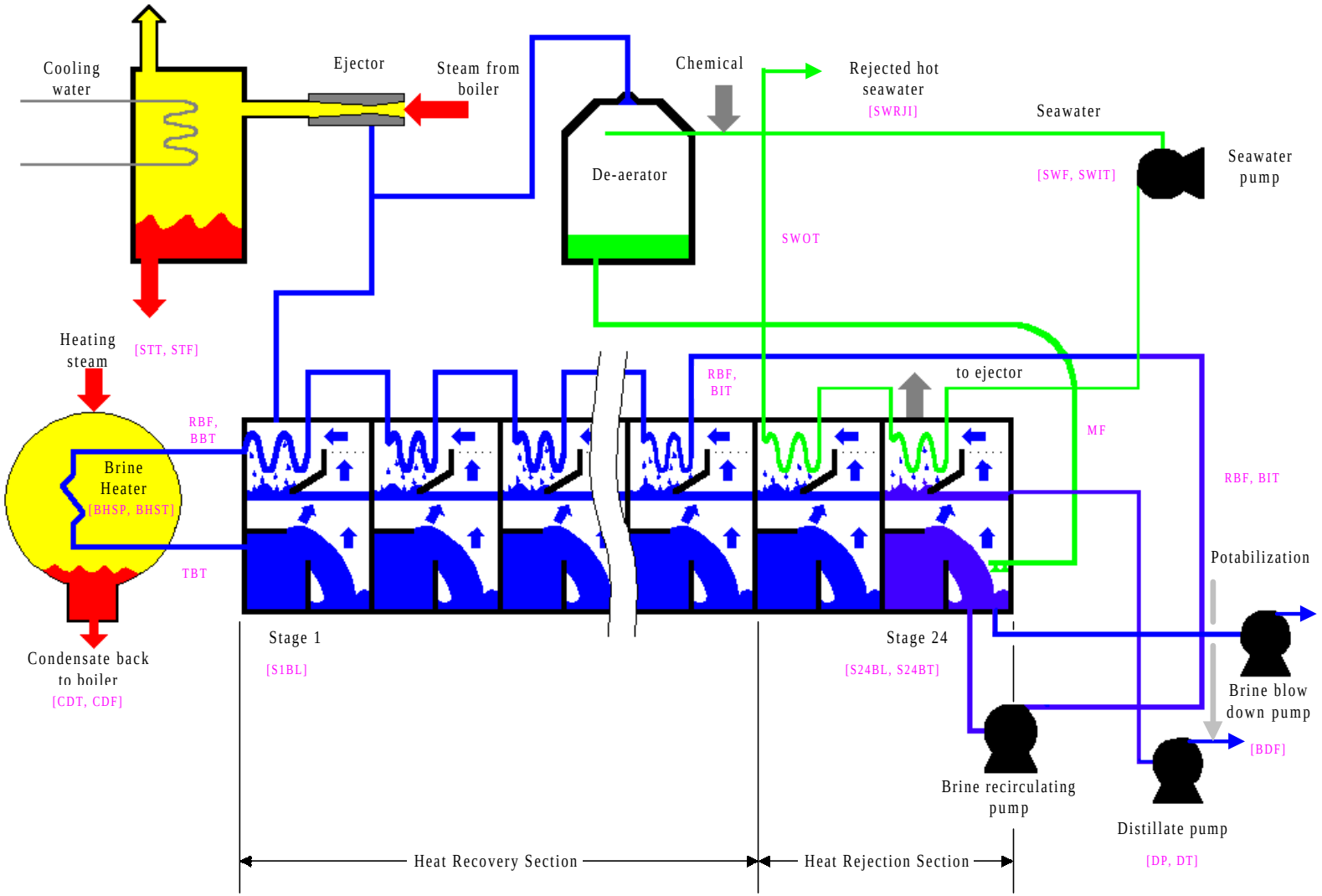

Figure 4.2: Schematic diagram of a multistage flash (MSF) desalination plant

Table 4.1: Design information for AZ-ZOUR SOUTH distillation unit.

Unit	AZ-OUR SOUTH Distillation Units
Manufacturer	Sasakura Engineering Co. Ltd., Mitsubishi Heavy Industries and Mitsui and Company, Ltd.
Year of commissioning	1988
Type	cross-tube recirculating multistage flash (MSF)
Number of distillation units	8
Heat-input section (brine heater)	
Number of passes	1
Number of tubes	1367
Tube size	43.8 mm (O.D.) x 1.219 mm (avg. thickness) x 18,991 mm (length)
Heat-transfer area	3,544 m^2
Tube material	Copper-nickel alloy 66% Cu, 30% Ni, 2% Mn, 2% Fe
Heat-recovery section (H.R.S.)	
Number of passes	23
Number of tubes	1,451
Tube size	43.8 mm (O.D.) x SWG. 18 (avg.)
Heat-transfer area	77,206 m^2
Tube material:	
Stages 1 and 2	Copper-nickel alloy 66% Cu, 30% Ni, 2% Mn, 2% Fe
Stages 3-21	Aluminum alloy 76% Cu, 22% Zn, 2% Al
Heat-rejection section (H.J.S.)	
Number of passes	3
Number of tubes	1,588
Tube size	34.2 mm (O.D.) x SWG. 18 (avg.)
Heat-transfer area	9,444 m^2
Tube material	Copper-nickel alloy 66% Cu, 30% Ni, 2% Mn, 2% Fe

Table 4.2: Operating variables of AZ-ZOUR SOUTH distillation units during winter months.

Variable	Symbol	Unit	Winter design value
Seawater flowrate	SWF	T/hr	8497
Makeup feed flowrate	MF	T/hr	2898.4
Seawater recirculating flowrate	SWRF	T/hr	4945
Recirculating brine flowrate	RBF	T/hr	13386
Blowdown flowrate	BDF	T/hr	1770.7
Low-pressure steam flowrate	STF	T/hr	140.96
Condensate flowrate	CDF	T/hr	140.96
Distillate produced	DP	T/hr	1127.7
Seawater-inlet temperature	SWIT	°C	26.96
Seawater-outlet temperature	SWOT	°C	35.91
Brine inlet temperature	BIT	°C	36.54
Stage 24 brine temperature	S24BT	°C	36.85
Brine-heater inlet temperature	BBT	°C	84.51
Top brine temperature	TBT	°C	90.56
Steam temperature	STT	°C	100
Condensate temperature	CDT	°C	100
Brine-heater shell temperature	BHST	°C	100
Brine-heater shell pressure	BHSP	bar	1.033
First stage brine level	S1BL	m	0.5

B. Data Collection and Sampling Size

1. Plant Preparation

In order to ensure the relevance of data collected from the operational trial of the unit, it is imperative to carry out the modeling study on a high-performance distillation unit that is free of scale deposition and equipped with accurate instrumentation.

Based on the requirements, we utilize the D-8 distillation units (6.0-7.2 MGPD capacity)

at AZ-ZOUR SOUTH Power Generation and Water Production Station in the State of Kuwait for this study.

Two inspections (before and after the overall annual maintenance) are carried out on the D-8 Evaporator. The final inspection report after the maintenance reveals that the unit is in very good condition. Therefore, we select distillation unit D-8 for the study.

2. Instrumentation Selection and Calibration

There are two categories of unit instrumentation. The first consists of all instrumentation located in the distillation control room (DCR). The second category consists of instrumentation sited locally throughout the unit. Data from local instrument are used to double-check data levels. For consistency, we rely only upon the data generated by the DCR instrumentation.

In order to be able to collect accurate process data to determine process variables, as much unit instrumentation as possible is used. We verify the proper calibration of all instrumentation before attempting to collect data.

3. Sampling Size

To permit accurate monitoring of the operation of the distillation unit, we collect data of varied natures and log them properly. In any experiment, as the number of observations increases, the resulting statistical correlations become increasingly reliable. Therefore, the investigator should use a large sample size wherever possible. In this study, we utilize the operational variables from the MSF desalination plant measured every two hours for a month during winter and summer operations (300 data sets for each period).

Flowrates:

The following flowrate measurements are available to the plant:

- Seawater flow to the vent condenser
- Seawater flow to the heat-rejection section (SWF)
- Seawater recirculating flow (SWRF)
- Makeup feed flow (MF)
- Recirculating brine flow (RBF)
- Blowdown brine flow (BDF)
- Distillate flow (DP)
- Condensate flow (CDF)
- Low-pressure steam flow (STF) (desuperheater inlet, atomizing steam and ejector steam).

Flowrates of both the anti-scalant and the anti-foam chemicals are also available.

Temperatures:

The major temperature readings include the following :

- Brine-heater inlet brine (BBT)
- Brine-heater outlet brine (TBT)
- Brine-heater shell side (BHST)
- Brine-heater steam condensate (CDT)
- Low-pressure steam to desuperheater
- Low-pressure steam to brine-heater (STT)
- Ejector steam
- Vent-condenser outlet seawater
- Vent-condenser outlet distillate
- Heat-rejection inlet cooling seawater
- Heat-rejection outlet cooling seawater (makeup)

- Stage 1 vapor
- Stage 21 vapor
- Stage 22 vapor
- Stage 24 vapor
- Stage 1 flashing brine
- Stage 21 flashing brine
- Stage 22 flashing brine
- Stage 24 flashing brine (Blowdown)
- Distillate (DT)

Pressures:

A number of pressure readings are available.

- Stage nos. 1 and 24
- Brine-heater vapor space
- Brine-heater steam supply (after the desuperheater)
- Brine-heater steam supply (prior to the desuperheater)
- Turbine extraction steam
- Steam supply to both the desuperheater and the ejector
- Brine-heater shell
- Brine-heater inlet brine
- Brine-heater outlet brine

Levels:

The levels of the flashing brine in the flashing chambers of stages 1 and 24 are monitored daily, as displayed in the control room and as measured locally. These levels are indicative of the flashing behavior throughout the flashing chambers. Furthermore, the level drops of both the anti-scaling additive and antifoaming agent in their respective storage tanks are continuously recorded. The distillate level in the last stage is also recorded.

Table 4.3 summarizes 19 operating variables monitored in the distillation control room (DCR) that most affect the plant performance. These variables are also indicated in Figure 4.1. The main performance variables for the plant include: top brine temperature (TBT), distillate produced (DP), and steam flowrate (STF). The control of these performance variables is the main objective of plant optimization. Section 2.4 in Chapter 2 discusses the significance of these performance variables.

Table 4.3: Operational variables affecting the MSF distillation plant performance (see also Figure 4.1).

Name	Nomenclature
Seawater flowrate	SWF
Makeup flowrate	MF
Seawater recirculating flowrate	SWRF
Recirculating brine flowrate	RBF
Blowdown flowrate	BDF
Low-pressure steam flowrate	STF
Condensate flowrate	CDF
Distillate produced	DP
Seawater-inlet temperature	SWIT
Seawater-outlet temperature	SWOT
Brine-inlet temperature	BIT
Stage 24 brine temperature	S24BT
Brine-heater inlet temperature	BBT
Top brine temperature	TBT
Steam temperature	STT
Condensate temperature	CDT
Brine-heater shell temperature	BHST
Brine-heater shell pressure	BHSP
Stage 1 brine level	S1BL

C. Data Preparation and Analysis

Real-life data obtained from the plant must be filtered to remove unmeasured noise, outliers, and fault-contaminated measurements. We describe the strategy of data analysis to find the simplest model adequate for data description and inference.

Real-life data often contain outliers, which are observations that do not reasonably fit within the pattern of the bulk of the data points and are not typical of the rest of data. Some outliers are the result of incorrect measurements and can be immediately rejected and removed from the data set. Other outliers are observations resulting from unusual process phenomena that are of vital interest. Data require careful inspection and examination in order to observe this distinction.

Outliers are given particular attention in a neural network and in a statistical analysis in order to determine the reasons behind large discrepancies between those points and the remainder of the data set. The inclusion of outliers in training data forces the network to consider a larger solution space, and can therefore reduce the overall precision of the resulting network. This is observed as occasional large differences between actual and predicted values of output variables. Figure 4.3 gives an example of the potential influence of outliers on the network performance for predicting the top brine temperature (TBT). The root-mean-squares (RMS) error decreases from 0.114835 to 0.054592 in the TBT network after removing the outliers. Removing outliers generally improves network performance.

One of the simplest techniques for detecting outliers is to examine the frequency histogram of the data, plotting the number of occurrence of the observed data within a specific range of a selected operating variable. Figure 4.4 illustrates the frequency distribution of the brine-heater shell temperature (BHST). Point (a) is out of the normal operating range, and by checking the other operational variables, we find that point (a) results from incorrect measurement. Figure 4.5 shows the frequency distribution of the 19 operational variables after removing the outliers. The frequency distribution becomes to be continuous and normally distributed with a bell shape, with the exception of a few outliers that are observations of unusual phenomena.

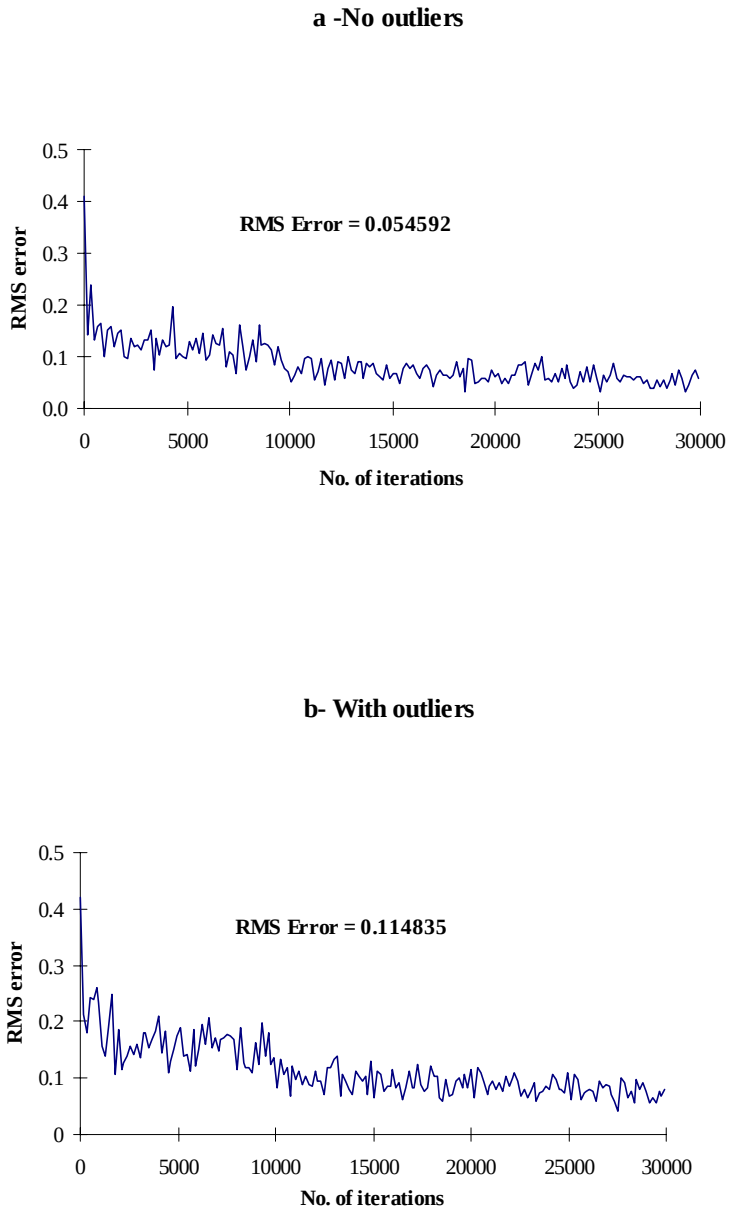

Figure 4.3: RMS error of the top-brine-temperature network: (a) no outliers; and (b) with outliers

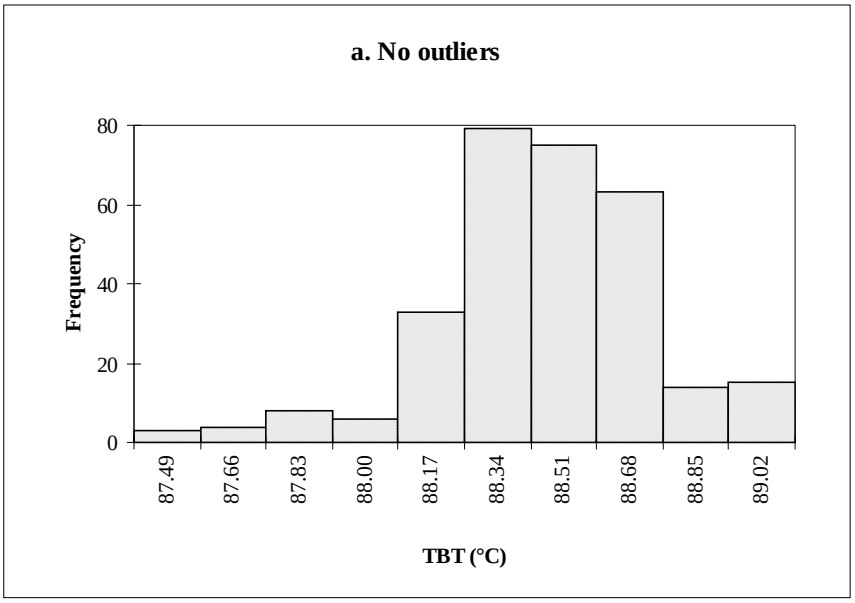

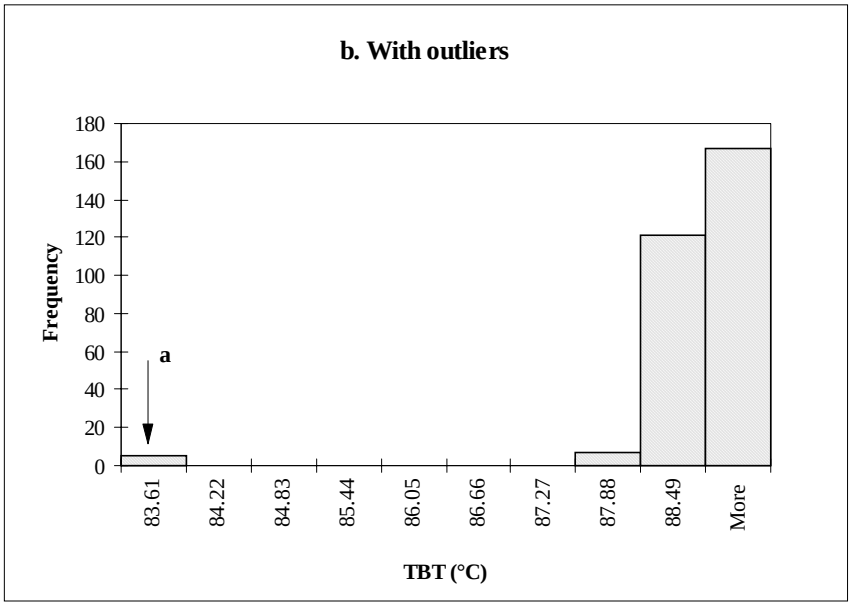

Figure 4.4: Frequency histogram of the top brine temperature (TBT): (a) no outliers; and (b) with outliers (indicated by “a”)

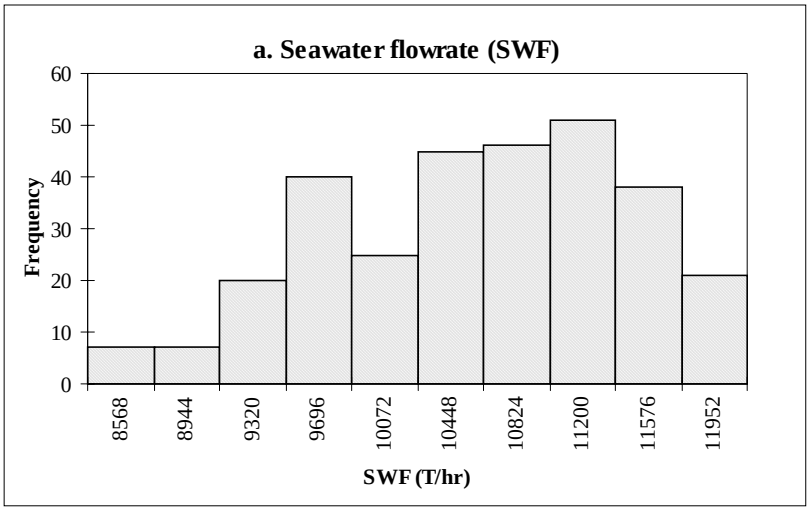

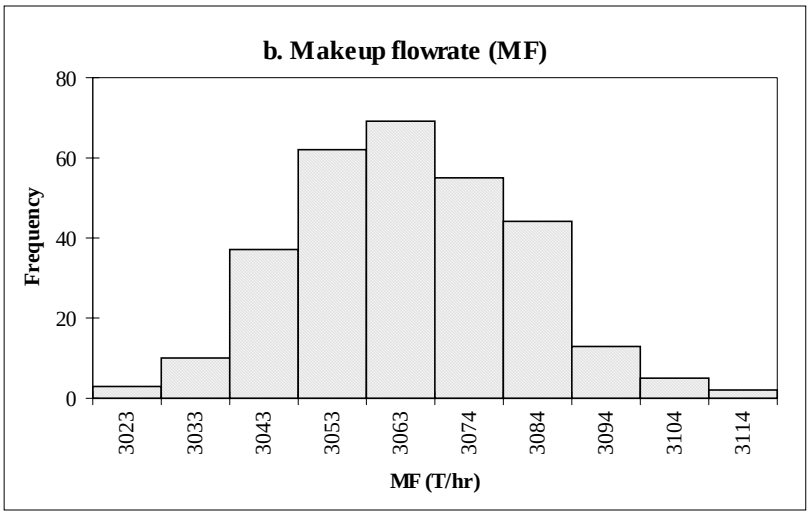

Figure 4.5: Frequency histograms of data from the MSF Plant.

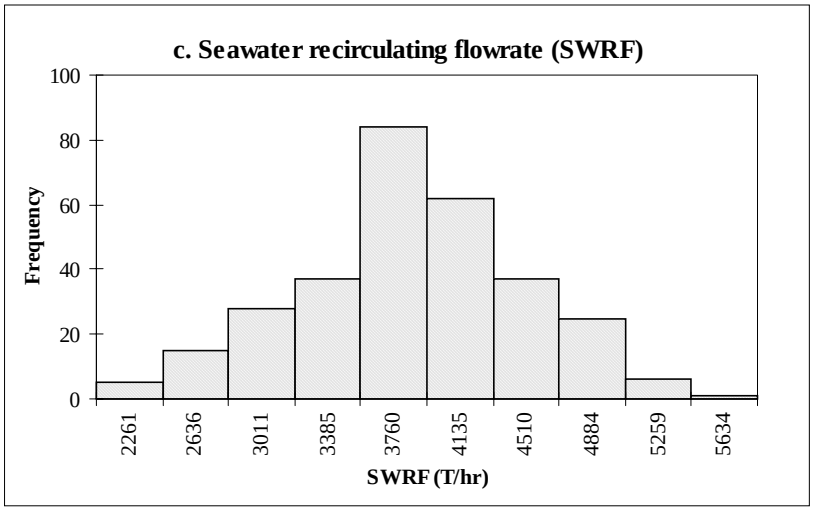

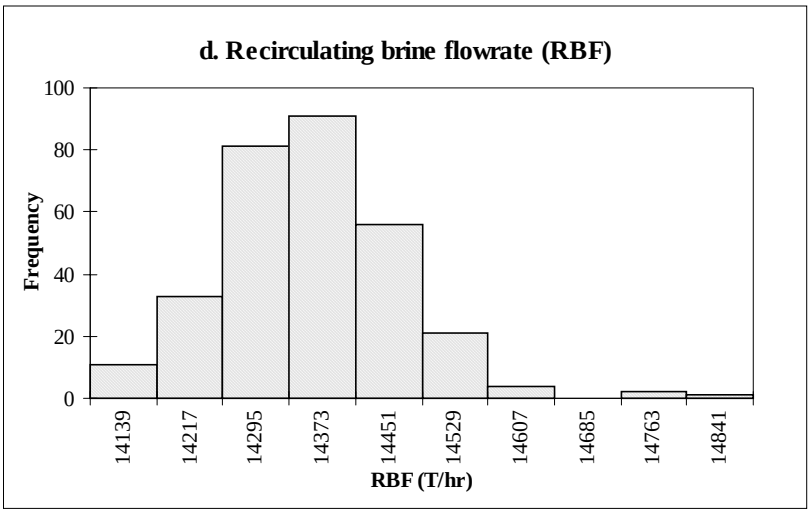

Figure 4.5: Frequency histograms of data from the MSF Plant (continued).

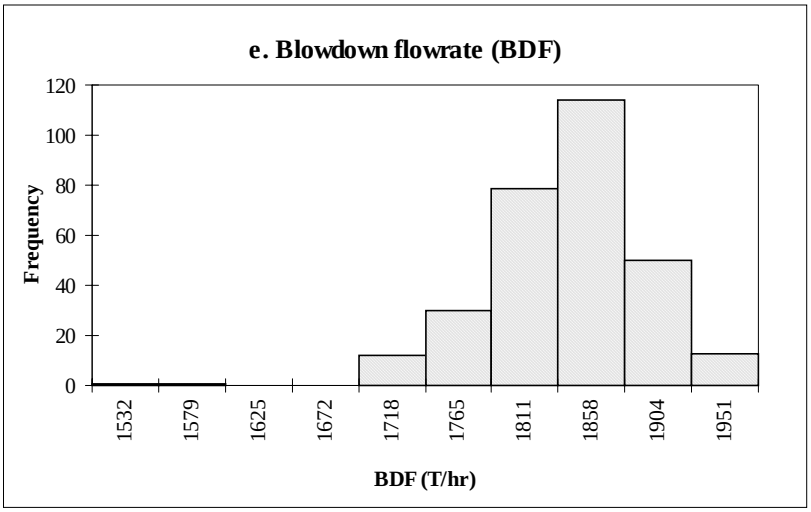

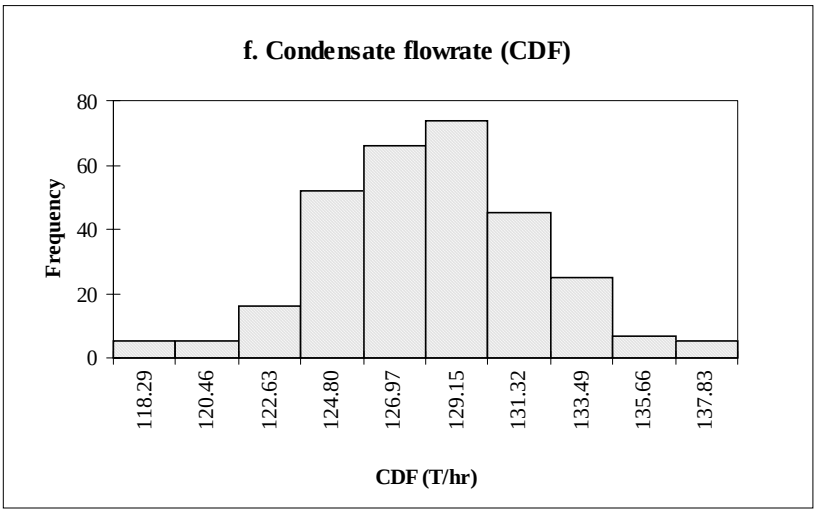

Figure 4.5: Frequency histograms of data from the MSF Plant (continued).

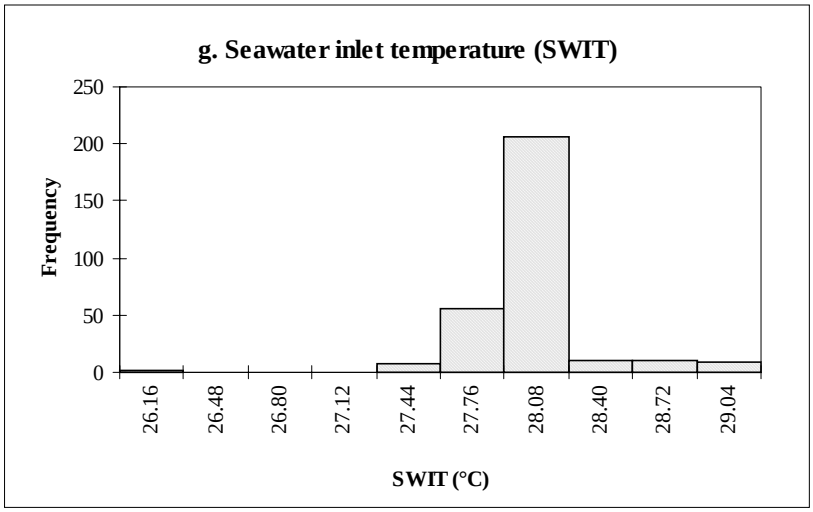

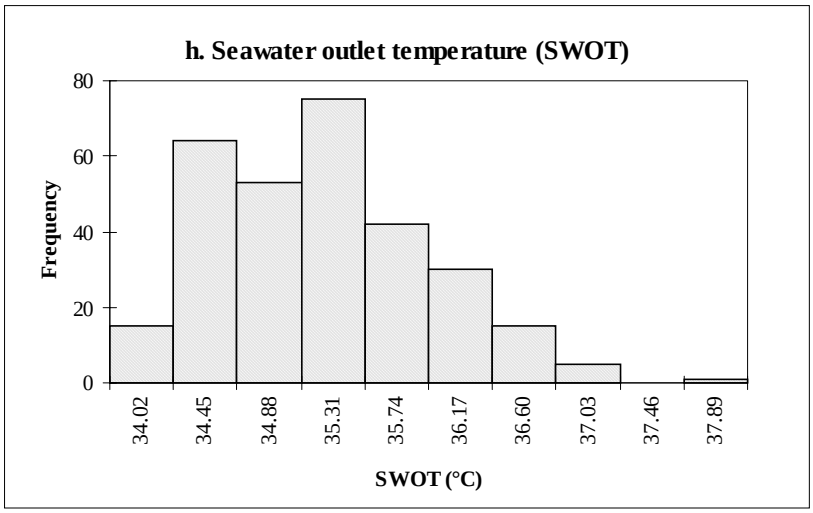

Figure 4.5: Frequency histograms of data from the MSF Plant (continued).

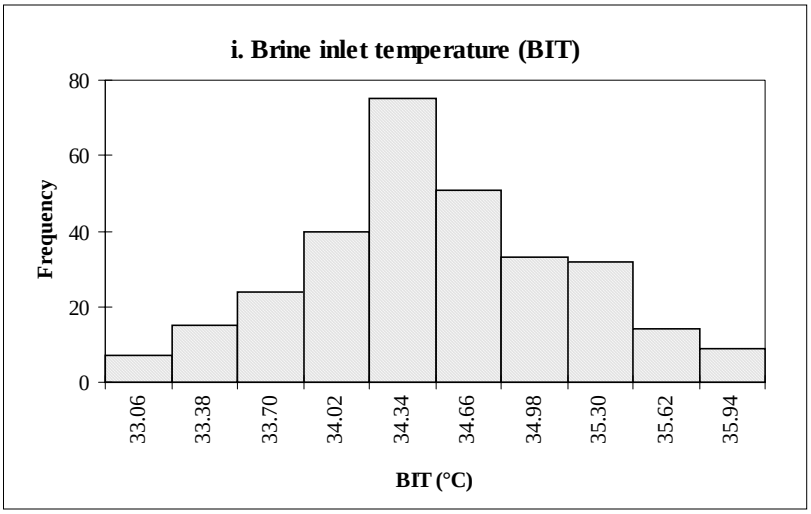

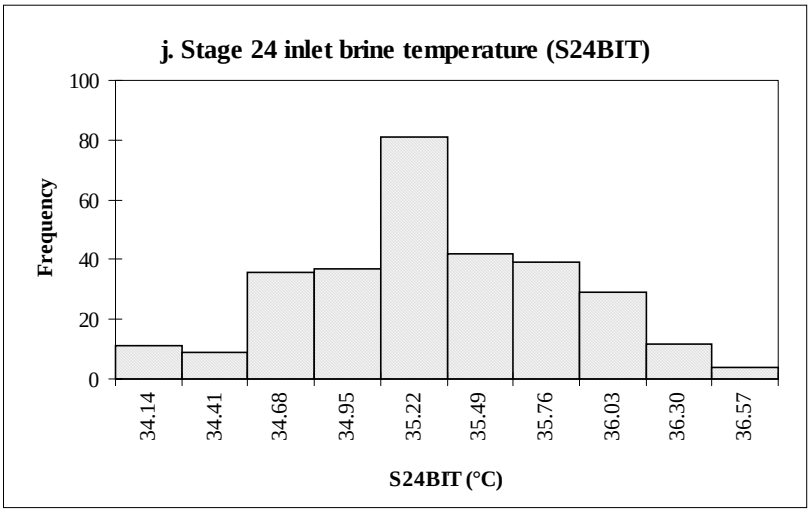

Figure 4.5: Frequency histograms of data from the MSF Plant (continued).

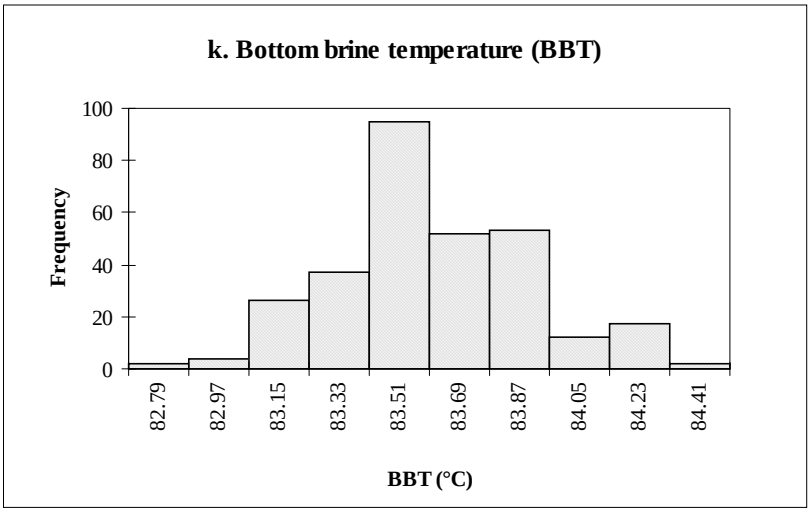

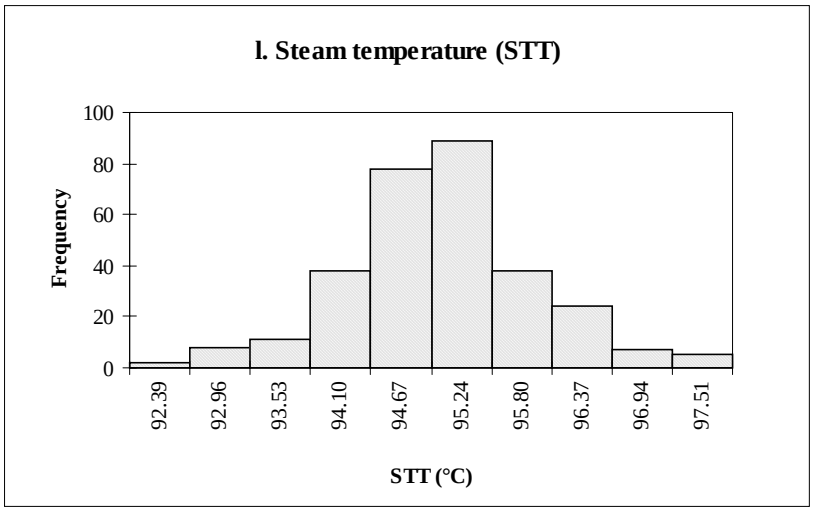

Figure 4.5: Frequency histograms of data from the MSF Plant (continued).

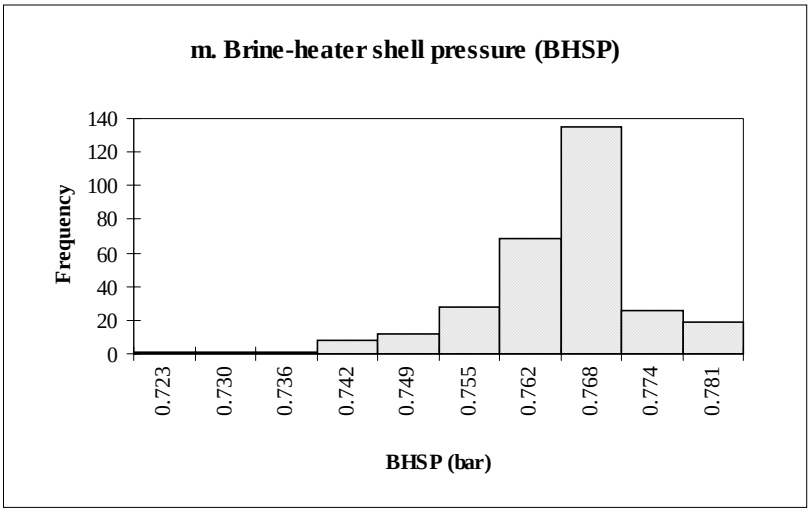

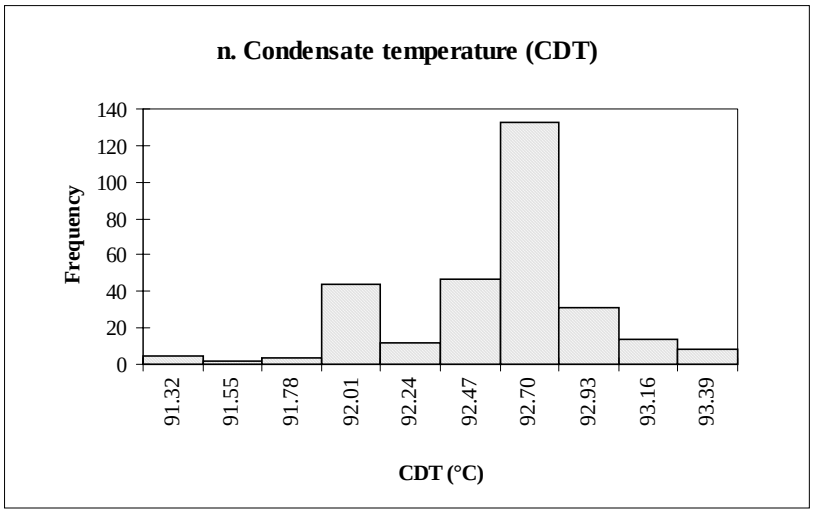

Figure 4.5: Frequency histograms of data from the MSF Plant (continued).

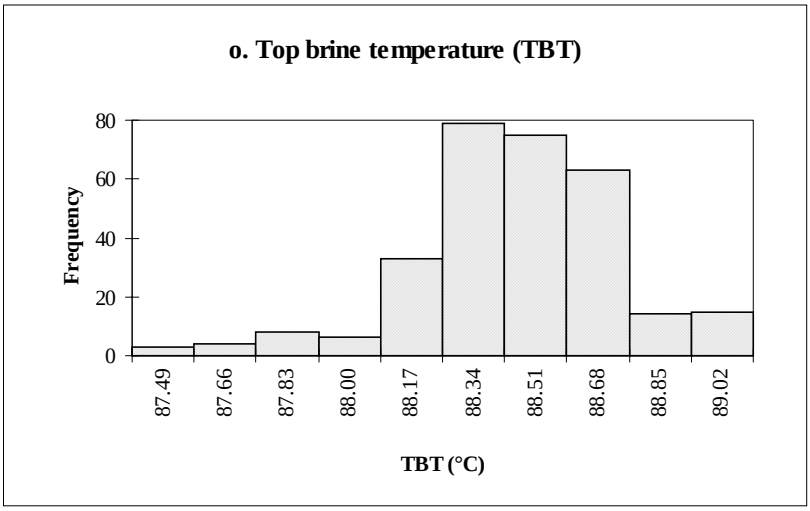

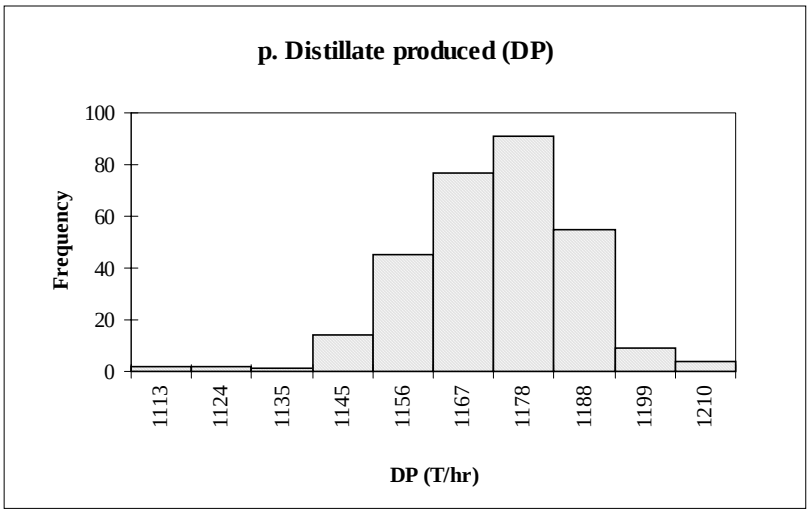

Figure 4.5: Frequency histograms of data from the MSF Plant (continued).

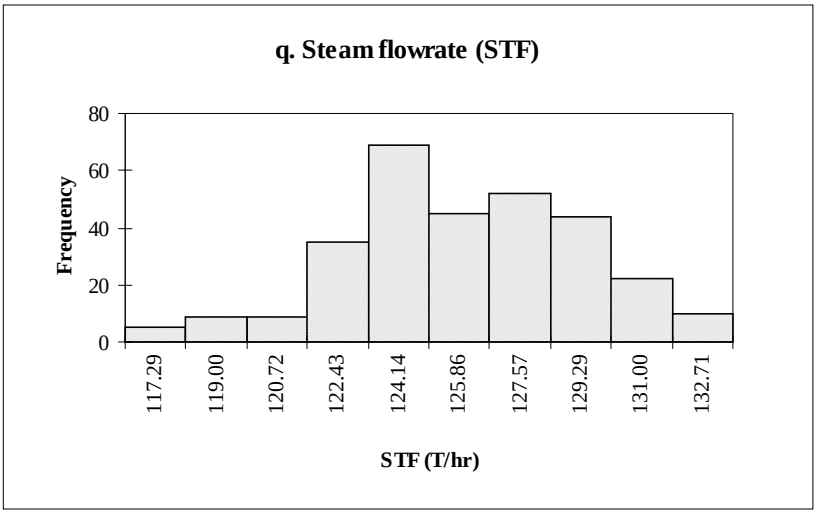

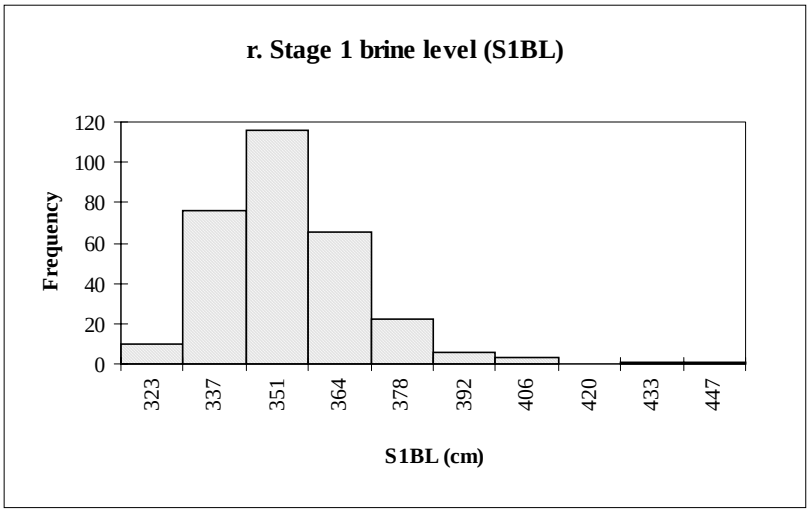

Figure 4.5: Frequency histograms of data from the MSF Plant (continued).

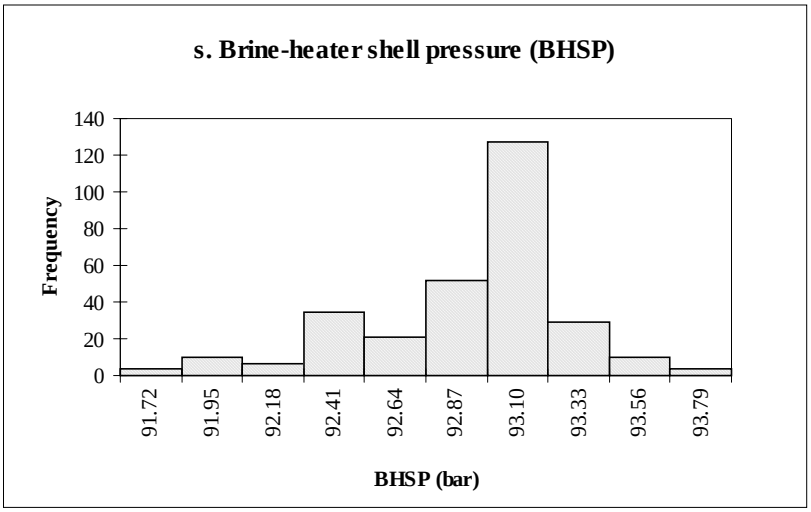

Figure 4.5: Frequency histograms of data from the MSF Plant (continued).

D. Input-Variable Selection

1. Factor Analysis: Principal Component Analysis

A number of multivariable statistical methods are available to reduce the data dimensionality and to extract useful information from process data involving large numbers of measured variables. Utojo and Bakshi (1995) give an excellent overview and comparison of multivariable statistical methods and neural networks for data processing.

Factor analysis is a technique of multivariate analysis that attempts to account for the covariation among a set of observable random variables (denoted as X) in term of a minimal number of unobservable or latent random variables called factors. These unobserved factors are assumed to be linear combinations of the variables which make up the set X. Thus, the objective becomes one of reducing the complexity of the set X into

as few linear combinations of those variables within X as possible. There are numerous strategies for performing this reduction of the set X. One such approach is *Principal Component Analysis (PCA)* that reduces the complexity of the set X via a canonical analysis of the correlation matrix of X. The dominant eigenvectors of the matrix X are then taken to be the principal factors of X. The elements comprising the eigenvectors are then taken to be the weights which produce the linear combination of the set of variables within X. For instance, if we denote the first factor as F_1, then F_1 is simply a linear combination of the variables in X, where the weights are determined by the elements of the first (most dominant) eigenvector of the correlation matrix of X.

$$F_1 = e_{11}x_1 + e_{21}x_2 + \ldots + e_{p1}x_p ,$$

where $e_1=(e_{11}e_{21}\ldots e_{p1})$ denotes the most dominant eigenvector of the correlation matrix of X. The elements of e_1 are known as factor loading for each of the p variables that comprise X. These factor loadings are always between -1.0 and 1.0, *and a useful heuristic is that variables whose factor loadings have absolute value greater than 0.5 are related highly to the corresponding factor.*

The rotated principal component analysis generally involves the following major steps:

a) selecting the variables,
b) computing the matrix of correlations among the variables,
c) extracting the unrotated factors,
d) rotating the factors, and
e) interpreting the rotated factor matrix.

Current estimation and rotation methods require iterative calculations that must be done on a computer. Several computer programs are now available for this purpose. SAS statistical software (SAS Institute Inc., 1996) is used to carry out the factor analysis test.

As presented previously in Table 4.3, the important operational variables from those collected in the DCR are 19 variables, of which the performance variables of desalination plants are TBT, DP, and STF. We apply the factor analysis to test 19 variables with 4 factors. Table 4.5 summarizes the resulting rotated factor loadings.

Table 4.4: Estimated rotated factor loading for 19 operating variables.

Operating variables	**Estimated rotated factor loading (300 observations)**			
	F_1	F_2	F_3	F_4
SWF	0.90878	-0.31166	0.04798	0.14892
SWRF	0.29574	-0.23082	0.85593	0.03245
MF	0.61270	0.38589	-0.52136	0.07086
RBF	-0.49449	0.02260	-0.05117	-0.64233
BDF	0.73723	0.02992	-0.63621	0.00386
CDF	0.73776	0.19164	-0.09635	0.40617
SWIT	-0.37805	-0.15163	-0.36583	0.49778
SWOT	-0.94760	0.26669	-0.12396	-0.03743
BIT	-0.77128	0.48112	-0.27091	0.07592
BBT	-0.37288	0.86703	0.12281	-0.15522
S24BT	-0.96054	0.09331	-0.09121	0.04516
STT	-0.06584	0.10695	0.05327	0.78844
CDT	-0.04327	0.95970	-0.09453	0.05409
BHSP	-0.05189	0.94665	-0.02183	0.01674
BHST	0.16472	0.73829	-0.21171	0.08723
S1BL	-0.10277	-0.71761	0.02479	-0.52569
TBT	-0.11481	**0.95700**	0.05019	0.01441
DP	**0.85905**	0.22651	-0.16289	-0.25749
STF	-0.17205	0.54827	**0.59606**	0.01470

According to the preceding heuristic, the variables whose loading values are greater than 0.5 for a particular factor are taken to represent that factor. Factor 1 (F_1) has high loading

values for variables 24BT, SWOT, SWF, DP, BIT, CDF, BDF, and MF, and much lower values for all the rest. Factor 2 (F_2) has high loadings for variables CDT, TBT, BHSP, BBT, BHST, S1BL, and STF, with much lower loadings for all the other variables. Finally, Factor 3 (F_3) has high loadings only for variables SWRF, BDF, STF, and MF. Each factor, then, in Table 4.5 is related highly to only a few variables (indicated by numbers in **bold**), and the set of related variables differs for each factor.

The performance variables of desalination plants are the top brine temperature (TBT), the distillate produced (DP), and the steam flowrate (STF), as listed as the last three variables in Table 4.5. The factor columns in the matrix represent the output variables. In order to determine the relationship between significant input variables and output variables, each output variable must be matched to a factor column. To match an output variable to a factor column, we examine the output variable's row of loading values. Specifically, we identify the largest loading value in that row, and the column in which this value is located indicates the appropriate factor match for that output variable. We repeat this process for each of the output variables, and if there are fewer output variables than columns, we discard the extraneous columns.

As seen in Table 4.5, marked by the circle, we find F_1, F_2, and F_3 to be DP, TBT, and STF variables, respectively.

2. Engineering Knowhow

Variable selection comprises decisions to include or exclude input variables and these decisions are necessarily made on only the specifications determined by the researcher. Often as an aid in this process, we use the factor analysis, R^2 test or some other statistical method to examine relationships between inputs and outputs, and to select input

variables. In using these methods, there is always the risk that significant input variables may be excluded if we do not utilize the particular functional relationship in that testing method. Our emphasis is on selecting an appropriate subset of these variables for use in a final prediction model. Therefore, we investigate various specifications of the input variables, based on the plant design and engineering knowhow, and retained any that are deemed worthy of further study. Ultimately, based on engineering knowhow, we conclude to include the 19 variables in training the MSF network.

Table 4.6 presents the input variables recommended by engineering knowhow and by factor analysis. Figure 4.6 compares the neural network performance based on factor analysis and engineering knowhow for variable selection. It is clear that the network with variables selected based on engineering knowhow, with more input variables, performs better than that with less variables selected based on factor analysis. Table 4.7, and Figure 4.7 illustrate that the RMS error for the engineering-knowhow network is much less in value and fluctuation than those for factor analysis.

Table 4.5: Input variables recommended for the MSF network by engineering knowhow and by factor analysis.

Engineering Knowhow	**Factor Analysis**		
	Top brine temperature	Distillate produced	Steam flowrate
1. Seawater flowrate 2. Seawater recirculating flowrate 3. Makeup flowrate 4. Recirculating brine flowrate 5. Blowdown flowrate 6. Condensate flowrate 7. Seawater-inlet temperature 8. Seawater-outlet temperature 9. Brine inlet temperature 10. Brine-heater inlet temperature 11. Stage 24 brine temperature 12. Steam temperature 13. Condensate temperature 14. Brine-heater shell pressure 15. Brine-heater shell temperature 16. Stage 1 brine level 17. Top brine temperature 18. Distillate produced 19. Steam flowrate	1. Condensate temperature 2. Brine-heater shell pressure 3. Brine-heater inlet temperature 4. Steam temperature 5. Brine-heater shell temperature 6. Stage 1 brine level 7. Recirculating brine flowrate 8. Steam flowrate 9. Seawater-inlet temperature	1. Stage 24 brine temperature 2. Seawater-outlet temperature 3. Seawater flowrate 4. Steam temperature 5. Brine inlet temperature 6. Condensate flowrate 7. Blowdown flowrate 8. Recirculating brine flowrate 9. Makeup flowrate 10. Stage 1 brine level 11. Seawater-inlet temperature	1. Seawater recirculating flowrate 2. Steam temperature 3. Recirculating brine flowrate 4. Blowdown flowrate 5. Stage 1 brine level 6. Makeup flowrate 7. Seawater-inlet temperature

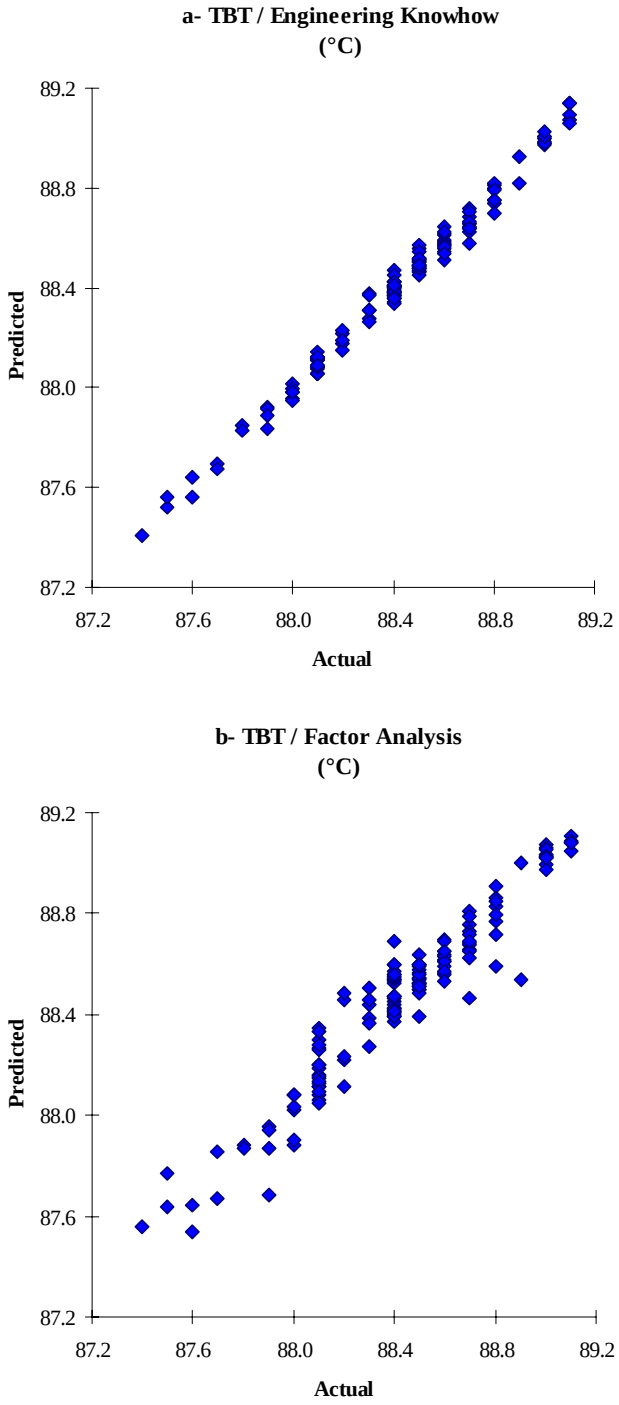

Figure 4.6: Actual and predicted output variables for the MSF network by engineering knowhow and by factor analysis: (a), (b) Top brine temperature; (c),(d) Distillate produced; and (e), (f) Steam flowrate.

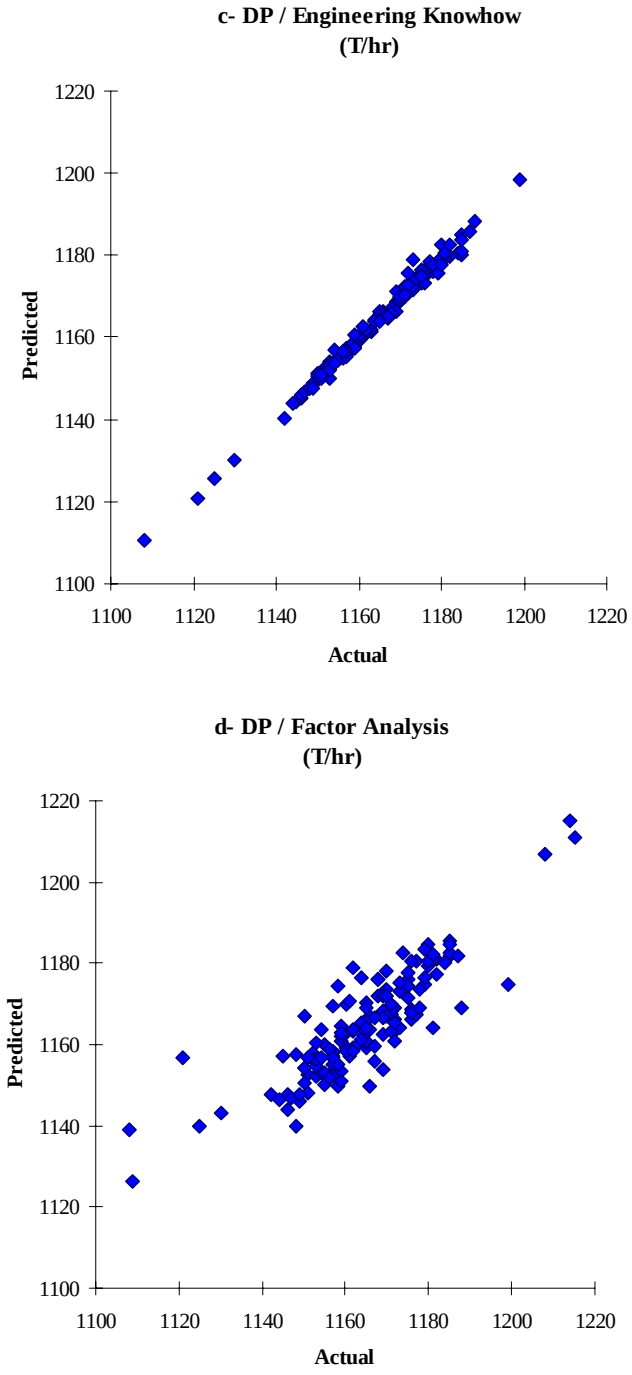

Figure 4.6: Actual and predicted output variables for the MSF network by engineering knowhow and by factor analysis: (a), (b) Top brine temperature; (c),(d) Distillate produced; and (e), (f) Steam flowrate (continued).

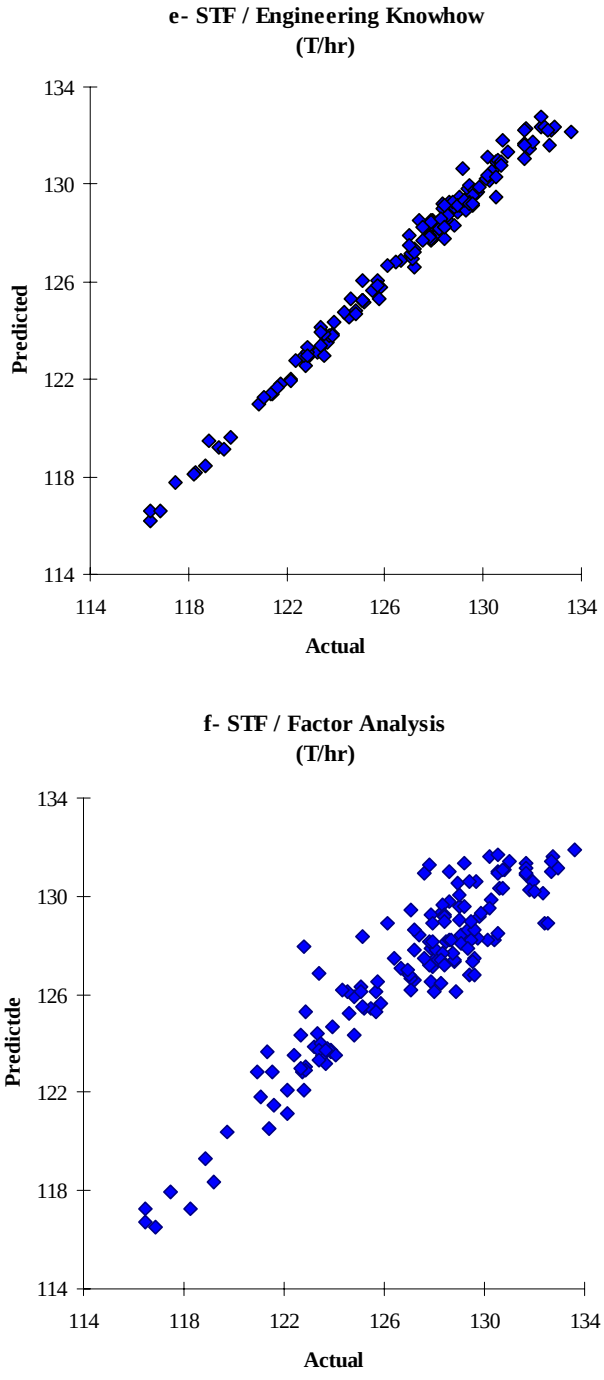

Figure 4.6: Actual and predicted output variables for the MSF network by engineering knowhow and by factor analysis: (a), (b) Top brine temperature; (c),(d) Distillate produced; and (e), (f) Steam flowrate (continued).

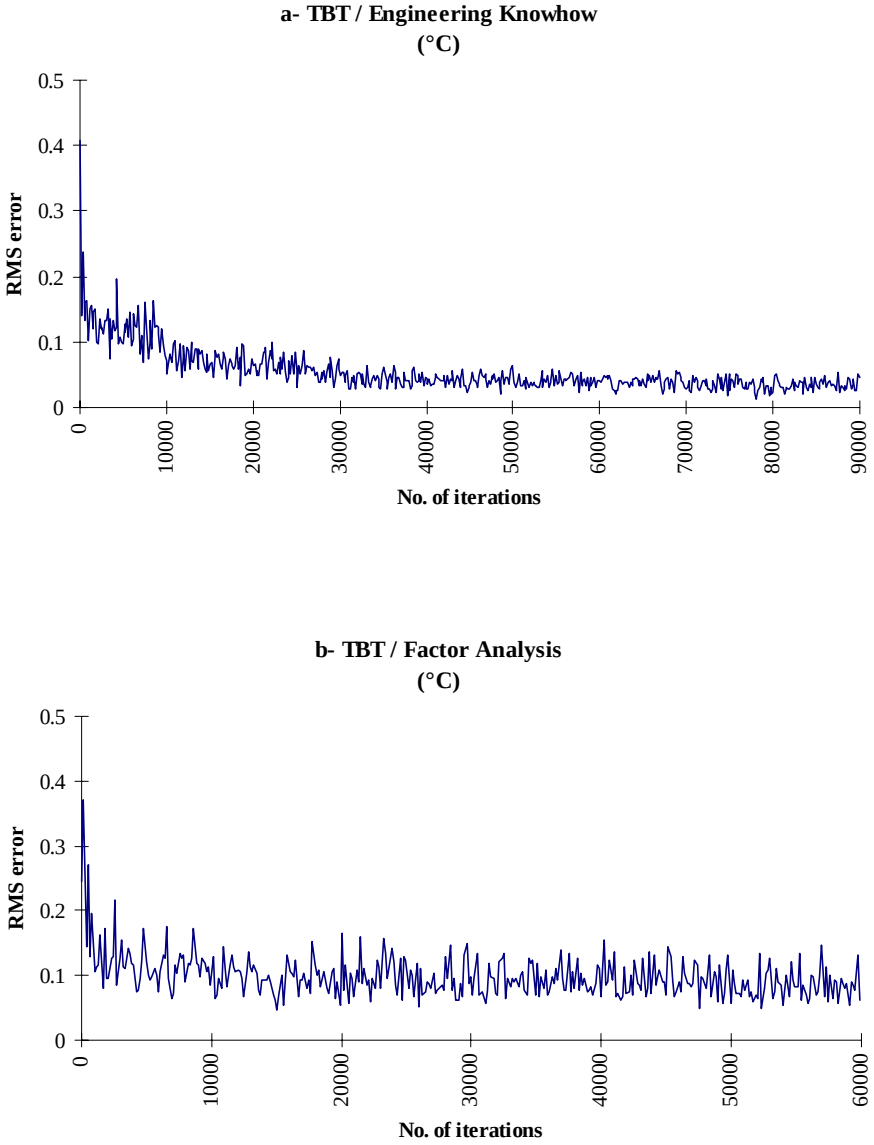

Figure 4.7: RMS errors for the MSF network by engineering knowhow and by factor analysis: (a), (b) Top brine temperature; (c),(d) Distillate produced; and (e), (f) Steam flowrate.

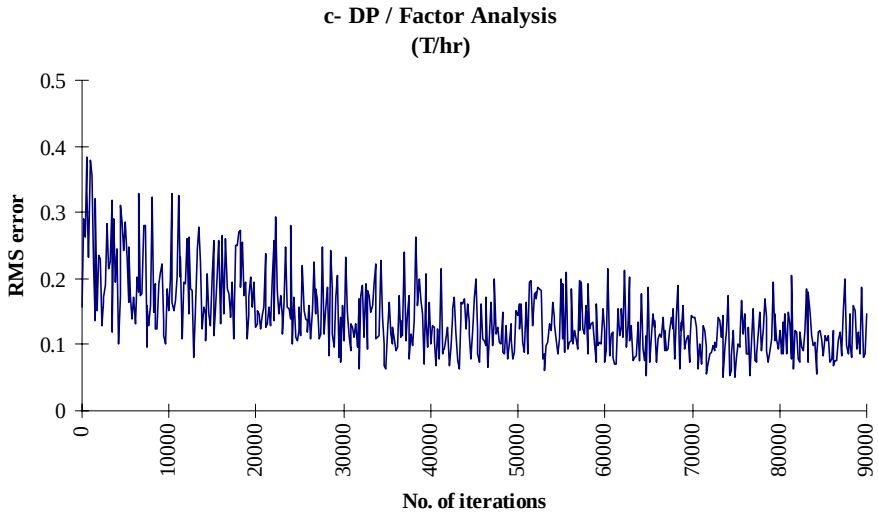

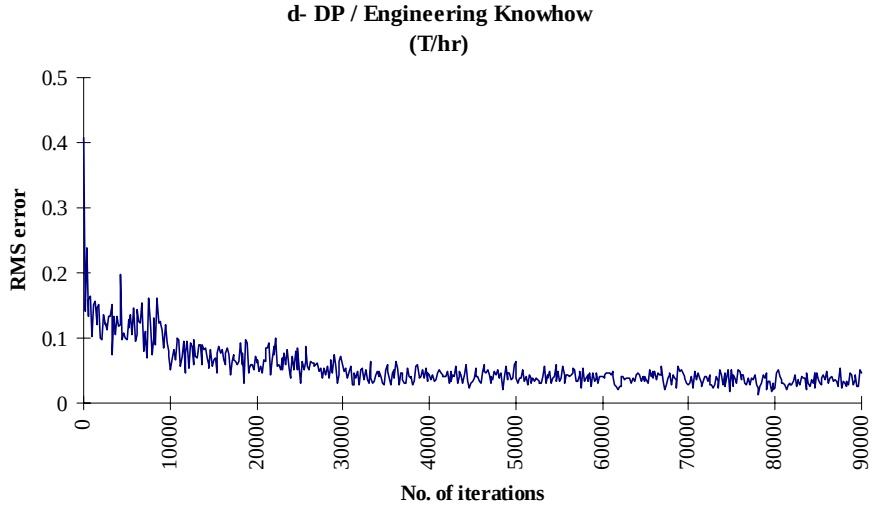

Figure 4.7: RMS errors for the MSF network by engineering knowhow and by factor analysis: (a), (b) Top brine temperature; (c),(d) Distillate produced; and (e), (f) Steam flowrate (continued).

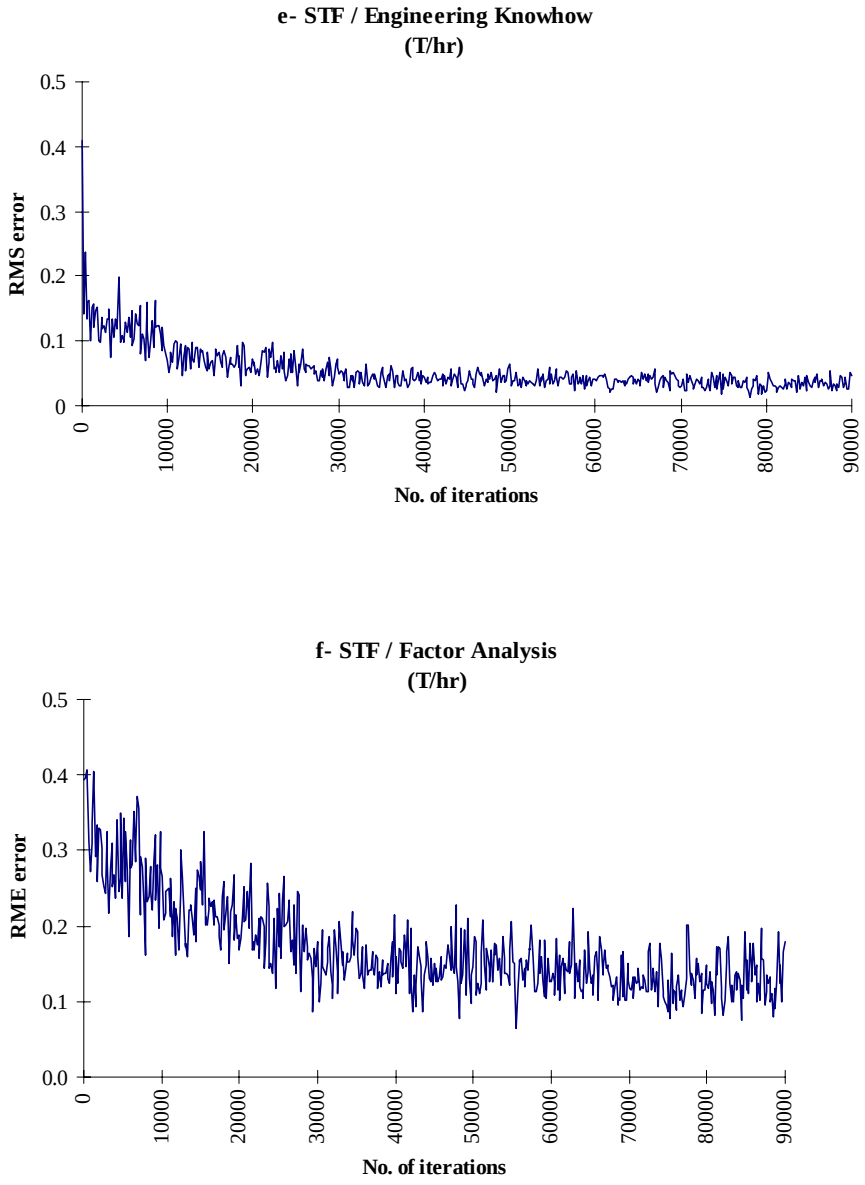

Figure 4.7: RMS errors for the MSF network by engineering knowhow and by factor analysis: (a), (b) Top brine temperature; (c),(d) Distillate produced; and (e), (f) Steam flowrate (continued).

Table 4.6: RMS errors of the top brine temperature (TBT), distillate produced (DP), and steam flowrate (STF) based on different approaches to input-variables selection.

Variable-selection method	**TBT (°C)**	**DP (T/hr)**	**STF (T/hr)**
Engineering knowhow	0.0546	0.0621	0.0679
Factor analysis	0.0986	0.1425	0.1705

We conclude that the degree of success in variable selection greatly influences the resulting network's ability to predict. Statistical methods can aid in the process of variable selection, but the wise engineer will not hesitate to use his knowhow when it comes down to the final decisions. In all cases investigated here, the results show that networks using variable selections based on engineering judgment equal or surpass the performance of networks using statistical methods.

E. Training and Testing Sets

Two subsets of data are used to build a model: a training set and a testing set. The training phase needs to produce a neural network that is both stable and convergent. Therefore, selecting what data to use for training a network is one of the most important steps in building a neural network model.

Neural networks interpolate data very well, but they do not extrapolate. Therefore, the training set should be selected in such a way that it includes data from all regions of desirable operation.

An important aspect of developing neural networks is determining how well the network performs once training is complete. Checking the performance of a trained network involves two main criteria: (1) how well the neural network recalls the predicted response from data sets used to train the network (called *the recall step*); and (2) how well the network predicts responses from data sets that were not used in training (called *the generalization step*).

In the recall step, we evaluate the network's performance in recalling (retrieving) specific initial input used in training. Thus, we introduce a previously used input pattern to the trained network. A well-trained network should be able to produce an output that deviates very little from the desired value.

In the generalization step, we feed new input patterns (whose results are known for us, but not to the network) to the trained network. The network generalizes well when it sensibly interpolates these new patterns. Generalization is affected by three factors: the size and the efficiency of the training data set, the architecture of the network, and the physical complexity of the problem.

To effectively visualize how well a network performs recall and generalization, we often generate *a learning curve,* which represents the average error for both the recall of training data sets and the generalization of the testing sets as a function of the number of examples in the training data set. The two main uses of a learning curve are (Baughman, and Liu, 1995):

- to find the number of training example required to achieve a fixed average error. In Figure 4.8, the network reaches a fixed average error at approximately the t4 time interval.

- to estimate the minimum average error attainable through adding data sets.

  In Figure 4.8, the network shows low average error for recall with small training data sets, and the recall error increases slightly as more examples are included. In contrast, the generalization is very poor (high average error) for small training data sets and the error decreases as more examples are included. For a well-trained network, as it receives more information, the recall and generalization curves approach each other. The minimum average error for generalization is 0.1.

  Figure 4.9 shows that the RMS errors become more stable as the number of examples in the training sets increase. This figure displays the lowest RMS error with 150 training examples. Therefore, we use a training data set and a testing data set of 150 samples each throughout this study.

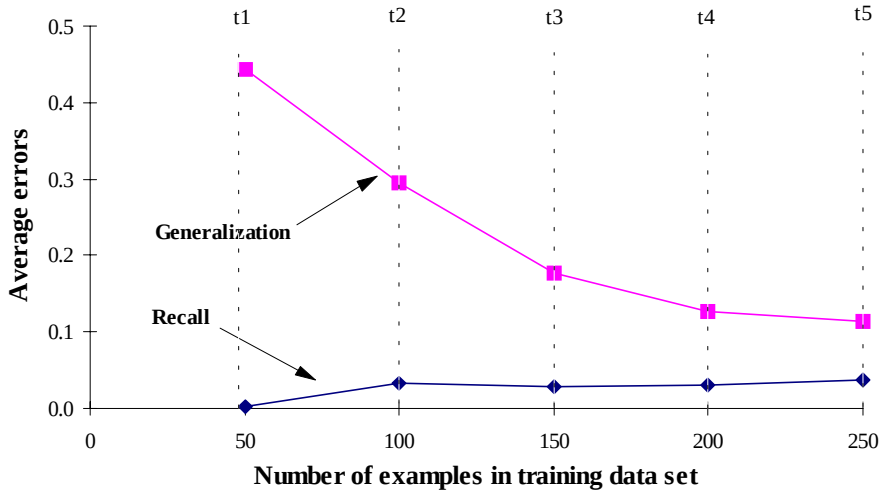

Figure 4.8: The learning curve for training the TBT network.

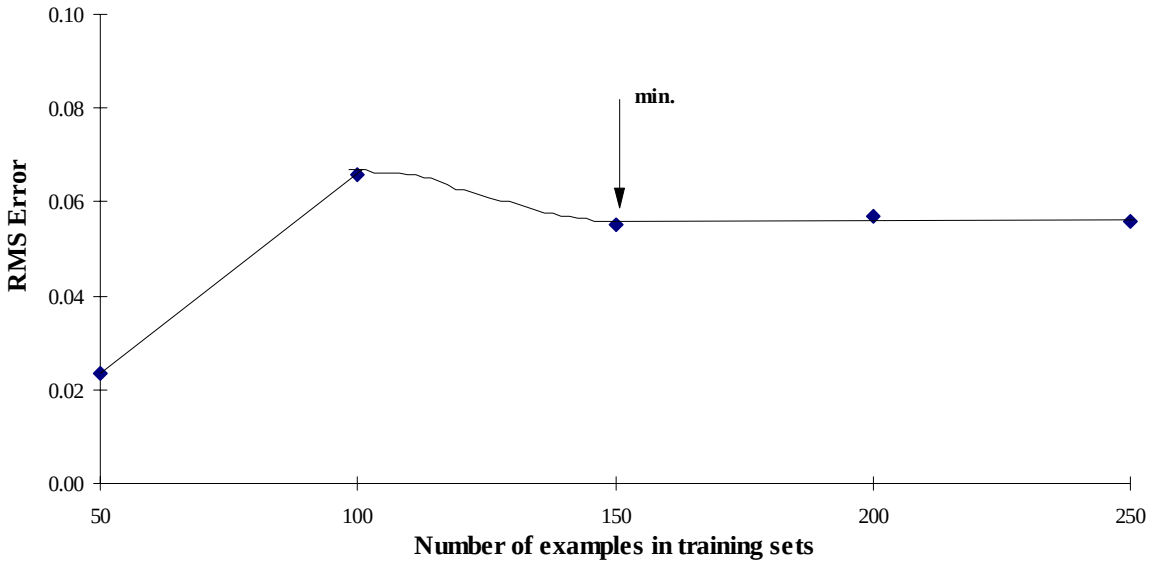

Figure 4.9: RMS errors for the TBT network with increasing number of examples in training sets.

F. Model Development and Optimization

In developing a neural network model for our application, we try to maximize the performance of the model developed (speed of convergence and accuracy of prediction) by investigating the following network characteristics before experimenting with any future tests:

- Weight initialization.
- Normalizing input and output data sets
- Optimum network architecture:
    - Epoch size
    - Transfer function.
    - Learning rates and momentum coefficients
    - Number of nodes in the hidden layer(s).
- Network configuration:
    - Multiple-input-single-output (MISO)
    - Multiple-input-multiple-output (MIMO)
- Neural networks versus statistic regression

1. Weight Initialization

The first step in neural computing, prior to training a neural network, is to initialize the weight factors between the nodes of the hidden layers. Since no prior information about the system being modeled is available, it is preferable to set all the free parameters of the network to random numbers that are uniformly distributed inside a small zero-mean range of values, say, between ±0.5.

The initial distribution set by the software package, NeuralWare's NeuralWork Professional II/Plus (1993), for instance, sets the initial weight-factor distribution to a fairly narrow range, based on the number of input variables and total number of nodes in the hidden layer(s), and allows it to broaden using high learning rate and momentum coefficient in the early stages of the training process.

Table 4.8 lists effective initial weight factor distribution used in training backpropagation networks recommended in Baughman, and Liu (1995).

Table 4.7: A recommended set of weight-factor distributions featuring good initial Gaussian distributions for varying total number of nodes in the hidden layer(s) for neural networks with 1 to 3 hidden layers (Baughman and Liu, 1995).

Number of input variables (nodes)	**Total number of nodes in the hidden layer(s)**		
	30	45	100
5	-0.70 to 0.70	-0.50 to 0.50	-0.35 to 0.35
10	-0.50 to 0.50	-0.40 to 0.40	-0.30 to 0.30
20	-0.45 to 0.45	-0.35 to 0.35	-0.30 to 0.30
30	-0.40 to 0.40	-0.30 to 0.30	-0.25 to 0.25
50	-0.30 to 0.30	-0.20 to 0.20	-0.20 to 0.20
100	-0.25 to 0.25	-0.20 to 0.20	-0.20 to 0.20

2. Normalizing Input and Output Data Sets

NeuralWare's NeuralWorks (NWorks) Professional II/Plus (1993), normalizes the input and output data sets for the user using the zero-mean normalization method, explained in Section 3.9 of Chapter 3. The pre-processing facilities in Nworks computes the lows and

highs of each data field for all the data fields to be used with a given network, and stores in a table called MinMax table. The ranges to which the input and output should be scaled, for presentation to the network is set between limits of -1 and 1, having the average value set at 0. NWorks then computes the proper scale and offset for each data field. Real world values are then scaled to network ranges for presentation to the network. After the network has produced a network-scaled results, the result is de-scaled to real world units.

Section 3.9 of Chapter 3 presents more information on types of normalization procedures.

3. Optimal Network Architecture.

a. Epoch size

The optimum epoch size should be determined for better training. An epoch is defined as a sequence of training data sets presented to the network (learning cycle) between weight updates. We choose the epoch size such that the total number of training patterns used for each run is constant. Setting the epoch size to the size of the training data set will allow the RMS error graph to show the performance of the entire training data set.

When using backpropagation, the optimal epoch size is a function of the data. Therefore, determining the epoch size is important for better training. This can be done by setting the epoch size to different fractions of the total training set (1/10, 2/10, ….., 9/10, full training set size) and testing the R values of different networks. Select the epoch size produce the highest R value (lowest R^2 value). This method is particularly successful on noisy data.

Since we are using the Delta Rule as a learning rule and the data are not very noisy, a default epoch size of 16 is used.

b. Transfer Function

Another factor governing a node's output is the transfer function. The most common transfer functions are the sigmoid, hyperbolic tangent, and radial-basis functions. The hyperbolic tangent transfer function performs well for the prediction networks, while the radial-basis-transfer function works best in classification problems (Baughman and Liu, 1995).

A multilayer prediction network trained with the backpropagation algorithm will, in general, learn faster when the transfer function built into the network is symmetric (hyperbolic tangent, with output value between -1.0 and +1.0) rather than nonsymmetric (sigmoid, with output value between 0.0 and 1.0), as previously described in Chapter 3. Therefore, we use the hyperbolic tangent transfer function throughout this study.

c. Setting the Learning Rate and Momentum Coefficient

The learning rate and momentum coefficient are two important parameters that control the effectiveness of the training algorithm. The learning rate is a positive parameter that regulates the relative magnitude of weight changes during learning. However, how would a change in the learning rate change the performance of the algorithm? To understand the effect of the learning rate on the network training, let us consider the prediction network for the top brine temperature (TBT) with 150 training examples. We use a backpropagation network with the 30:15 hidden-layer configuration, the delta learning rule, the hyperbolic tangent transfer function, and zero momentum coefficient.

Figure 4.10 compares the RMS error using a low learning rate of 0.01, a moderate learning rate of 0.3, and a high learning rate of 5.0. In general, a smaller learning rate results in slower convergence. When the learning rate is low (0.01), the network takes a

longer time (4,000 iterations) to reach an RMS error of 0.16 (point b). This is due to the fact that the smaller the learning rate, the smaller will the changes to the weights in the network be from one iteration to the next, and the larger the number of update steps needed to reach a minimum.

However, when the learning rate is 0.3, the network reaches an RMS error of 0.16 (point a) in a shorter time (200 iterations). If increase the learning rate to 5.0, such that we will be taking larger steps, the algorithm will become unstable; the oscillating error fluctuations will increase instead of decaying and thus not reaching a minimum (see Figure 4.11).

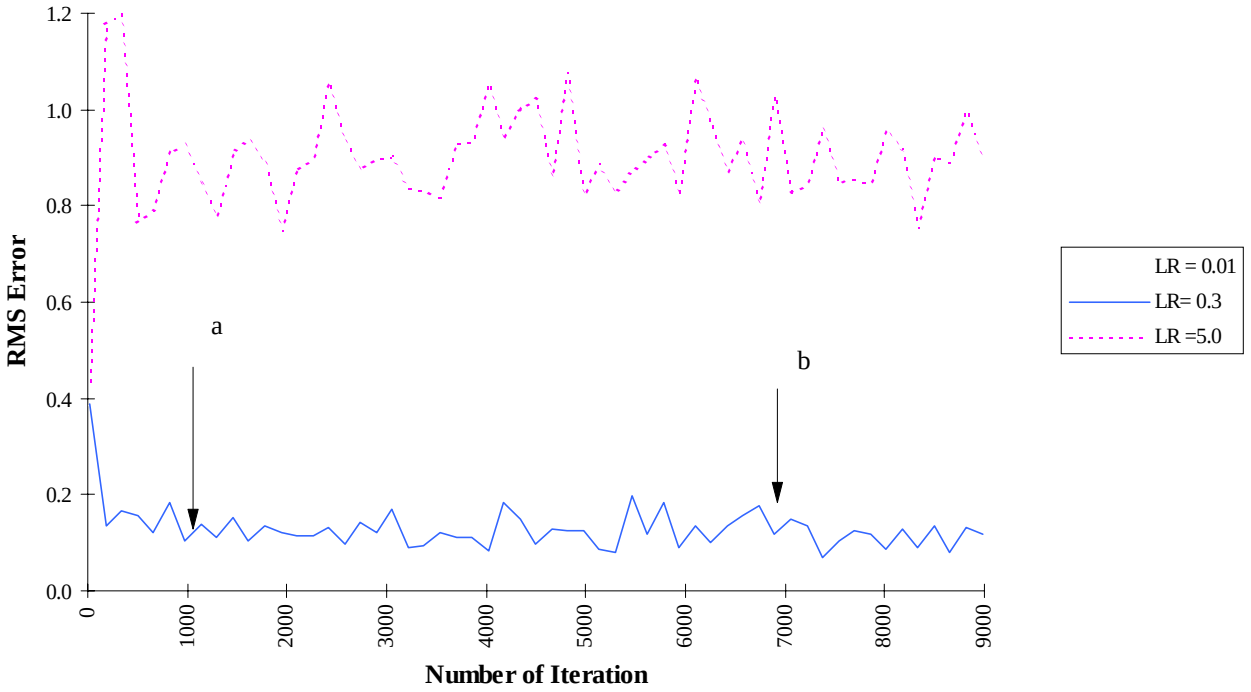

Figure 4.10: A comparison of the RMS error in training the TBT network with different learning rates (LRs).

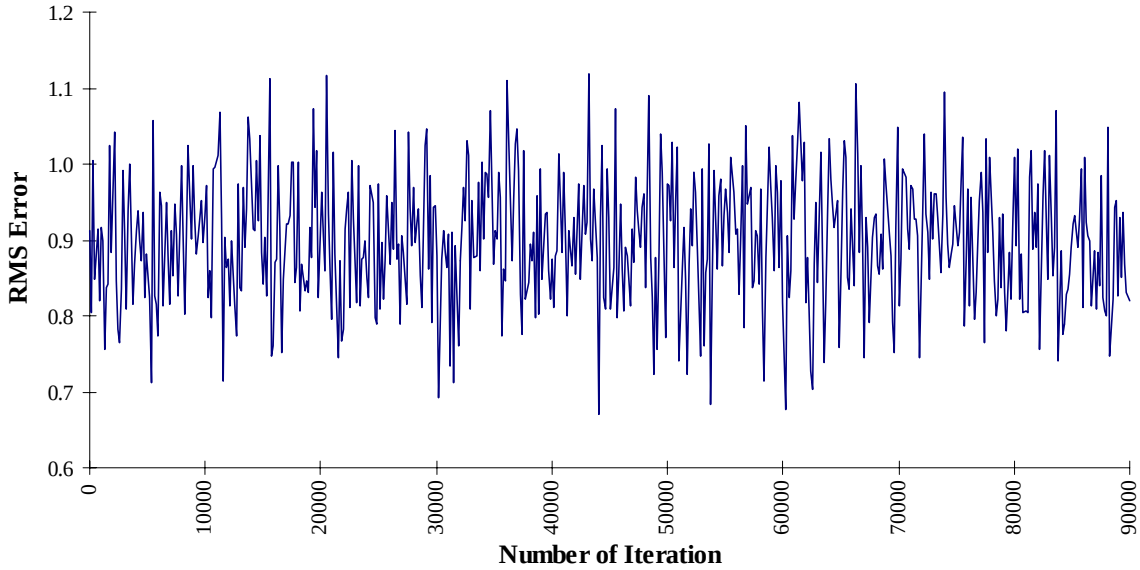

Figure 4.11: Network training with high initial learning rate (5.0) and momentum coefficient (0.8).

Therefore, to avoid the danger of instability and improve convergence as we increase the learning rate, a momentum coefficient is introduced, which will smooth out the oscillation. The momentum coefficient is a constant, between 0 and 1, used to promote stability of weight adaptation in a learning rule, and it tends to accelerate descent in a steady downhill direction. In backpropagation with momentum, the weight changes in a direction that is a combination of the current gradient and the previous gradient. This will help in moving the minimization routine out, if during training, it is trapped in a local minimum, as Figure 4.12 illustrates. To prevent excessive weight changes and possible oscillation, the algorithm slows down the weight changes by a term that is proportional to the previous weight change and the momentum coefficient.

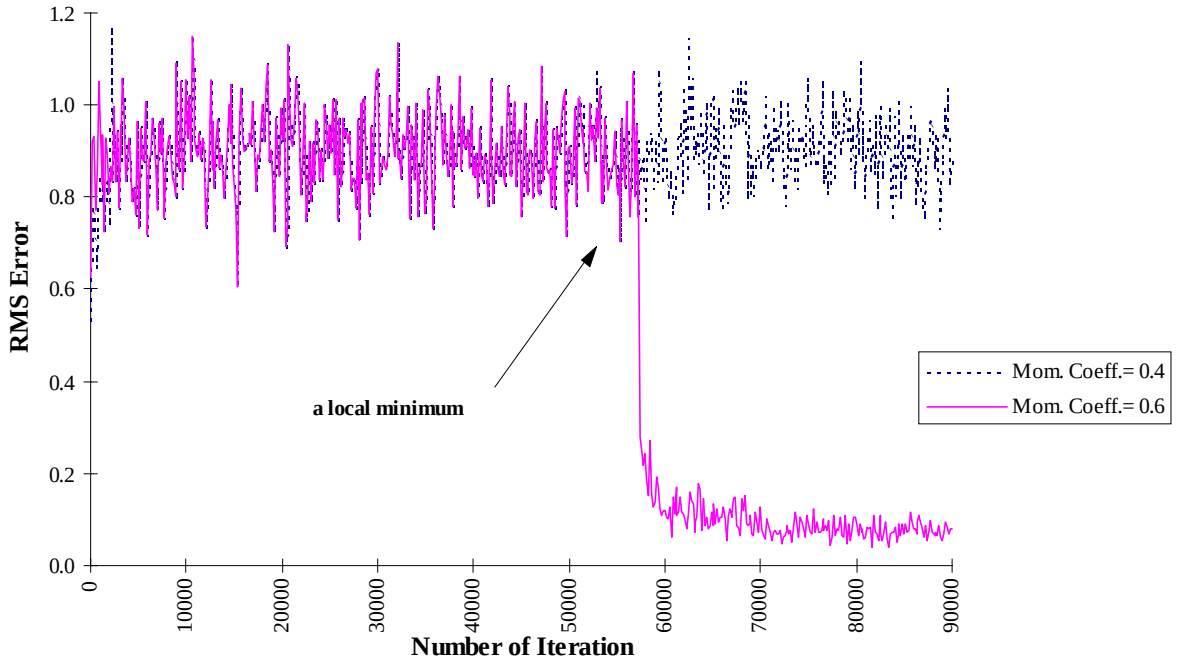

Figure 4.12: The effect of introducing a momentum coefficient on the local minimum.

To observe the effects of both learning rate and momentum coefficient on the convergence of the prediction network for the top brine temperature (TBT), we train with different learning rates {0.01,0.1, 0.3, 0.5, 0.7, 0.9, 1.0, 3.0} and momentum coefficients {0.0, 0.2, 0.4, 0.6, 0.8}. Table 4.9 lists the RMS errors for training the top brine temperature (TBT) network after 90,000 iterations. Figure 4.13 illustrates the effect of increasing the momentum coefficient on the speed of convergence. The network takes a longer time (8,000 iterations) to reach an RMS error of 0.15 when no momentum coefficient is used (Point b). By contrast, it reaches the same error at a shorter time (3,000 iterations) when the momentum coefficient is increased to 0.6 (Point a).

Table 4.8: RMS errors for the TBT network, over different learning rates and momentum coefficients.

Learning rate	**Momentum coefficient**				
	0	**0.2**	**0.4**	**0.6**	**0.8**
0.01	0.1582	0.1564	0.1541	0.1513	0.1474
0.1	0.1188	0.1163	0.1123	0.1081	0.1028
0.3	0.0951	0.0927	0.0895	0.0909	0.0968
0.5	0.0823	0.0800	0.0788	0.0841	0.0641
0.7	0.0755	0.0754	0.0736	0.0719	1.0151
0.9	0.0896	0.9302	0.0693	0.2756	1.0238
1	0.0910	0.0852	0.0637	0.5719	1.3695
3	0.0288	0.1282	1.0238	0.0858	1.0238

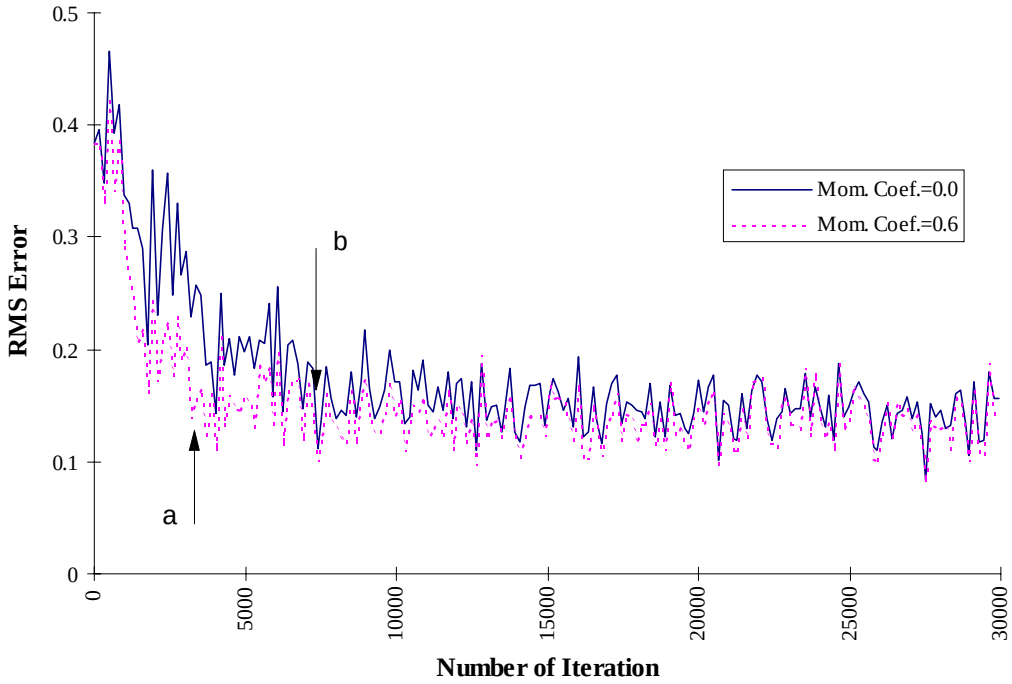

Figure 4.13: The effect of introducing a momentum coefficient on the speed of learning.

The results reached above suggest the following trends:

- In general, a smaller learning rate results in a slower convergence. Table 4.9 indicates that as the learning rate decreases, a larger momentum coefficient increases the speed of convergence. In other words, it decreases the training time.
- Table 4.9 suggests that the effective initial values for both the learning rate and the momentum coefficient are {0.3, 0.5 and 0.7}, and {0.4}, respectively. Those values agree with what Baugham and Liu (1995) recommend as effective ranges of learning rate and momentum coefficient in their text.
- The use of high learning rate and momentum coefficient causes oscillation in the RMS error during learning.

The default values for the learning rate and momentum coefficient in NeuralWare's *Neural Works Professional II/Plus* (1993) for a backpropagation algorithm are 0.3 and 0.4, respectively, which will be used throughout the study.

In general, the learning rate should be assigned a smaller value in the last layers than the front-end layers, because the last layers tend to have larger local gradients than the layers at the front-end of the network. In contrast, the momentum coefficient should be kept constant between layers and decrease with increasing in the number of iterations. Table 4.10 illustrates the typical learning schedule for a 2-hidden-layer backpropagation network used throughout this research.

Table 4.9: A typical learning schedule for a 2-hidden-layer backpropagation network (Baughman and Liu, 1995, p.62).

Hidden Layer 1				
Training iteration	0-10,000	10,001-30,000	30,001-70,000	70,001-150,000
Learning rate	0.3	0.15	0.375	0.234
Momentum coefficient	0.4	0.2	0.05	0.00312

Hidden Layer 2				
Training iteration	0-10,000	10,001-30,000	30,001-70,000	70,001-150,000
Learning rate	0.25	0.125	0.03125	0.0195
Momentum coefficient	0.4	0.2	0.05	0.00312

d. Number of nodes in the hidden layer(s).

The number of input and output nodes corresponds to the number of inputs into the network and the number of desired outputs of the network, respectively. The choice of the number of nodes in the hidden layer(s) depends on the network application. Although using a single hidden layer is sufficient in solving many functional approximation problems, some problems may be easier to solve with a two-hidden-layer configuration.

Consider the prediction network for the top brine temperature (TBT) specified in Tables 4.11 and 4.12. The network consists of 18 input variables, and 1 output variable. It uses a backpropagation network, the delta learning rule, the hyperbolic tangent transfer function, 0.3 for the learning rate, and 0.4 for the momentum coefficient. We use 150 data sets to train these configurations with 60,000 iterations. The network is tested with 1- and 2- hidden-layer configurations with an increasing number of nodes in each hidden layer(s). Figure 4.14 illustrates the network response as the number of nodes in one- and two-hidden-layer networks increases The results show that the 2-hidden-layer network

performs significantly better than the 1-hidden-layer network. The optimal configuration in 2-hidden-layer networks with minimum average error is 30:15. This configuration agrees with what Baugham and Liu (1995) recommend as effective hidden nodes in their text.

Figure 4.15 shows that the trained 30:15 network can predict the top brine temperature (TBT) very well. This configuration will be used throughout our work.

Table 4.10: The format of data files used for training the TBT prediction network.

Column No.	**Variable name**	**Variable type**	**Nomenclature**
1	Seawater flowrate	Input	SWF
2	Make-up flowrate	Input	MF
3	Seawater recirculating flowrate	Input	SWRF
4	Seawater inlet temperature	Input	SWIT
5	Seawater outlet temperature	Input	SWOT
6	Blow-down flowrate	Input	BDF
7	Brine inlet temperature	Input	BIT
8	Stage 24 brine temperature	Input	S24BT
9	Brine-heater (BH) inlet temperature	Input	BBT
10	Stage 1 brine level	Input	S1BL
11	Brine-heater shell pressure	Input	BHSP
12	Brine-heater shell temperature	Input	BHST
13	Steam temperature	Input	STT
14	Condensate temperature	Input	CDT
15	Condensate flowrate	Input	CDF
16	Recirculating brine flowrate	Input	RBF
17	Low-pressure steam flowrate to BH	*Output 1*	STF
18	Distillate produced	*Output 2*	DP
19	Top brine temperature	*Output 3*	TBT

Table 4.11: Specification of top-brine-temperature (TBT) prediction network.

Network type	Backpropagation
Training file name	*WTBT.nna*
Transfer function (input layer)	Linear
Transfer function (hidden layer)	tanh
Transfer function (output layer)	tanh
Learning rule	Delta rule
summation	Sum
Error	Standard
Network weight distribution	Normal distribution:3σ limits of [-1,1]

Input Layer

Training iteration	5,000
Noise	0.0
Learning rate	0.9
Momentum coefficient	0.6
Error tolerance	0.0

Hidden Layer 1

Training iteration	10,000	30,000	70,000
Noise	0.0	0.0	0.0
Learning rate	0.3	0.15	0.375
Momentum coefficient	0.4	0.2	0.05
Error tolerance	0.1	0.1	0.1

Hidden Layer 2

Training iteration	10,000	30,000	70,000
Noise	0.0	0.0	0.0
Learning rate	0.25	0.125	0.03125
Momentum coefficient	0.4	0.2	0.05
Error tolerance	0.1	0.1	0.1

Output Layer

Training iteration	10,000	30,000	70,000
Noise	0.0	0.0	0.0
Learning rate	0.15	0.075	0.01875
Momentum coefficient	0.4	0.2	0.05
Error tolerance	0.1	0.1	0.1

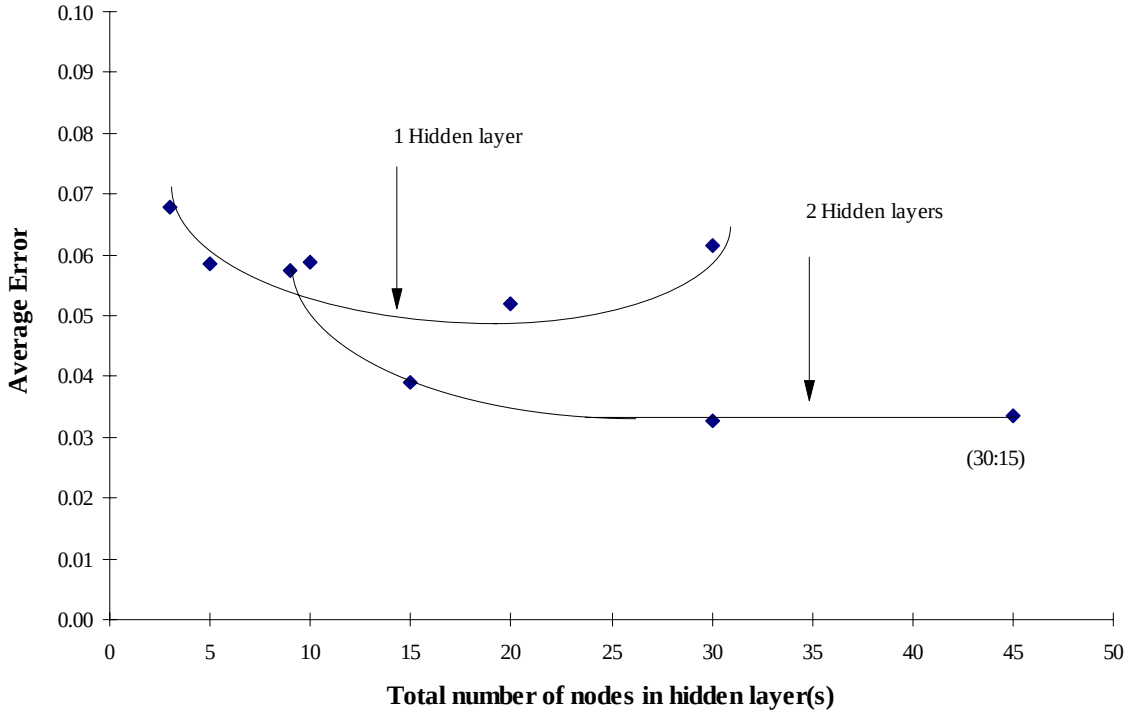

Figure 4.14: A comparison of the average errors for the prediction network for the top brine temperature (TBT) trained with various one- and two-hidden-layer configurations.

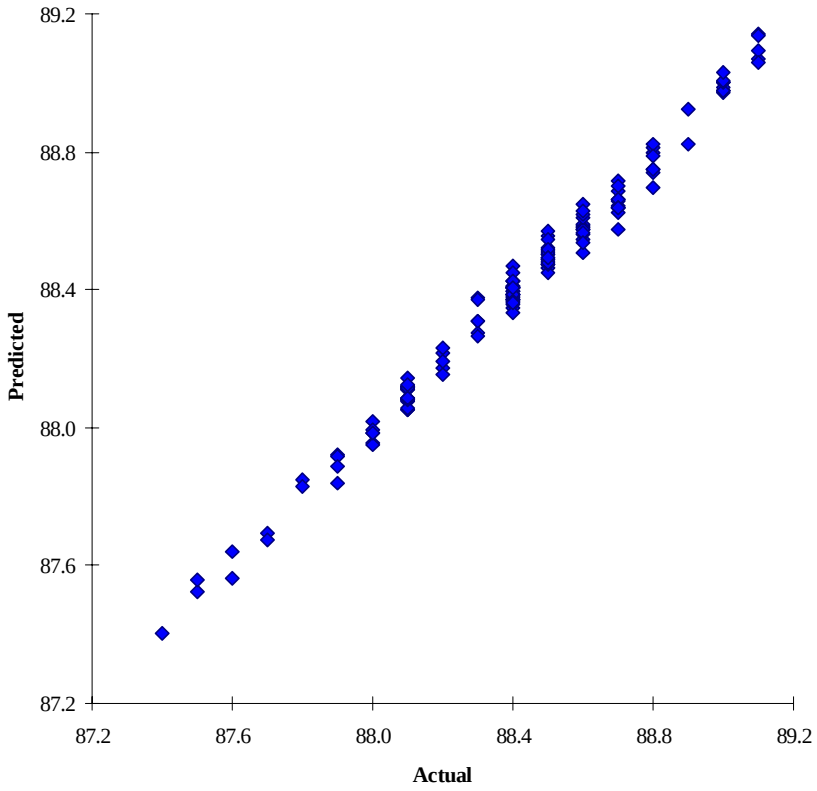

Figure 4.15: Actual and predicted TBT in °C for 30:15 hidden-layer configuration.

Based on the above results, the optimal network architecture recommended for the MSF network is one based on a backpropagation algorithm, using the delta learning rule, and the hyperbolic tangent transfer function. The learning rate is set to 0.3 and it decreases with increasing number of hidden layers, and with increasing number of iterations increases. The momentum coefficient is set to 0.4 and remains constant between the hidden layers, but decreases as the number of iterations increases. The two hidden layers have 30 and 15 nodes, respectively, whereas the maximum number of training iterations is 30,000 and the epoch size is fixed at 16 examples. The data are divided into two equal portions (150 points in each set) for the training and the testing sets.

4. Network Configuration (Multiple-input-single-output versus multiple-input-multiple-output).

In developing a neural-network model, the goal is to develop a network that produces the lowest error between the actual and predicted values for each output variable. The question then arises whether a network predicting multiple output variables (multiple-input-multiple-output, MIMO) or a network predicting only a single output variable (multiple-input-single-output, MISO), would more accurately represent the process.

In using a MISO network, it would be necessary to train a separate network for each of the output variables that are to be predicted. This would require more overall training time than for a single MIMO network. In the MIMO network, all output variables are predicted simultaneously using one network. The development and execution of this model would be simpler, more convenient and cheaper than using a set of MISO networks, especially in an on-line application of the network. An important factor in deciding between MISO and MIMO approaches is the comparative accuracy of the model

that each method produces. In this investigation, we develop MISO and MIMO networks with the same input data in order to determine which network performs (predicts) better.

We test both multiple-input-single-output (MISO) and multiple-input-multiple-output (MIMO) configurations using the same number of training and testing example sets (150 example sets) for both winter and summer data from the plant. In training a separate MISO network for each of the three outputs (TBT, DP, and STF), we use networks with 18 inputs and one output for winter data and 17 input and one output for summer data. The architecture of the MISO network for the winter data is[18:30:15:1], including a total of 1051 weights. We train the MIMO network for the three outputs together, with 16 inputs and three outputs. Therefore, the network architecture is [16:30:15:3], with a total of 991 weights.

Similarly, the architecture of the MISO network for the summer data is represented as [17:30:15:1], and of the MIMO network is [15:30:15:3]. Tables 4.13 and 4.14 show the formats of the data files used for training the MIMO and MISO networks, and the prediction network specification, respectively.

Table 4.12: The format of data files used for training the MISO TBT, DP, and STF prediction networks under winter conditions.

Column no.	**Variable name**	**Nomen-clature**	**Variable type for TBT network**	**Variable type for DP network**	**Variable type for STF network**
1	Seawater flowrate	SWF	Input	Input	Input
2	Make-up flowrate	MF	Input	Input	Input
3	Seawater recirculating flowrate	SWRF	Input	Input	Input
•	Seawater inlet temperature	SWIT	•	•	•
•	Seawater outlet temperature	SWOT	•	•	•
•	Blow-down flowrate	BDF	•	•	•
•	Brine inlet temperature	BIT	•	•	•
•	Stage 24 brine temperature	S24BT	•	•	•
•	Brine-heater inlet temperature	BBT	•	•	•
•	Stage 1 brine level	S1BL	•	•	•
•	Brine-heater shell pressure	BHSP	•	•	•
•	Brine-heater shell temp.	BHST	•	•	•
•	Steam temperature	STT	•	•	•
•	Condensate temperature	CDT	•	•	•
•	Condensate flowrate	CDF	•	•	•
•	Recirculating brine flowrate	RBF	Input	Input	Input
17	LP Steam flowrate to BH	STF	Input	Input	*Output*
18	Distillate produced	DP	Input	*Output*	Input
19	Top brine temperature	TBT	*Output*	Input	Input

Table 4.13: Network specification for the MISO and MIMO prediction networks under winter condition.

Network type			Backpropagation
Training file name			*WMIMO.nna, WTBT.nna, WDP.nna, and WSTF.nna*
Transfer function (input layer)			Linear
Transfer function (hidden layer)			tanh
Transfer function (output layer)			tanh
Learning rule			Delta rule
summation			Sum
Error			Standard
Network weight distribution			Normal distribution:3σ limits of [-1,1]
Input Layer			
Training iteration			5,000
Noise			0.0
Learning rate			0.9
Momentum coefficient			0.6
Error tolerance			0.0
Hidden Layer 1			
Training iteration	10,000	30,000	70,000
Noise	0.0	0.0	0.0
Learning rate	0.3	0.15	0.375
Momentum coefficient	0.4	0.2	0.05
Error tolerance	0.1	0.1	0.1
Hidden Layer 2			
Training iteration	10,000	30,000	70,000
Noise	0.0	0.0	0.0
Learning rate	0.25	0.125	0.03125
Momentum coefficient	0.4	0.2	0.05
Error tolerance	0.1	0.1	0.1
Output Layer			
Training iteration	10,000	30,000	70,000
Noise	0.0	0.0	0.0
Learning rate	0.15	0.075	0.01875
Momentum coefficient	0.4	0.2	0.05
Error tolerance	0.1	0.1	0.1

As shown in Table 4.14 and 4.15, and Figures 4.16 and 4.17, the prediction of the outputs for the recall and generalization sets is very good. In general, the MISO network shows smaller recall error, and the MIMO networks gives a lower generalization error. Figure 4.18 and 4.19 illustrate that the RMS errors for the three MISO (TBT, DP, and STF) and the single MIMO networks, for both winter and summer operational data, are less than 0.08.

Table 4.14: Average absolute recall and generalization errors for MISO and MIMO networks with winter data.

Error	**MIMO network**			**MISO network**		
	TBT (°C)	DP (T/hr)	STF (T/hr)	TBT (°C)	DP (T/hr)	STF (T/hr)
Recall average absolute Generalization average absolute	0.0371 0.1743	1.0582 13.568	0.2475 4.2798	0.0287 0.1764	0.9329 13.088	0.3067 3.5910
RMS error	0.0765			0.0517	0.0249	0.1258

Table 4.15: Average absolute recall and generalization errors for MISO and MIMO networks with summer data.

Error	**MIMO network**			**MISO network**		
	TBT (°C)	DP (T/hr)	STF (T/hr)	TBT (°C)	DP (T/hr)	STF (T/hr)
Recall average absolute Generalization average absolute	0.0410 0.1430	3.9050 8.7080	0.5400 4.9430	0.0287 0.1764	0.9329 13.088	0.3067 3.5910
RMS error	0.0650			0.0461	0.0265	0.0408

In the MISO network, the RMS errors for the winter data are more stable than that for the summer data. It starts at about 0.2 and converges rapidly after 10,000 iteration to 0.0461, 0.0265, and 0.0407 for the TBT, DP and STF, respectively, whereas the RMS errors for the summer data are unstable and fluctuating, starting at 0.35 and converging after 30,000 iteration to 0.0516, 0.0249, and 0.0125 for the TBT, DP and STF respectively. In the MIMO network, the RMS errors follow the same trend as the MISO network for the summer and winter data. This could be attributed to the stable operation of the plant during the winter time.

We see no significant difference in the prediction accuracy between the MISO and MIMO networks.

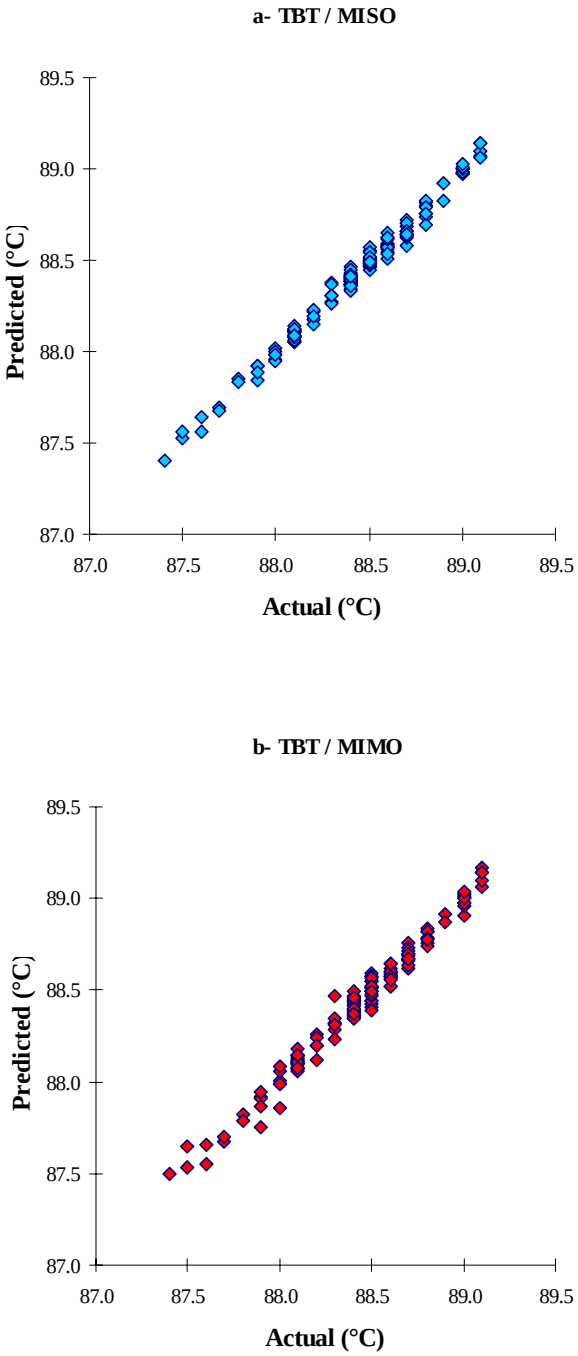

Figure 4.16: Actual and predicted outputs from the MISO and MIMO networks with winter data: (a), (b) TBT networks; (c), (d) DP networks; and (e), (f) STF networks.

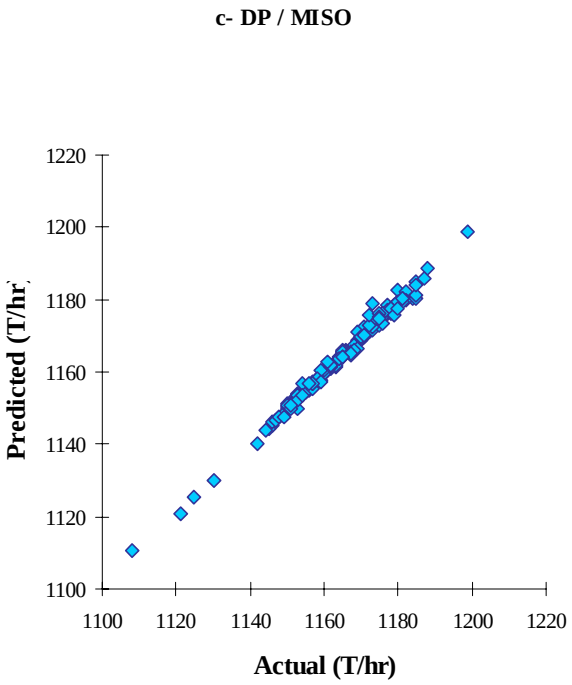

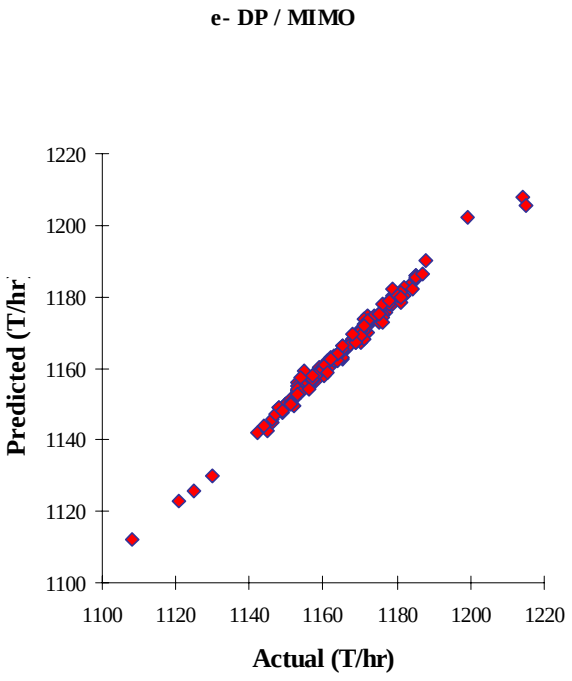

Figure 4.16: Actual and predicted outputs from the MISO and MIMO networks with winter data: (a), (b) TBT networks; (c), (d) DP networks; and (e), (f) STF networks (continued).

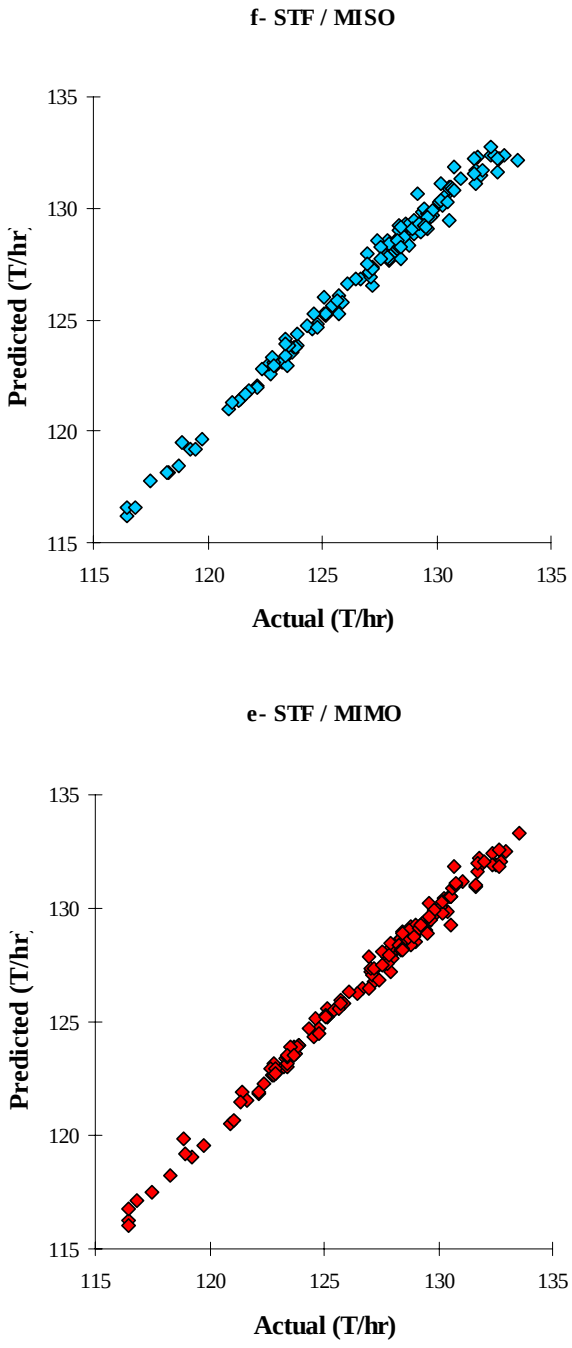

Figure 4.16: Actual and predicted outputs from the MISO and MIMO networks with winter data: (a), (b) TBT networks; (c), (d) DP networks; and (e), (f) STF networks (continued).

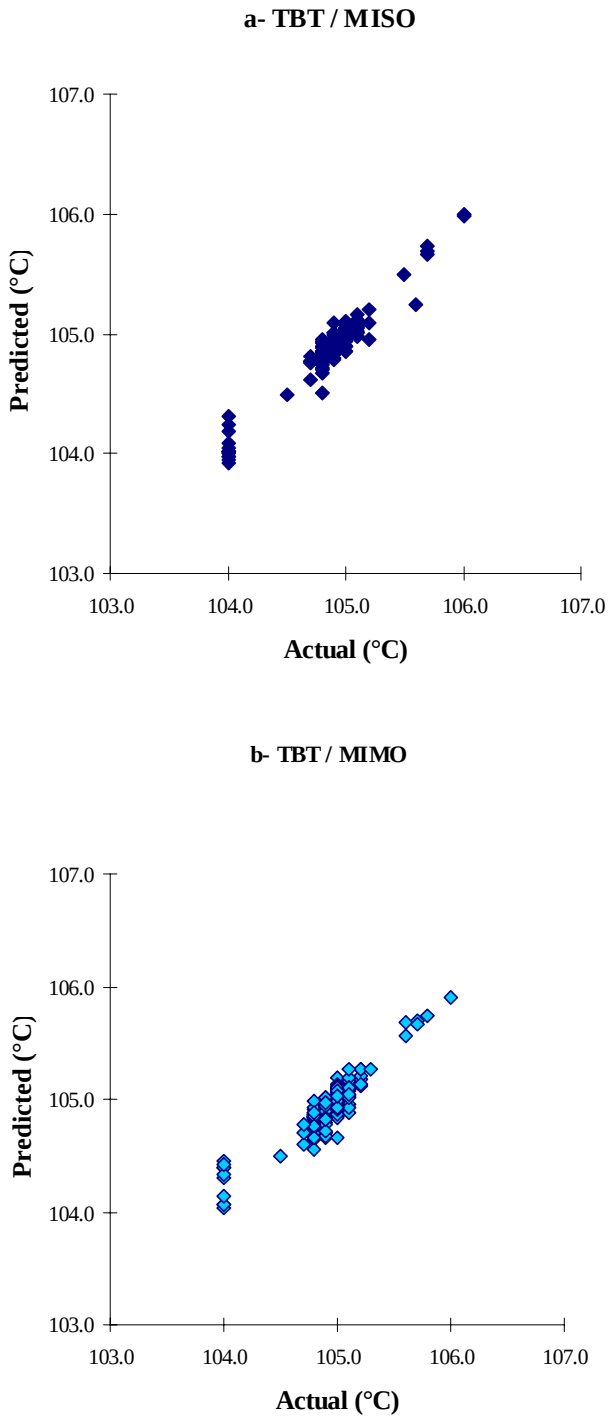

Figure 4.17: Actual and predicted outputs from the MISO and MIMO networks with summer data: (a), (b) TBT networks; (c), (d) DP networks; and (e), (f) STF networks.

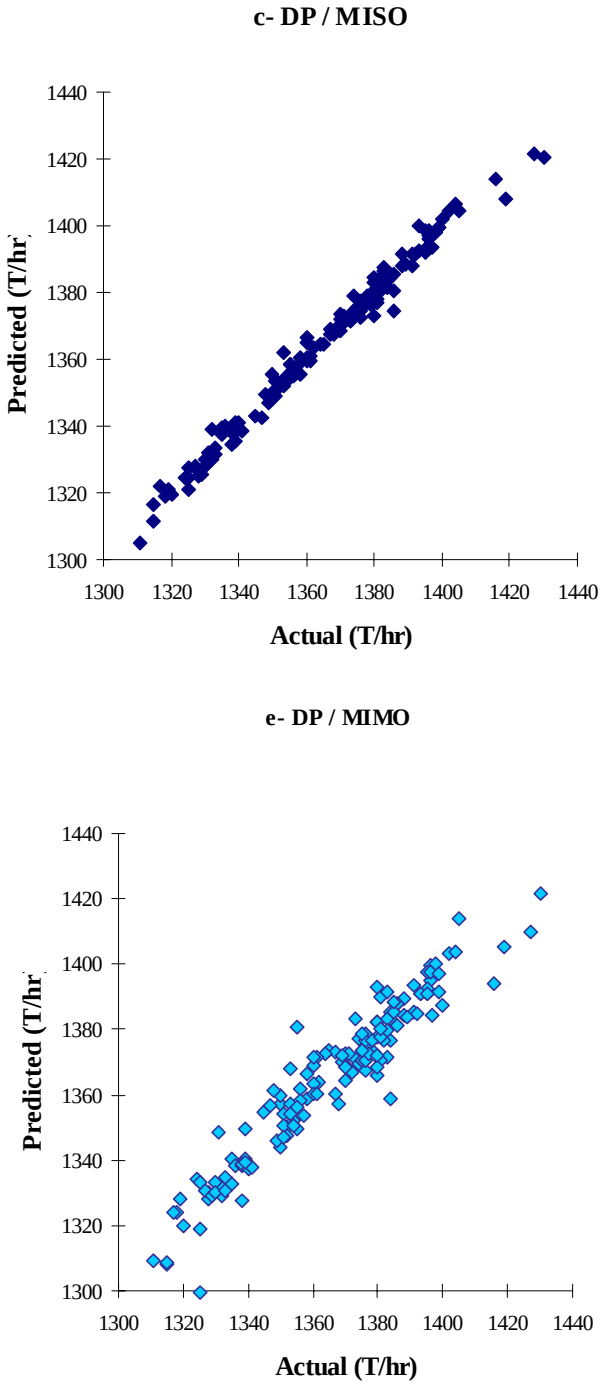

Figure 4.17: Actual and predicted outputs from the MISO and MIMO networks with summer data: (a), (b) TBT networks; (c), (d) DP networks; and (e), (f) STF networks (continued).

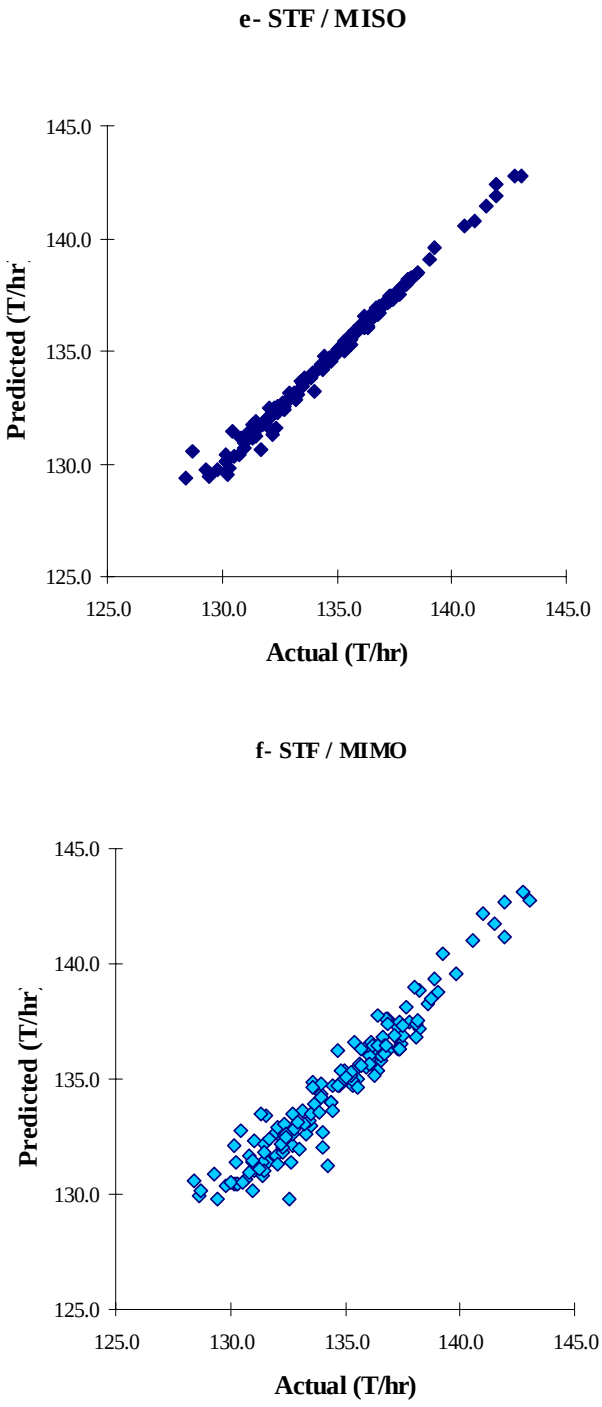

Figure 4.17: Actual and predicted outputs from the MISO and MIMO networks with summer data: (a), (b) TBT networks; (c), (d) DP networks; and (e), (f) STF networks (continued).

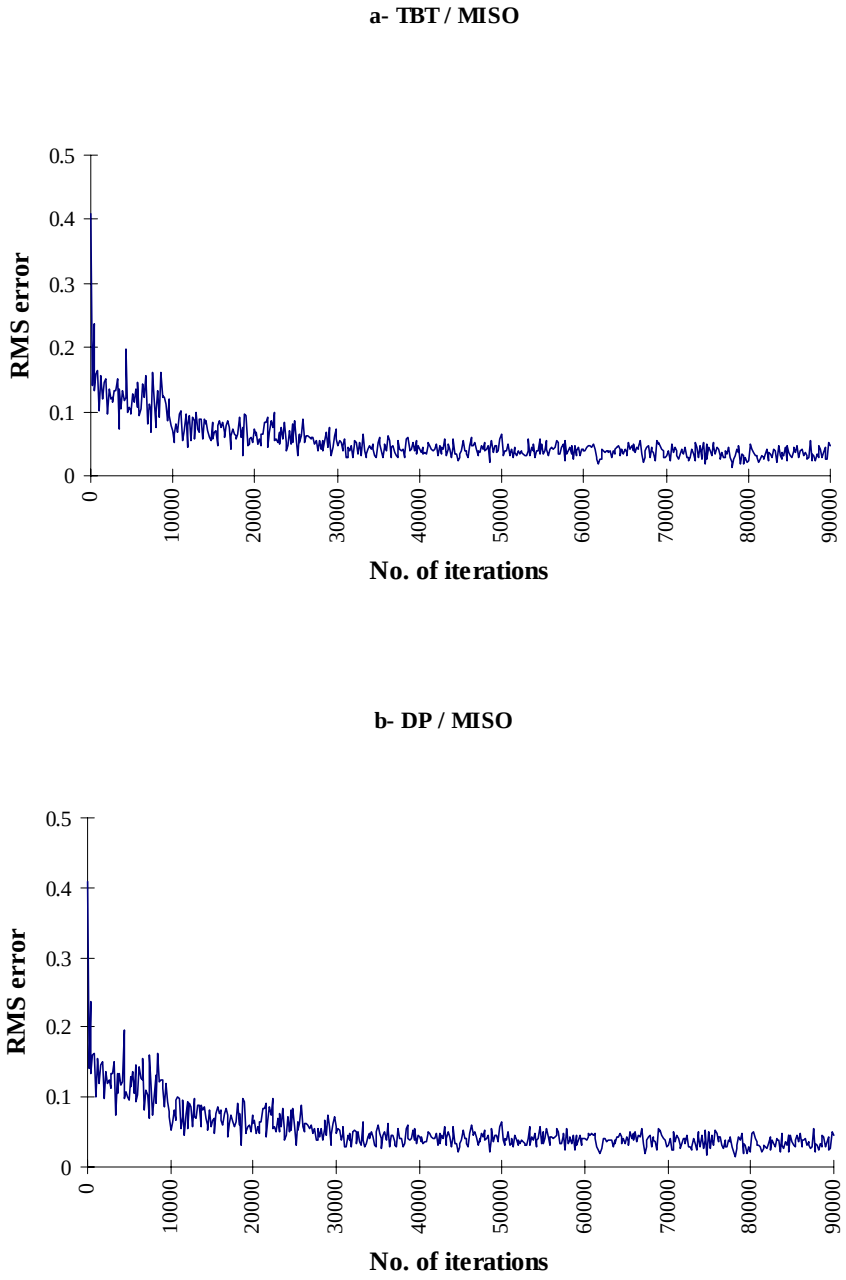

Figure 4.18: RMS errors for the three MISO networks (a), (b), and (c), and for the single MIMO network (d) with winter data.

c- STF / MISO

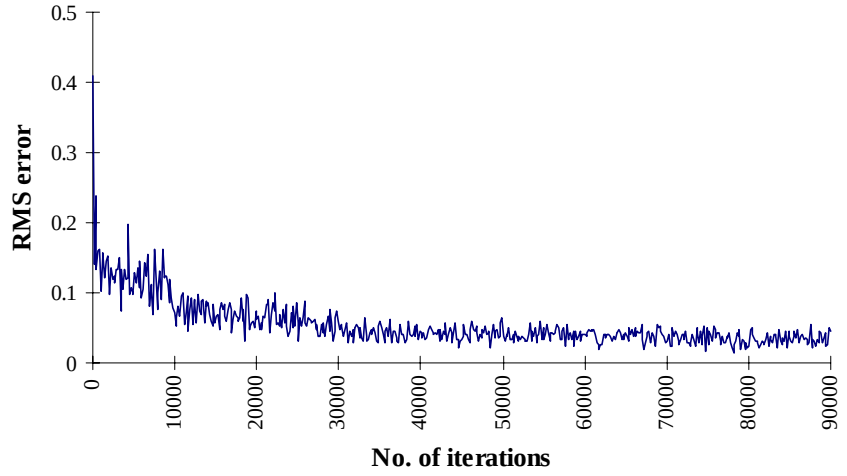

d- MIMO

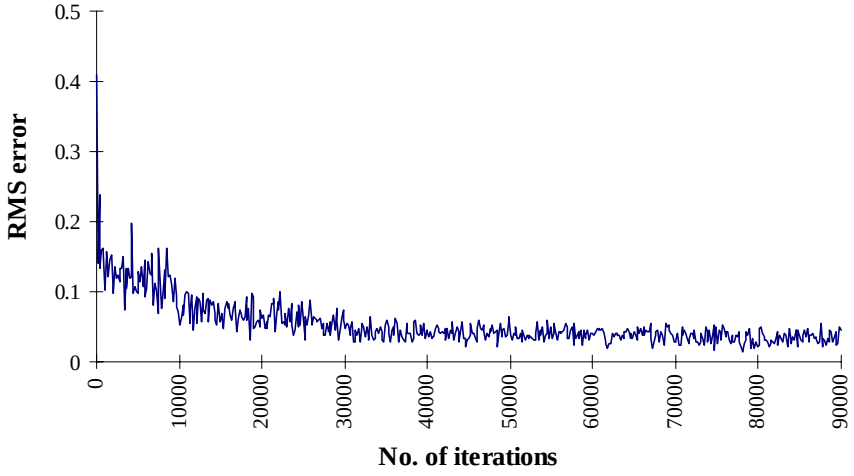

Figure 4.18: RMS errors for the three MISO networks (a), (b), and (c), and for the single MIMO network (d) with winter data (continued).

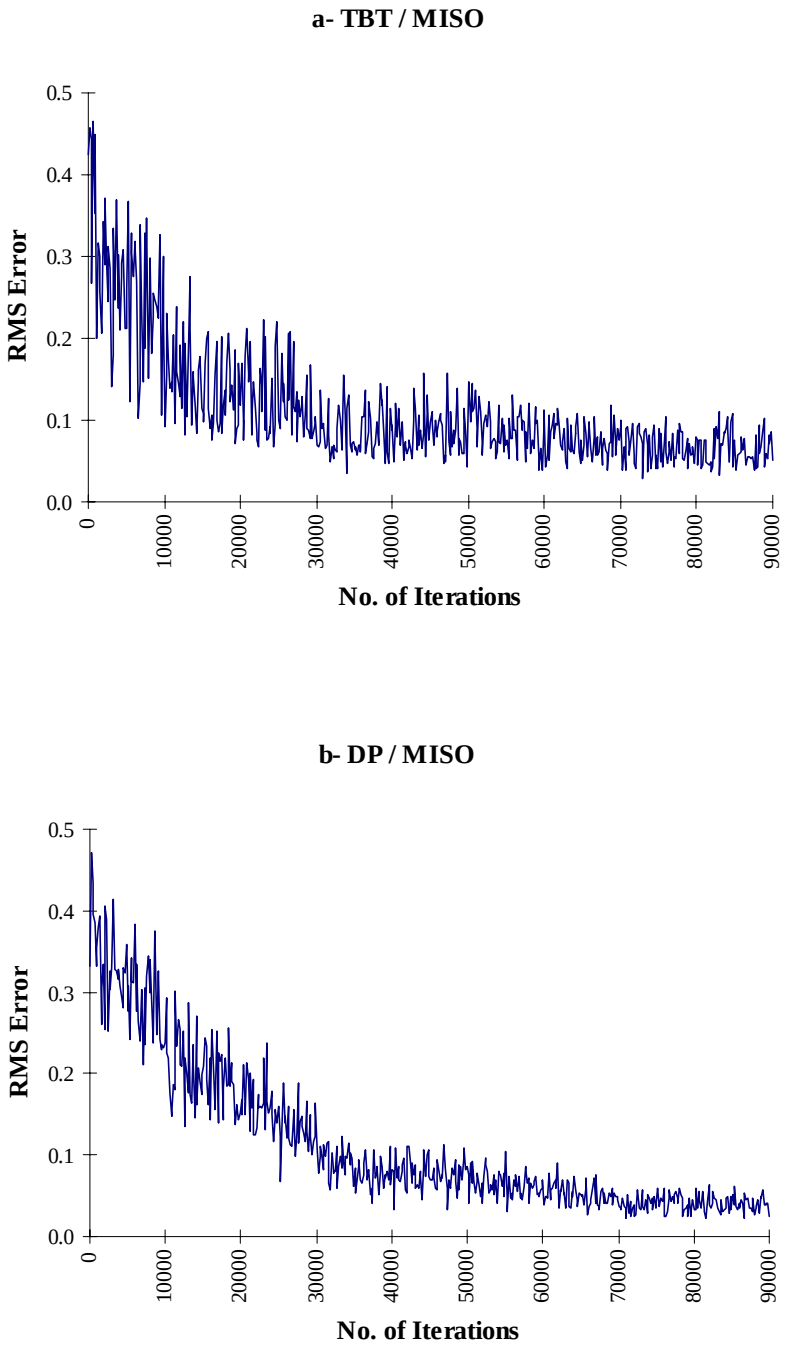

Figure 4.19: RMS errors for the three MISO networks (a), (b), and (c), and for the single MIMO network (d) with summer data.

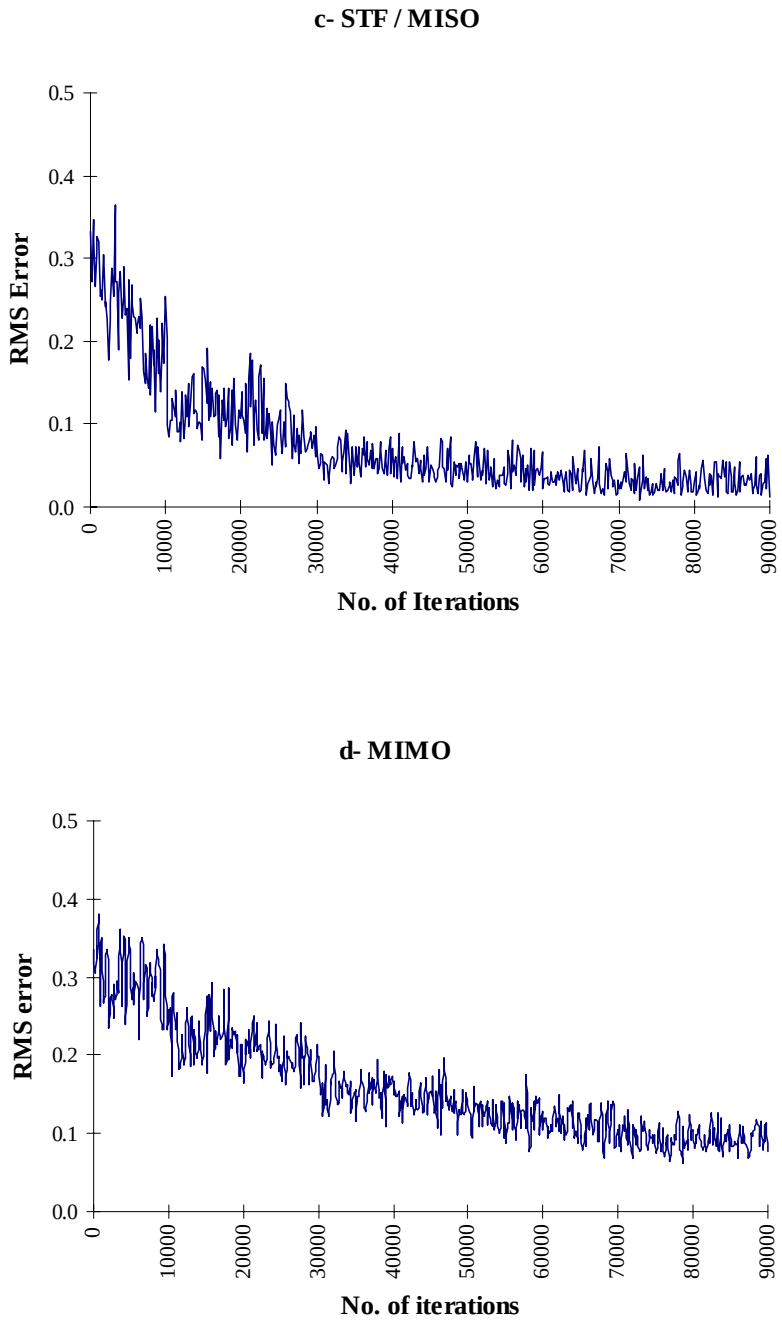

Figure 4.19: RMS errors for the three MISO networks (a), (b), and (c), and for the single MIMO network (d) with summer data (continued).

The decision on whether to use a MIMO or MISO network is affected by a number of considerations. While the MIMO network may be easier to develop and implement, the MISO networks may offer better modeling ability. The network architecture (learning rate, momentum coefficient, etc.), complexity (number of input and output variables) and costs (training time) must be weighed to determine which network design works better. However, the use of MIMO networks may not sacrifice much, if any, model performance. In this investigation, no significant differences exist between the models produced by the MIMO and MISO networks. Although this result is highly dependent upon the problem being modeled and the data used to train the network, the use of MIMO networks should definitely be viewed as a viable method of process modeling.

5. Neural Networks versus Statistical Regression

Figures 4.20 compares the predicted and the actual outputs from the multiple-input-single-output neural networks (MISO) and from statistical regression. The results show that the neural network outperforms the statistical regression, especially for noisy data such as the distillate produced (DP) and the steam flowrate (STF). Table 4.17 shows the average absolute error and the RMS error of both models. The RMS errors for the TBT, DP, and STF in the statistical regression model are 57.5%, 99.5%, and 97.7%, respectively, larger than those of the neural network model.

After fitting the regression model to the given data, we evaluate its adequacy of fit to the data. The most widely used measure is the multiple correlation coefficient R, or more frequently, the square of the multiple correlation coefficient R^2.

R^2 has a range between 0 and 1. When the model fits the data well, the value of the R^2 is close to unity. With a good fit, the observed and the predicted values are close to each other and the residual is small. Therefore, we can use the R^2 value as an overall measure

to judge the model fit to a given data set. We often multiply the R^2 value by 100 to give a percentage fit to regression.

The R^2 values for the TBT, DP, and STF models are: 0.767846, 0.433603, and 0.184604, respectively. These values are indicative of a good model.

Neural networks have been very effective in predicting and optimizing the performance variables of the MSF desalination plants and are capable of handling complex and nonlinear problems. It also outperforms the regression models in prediction problems.

Table 4.16: Average absolute error and RMS error for the MSF plant outputs predicted by the neural network and the statistical regression.

Error type	**Top brine temperature (°C)**		**Distillate produced (T/hr)**		**Steam flowrate (T/hr)**	
	Neural network	Statistical regression	Neural network	Statistical regression	Neural network	Statistical regression
Average abs. error	0.02867	0.09181	0.93293	7.61922	0.30672	2.37108
Max.	0.12483	0.52280	6.08826	79.1100	1.50449	8.29000
Min.	0.00020	0.0001	0.00256	0.03000	0.00063	0.01900
RMS error	0.05459	0.12853	0.06208	11.6521	0.06786	2.99627

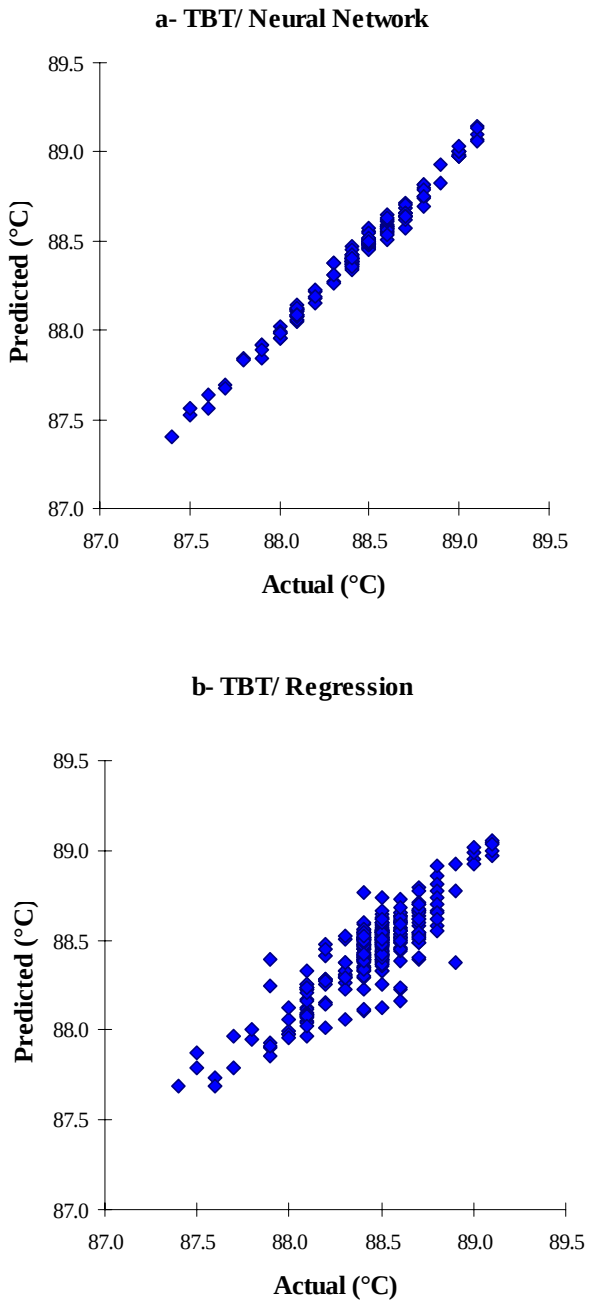

Figure 4.20: Actual and predicted MSF plant outputs from neural network and statistical regression: (a), (b) top brine temperature; (c), (d) distillate produced; and (e), (f) steam flowrate.

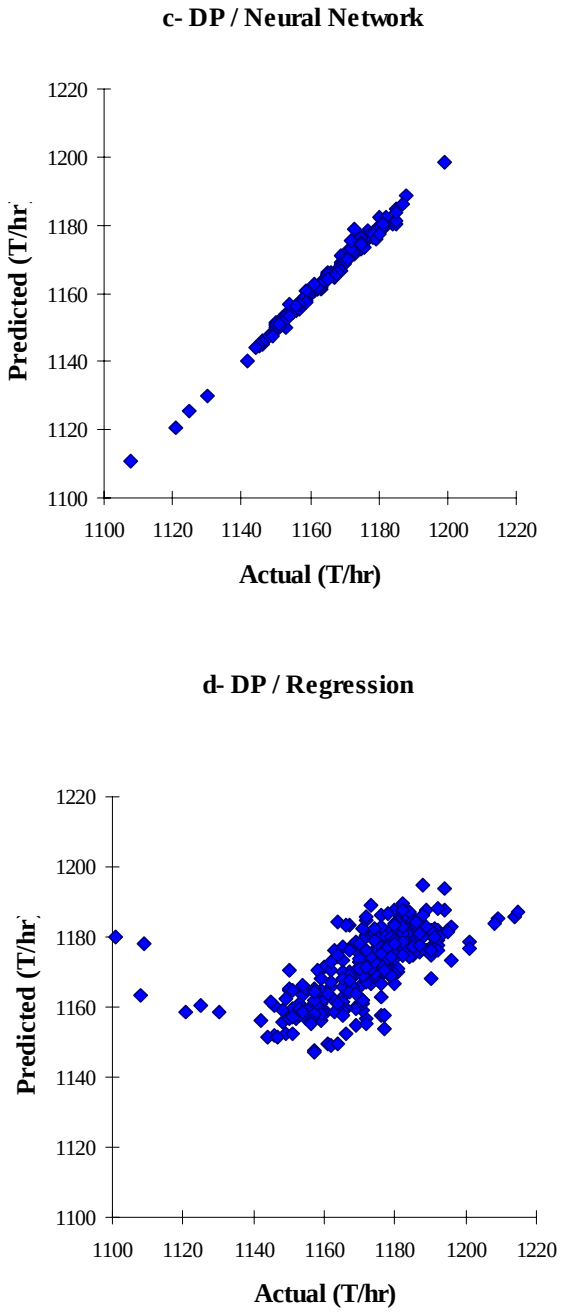

Figure 4.20: Actual and predicted MSF plant outputs from neural network and statistical regression: (a), (b) top brine temperature; (c), (d) distillate produced; and (e), (f) steam flowrate (continued).

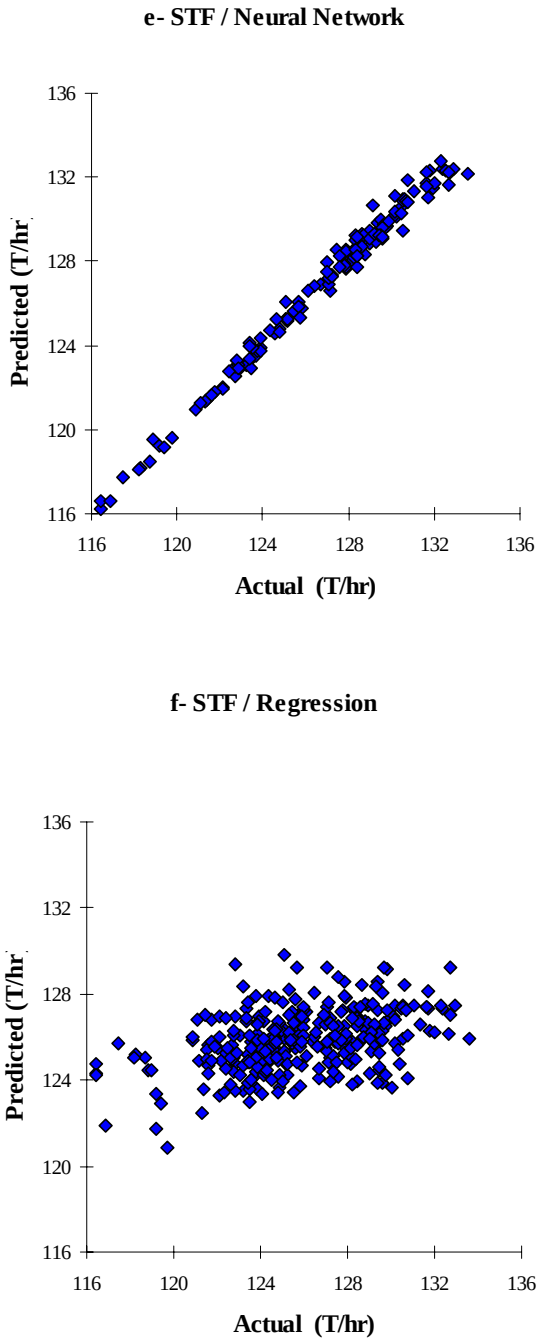

Figure 4.20: Actual and predicted MSF plant outputs from neural network and statistical regression: (a), (b) top brine temperature; (c), (d) distillate produced; and (e), (f) steam flowrate (continued).

4.3 Reverse-Osmosis (RO) Desalination Plant

Jeddah 1-Phase II Seawater Reverse Osmosis Plant in the Kingdom of Saudi Arabia with a capacity of 15 MGPD is the largest seawater reverse-osmosis plant in the world, constructed with the latest and most advanced technology. Therefore, we decide to utilize this plant for our study. The plant specification and design parameters follow.

A. Jeddah 1-Phase II Seawater RO Plant

The Jeddah Seawater RO plant phase II has been in operation since March 1994. It has a capacity of 15 MGPD (56,800 m^3/day). The owner of the plant is Saline Water Conversion Corporation (SWCC) in the Kingdom of Saudi Arabia. Mitsubishi Heavy Industries, Ltd. constructed the plant on a turnkey basis under the supervision of SWCC technical committee in Jeddah. Jeddah 1 RO Plant has a production capacity of 30 MGPD (113,600 m^3/day). Combining phase I and phase II plants gives the largest reverse osmosis desalination plant in the world. TOYOBO double-element-type, hollow-fine-fiber RO modules are used for both plants.

Table 4.17 summarizes the plant specification. The plant capacity is 15 MGPD and guaranteed product quality is 625 mg/l as chloride.

Table 4.17 : Jeddah 1-Phase II Seawater RO plant specification.

Plant:	
Number of trains	10 (trains k to T)
Capacity	1.5 MGPD x 10 trains (5,680 m^3/day each)
Permeate quality (Cl^-)	< 625 mg/l
Operation condition:	
Seawater TDS	43,300 mg/l
Temperature	24-35 C
Recovery ratio	35%
Max feed pressure	70.42kg/cm^3
Silt density index (SDI)*	< 3.0
Module:	
Model	TOYOBO HOLLOSEP HM10255FI
Number of modules	148 pieces x 10 trains
Membrane guarantee	5 years with 10% annual replacement

*: Silt density index (SDI) is the rate of plugging of 0.45-micron filter when the water is passed through the filter at 30 psig.

Figures 4.21 and 4.22 show the process diagram and the plant flowsheet, respectively. The raw seawater from the Red Sea goes through the following pretreatment steps as it enters the plant:

1. Sodium hypochlorite as a disinfectant produced by chlorine generator is injected into seawater. Phase II Plant adopts ”Intermittent Chlorine Injection Method (ICI)”, instead of the conventional “Continuous Chlorine Injection Method (CCI)” in order to prevent membrane degradation by oxidation reaction under the coexistence of special heavy metals and chlorine.
2. A coagulant, ferric chloride is injected before dual-media filter which contains sand and anthracite.
3. Sulfuric acid is injected to control the pH of filtered seawater to prevent formation of scale and membrane degradation.

4. Micron-cartridge filters are installed as a final guard filter for high-pressure pump and modules to remove particles larger than 10 mm.
5. Sodium bisulfite (SBS) is injected into downstream seawater from micron cartridge filters for 7 hours per 8 hours to decompose chlorine. In other words, for one hour per 8 hours, chlorine in seawater disinfect the pipings after injection point of SBS, high-pressure pump and RO modules

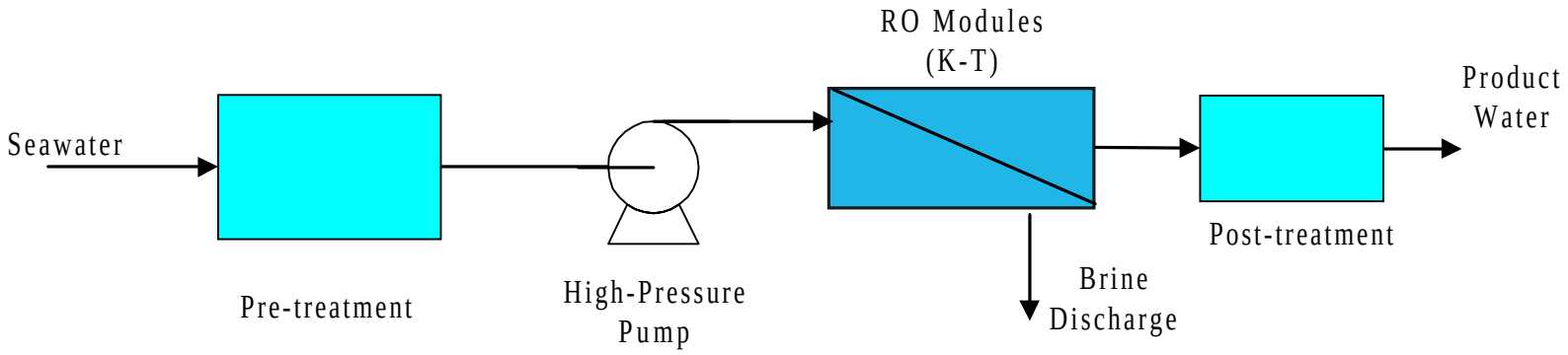

Figure 4.21: Process diagram for a reverse osmosis plant.

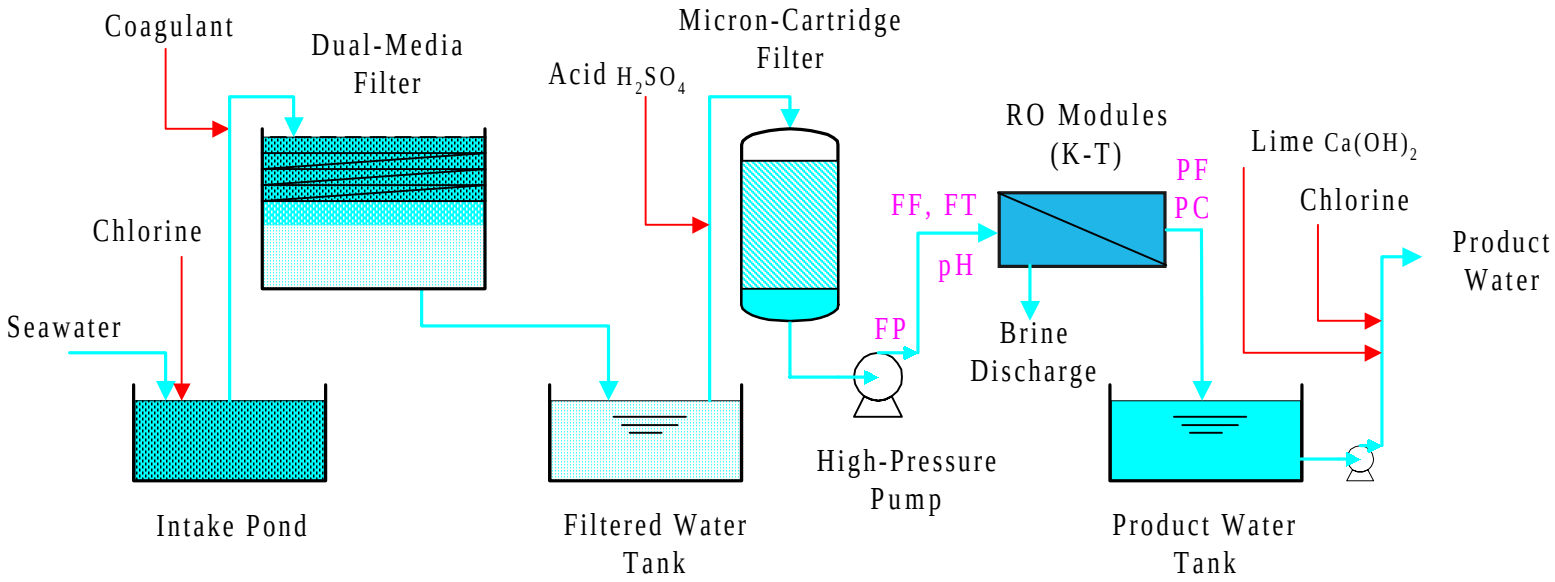

Figure 4.22: Jeddah 1-Phase II RO plant flowsheet.

B. Sampling Size, and Data Collection, Preparation, and Analysis.

In order to monitor accurately the operation of the RO Plant, data of varied nature were logged periodically on log sheets, presented in Appendix A. We record the operating variables from the RO Plant every hour for a period of one month (568 points). The most important operating variables from those collected in the distillation control room (DCR) are feed temperature (FT), feed pressure (FP), feed flowrate(FF), feed pH (pH), product flowrate (PF), product conductivity (PC) of which the most significant are the PF and PC, as describes in section 2.5 of Chapter 2. Figure 4.23 shows the frequency histogram of 6 variables from the RO Plant.

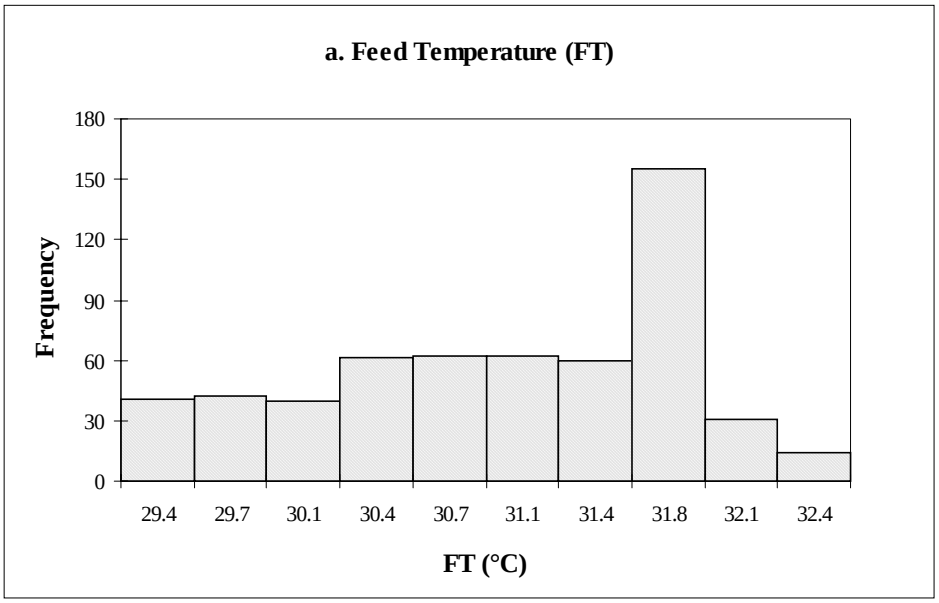

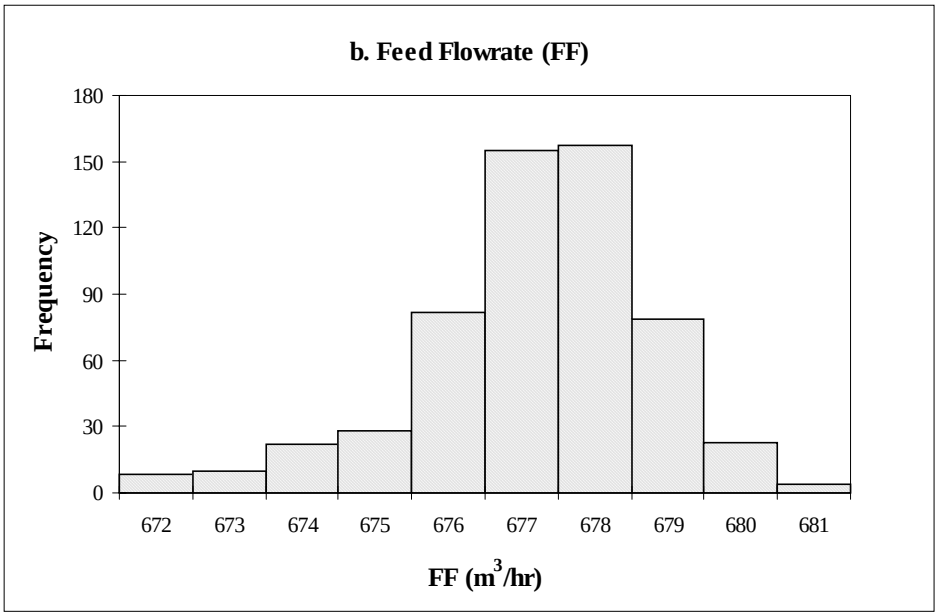

Figure 4.23: Frequency histogram of data from the RO Plant.

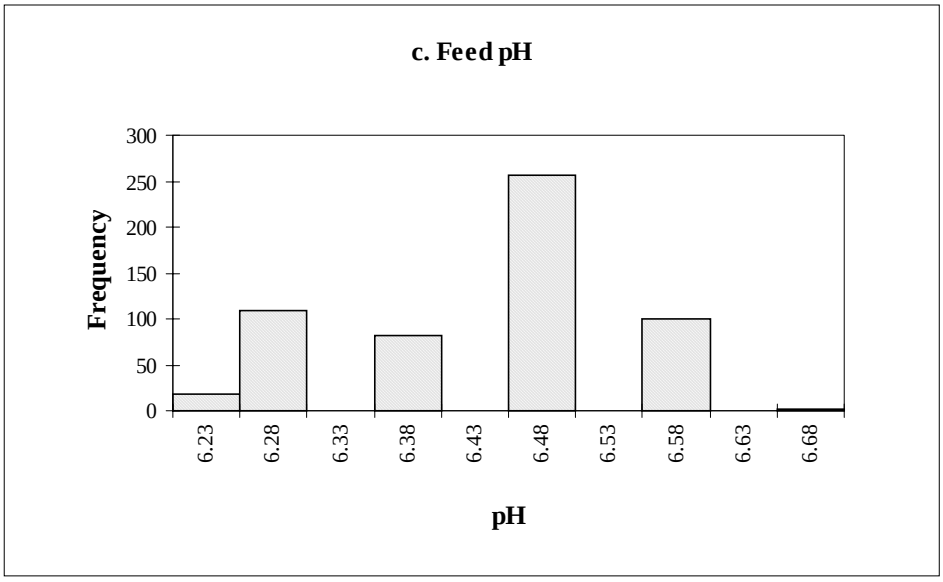

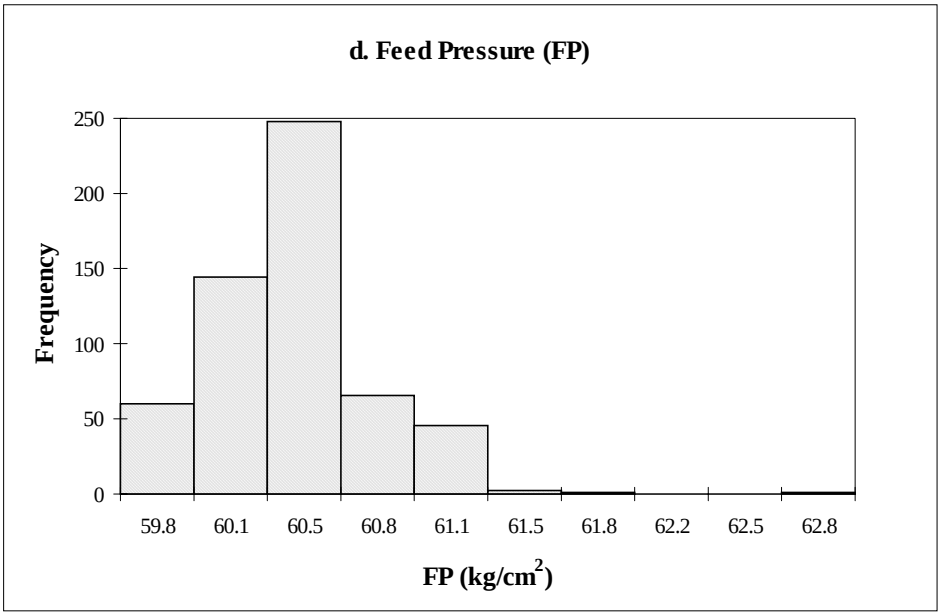

Figure 4.23: Frequency histogram of data from the RO Plant (continued).

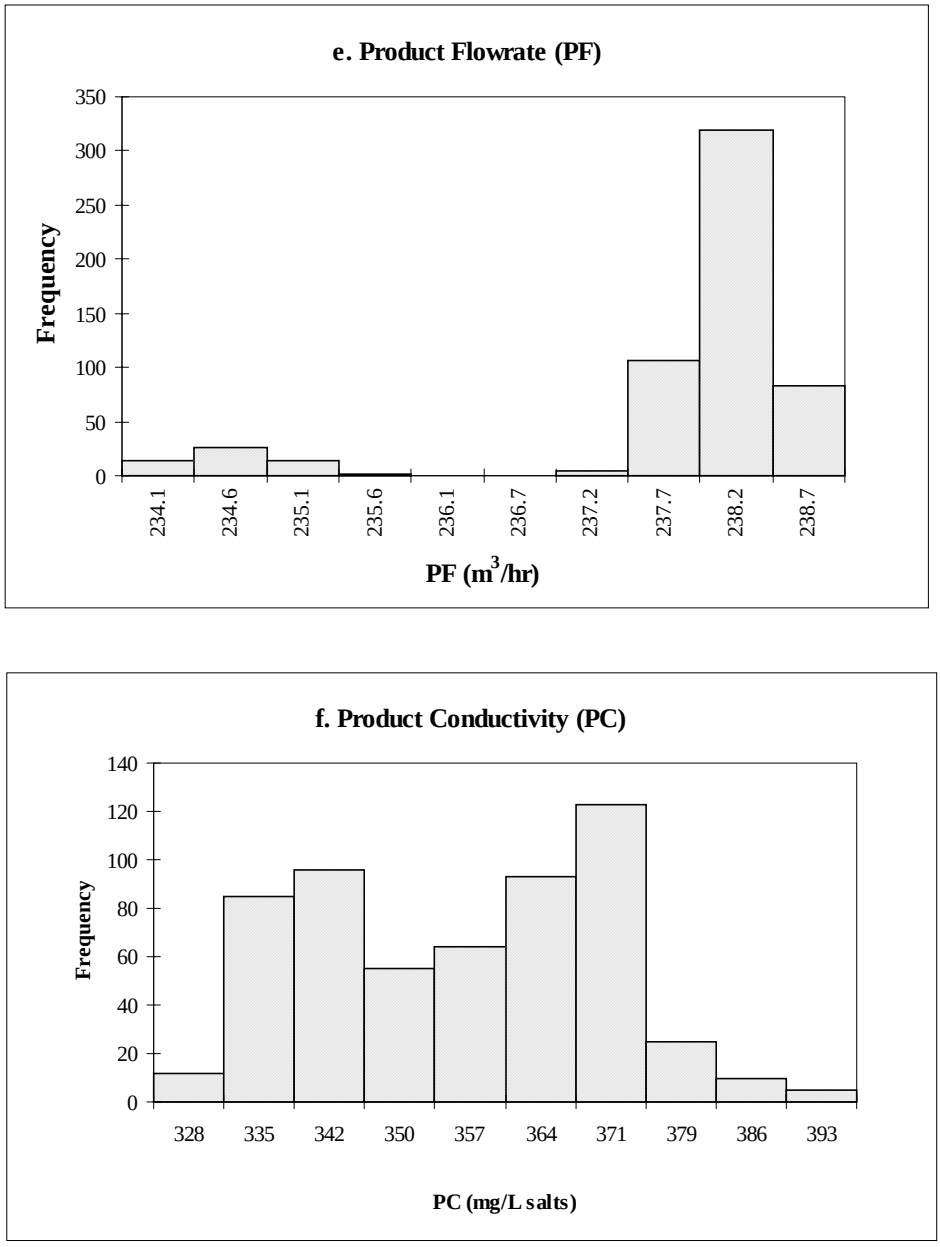

Figure 4.23: Frequency histogram of data from the RO Plant (continued).

C. Input-Variable Selection

The factor analysis for variable selection in the MSF networks is also used for the RO networks. Table 4.18 shows the resulting factor loadings with 6 variables and 2 factors.

Table 4.18: Estimated rotated factor loading with 6 variables.

Variable	**Estimated rotated factor loading (568 observations)**	
	F_1	F_2
PC	**0.72389**	0.05759
PF	-0.03261	**0.98320**
FT	**0.82904**	0.07543
FP	**-.069526**	0.32906
FF	0.00044	**0.97995**
pH	**0.60261**	0.01748

Factor 1 (F_1) in Table 4.18 has high loadings for variables FT, PC, FP, and pH, and smaller loadings for the rest. Factor 2 (F_2) has high loadings for variables PF, FF, and FP with much lower loadings for the other variables.

Factor columns in the matrix represent the dependent variables. As in the MSF analysis, the dependent variable's row with the largest loading is determined, and the column in which this value is located indicates the appropriate factor match for the dependent variable. From the table, we identify the most significant dependent variables as the product flux (PF) and product conductivity (PC).

Table 4.19 illustrates the variables selected based on engineering knowhow and factor analysis for the prediction network for the product flux (PF) and product conductivity (PC).

We compare the performance of the RO models using the two approaches for variable selection involving four multiple-input-single-output (MISO) networks for the two dependent variables, product flux (PF) and the product conductivity (PC). We use the same network architecture as that used previously for the MSF network (Table 4.14).

Table 4.20 and Figures 4.24 and 4.25 show the recall and generalization results from training all MISO networks using engineering knowhow and factor analysis for input-variable selection. Table 4.20, the recall and generalization tests results of the four MISO networks, indicate that the networks using engineering knowhow for input-variable selection are superior to those using factor analysis.

Table 4.19: Input variables recommended for the RO network by engineering knowhow and by factor analysis.

Engineering knowhow	**Factor analysis**	
Product flux and conductivity (PF and PC)	Product flux (PF)	Product conductivity (PC)
Feed temperature Feed pressure Feed flowrate Product pH	Feed flowrate Feed pressure	Feed temperature Feed pressure Product pH

Table 4.20: Average absolute recall and generalization errors for the MISO Networks.

Error type	**Factor analysis**		**Engineering knowhow**	
	PF (2 inputs)	PC (3 Inputs)	PF (4 inputs)	PC (4 Inputs)
Recall average absolute error				
Max.	0.25512	4.05776	0.22478	3.88995
Min.	3.62289	15.74759	0.76678	14.91415
	0.00391	0.00430	0.00067	0.03540
Generalization average absolute error				
Max.	0.28948	5.98129	0.23897	4.98043
Min.	4.09080	23.89441	1.05955	19.42749
	0.00095	0.01904	0.00049	0.00348

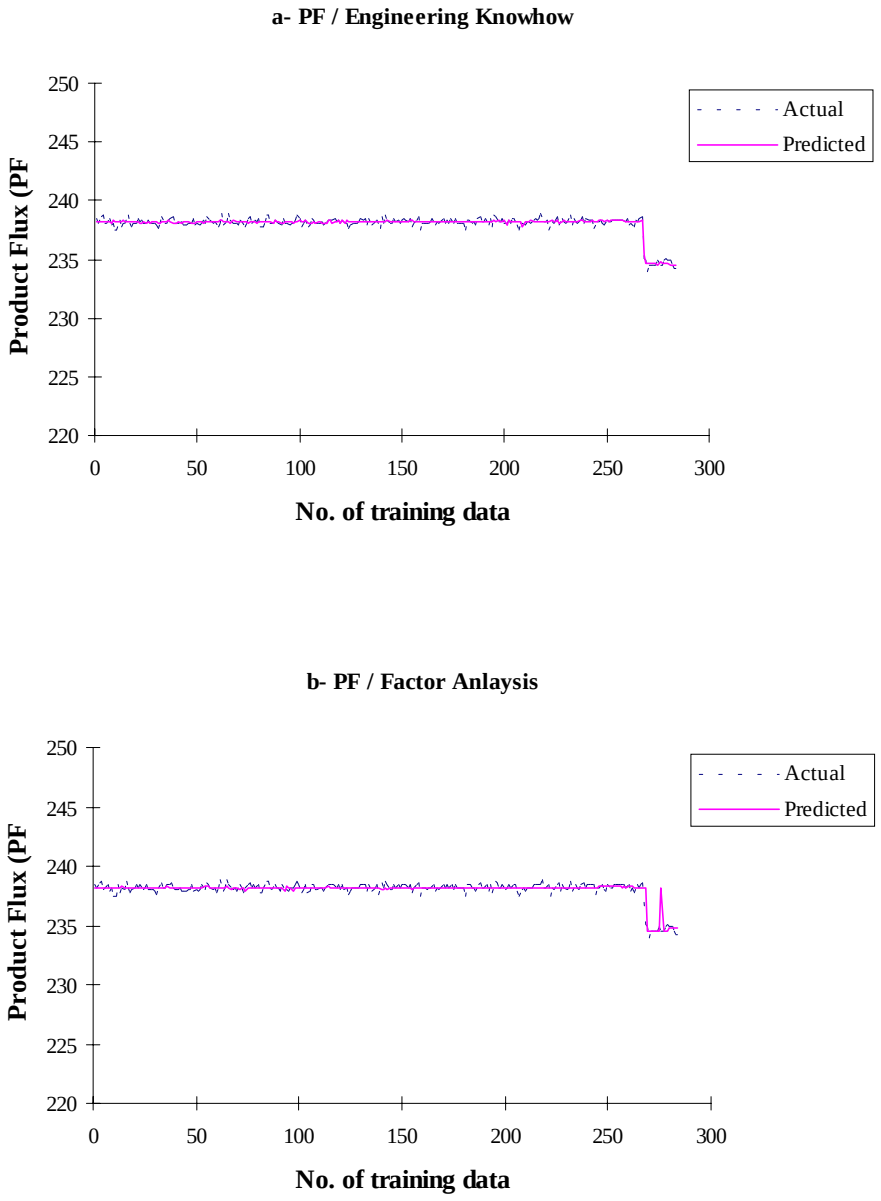

Figure 4.24: Actual and predicted product fluxes (PFs) and product conductivities (PCs) from recall networks based on engineering knowhow and factor analysis for input-variable selection.

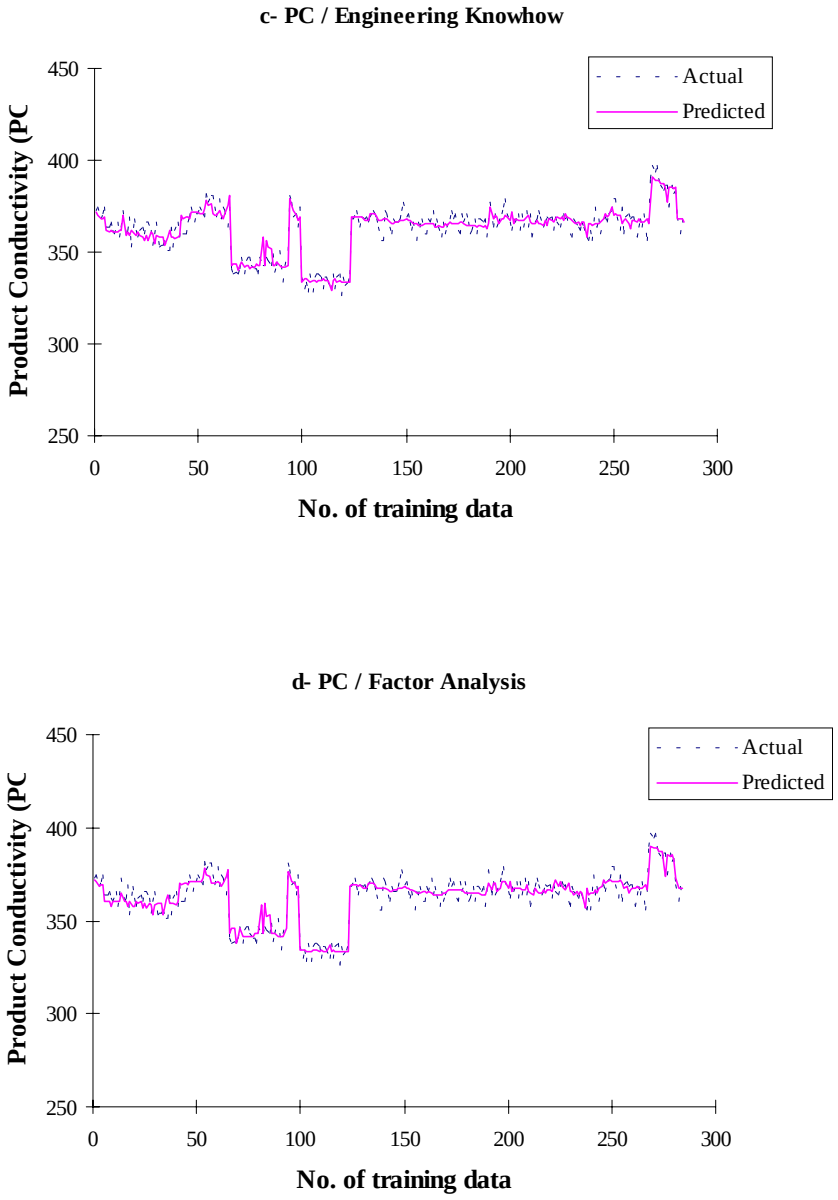

Figure 4.24: Actual and predicted product fluxes (PFs) and product conductivities (PCs) from recall networks based on engineering knowhow and factor analysis for input-variable selection (continued).

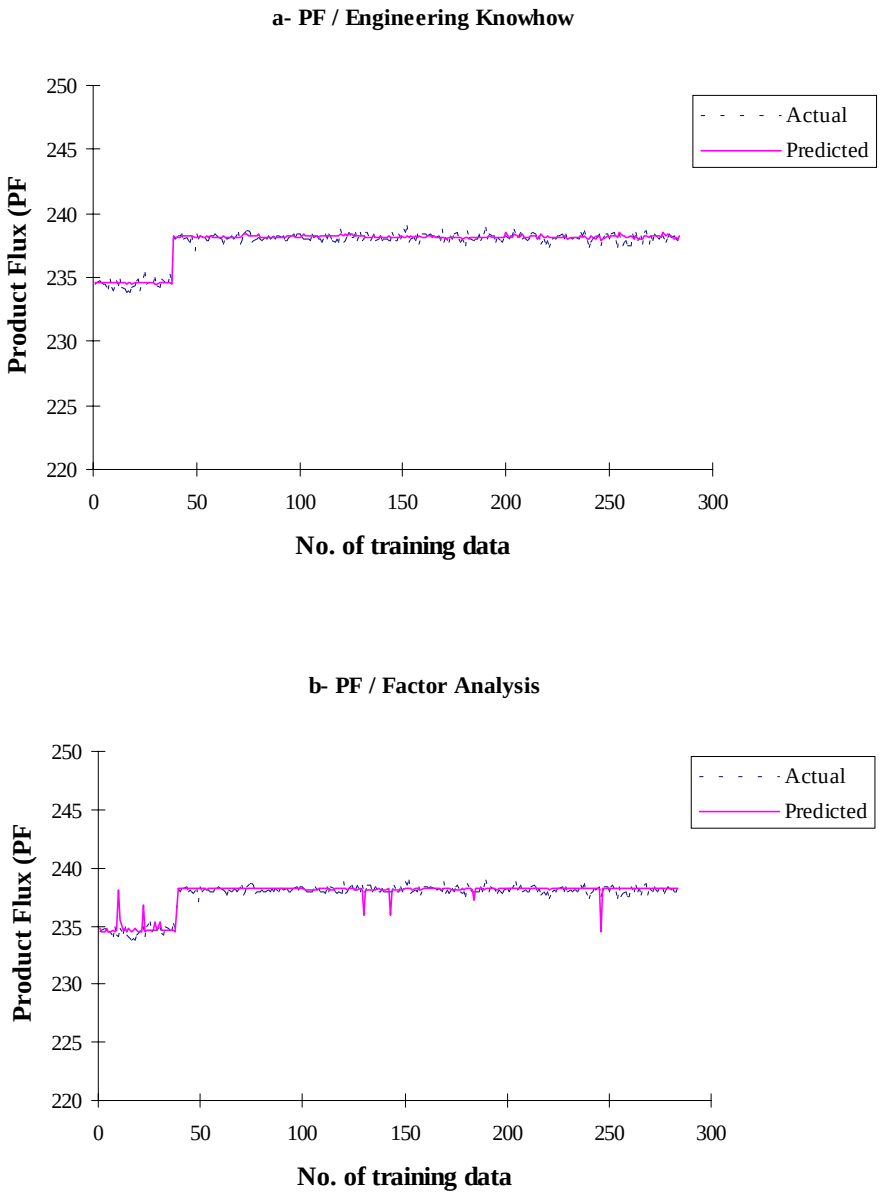

Figure 4.25: Actual and predicted PFs and PCs from generalization networks based on engineering knowhow and factor analysis for input-variable selection.

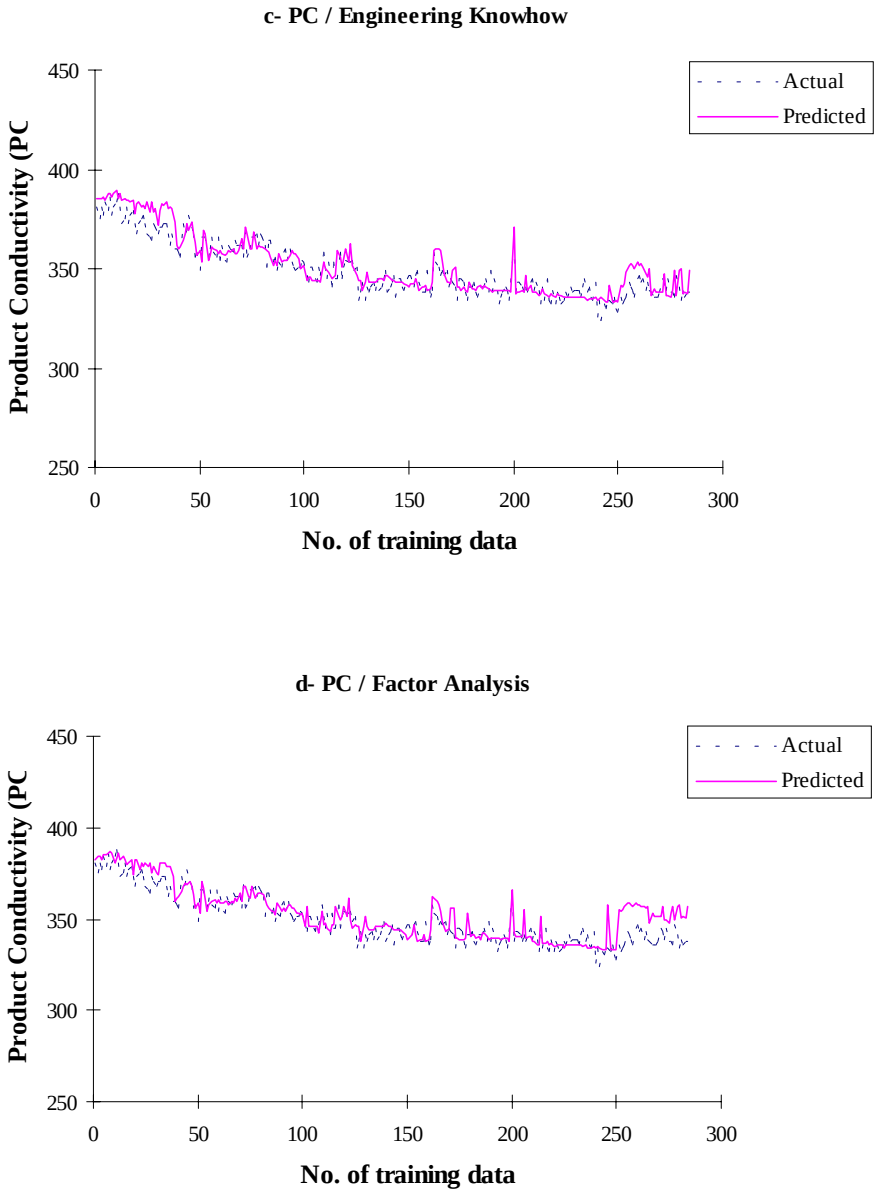

Figure 4.25: Actual and predicted PFs and PCs from generalization networks based on engineering knowhow and factor analysis for input-variable selection (continued).

Table 4.21 shows that the RMS errors for engineering-knowhow networks are lower than those of factor-analysis networks. This is seen in Figure 4.26 for both PF and PC networks, although the differences are only minor.

Table 4.21: RMS errors for PFs and PCs networks based on engineering knowhow and factor analysis for input-variable selection.

Variable-selection approach	**Product flux (PF)**	**Product conductivity (PC)**
Engineering knowhow	0.09914	0.12072
Factor analysis	0.11711	0.12276

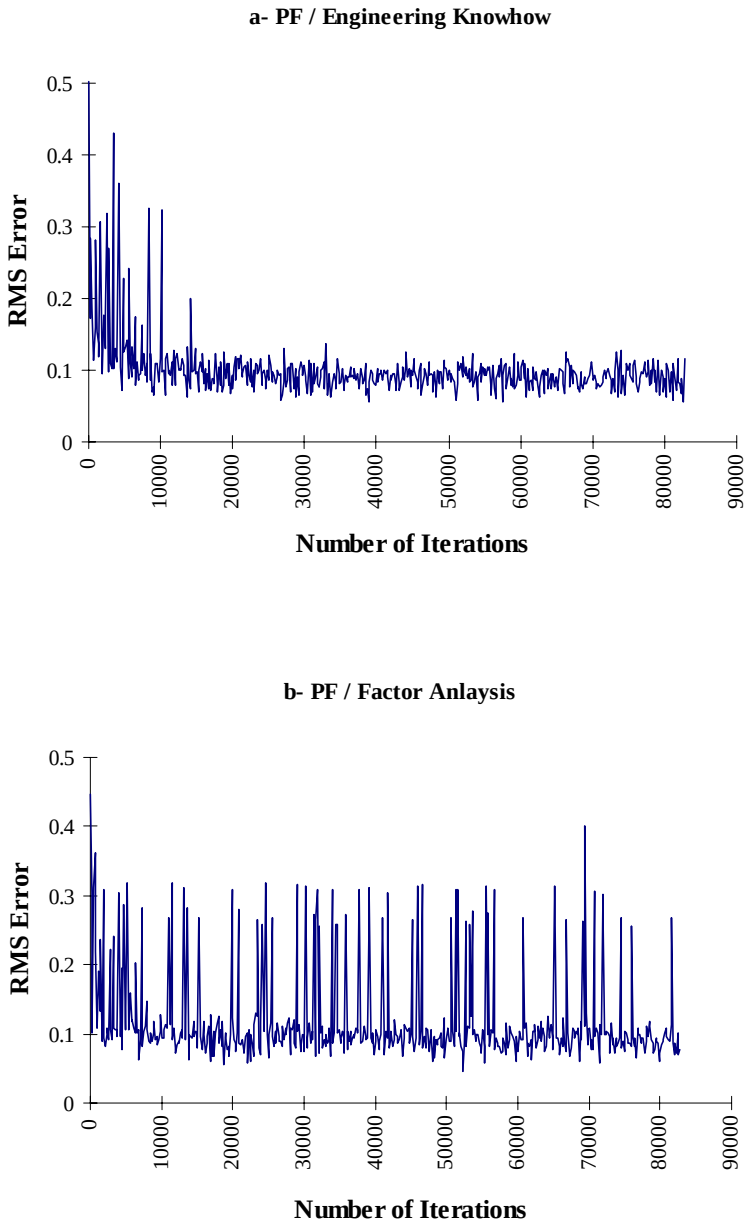

Figure 4.26: RMS errors for PFs and PCs networks based on engineering knowhow and factor analysis for input-variable selection.

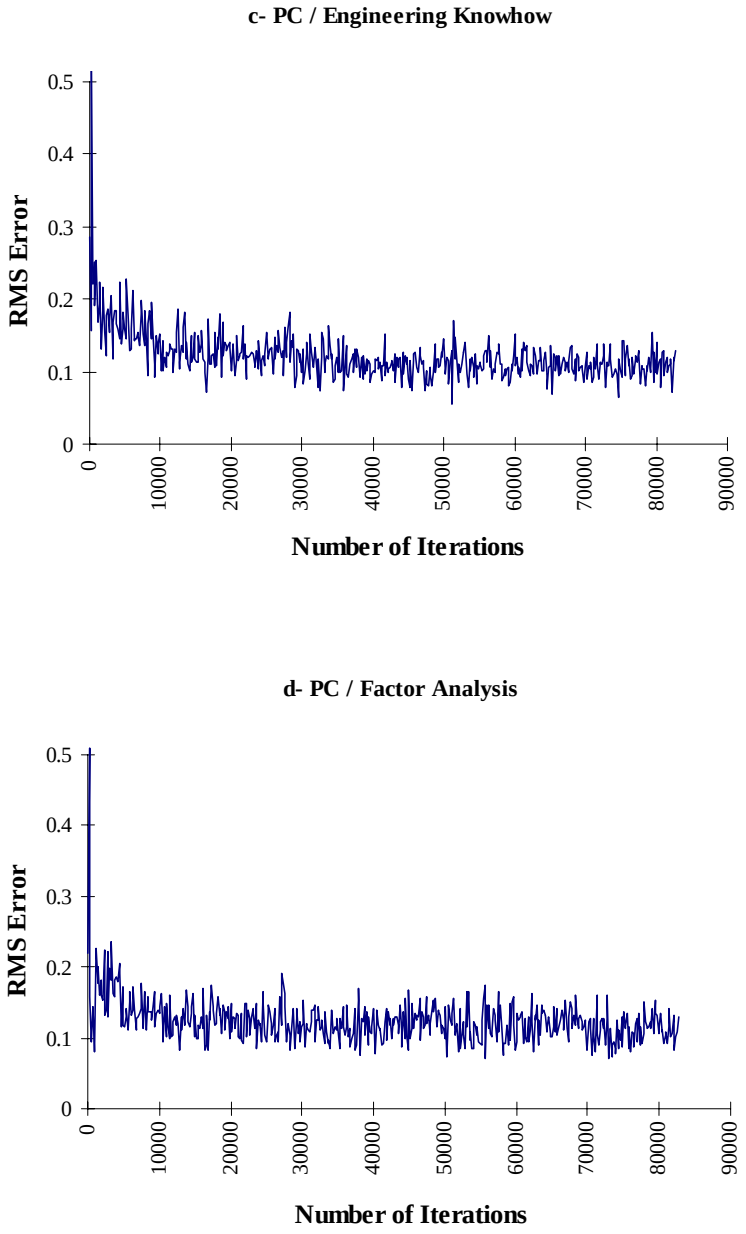

Figure 4.26: RMS errors for PFs and PCs networks based on engineering knowhow and factor analysis for input-variable selection (continued).

D. Model Development and Optimization

We compare the two types of networks, MISO and MIMO, using three networks. Specifically, we develop two MISO networks, each using one of the two identified output variables, product flux (PF) and product conductivity (PC). The architecture of the MISO network is [4:30:15:1]. We also develop one MIMO network and train it using the two outputs together. Therefore, the network architecture is [4:30:15:2]. The input variables for all three networks are feed tmperature (FT), feed pressure (FP), feed flowrate (FF), and feed pH (pH). The same network architecture used for the MSF prediction network is used here for the RO prediction network. We choose data from Train T (568 points) for their good trend to accomplish this work. The data are divided into two equal portions (284 points in each set) for the training and the testing sets. Table 4.22, and Figures 4.27 and 4.28 show recall and generalization results from training the MIMO and the MISO networks.

Table 4.22: Average absolute recall and generalization errors for MISO and MIMO networks.

Error type	**MIMO network**		**MISO network**	
	PF	PC	PF	PC
Recall average absolute error	0.22209	3.87751	0.22478	3.88995
Max.	0.79578	13.34421	0.76678	14.91415
Min.	0.00314	0.03586	0.00067	0.03540
Generalization average absolute error	0.24698	4.77423	0.23897	4.98043
Max.	1.02112	17.65421	1.05955	19.42749
Min.	0.00011	0.00418	0.00049	0.00348

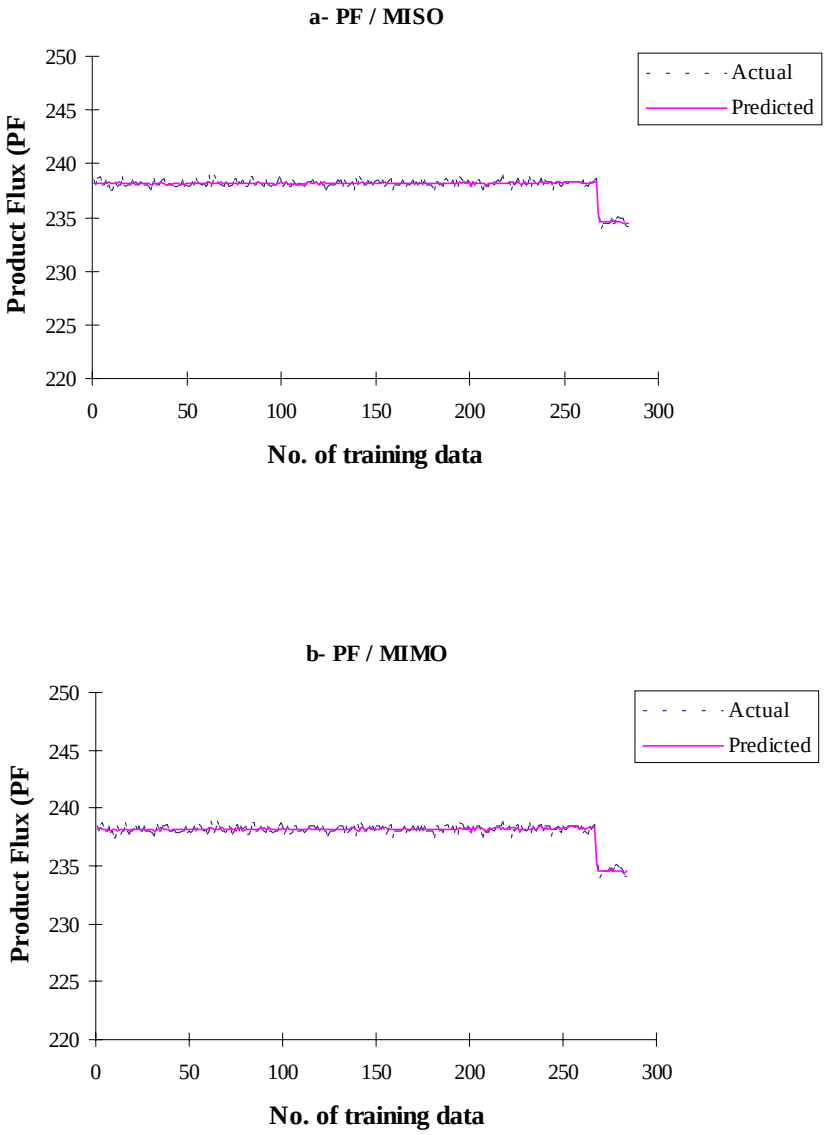

Figure 4.27: Actual and predicted PFs and PCs from recall test for MISO and MIMO networks.

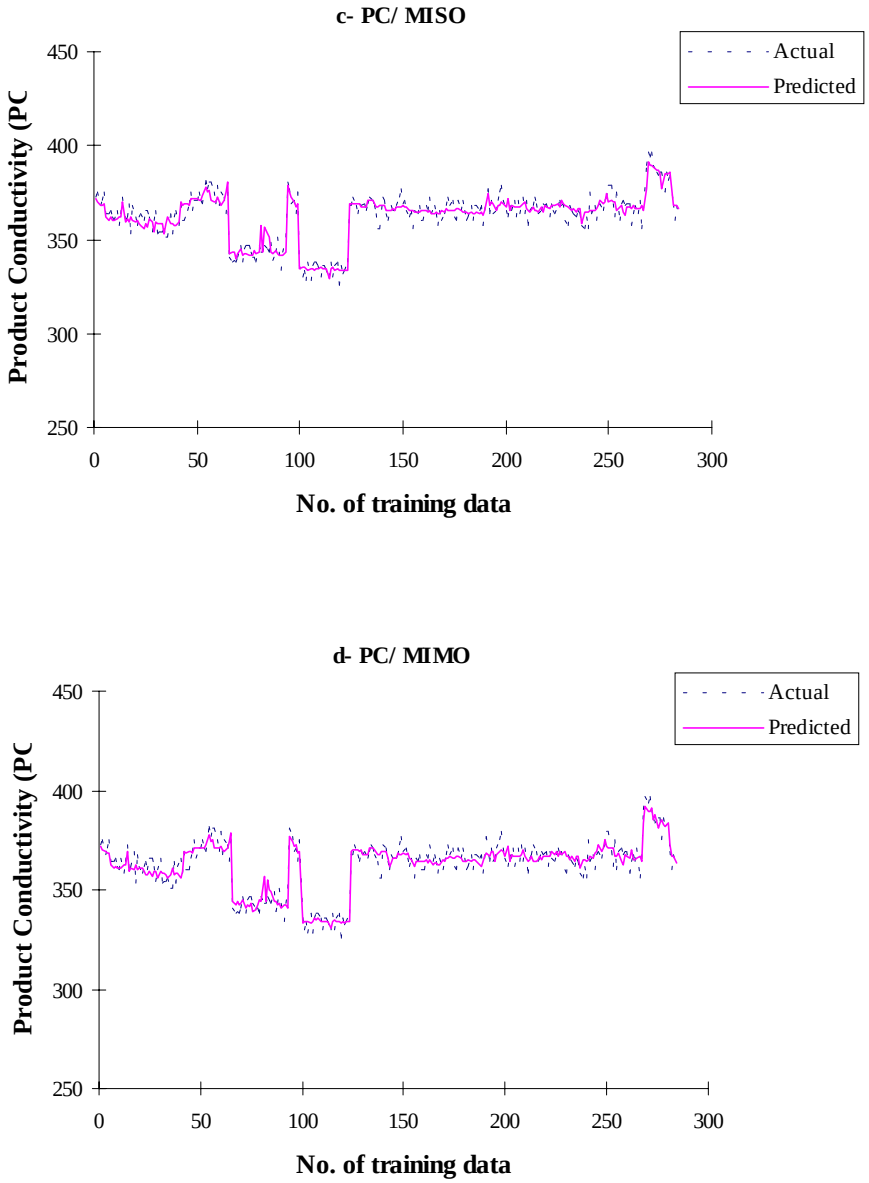

Figure 4.27: Actual and predicted PFs and PCs from recall test for MISO and MIMO networks (continued).

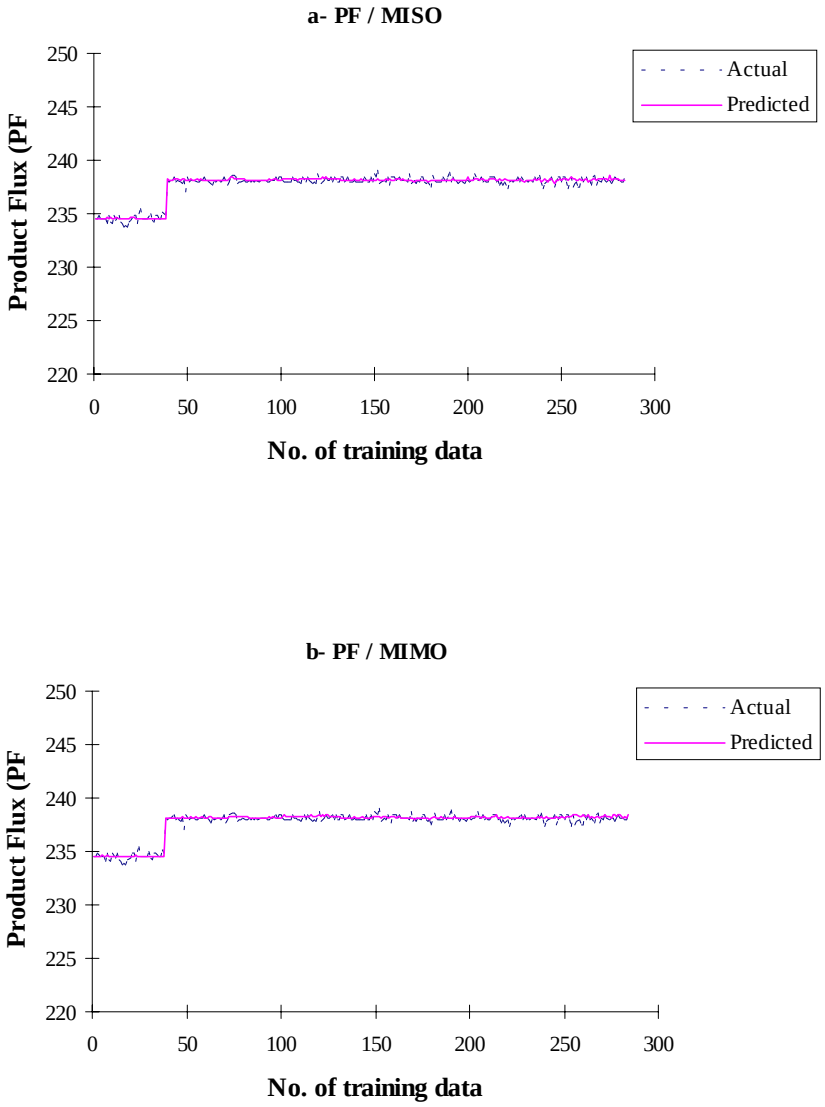

Figure 4.28: Actual and predicted PFs and PCs from generalization test for MISO and MIMO networks.

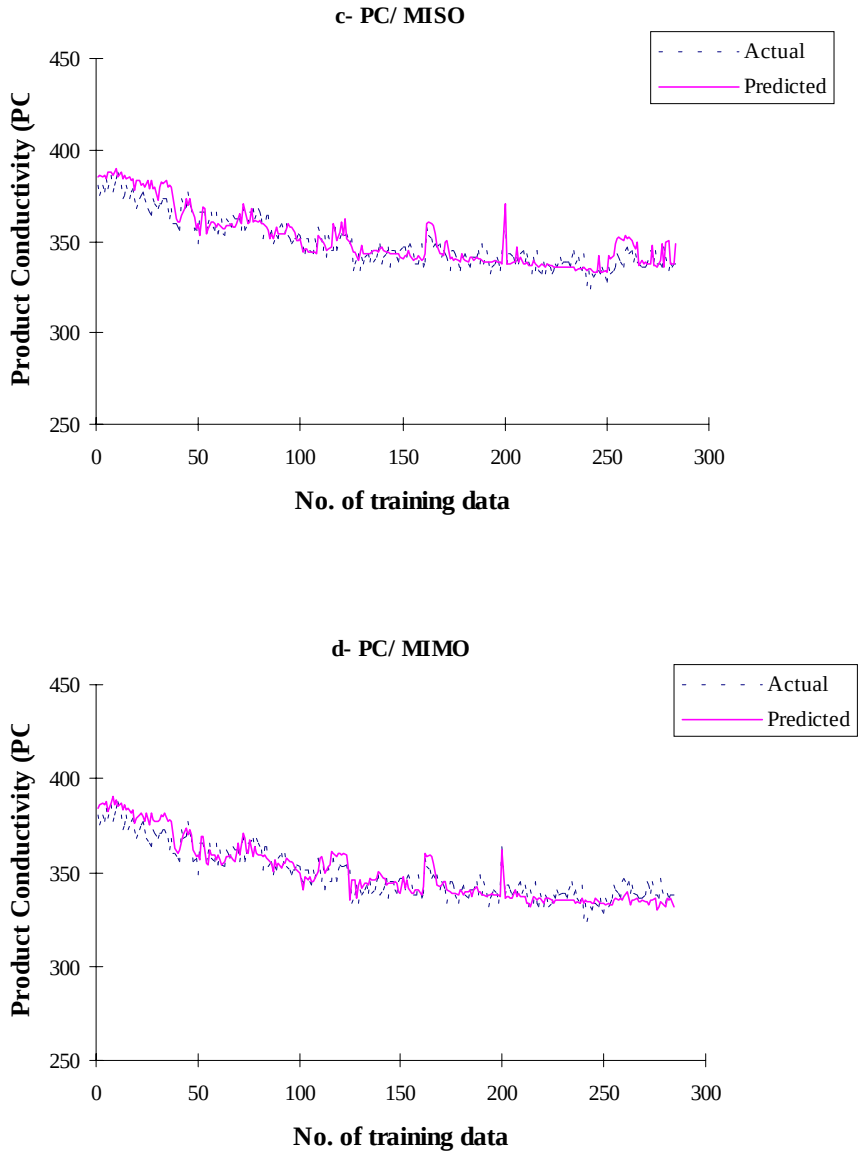

Figure 4.28: Actual and predicted PFs and PCs from generalization test for MISO and MIMO networks (continued).

The results for recall tests indicate that there is no significant difference between the MISO and MIMO networks. For PF, the average absolute error only differs in the thousandths, and the maximum error differs by only 0.03 m^3/hr, or 0.013% of the average flux. For PC, the largest difference between MISO and MIMO networks is about 1.6 mg/l, or 0.36% of the average conductivity. These differences are too small to be significant.

The generalization results also provide evidence that MISO and MIMO networks produce models of similar accuracy. The PF generalization results for both types of networks are almost identical. The average error differs by only 0.01 m^3/hr, or 0.004% of the average flux. The differences between the maximum and minimum errors are similarly insignificant. For PC, the largest difference between the MISO and MIMO networks is about 0.5% of the average conductivity. Again, no real difference in prediction accuracy results between MISO and MIMO networks.

As illustrated in Table 4.23, and Figure 4.29, the RMS errors for all three networks are in the range of 0.1. The difference between RMS results can be attributed to the type of output data with which the network is trained, rather than the number of output variables used.

Table 4.23: RMS errors for MIMO and MISO networks.

MIMO network (PF and PC)	**MISO network** (PF)	(PC)
0.11157	0.09914	0.12072

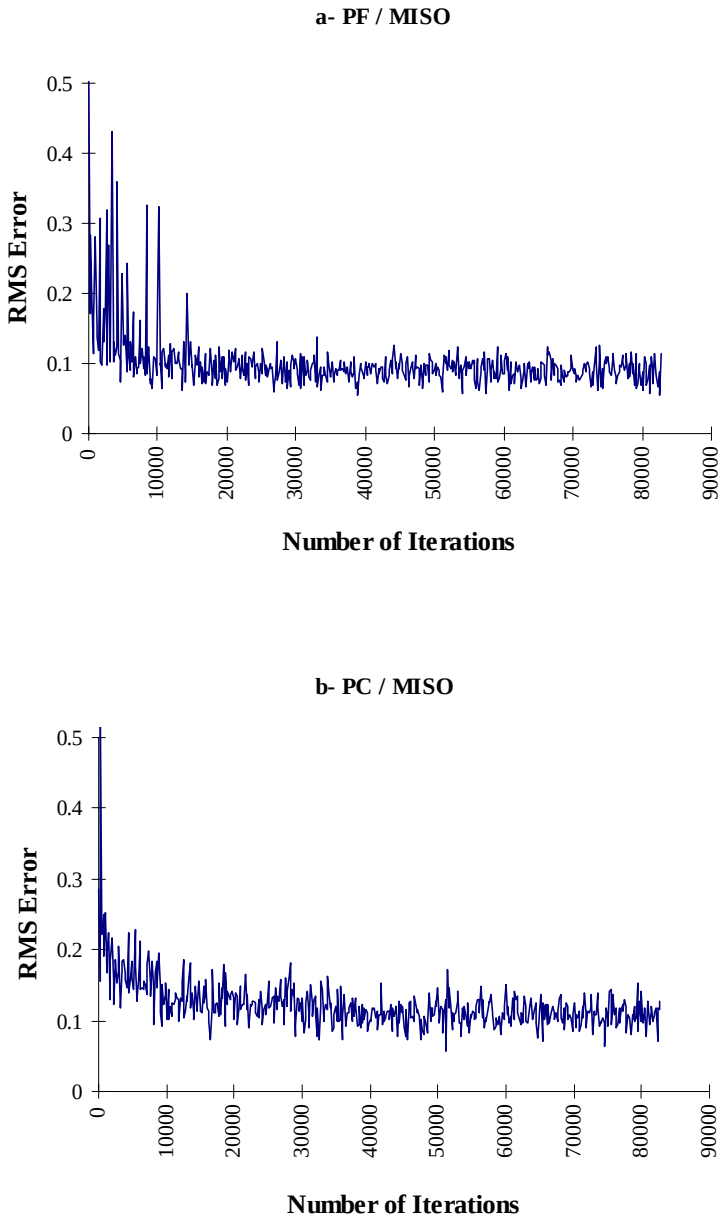

Figure 4.29: RMS errors: (a), (b) MISO network; and (c) MIMO network.

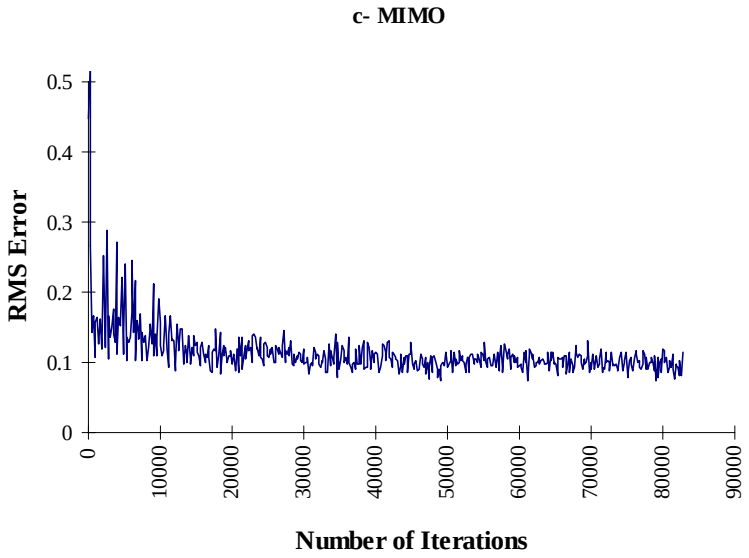

Figure 4.29: RMS errors: (a), (b) MISO network; and (c) MIMO network (continued).

E. Training and Generalization Tests for RO Trains

Based on the above results, we train the RO model with input variables selected on the basis of engineering knowhow. As presented in Table 4.17, Jeddah 1-Phase II Seawater RO Plant consists of ten trains (K-T). We model all the trains as follows.

The recommended effective ranges of learning rate, momentum coefficient and hidden nodes as mentioned in Baughman and Liu (1995) and successfully tested for the MSF model are as follows: (1) a learning rate of 0.3 which decreases as we progress between the hidden layers and as the number of iterations increases, (2) a momentum coefficient of 0.4 which remains constant between the hidden layers but decreases as the number of iterations increases, and (3) two hidden layers with 30 and 15 nodes. Training and testing sets of 284 example sets are used for each network. We apply the backpropagation algorithm, the delta learning rule, and the hyperbolic tangent transfer function. The maximum number of training iterations is 90,000 and the epoch size is fixed at 16 examples.

Table 4.24, Figures 4.30 and 4.31 show that the prediction performance of the ten trains (K-T) is very good. Train O has the highest recall and generalization errors for the PF network, and train Q has the highest recall and generalization errors for the PC network. The recall and generalization errors for the product conductivity (PC) is higher than that for the product flux (PF), but are still within an acceptable range. The errors could be related to the noise and fluctuation in PC values during operation and to the physical nature of the PC variable. Figure 4.32 displays the RMS errors of trains K-T. Train S has the minimum RMS error of 0.0822 and train M has the maximum RMS error of 0.2403.

Table 4.24: Average absolute recall, generalization, and RMS errors for all trains in the MIMO RO networks.

Average absolute error for PF network	**Train number** K	L	M	N	O	P	Q	R	S	T
Recall	0.3087	0.178	0.375	0.237	0.881	0.4785	0.833	0.239	0.327	0.222
Generalization	0.3037	0.1638	0.3466	0.2488	1.0283	0.5002	1.001	0.4522	0.4517	0.2470

Average absolute error for PC network	**Train number** K	L	M	N	O	P	Q	R	S	T
Recall	2.3743	1.784	1.6379	3.8964	5.9465	1.9208	6.9335	2.738	2.4659	3.8775
Generalization	2.2799	1.9237	1.9561	3.0577	4.6481	2.0519	6.0894	2.8388	2.9403	4.7742

	Train number K	L	M	N	O	P	Q	R	S	T
RMS error	0.1940	0.1995	0.2403	0.2191	0.1235	0.1961	0.1219	0.1982	0.0822	0.1116

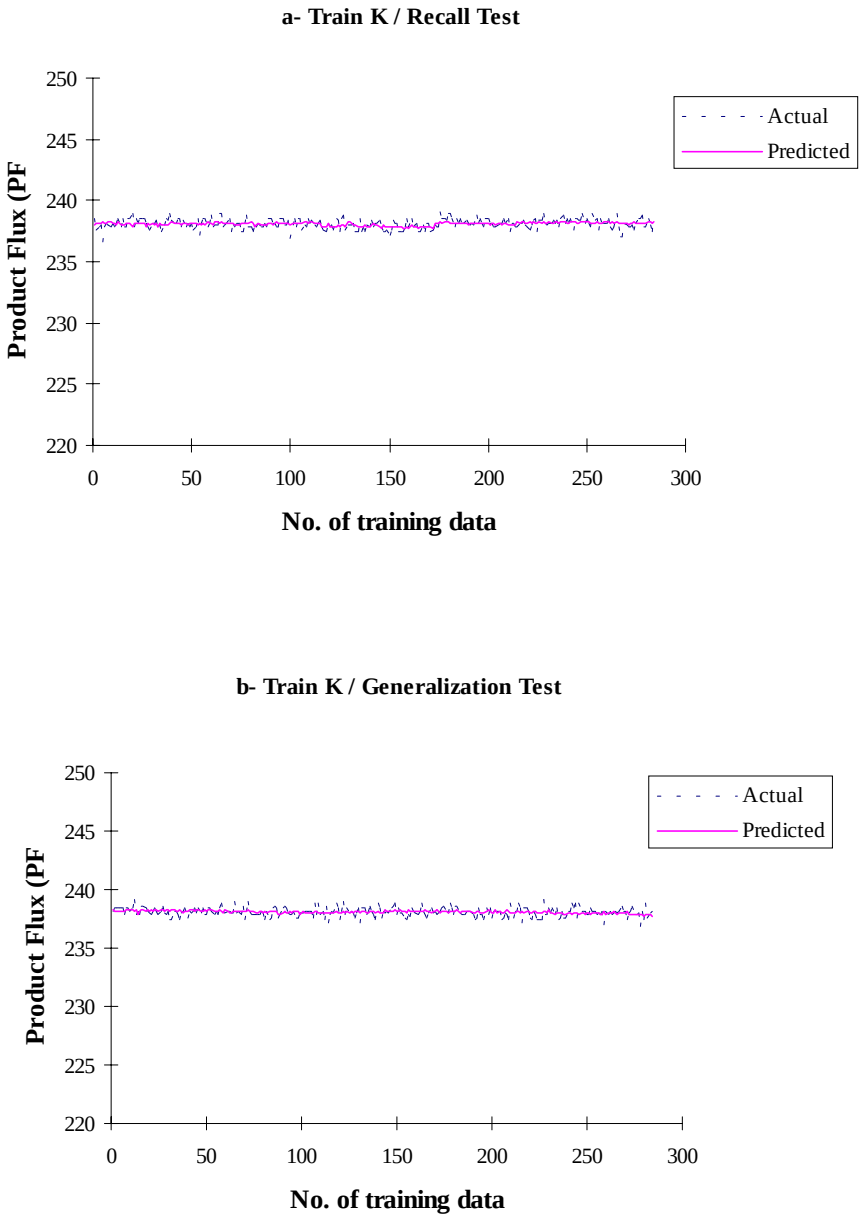

Figure 4.30: Actual and predicted product fluxes (PFs) from recall and generalization tests for RO trains K to T.

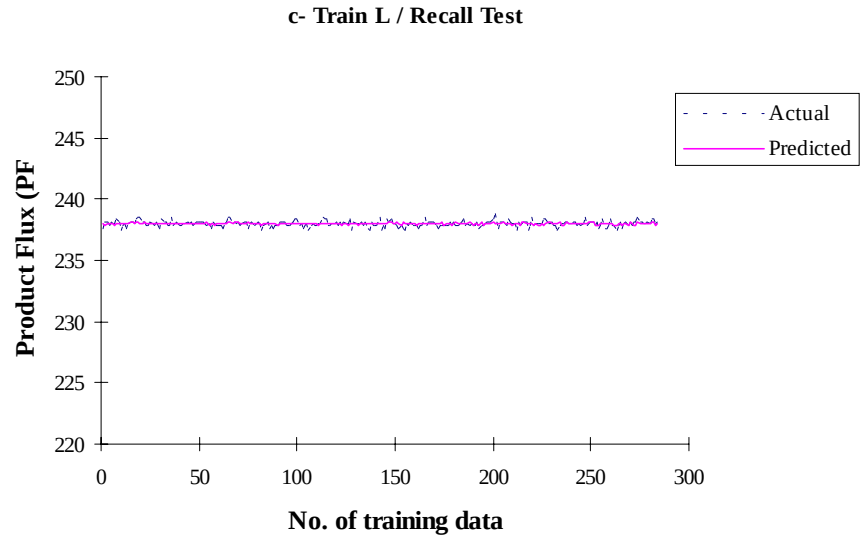

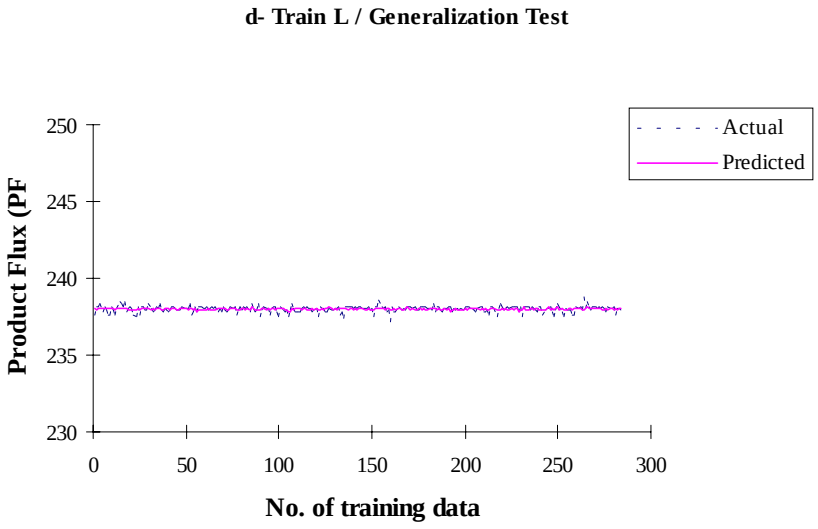

Figure 4.30: Actual and predicted product fluxes (PFs) from recall and generalization tests for RO trains K to T (continued).

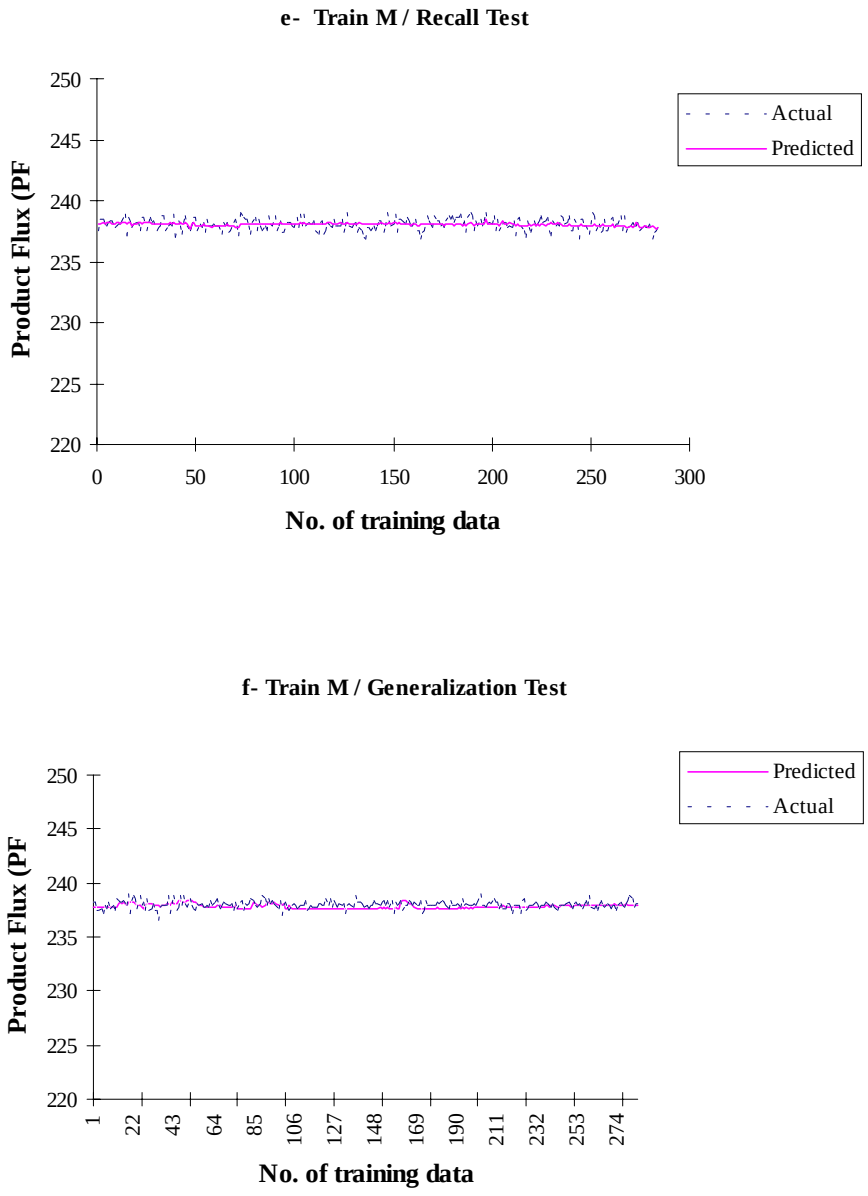

Figure 4.30: Actual and predicted product fluxes (PFs) from recall and generalization tests for RO trains K to T (continued).

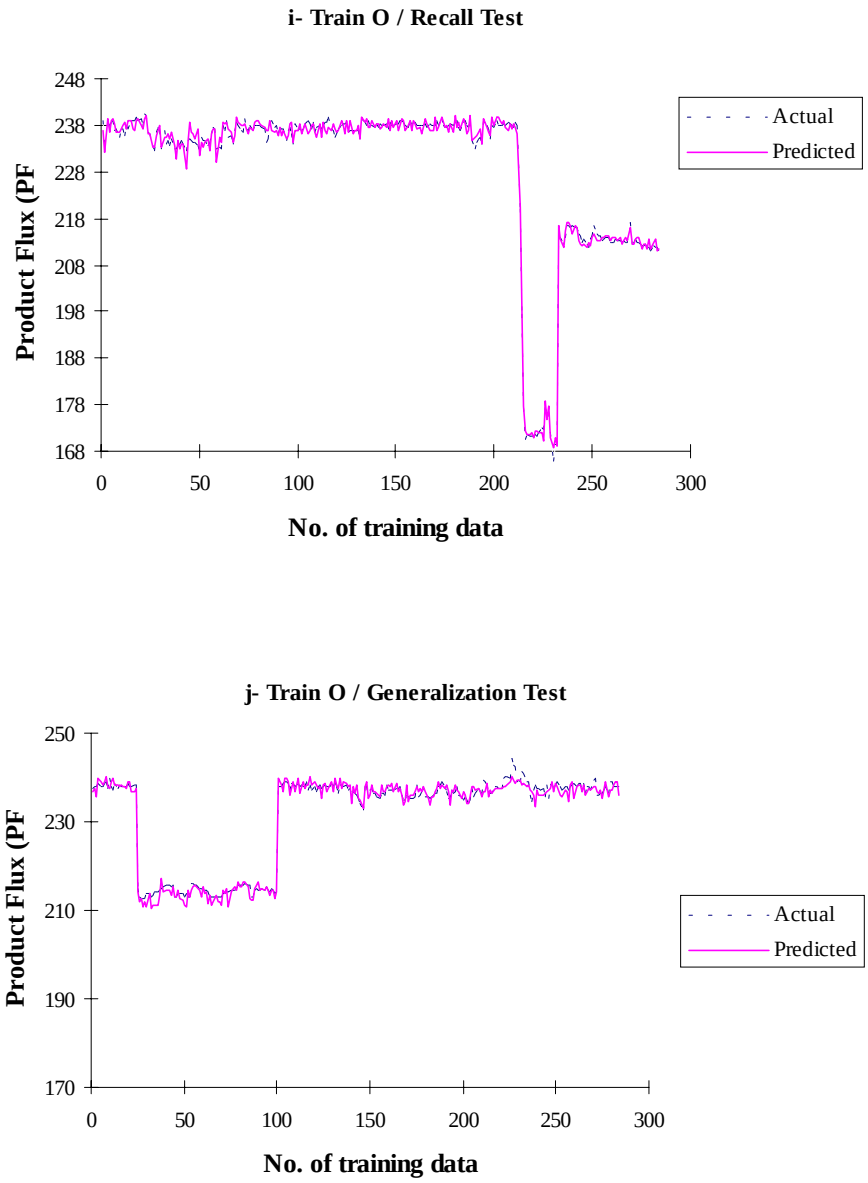

Figure 4.30: Actual and predicted product fluxes (PFs) from recall and generalization tests for RO trains K to T (continued).

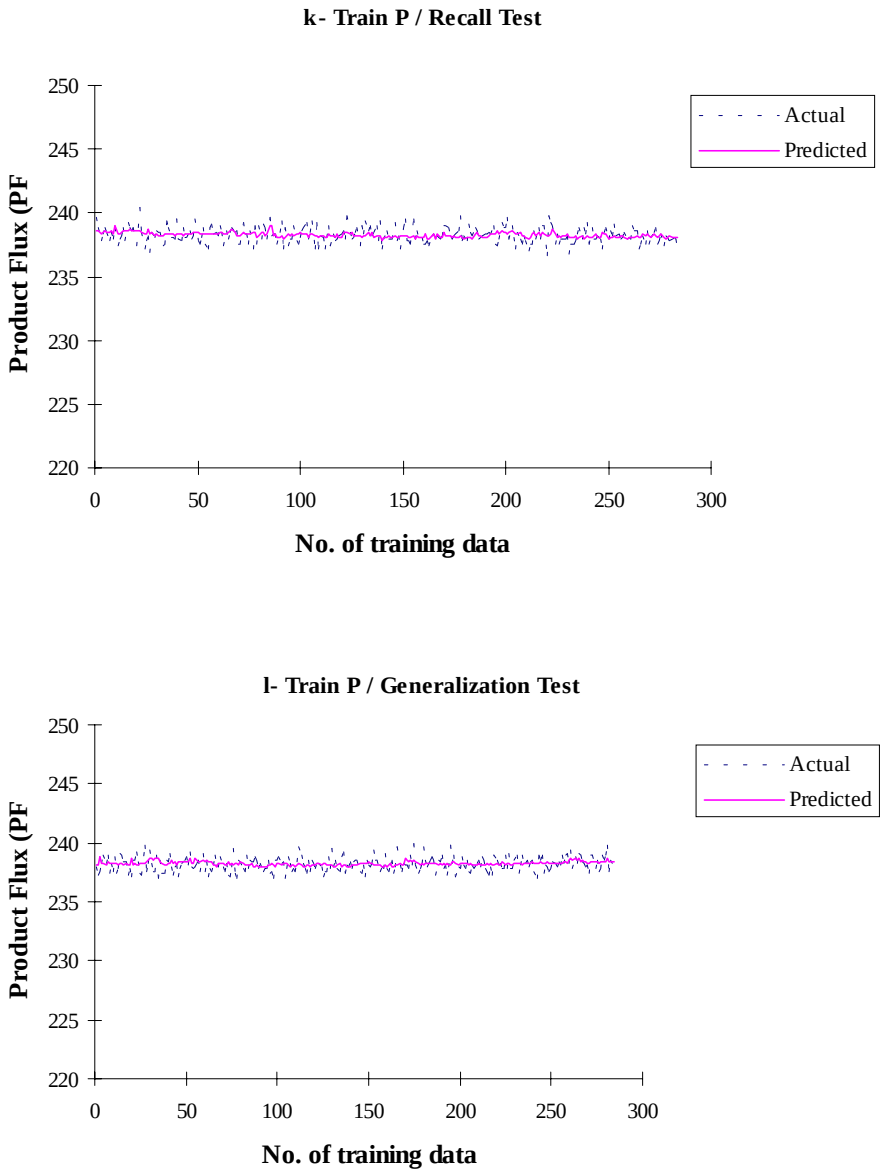

Figure 4.30: Actual and predicted product fluxes (PFs) from recall and generalization tests for RO trains K to T (continued).

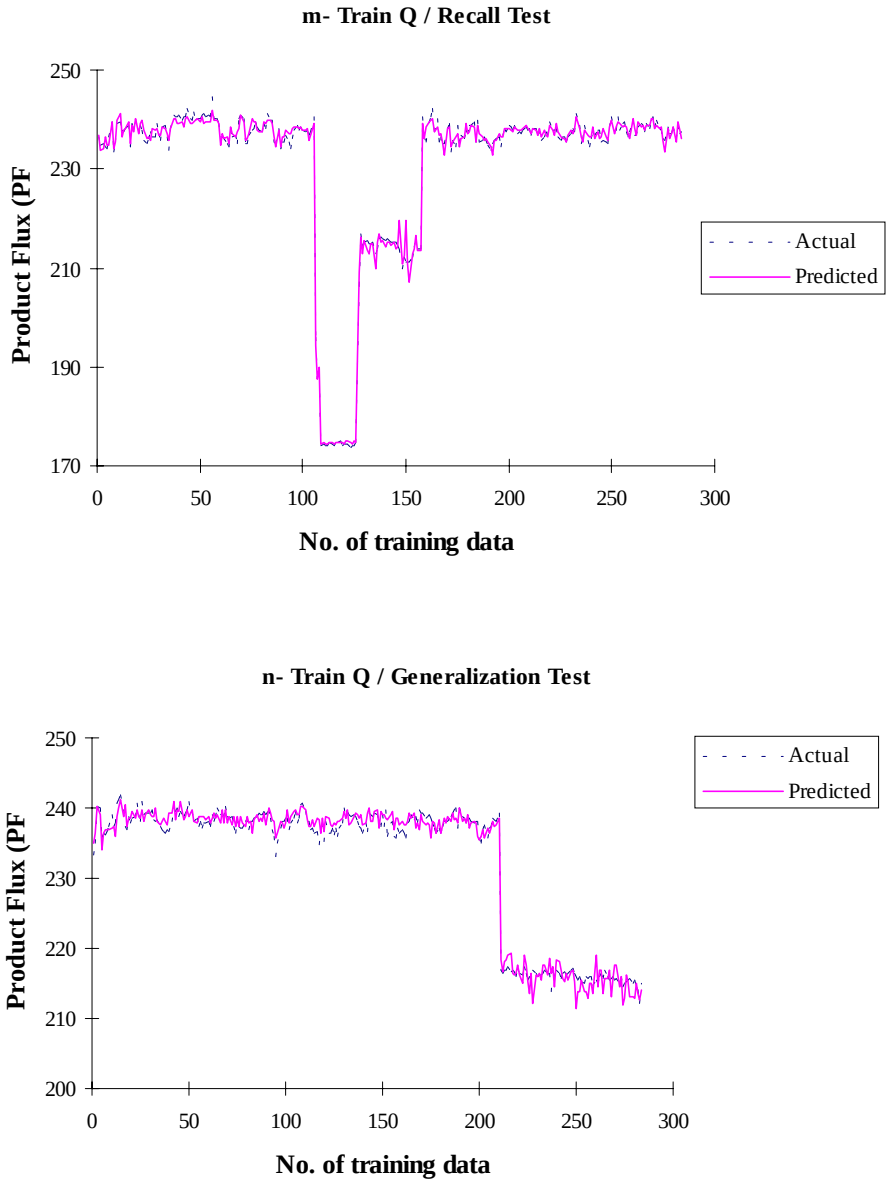

Figure 4.30: Actual and predicted product fluxes (PFs) from recall and generalization tests for RO trains K to T (continued).

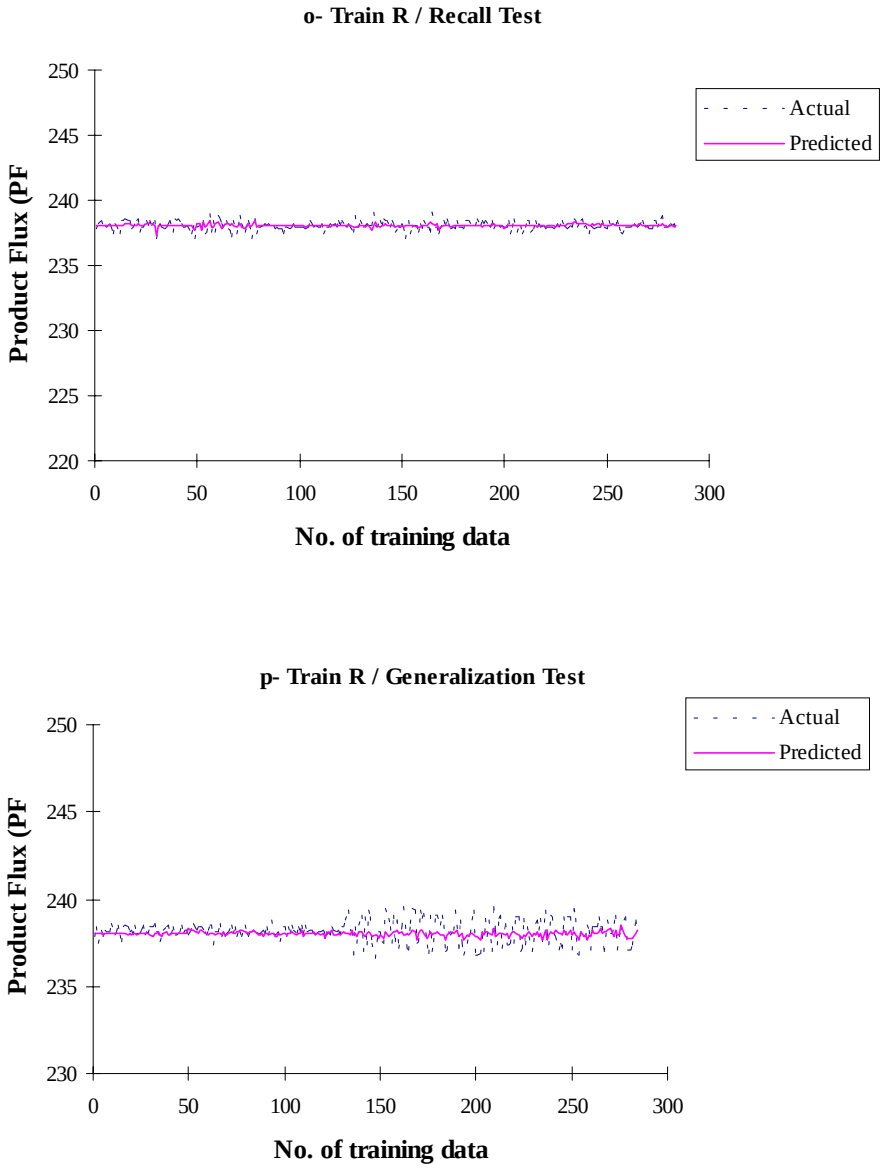

Figure 4.30: Actual and predicted product fluxes (PFs) from recall and generalization tests for RO trains K to T (continued).

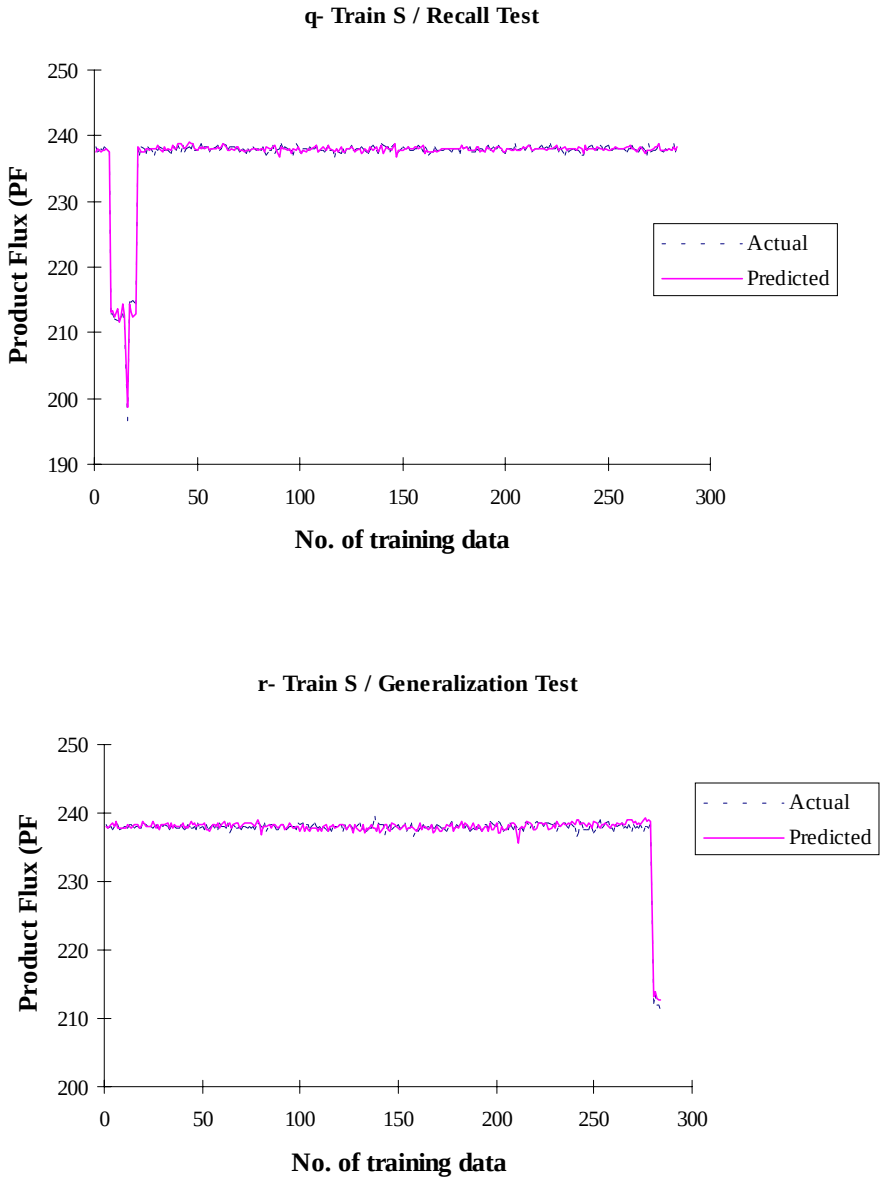

Figure 4.30: Actual and predicted product fluxes (PFs) from recall and generalization tests for RO trains K to T (continued).

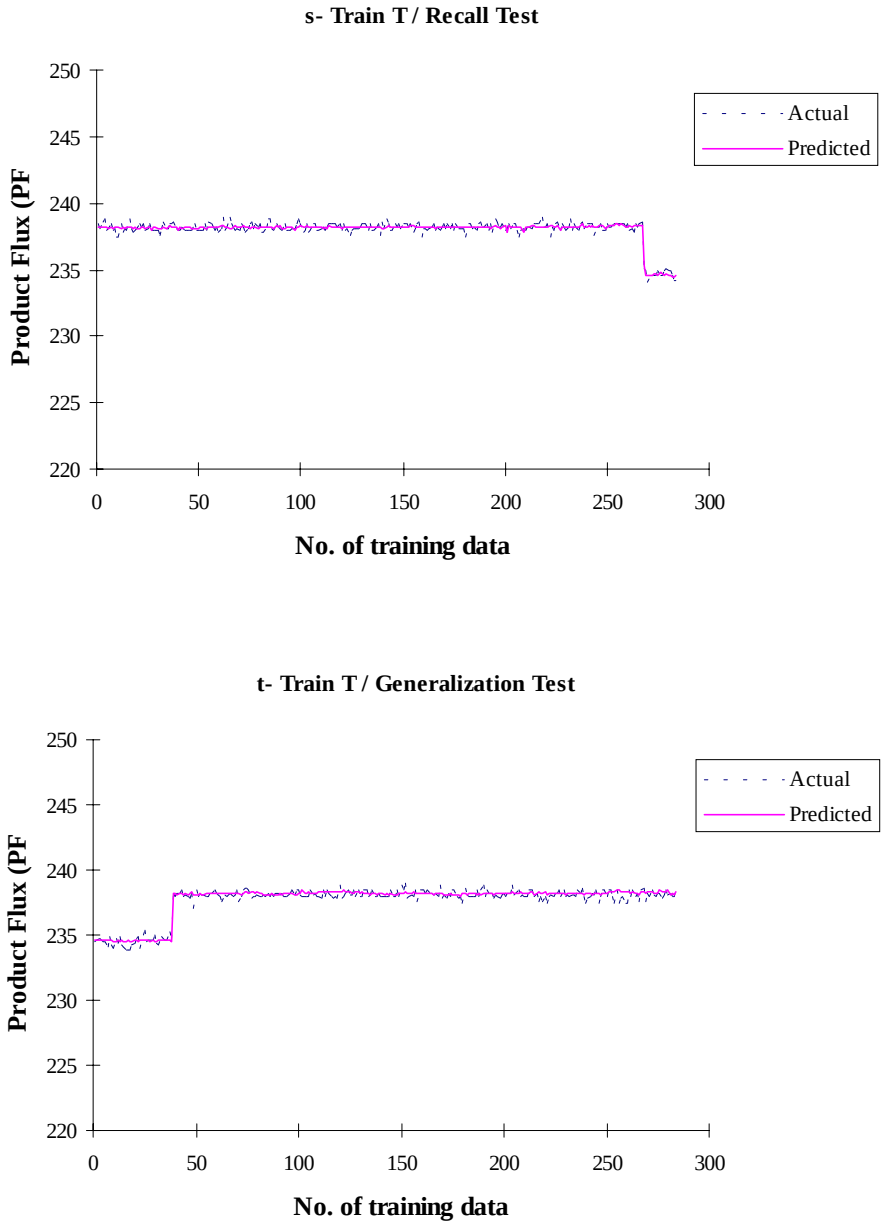

Figure 4.30: Actual and predicted product fluxes (PFs) from recall and generalization tests for RO trains K to T (continued).

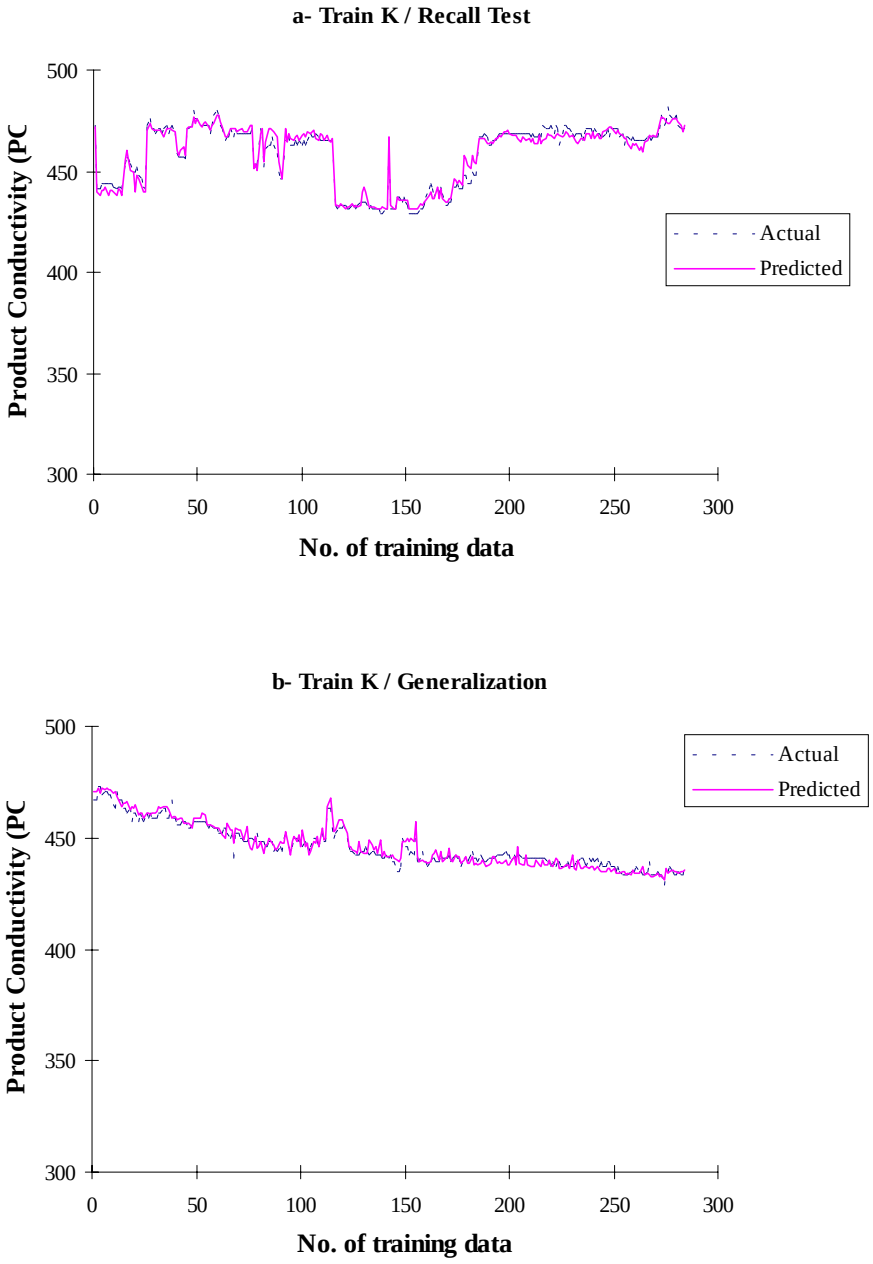

Figure 4.31: Actual and predicted product conductivities (PCs) from recall and generalization tests for RO trains K to T.

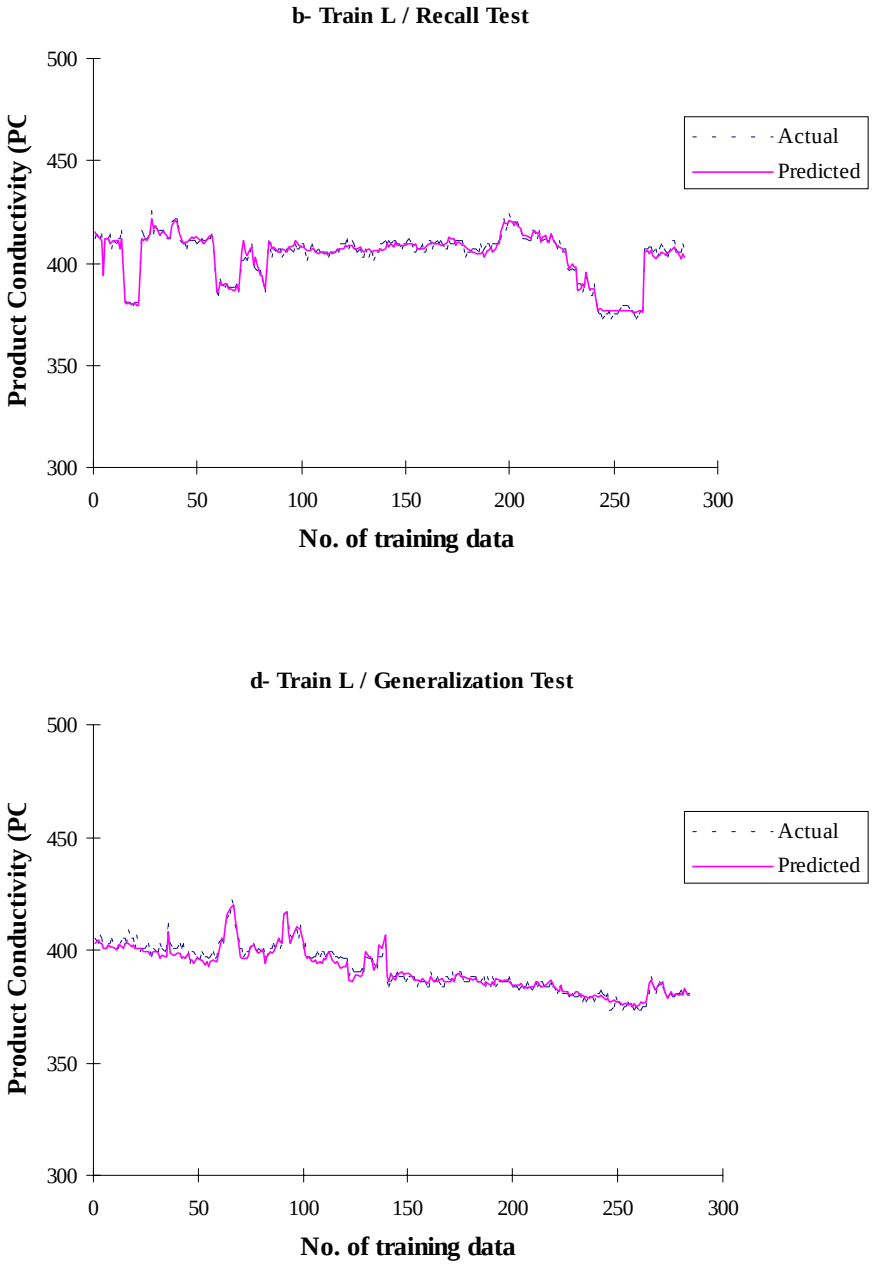

Figure 4.31: Actual and predicted product conductivities (PCs) from recall and generalization tests for RO trains K to T (continued).

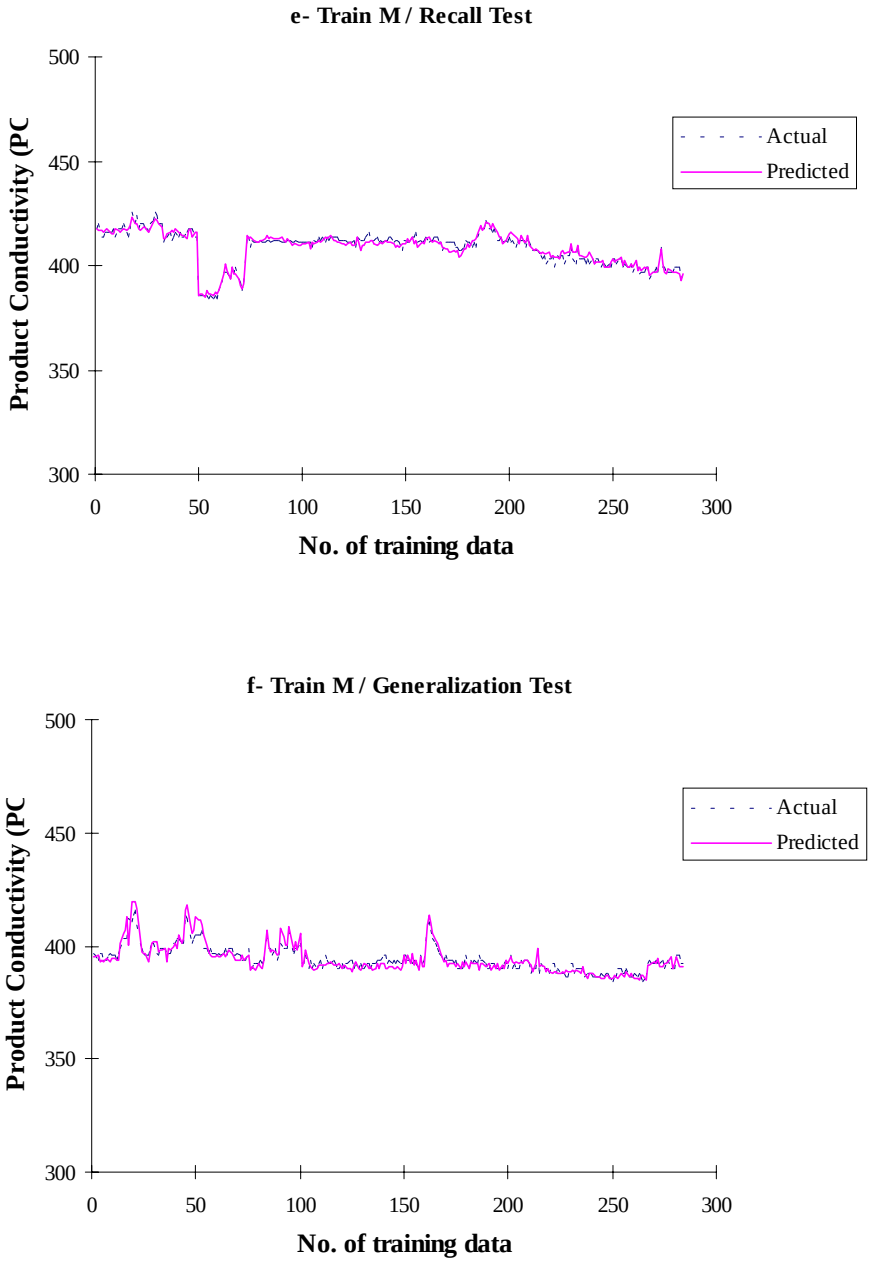

Figure 4.31: Actual and predicted product conductivities (PCs) from recall and generalization tests for RO trains K to T (continued).

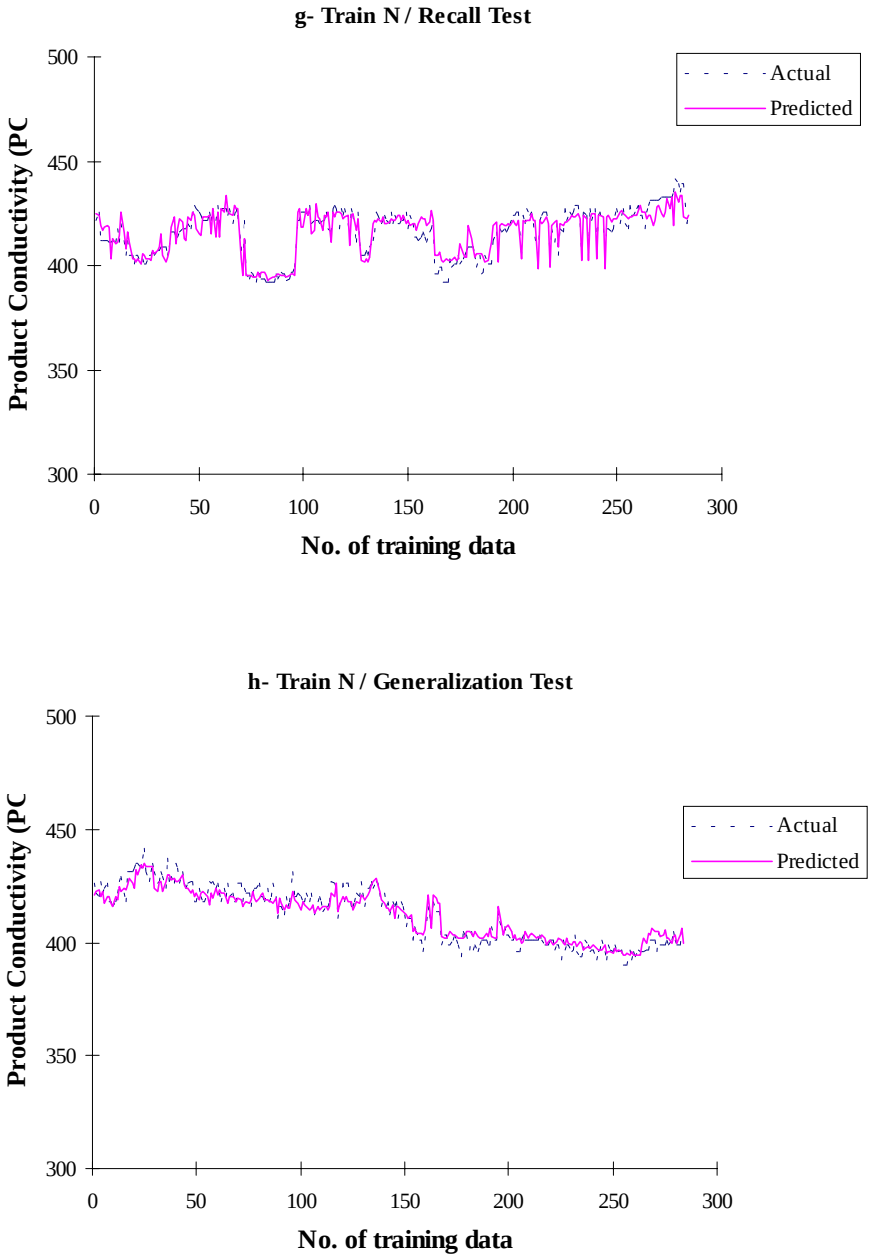

Figure 4.31: Actual and predicted product conductivities (PCs) from recall and generalization tests for RO trains K to T (continued).

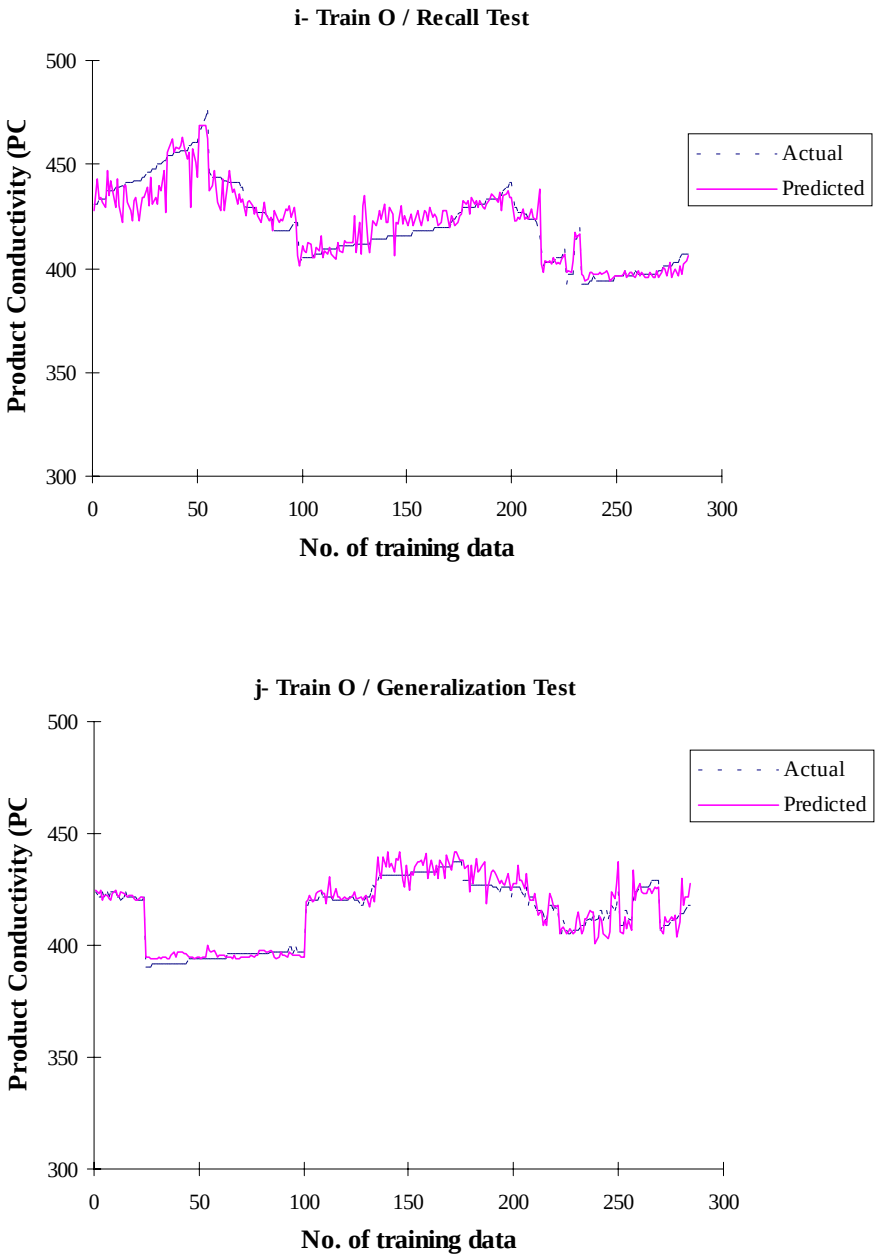

Figure 4.31: Actual and predicted product conductivities (PCs) from recall and generalization tests for RO trains K to T (continued).

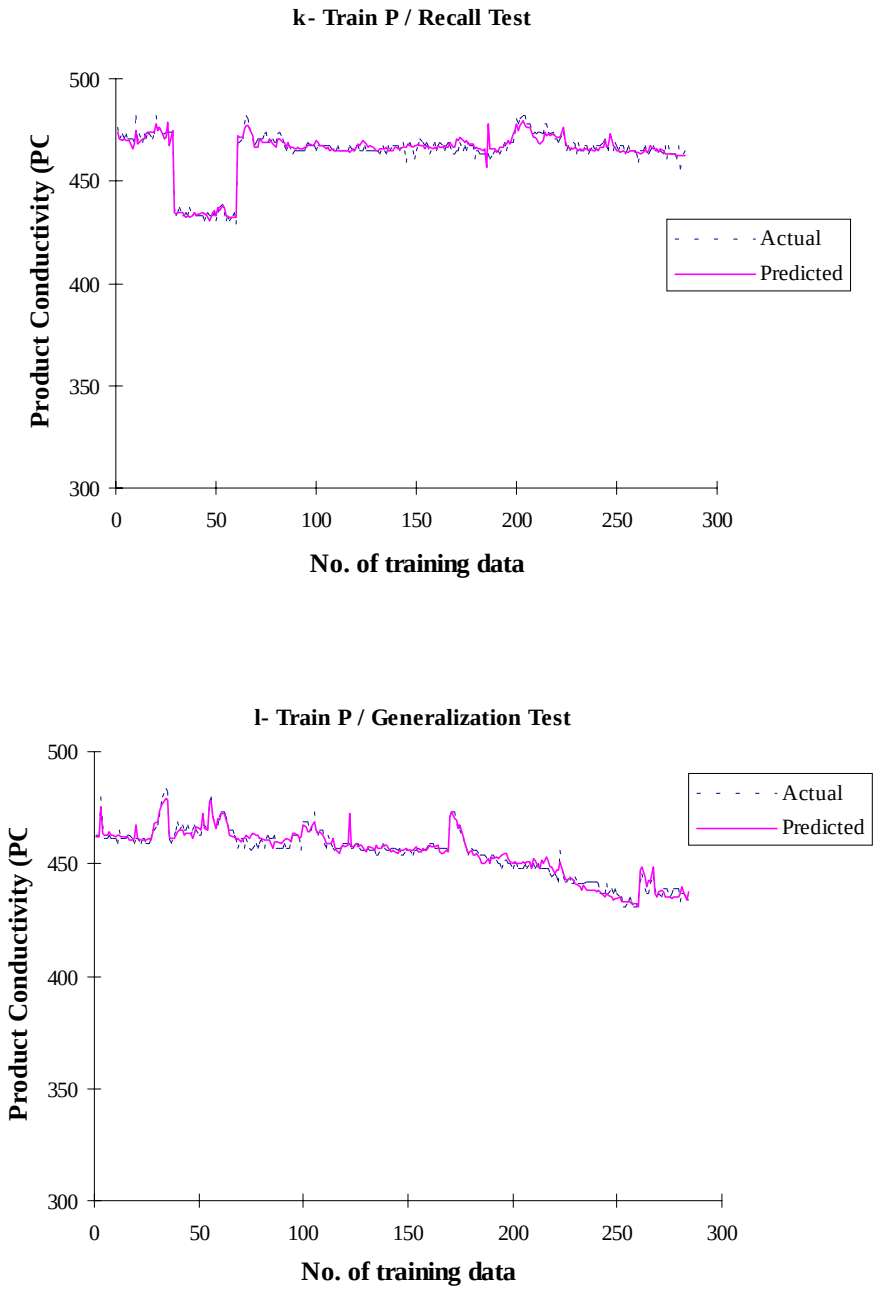

Figure 4.31: Actual and predicted product conductivities (PCs) from recall and generalization tests for RO trains K to T (continued).

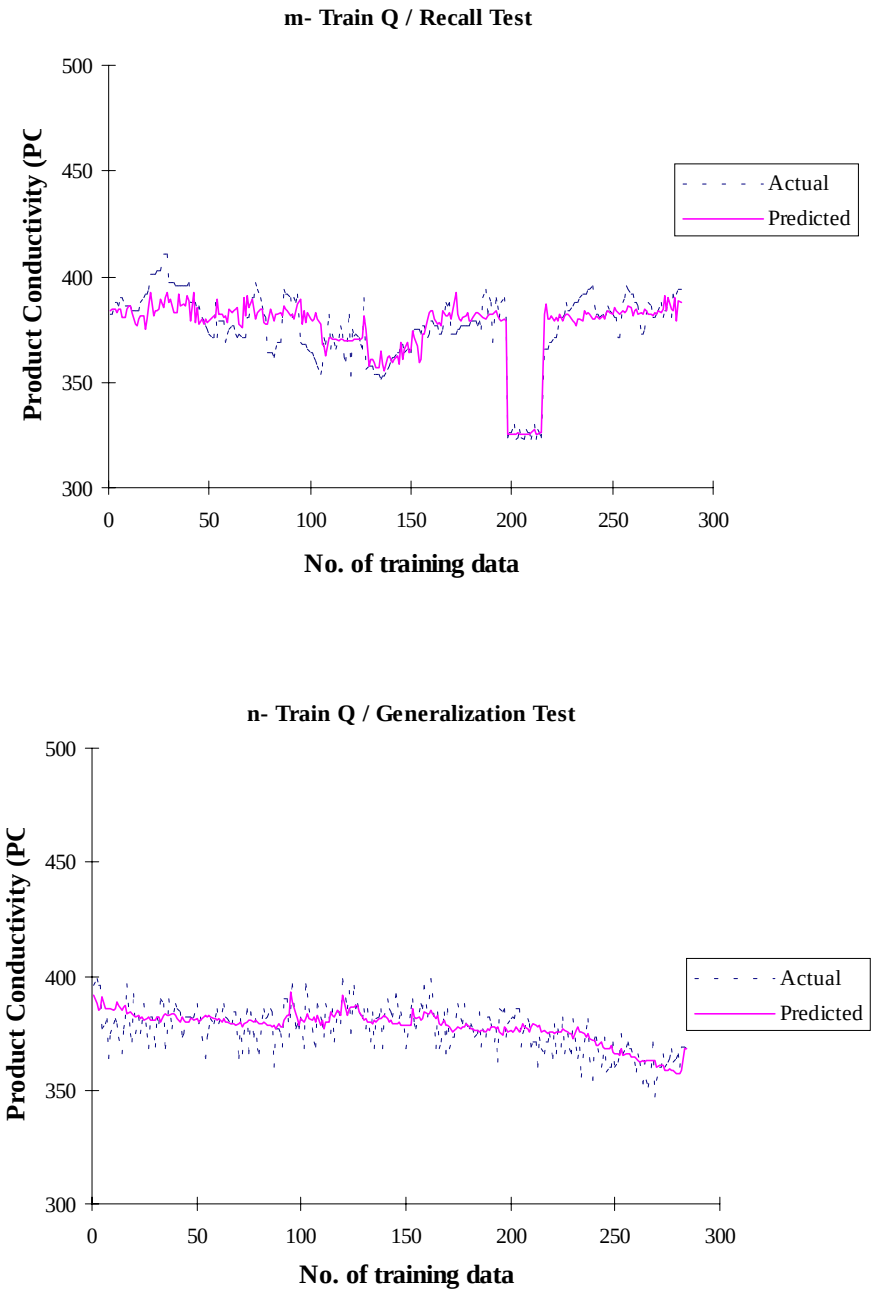

Figure 4.31: Actual and predicted product conductivities (PCs) from recall and generalization tests for RO trains K to T (continued).

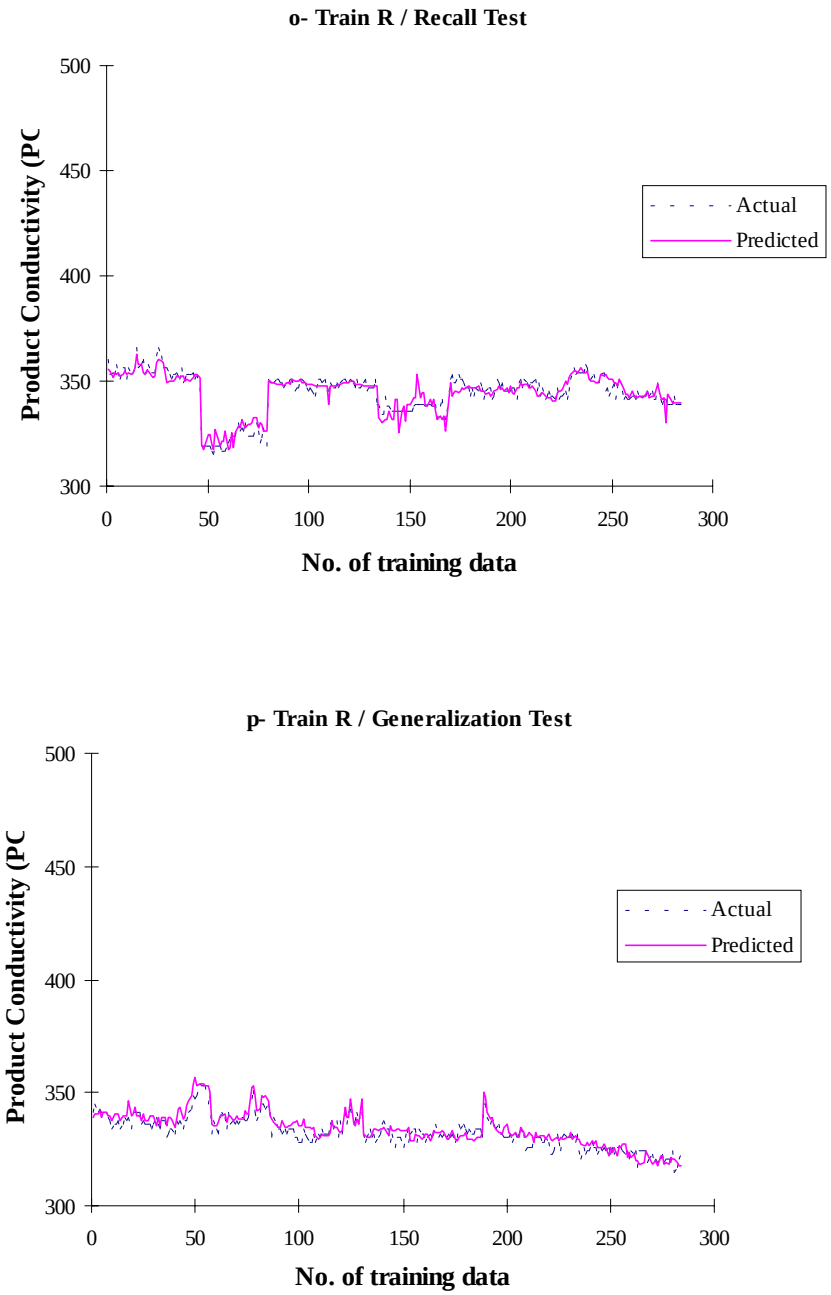

Figure 4.31: Actual and predicted product conductivities (PCs) from recall and generalization tests for RO trains K to T (continued).

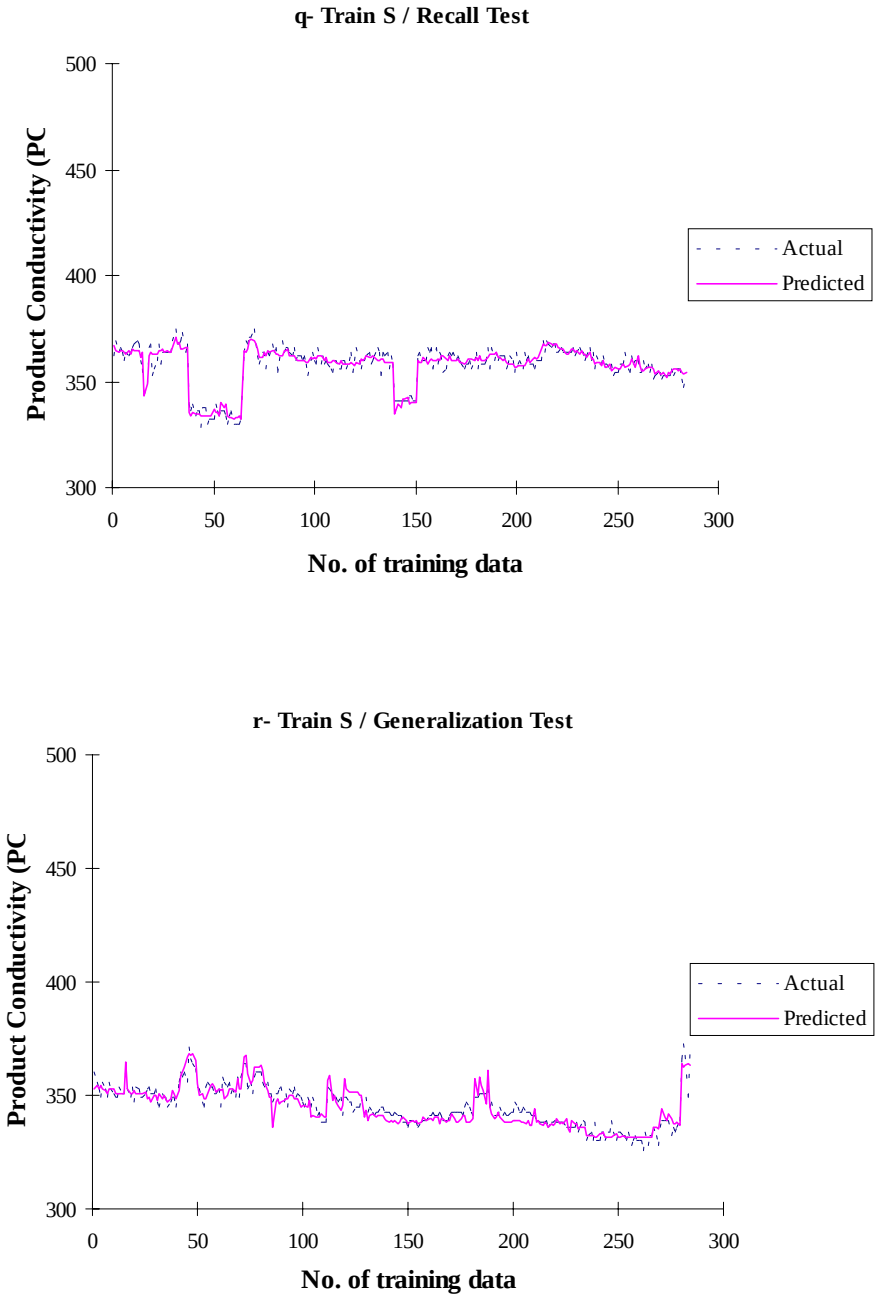

Figure 4.31: Actual and predicted product conductivities (PCs) from recall and generalization tests for RO trains K to T (continued).

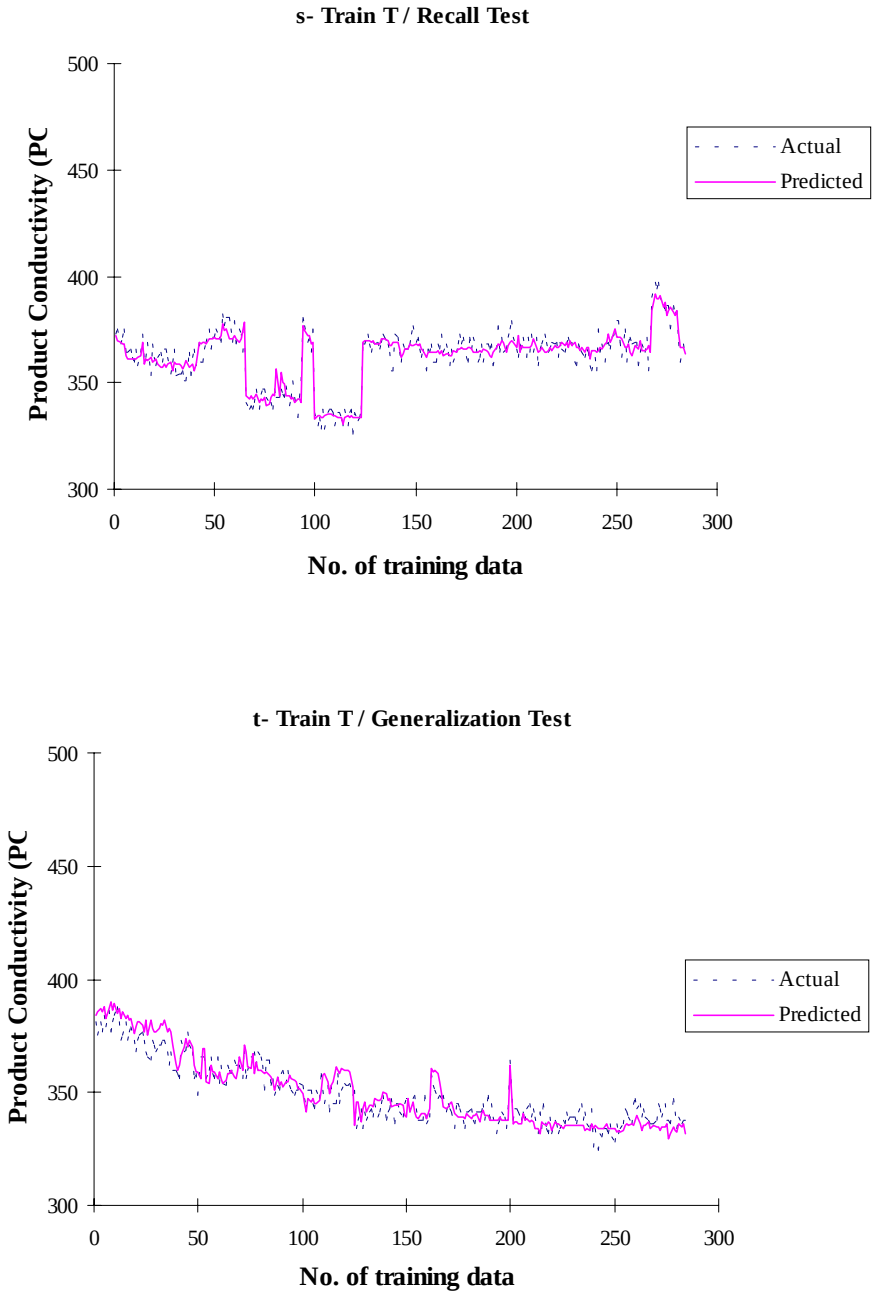

Figure 4.31: Actual and predicted product conductivities (PCs) from recall and generalization tests for RO trains K to T (continued).

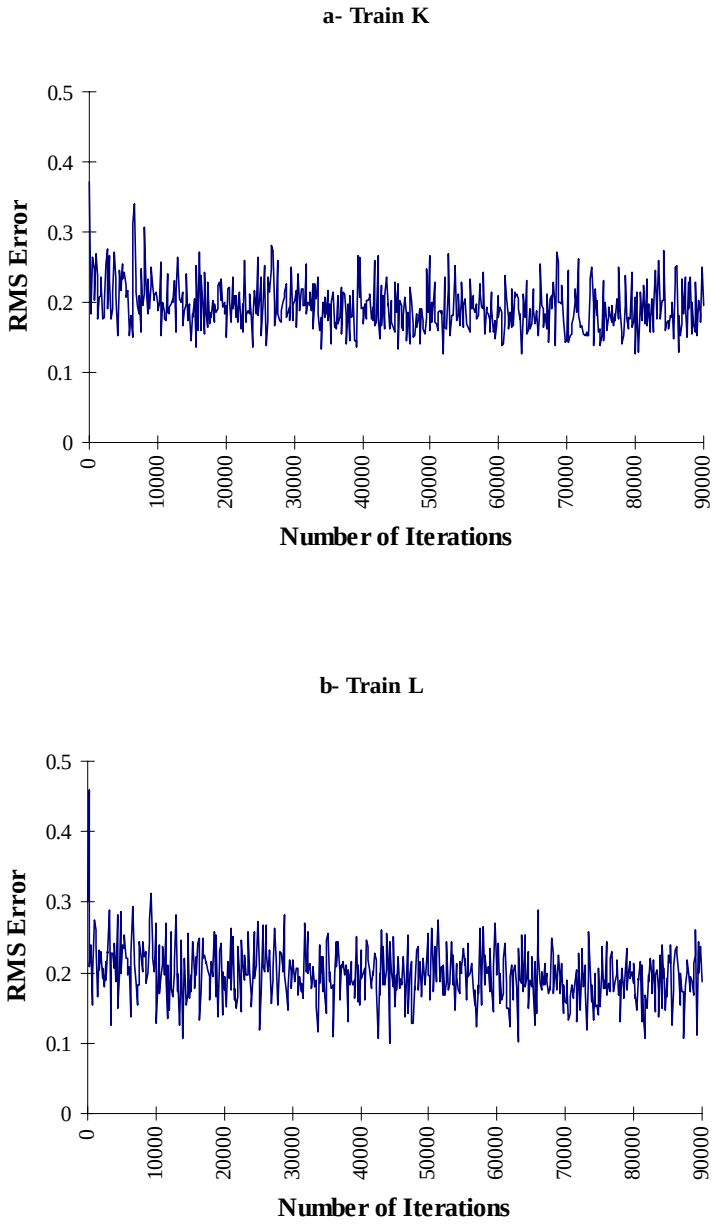

Figure 4.32: RMS errors for RO trains K to T.

c- Train M

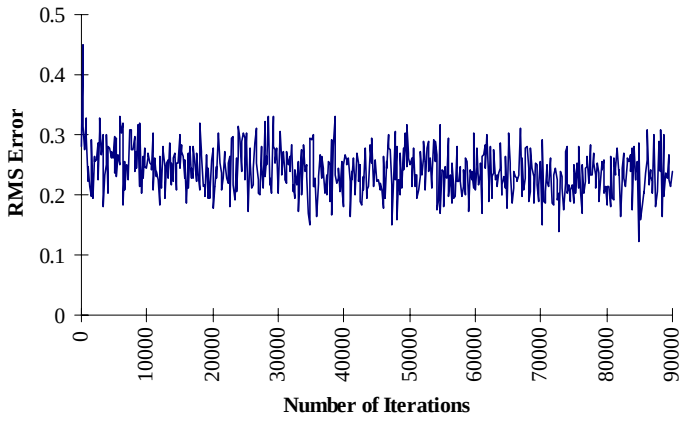

d- Train N

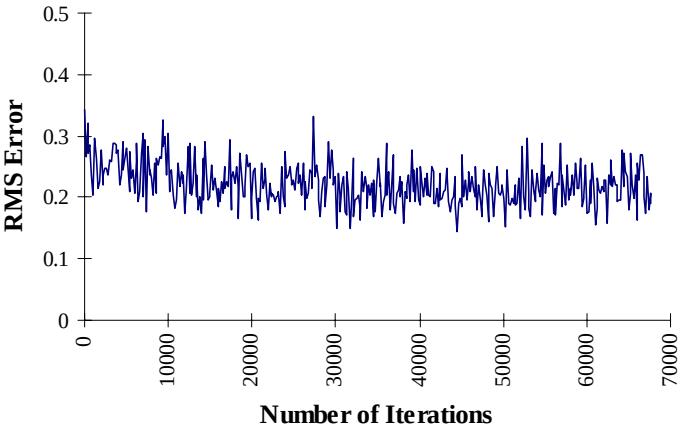

Figure 4.32: RMS errors for RO trains K to T (continued).

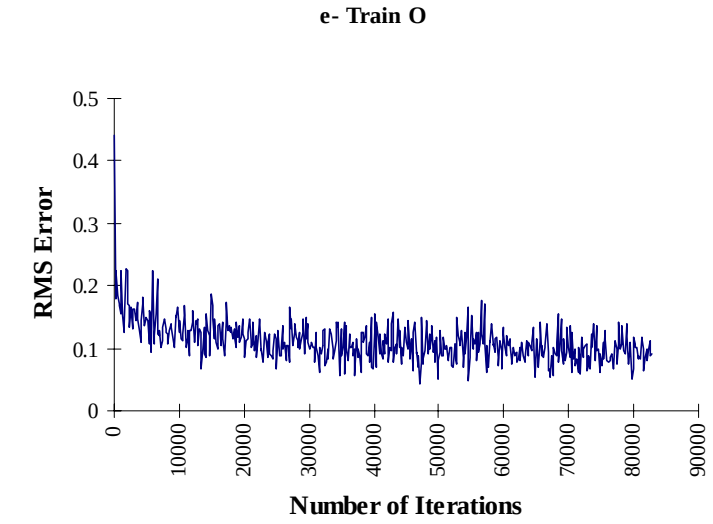

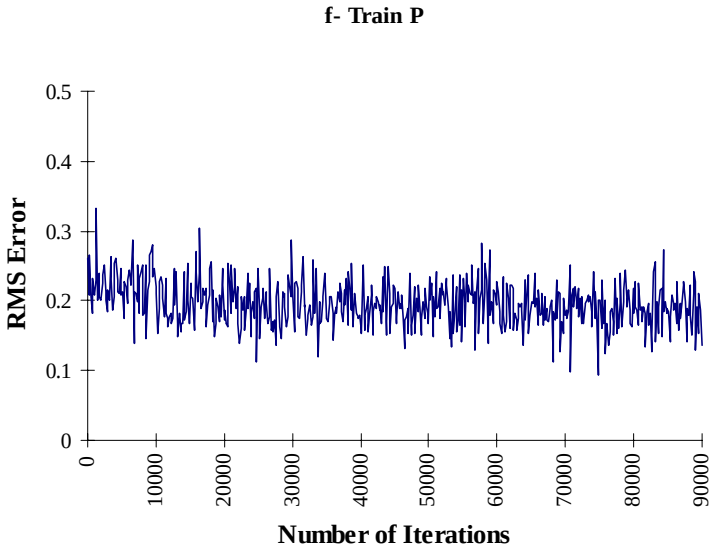

Figure 4.32: RMS errors for RO trains K to T (continued).

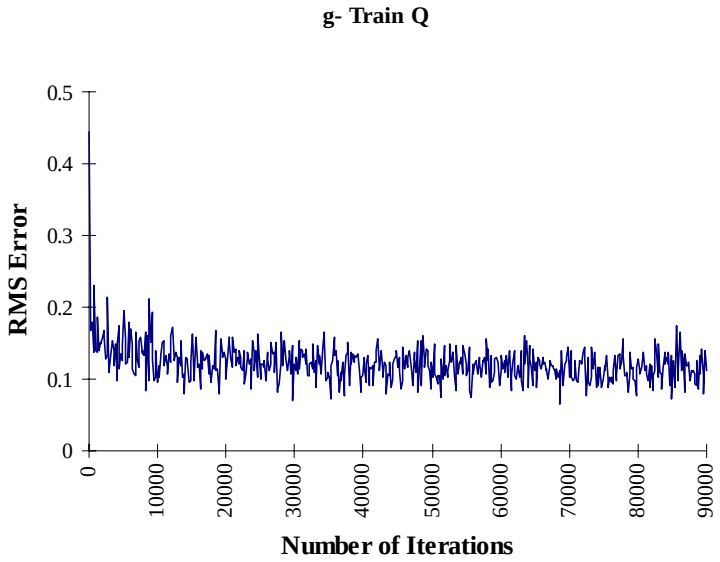

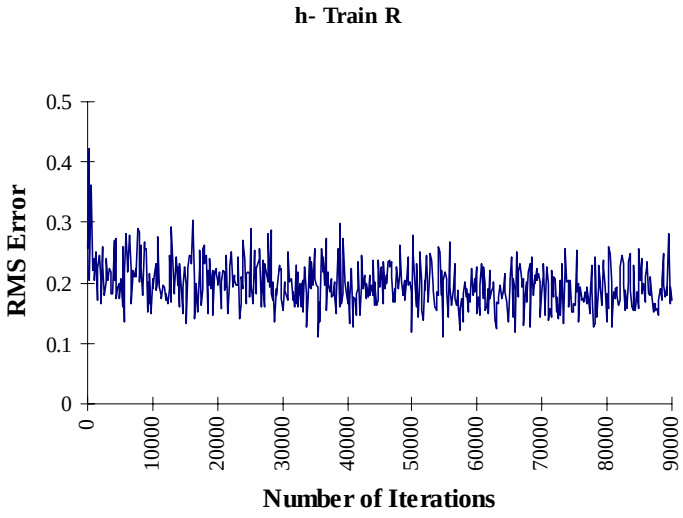

Figure 4.32: RMS errors for RO trains K to T (continued).

i- Train S

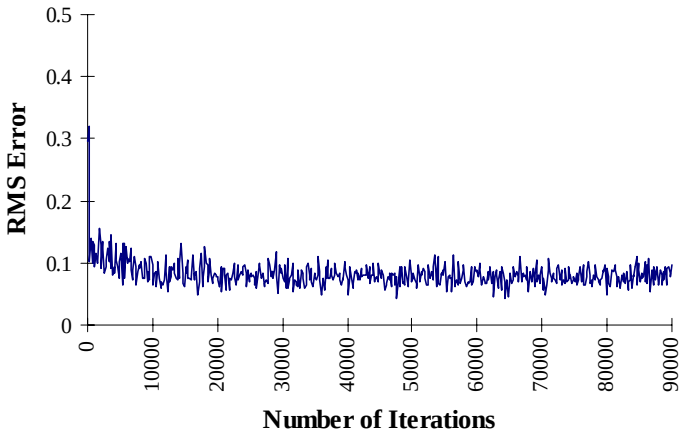

j- Train T

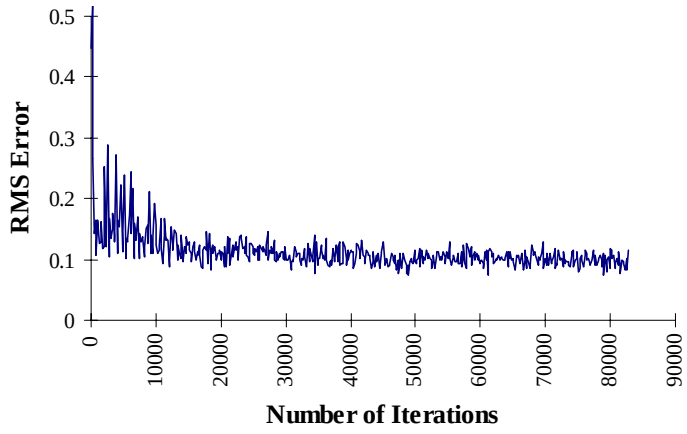

Figure 4.32: RMS errors for RO trains K to T (continued).

F. Neural Network versus Statistical Regression

Figure 4.33 presents the predicted and actual outputs from the multiple-input-single-output (MISO) neural networks and from statistical regression. The R^2 values for PF and PC are: 0.916704 and 0.95122, respectively. Despite the very good R^2 values, the neural network still outperforms the regression analysis. Table 4.25 shows the average absolute errors and the RMS errors of both models.

Neural networks have been very effective in predicting and optimizing the performance variables of the RO desalination plants. It also outperforms the regression models in prediction problems.

Table 4.25: Average absolute errors and RMS errors for the RO plant outputs predicted by neural network and statistical regression.

Error type	**Product flux (PF)**		**Product conductivity (PC)**	
	Neural network	Statistical regression	Neural network	Statistical regression
Average absolute error	0.22478	0.8686	3.88995	5.34856
Max.	0.76678	3.1770	14.91415	28.613
Min.	0.00067	0.0010	0.03540	0.01600
RMS error	0.09914	1.3934	0.12072	5.44070

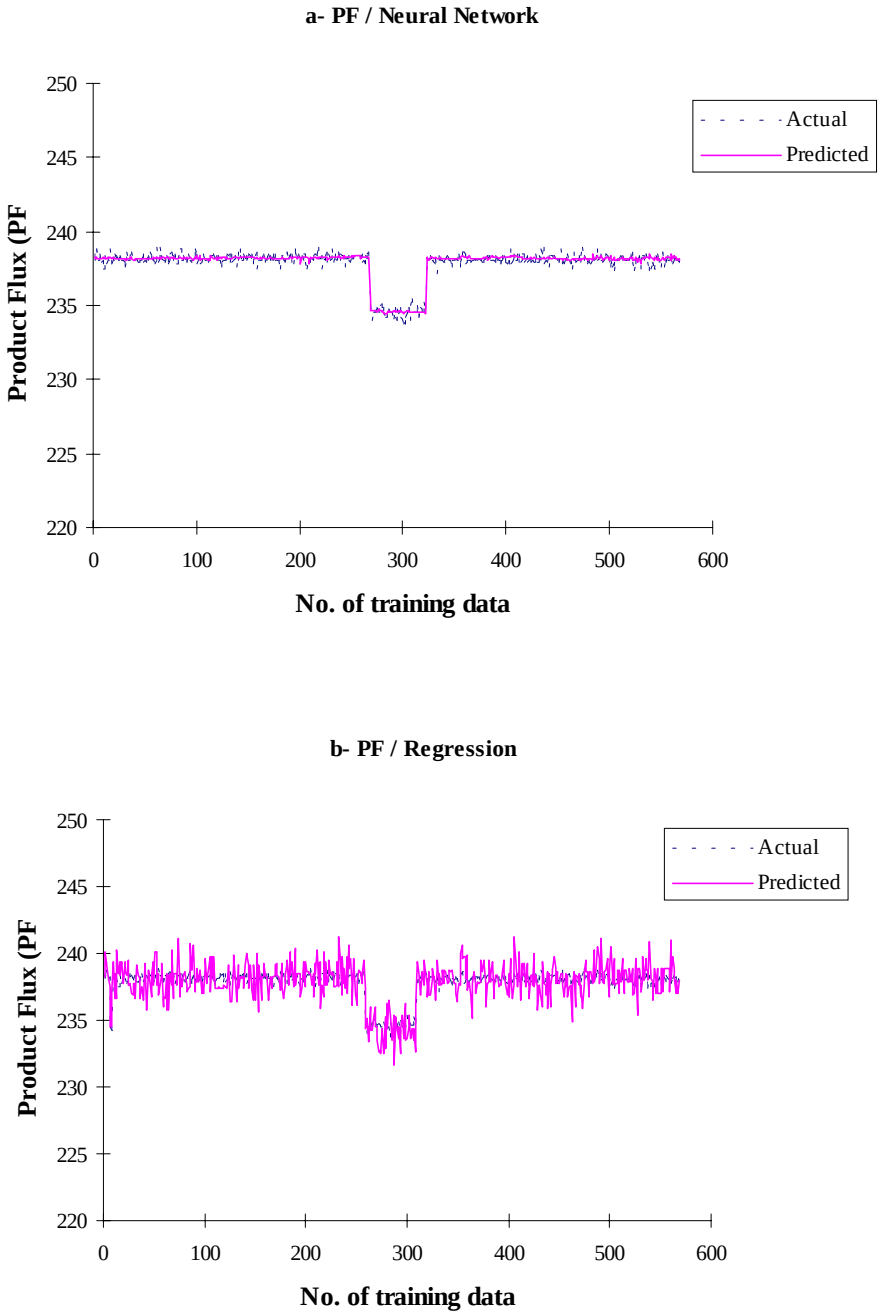

Figure 4.33: Actual and predicted PFs and PCs from neural network and statistical regression models.

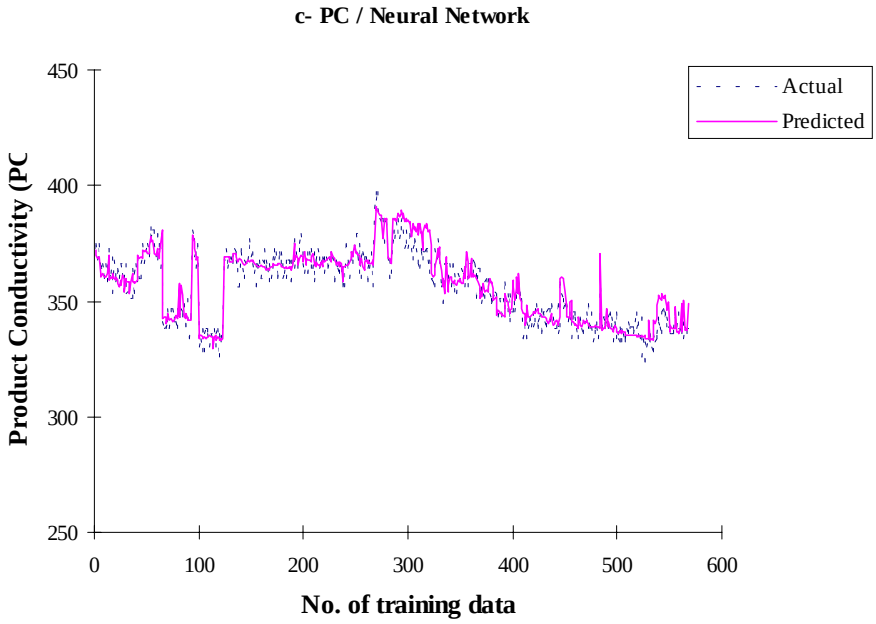

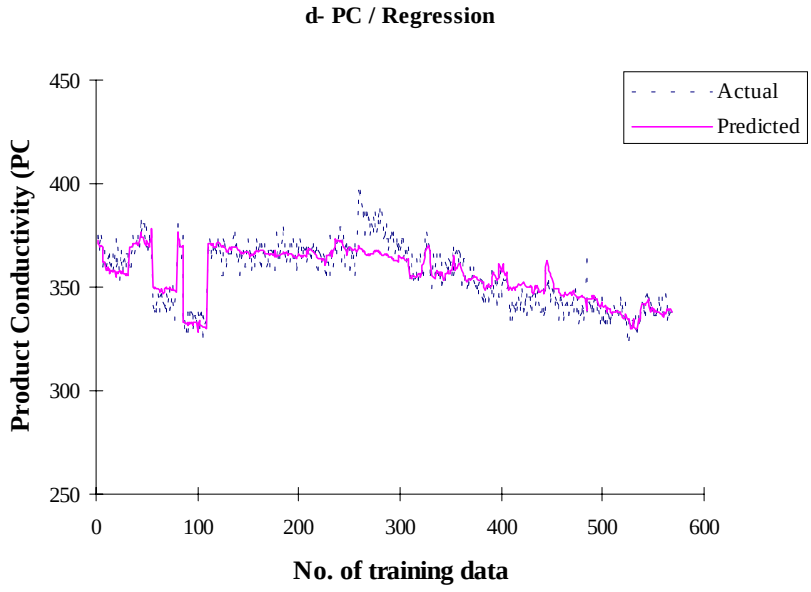

Figure 4.33: Actual and predicted PFs and PCs from neural network and statistical regression models (continued).

4.4 Comparison with Recent Studies

As presented earlier, we have developed a neural-network approach based on the backpropagation algorithm for the prediction and optimization of process performance variables of large-scale MSF and RO seawater desalination plants. In contrast to three recent studies by Abdulbary, et al., (1995), Parenis, et al., (1995), and Selvaraj and Deshpande, (1995) that use only simulated data for MSF processes, this work utilizes *actual operating data* from large-scale commercial MSF desalination plant (48 MGPD) and RO desalination plant (15 MGPD) located in the State of Kuwait, and the Kingdom of Saudi Arabia, respectively.

As discussed previously in section 4.2, the recommended effective ranges of learning rate, momentum coefficient and hidden nodes as mentioned in Baughman and Liu (1995) and successfully tested here for the MSF model are as follows: (1) a learning rate of 0.3 which decreases as we progress between the hidden layers and as the number of iterations increases, (2) a momentum coefficient of 0.4 which remains constant between the hidden layers but decreases as the number of iterations increases, and (3) two hidden layers with 30 and 15 nodes. We apply the backpropagation algorithm, the delta learning rule, and the hyperbolic tangent transfer function. The maximum number of training iterations is 90,000 and the effective epoch size is 16 examples. The input and output variables are selected based on engineering knowhow.

Tables 4.26 and 4.27 compare the network architectures between recent studies and the present work.

Table 4.26: A comparison of network architectures between the present work and recent studies.

Network architecture	**1. This work (1997)**	**2. Selvarajs and Deshpande (1995)**	**3. Abdulbary, et al. (1995)**	**Parentis, et al. (1995)**
Input variables (Table 4.2)	16	2	4	4
Output variables (Table 4.2)	3	3	3	8
Network parameters				
• learning rate	0.3	0.6	-	-
• momentum coefficient	0.4	0.8	-	-
• hidden layer(s) nodes	30:15	5	5	varies
• transfer function	Tanh	-	Sigmoid	Tanh
Training iterations	30,000 - 90,000	2,000	28,630 (Max.)	50,000

Note:
Models 2 to 4 used:
1. Simulated data form smaller-scale MSF Plant
2. One hidden-layer configuration
3. Less input variables, selected based on engineering knowledge

- : Unavailable information

Table 4.27: A comparison of input and output variables for the present work and recent studies.

No	1. This work		2. Selverajs and Deshpande (1995)		3. Abdulbary, et al. (1995)		4. Parentis, et al. (1995)	
	Input variables (16)	**Output variables (3)**	**Input variables (2)**	**Output variables (3)**	**Input variables (4)**	**Output variables (3)**	**Input variables (4)**	**Output variables (8)**
1	Seawater flowrate	Top brine temperature	Recirculating brine flowrate	Top brine temperature	Top brine temperature	Recirculating brine salinity	Recirculating brine flowrate	Steam flowrate
2	Makeup flowrate	Distillate produced	Steam flowrate	Distillate produced	Recirculating brine flowrate	Distillate produced	Recirculating brine temperature	Makeup flowrate
3	Seawater recycle flow	Steam flowrate		Stage 1 brine level	Makeup flowrate	Performance ratio	Recirculating brine salinity	Distillate produced
4	Seawater-inlet temperature				Steam temperature		Seawater-inlet temperature	Blowdown flowrate
5	Seawater-outlet temperature							Gain-output ratio
6	Blowdown flowrate							Evaporated brine out flow
7	Brine-inlet temperature							Evaporated brine out salinity
8	Stage 24 brine temperature							Evaporated brine out temperature
9	Brine-heater inlet temperature							
10	Stage 1 brine level							
11	Brine-heater shell temperature							
12	Brine-heater shell pressure							
13	Steam temperature							
14	Condensate temperature							
15	Condensate flowrate							
16	Recirculating brine flowrate							

We compare our model with Selvarajs' model in three different ways using winter and summer data, as follows:

Model 1: Selvarajs' variables + Selvarajs' network architecture + actual plant data.
Model 2: Selvarajs' variables + Our network architecture + actual plant data.
Model 3: Our variables + Selvarajs' network architecture + actual plant data.

The model response is the same with summer and winter data. We will limit our discussion of the three models with winter data

Table 4.28 compares of the recall, generalization, and RMS errors of TBT, DP and S1BL networks of our model with those of the other three models. In general, the three models perform inefficiently in comparison with our model.

Models 1 and 2 do not show a significant difference in their error values. Their RMS errors are trapped in local minima, unstable and fluctuating. The inefficient network performance in Models 1 and 2 could be attributed to the type of data used in their model (simulated data) and the variable selected.

Model 3 shows a better improvement in the network performance than Models 1 and 2. As Figure 4.34 illustrates, the RMS error in Model 3 is trapped in local minimum until it reached 10,000 iterations, where it converges. Even after the RMS error converges, the error is still unstable and fluctuating.

Figure 4.35 shows the actual and predicted output variables and the RMS errors from the above models.

Table 4.28: Average recall, generalization, and RMS errors of Selvarajs' model and our model.

Error	**TBT (°C)**	**DP (T/hr)**	**S1BL (cm)**
Model 1:			
Recall	0.2397	9.5117	12.3059
Generalization	0.1886	20.5378	14.8734
RMS	0.3054	0.2222	0.2055
Model 2:			
Recall	0.2400	9.5157	12.2910
Generalization	0.1892	20.5340	14.7740
RMS	0.2985	0.2164	0.2076
Model 3:			
Recall	0.0769	6.8592	12.7257
Generalization	0.1202	18.1674	12.8100
RMS	0.1311	0.1942	0.2563
Our Model			
Recall	0.0287	0.9329	*
Generalization	0.1764	13.0878	
RMS	0.0546	0.0621	

*: not considered as an output

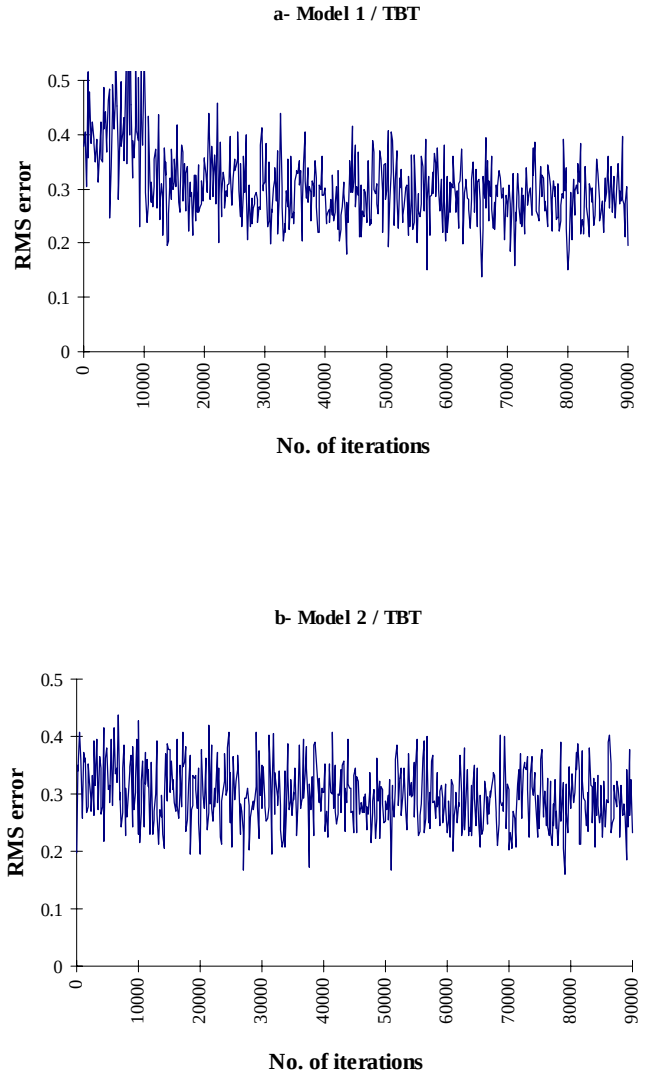

Figure 4.34: A comparison of RMS errors of TBT, DP, and S1BL networks of our model and three versions of Selveraj's model.

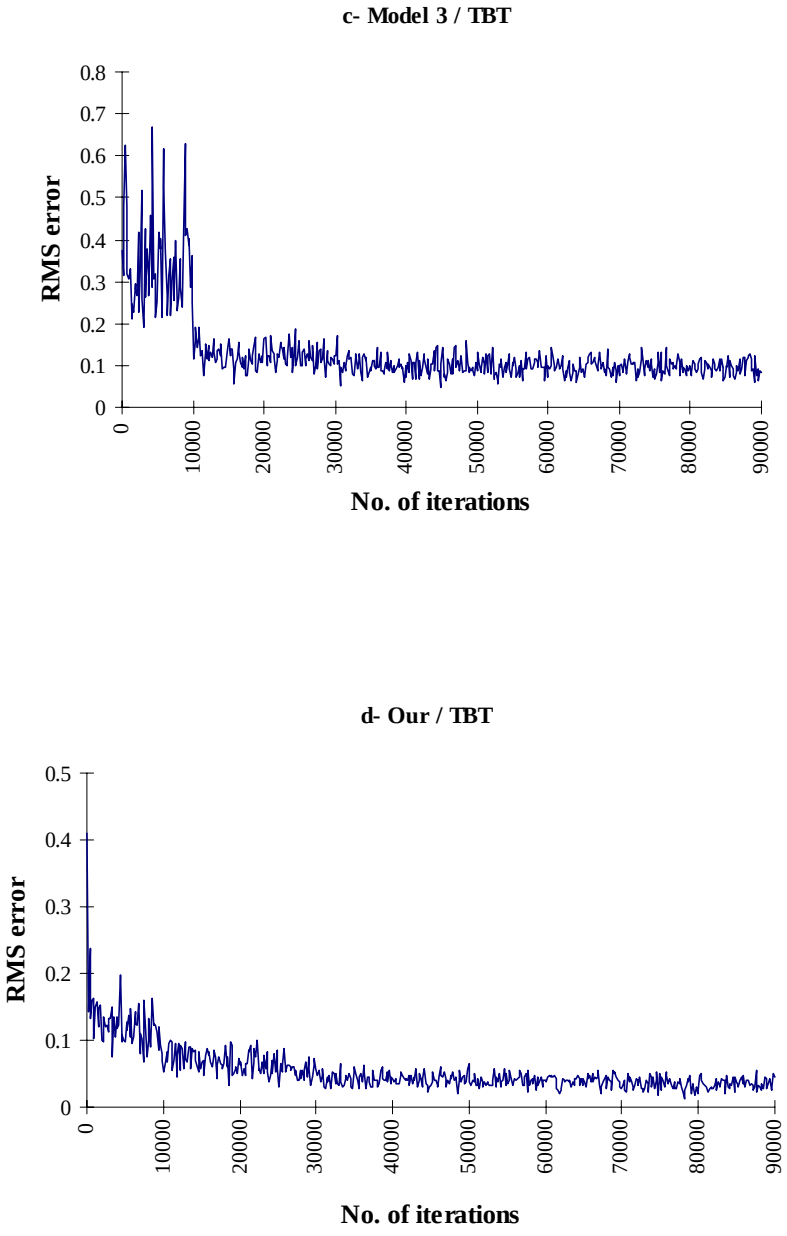

Figure 4.34: A comparison of RMS errors of TBT, DP, and S1BL networks of our model and three versions of Selveraj's model (continued).

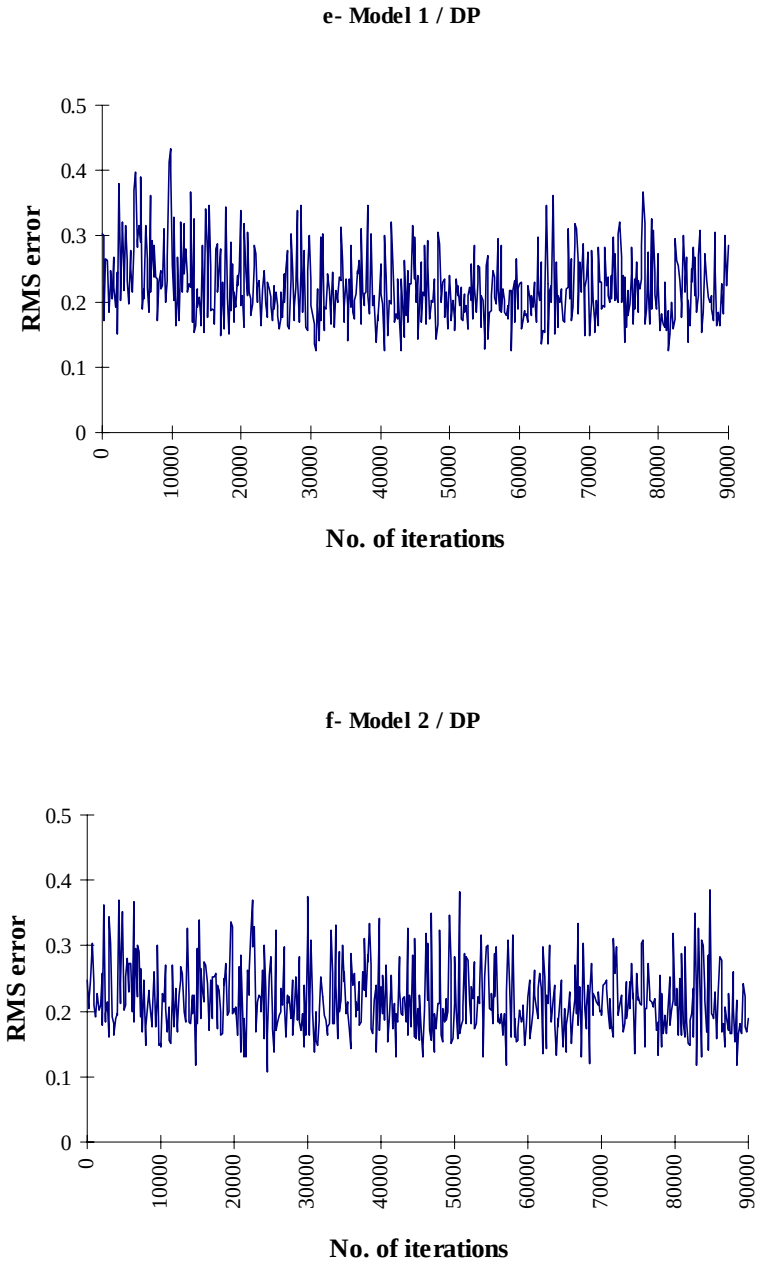

Figure 4.34: A comparison of RMS errors of TBT, DP, and S1BL networks of our model and three versions of Selveraj's model (continued).

g- Model 3 / DP

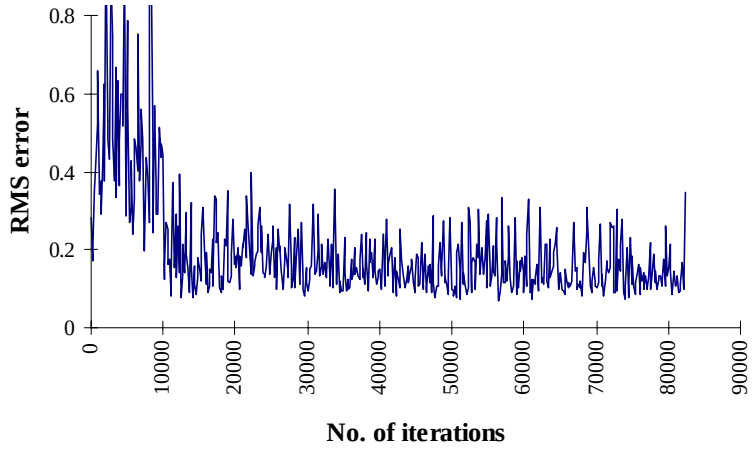

h- Our / DP

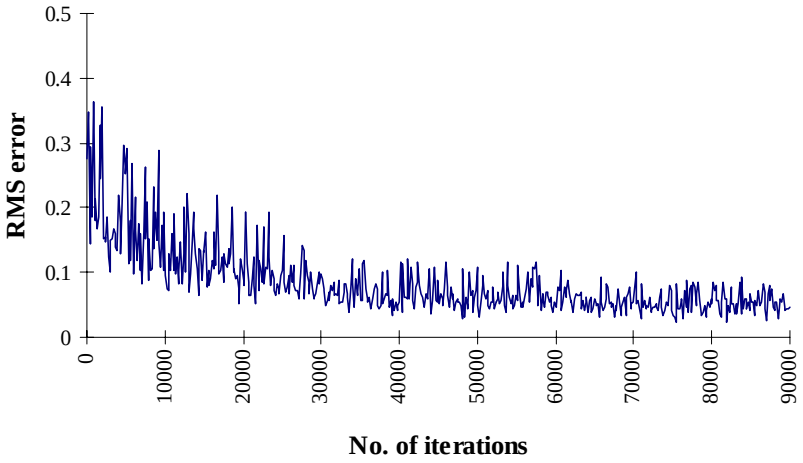

Figure 4.34: A comparison of RMS errors of TBT, DP, and S1BL networks of our model and three versions of Selveraj's model (continued).

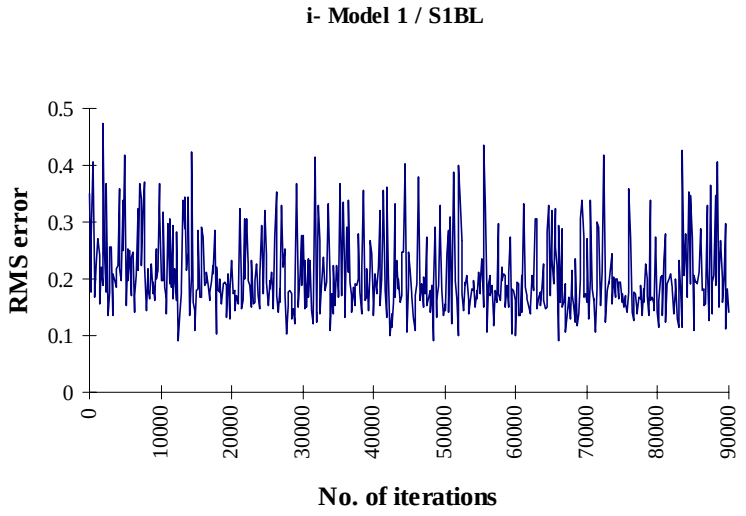

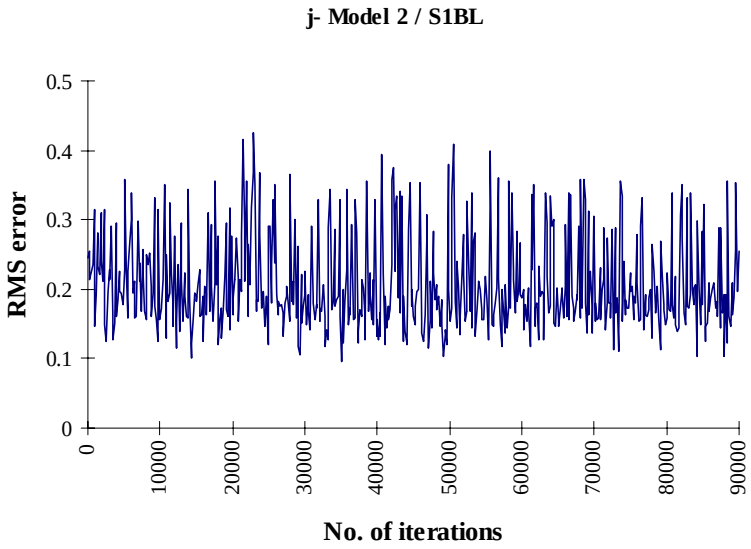

Figure 4.34: A comparison of RMS errors of TBT, DP, and S1BL networks of our model and three versions of Selveraj's model (continued).

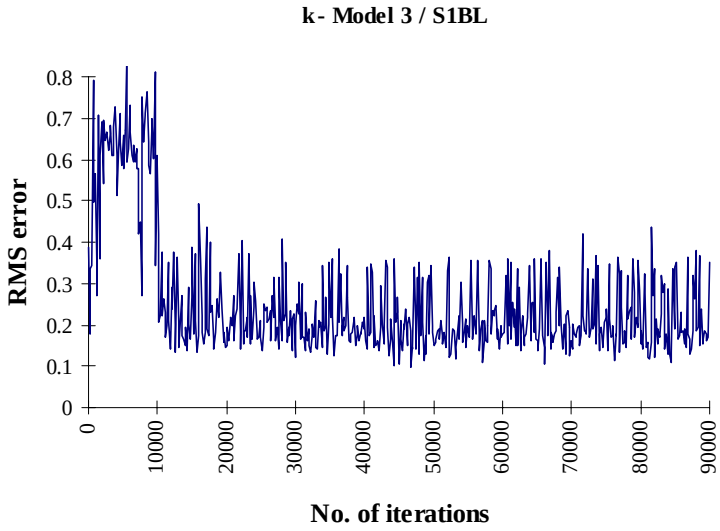

Figure 4.34: A comparison of RMS errors of TBT, DP, and S1BL networks of our model and three versions of Selveraj's model (continued).

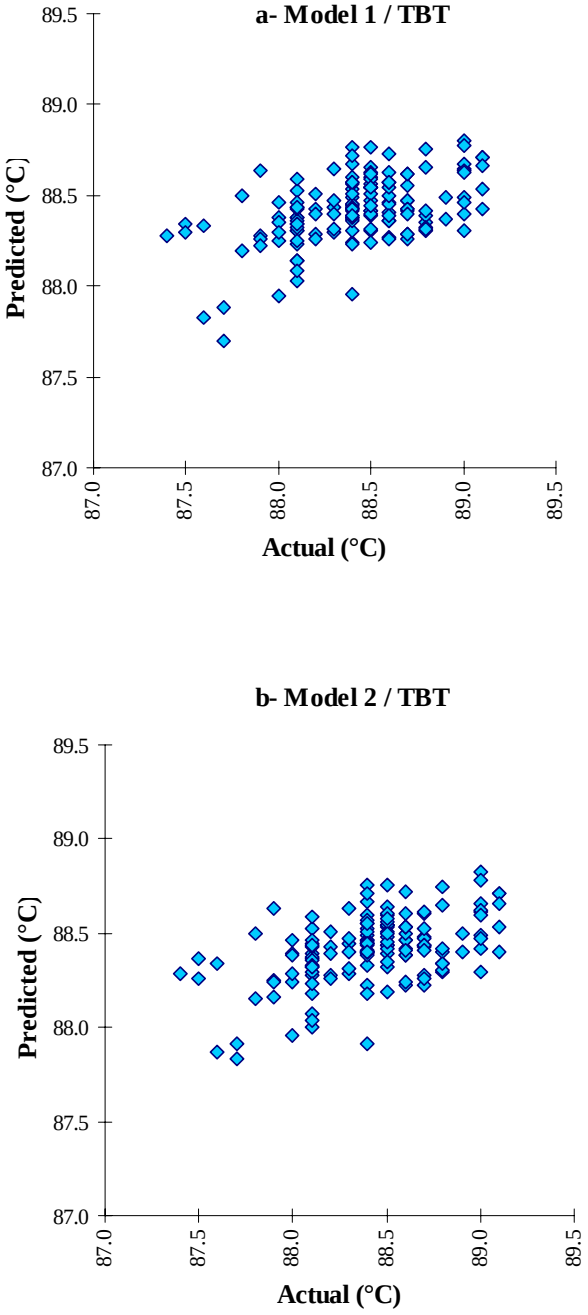

Figure 4.35: A comparison of actual and predicted output variables of our model and three versions of Selveraj's model.

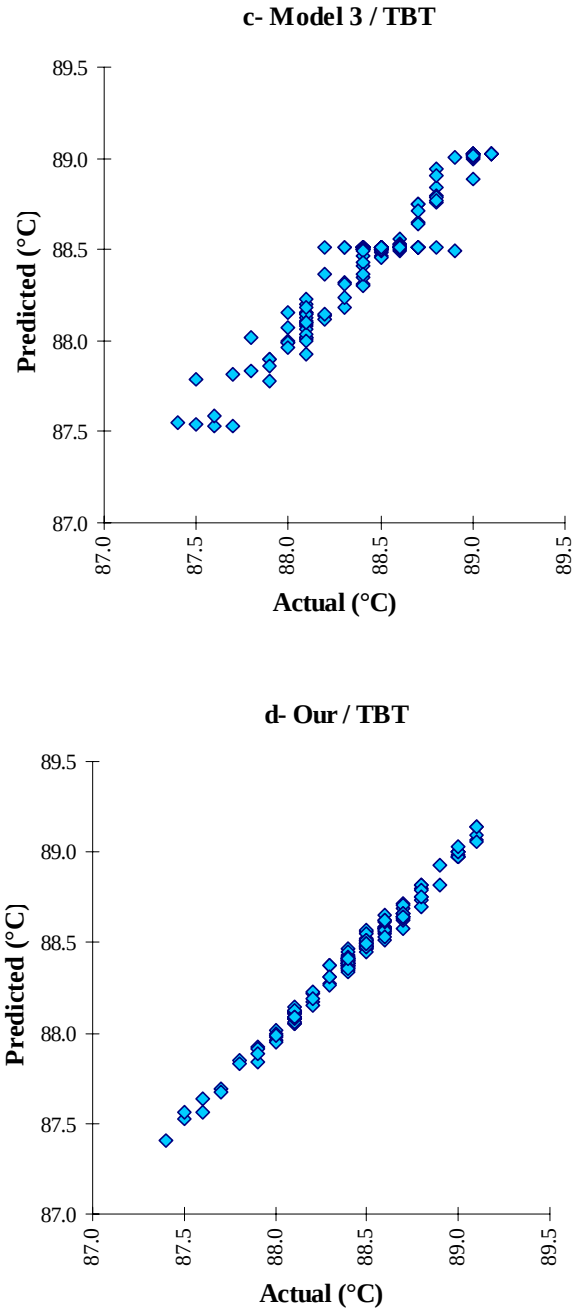

Figure 4.35: A comparison of actual and predicted output variables of our model and three versions of Selveraj's model (continued).

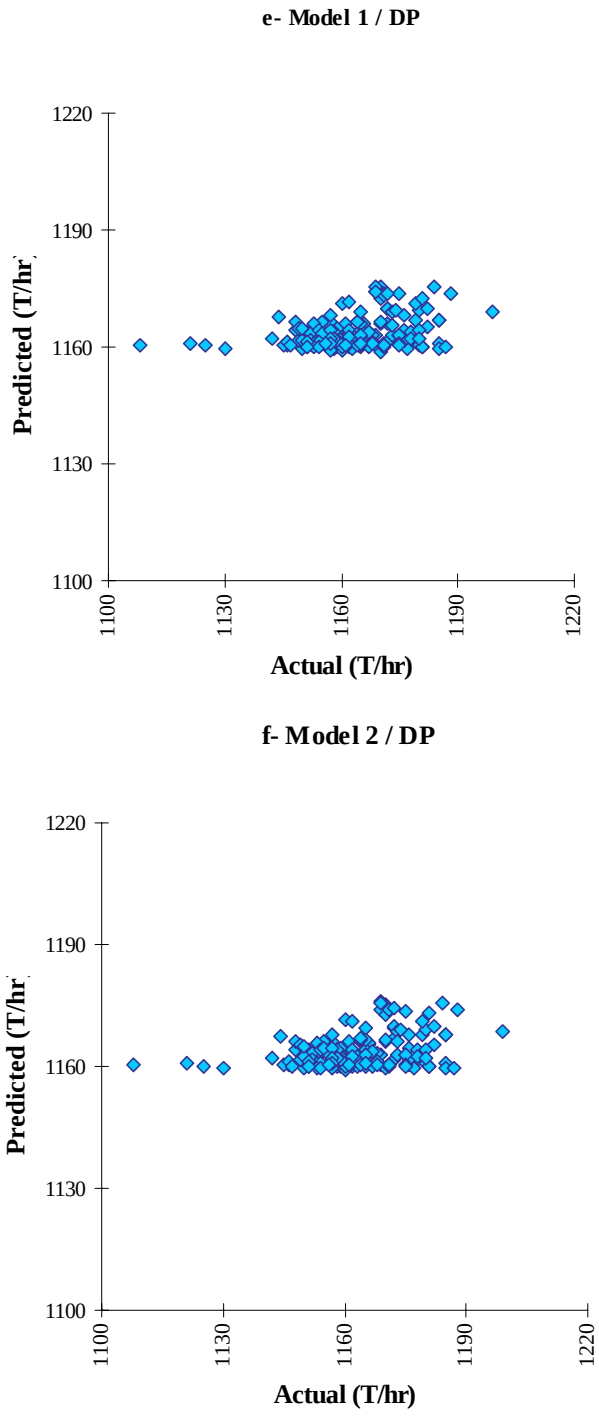

Figure 4.35: A comparison of actual and predicted output variables of our model and three versions of Selveraj's model (continued).

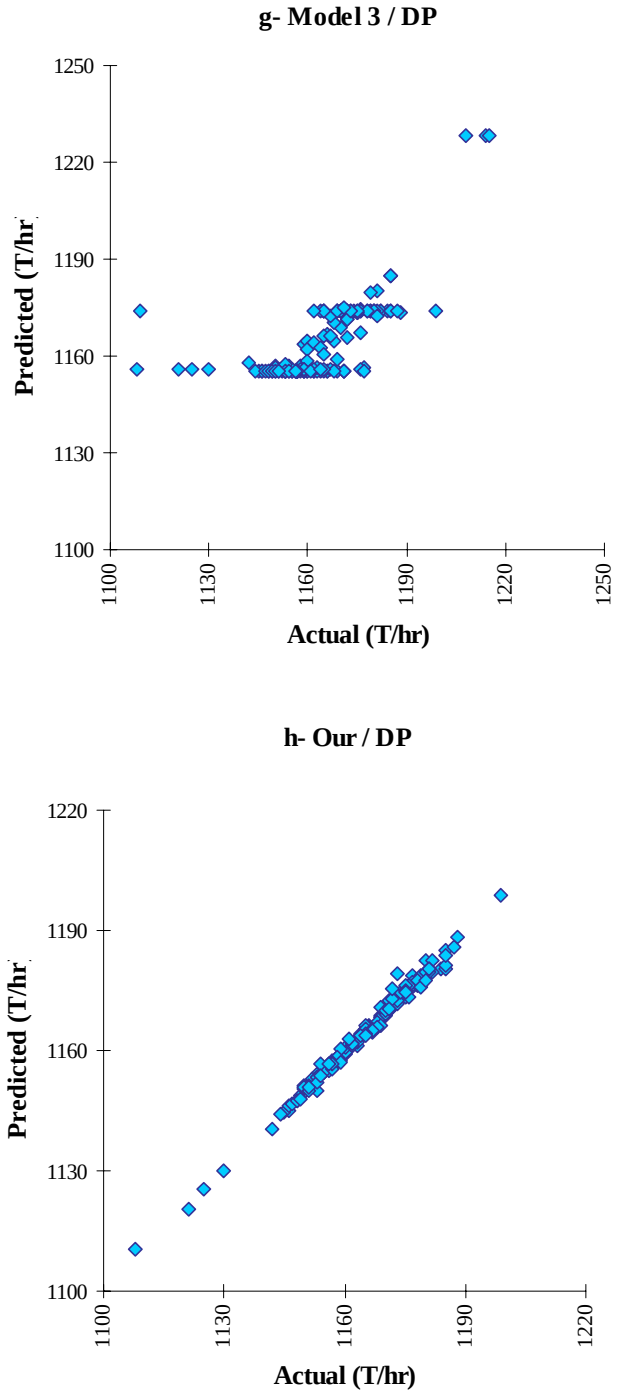

Figure 4.35: A comparison of actual and predicted output variables of our model and three versions of Selveraj's model (continued).

i- Model 1 / S1BL

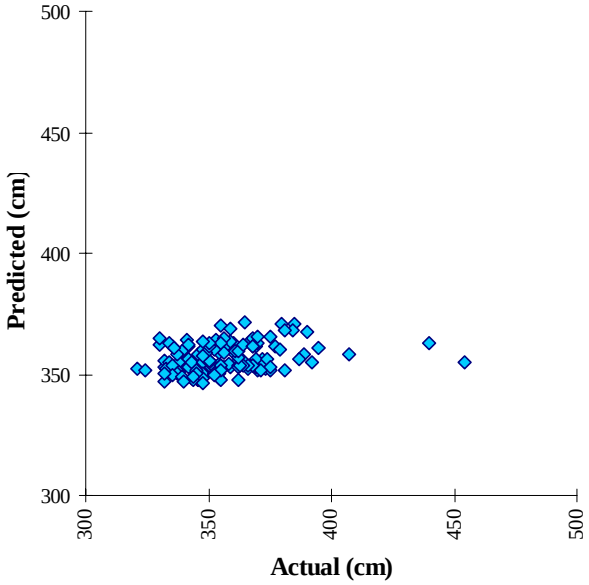

j- Model 2 / S1BL

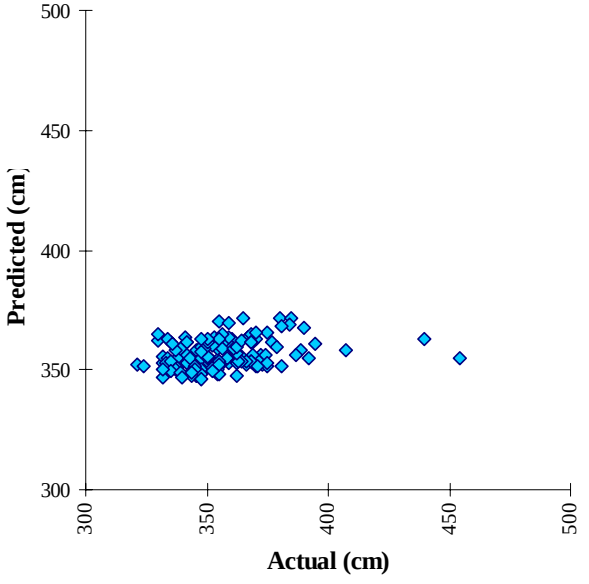

Figure 4.35: A comparison of actual and predicted output variables of our model and three versions of Selveraj's model (continued).

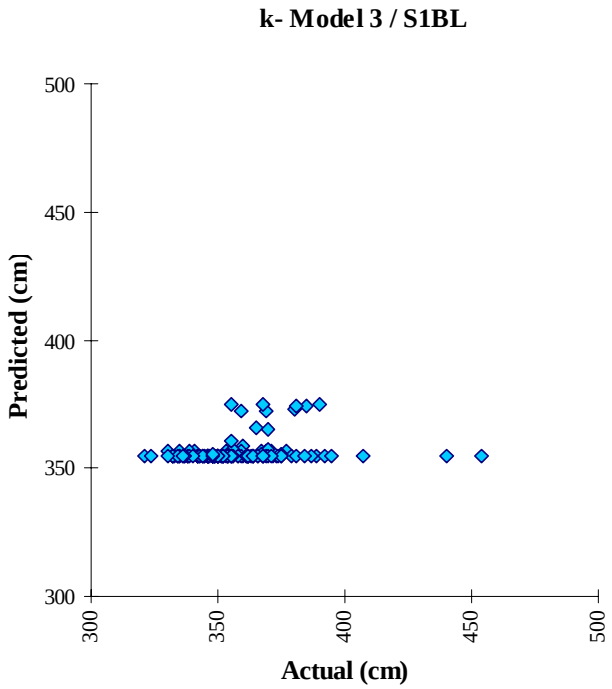

Figure 4.35: A comparison of actual and predicted output variables of our model and three versions of Selveraj's model (continued).

4.5 Conclusions

Neural networks have been very effective in predicting and optimizing the performance variables of the large-scale commercial MSF and RO desalination plants, and are capable of handling complex and nonlinear problems. They also outperform statistical regression models in prediction problems.

We conclude that the degree of success in variable selection greatly influences the resulting network's ability to predict. Statistical methods can aid in the process of variable selection, but the wise engineer will not hesitate to use engineering judgment when it comes to the final decision.

We recommend the following network parameters and functions for modeling a neural network for a large-scale, commercial desalination plant: (1) zero-mean normalization method for input variables; (2) Gaussian weigh-factor distribution for initial values; (3) hyperbolic tangent transfer function; (4) initial architecture: 30 nodes in hidden layer 1 and 15 nodes in hidden layer 2; and (5) initial values for both the learning rate and the momentum coefficient are {0.3, 0.5 & 0.7}, and {0.4}, respectively.
We conclude from comparative studies that our model performs favorably over recent models in accurately predicting commercial desalination plant data.

4.6 Nomenclature

BBT	:	Brine-heater inlet temperature
BDF	:	Blowdown flowrate
BHSP	:	Brine-heater shell pressure
BHST	:	Brine-heater shell temperature

BIT	:	Brine-inlet temperature
CDF	:	Condensate flowrate
CDT	:	Condensate temperature
DP	:	Distillate produced
FF	:	Feed flowrate
FP	:	Feed pressure
FpH	:	Feed PH
FT	:	Feed temperature
MF	:	Makeup flowrate
PC	:	Product conductivity
PF	:	Product flux
RBF	:	Recirculating brine flowrate
S1BL	:	Stage 1 brine level
S24BT	:	Stage 24 brine temperature
STF	:	LP steam flowrate
STT	:	Steam temperature
SWF	:	Seawater flowrate
SWIT	:	Seawater-inlet temperature
SWOT	:	Seawater-outlet temperature
SWRF	:	Seawater recirculating flowrate
TBT	:	Top brine temperature

4.7 References

Abdulbary, A. F., L.L. Lai, K. V. Reddy and D. M. Al-Gobaisi, “Artificial Neural networks as Efficient Tools of Simulation”, *Proceeding of the IDA World Congress*

on Desalination and Water Sciences, Abu Dhabi Printing & Publishing Co., Abu Dhabi, United Arab Emirates (1995).

Allen, D., *Analyzing Experimental Data by Regression,* Lifetime Learning Publications, Belmont, CA (1982).

Bastian, A. and J. Gasos, "Selection of Input Variables for Model Identification of Static Nonlinear Systems", *Journal of Intelligent and Robotic Systems*, **16**, 185 (1996).

Baughman, D. R. and Y. A. Liu, *Neural Network in Bioprocessing and Chemical Engineering*, Academic Press, San Diego, CA (1995).

Chatterjee, S. and B. Price, *Regression Analysis by Example*, John Wiley and Sons, Inc., New York, NY (1977).

Comrey, A.L. and H.B. Lee, *A first Course in Factor Analysis*, Lawrence Erlbaum Associates Publishers, Hilsdale, New Jersey (1992).

El-Hawary, M. E., "Artificial Neural networks and Possible Applications to Desalination", *Desalination*, **92**, 125 (1993).

Freeman, J. A. and D. M. Skapura, *Neural Networks: Algorithms, Applications, and Programming Techniques*, Addison-Wesley Publishing Company, Inc., New York, NY (1992).

Gunst, R. and R. Mason, *Regression Analysis and its Application, A Data-Oriented Approach*, Marcel Dekker, Inc., New York, NY(1980).

Khan, A.H., *Desalination and Water purification 1: Desalination Processes and Multistage Flash Distillation Practice*, Elsevier Science Publishers B.V., New York, NY (1986).

Lior, N., *Desalination and Water purification 2: Measurements and Control in Water Desalination*, Elsevier Science Publishers B.V., New York, NY (1986).

Meyer, S. L., *Data Analysis for Scientists and Engineers*, John Wiley and Sons, Inc., New York, NY (1975).

Parenti, R., S. Bogi, and A. Massarani, "Industrial Application of Real Time Neural Networks in Multistage Desalination Plant", *Proceeding of the IDA World Congress on Desalination and Water Sciences,* Abu Dhabi Printing & Publishing Co., Abu Dhabi, United Arab Emirates (1995).

Press, S. J., *Applied Multivariate Analysis: Using Bayesian and Frequentist Methods of Inference,* Robert E. Krieger Publishing Company, Malabar, Florida (1982).

Selvaragj, R. and P. B. Deshpande, "Neural Networks for the Identification of MSF Desalination Plants", *Desalination,* **101**, 185 (1995).

Tan, S. and M. Mavrovouniotis, "Reducing Data Dimensionality through optimizing Neural Network Inputs", *AICHE Journal*, **41**, 6, 1471 (1995).

Tukey, J., *Exploratory Data Analysis,* Addison-Wesley Publishing Company, New York, NY(1977).

Utojo, U. and B. R. Bakshi, "A Unified View of Artificial Neural Networks and Multivariate Statistical Methods", pp. 435-459, in *Neural Networks in Bioprocessing and Chemical Engineering*, by D.R. Baugham and Y.A. Liu, Academic Press, San Diego, CA (1995).

CHAPTER 5

MODELING AND SIMULATION OF A LARGE-SCALE COMMERCIAL MULTISTAGE FLASH DESALINATION PLANT

This chapter describes how to apply modular and equation-solving approaches for simulation of large-scale commercial MSF desalination plant using advanced commercial software tools. We first describe the application of the modular approach for the steady-state simulation through the use of ASPEN PLUS package. We next present the equation-solving approach for the steady-state and dynamic simulations through the use of SPEEDUP package. Finally, we compare the three steady-state models developed by neural network (Chapter 4), ASPEN PLUS and SPEEDUP.

5.1 Introduction

Modeling refers to formulating a set of equations that describe mathematically an industrial process under consideration. In the simulation phase, the formulated model is solved by using a suitable solution procedure, as well as by entering the values of independent process variables. We typically do this with the aid of a computer, which is termed as computer-aided simulation. The goals of modeling and simulation in the process industry include improving and optimizing designs, developing better insight into the working of the process, and ultimately leading to the optimal operation and control of the process.

In simulating a plant, we represent all the individual units in the process separately, and couple them together in accordance with physical interconnections to give the model for the whole plant. The basic approach to modeling is to utilize mathematical relationships

among process variables. These relationships define the physical laws, material, energy and momentum balances, etc. in the form of a set of generally nonlinear, algebraic and differential equations. The model should reflect all the important features of the process, and it should not be too complex to become unmanageable for computation.

For the preliminary checking of material and heat balances of a plant, a simplified model may be sufficient. For in-depth studies, however, we require more rigorous models.

According to the time-dependence, there are two kinds of process models: steady-state and dynamic models. The steady-state model is time-invariant. It describes the process through a set of algebraic equations. Design models of continuos processes are always steady-state models. Dynamic model are time-dependent, and they contain differential equations and supporting algebraic equations.

Different steady-state models are used for design purposes as well as for parametric studies of existing plants for performance evaluation and operational optimization. Dynamic models are used for unsteady-state simulations of the process and for control purposes. In both cases, the model of the process must be connected to the model of the control system to accomplish the simulation of the whole process.

Currently, there is an increasing interest in the development of advanced control system for the MSF desalination plant. Efforts to develop a steady-state model (Helal et al, 1986, and Husain et al, 1993) and a dynamic model (Husain et al, 1994, 1993) are continuing in the hope that considerable improvement in the operation of the plant can be achieved by applying advanced control strategies. Table 5.1 summarizes the reported approaches for solving nonlinear models for desalination processes using advanced commercial software tools. Little work exists on the development of dynamic models of commercial MSF

plants.

In this work, we use ASPEN PLUS for implementing the modular approach, and SPEEDUP for applying equation-solving approach for steady-state and dynamic simulations. We modify the SPEEDUP dynamic model for the MSF process developed by the International Center for Water and Energy Systems (ICWES) (Husain, 1995) for specifically applying it to the AZ-ZOUR South MSF desalination plant.

Table 5.1: Reported simulation studies which used advanced commercial software tools.

Investigators	**Remarks**	**Use of advanced commercial software tools**
Husain et al. (1993 and 1994)	Steady-state and dynamic simulations are carried out on 18-stage MSF desalination plant in Abu-Dhabi in United Arab Emirates.	SPEEDUP
Rahbar (1993)	• Explains how steady-state and dynamic simulations can lead to better design and improved control of 18-stage MSF desalination and co-generation plants in Abu-Dhabi in UAE. • Describes ASPEN PLUS and its applications in power-plant design. • Presents the facilities available in the SPEEDUP system for dynamic modeling and simulation and explains the interfaces available to control-system design packages.	ASPEN PLUS and SPEEDUP

The following sections introduce the MSF process, and the modular and equation-solving approaches used to develop the steady-state and dynamic simulations. We briefly describe ASPEN PLUS and SPEEDUP packages commercially available from Aspen

Technology, Massachusetts, USA, and illustrates the results of the steady-state simulations from both packages. Finally, we investigate the effect of introducing a step change in the set points of the key manipulated variables on the dynamic response of controlled variables through the use of SPEEDUP dynamic model.

Appendix A describes the mathematical model of a multistage flash desalination process. Appendix B lists all the physical property correlations used to develop a FORTRAN program to calculate the thermodynamic properties of different liquid and vapor streams.

5.2 Multistage Flash (MSF) Process Description and Model Formulation

A. Process Description

The MSF process is similar to multicomponent distillation, but there is no exchange of material between the countercurrent streams. Actually, the MSF process is a flash evaporation process in vacuum, where the vacuum changes from one stage to the next and the evaporation temperature decreases from the first to the last stage.

From the modeling point of view, it is easier to describe a single flash stage if it is split up into four compartments, which can be treated separately. The four compartments are: flash chamber, vapor space, product tray, and tube bundle. Figure 5.1 shows the graphical representation of a single compartmentalized stage. We indicate the liquid and vapor flows by solid and broken lines, respectively.

Each fluid stream communicating with the individual stage has four characterizing variables: flowrate, temperature, pressure, and salt concentration. From these variables, we calculate the physical properties, namely, enthalpy, density, and specific heat of the stream, as dependent variables.

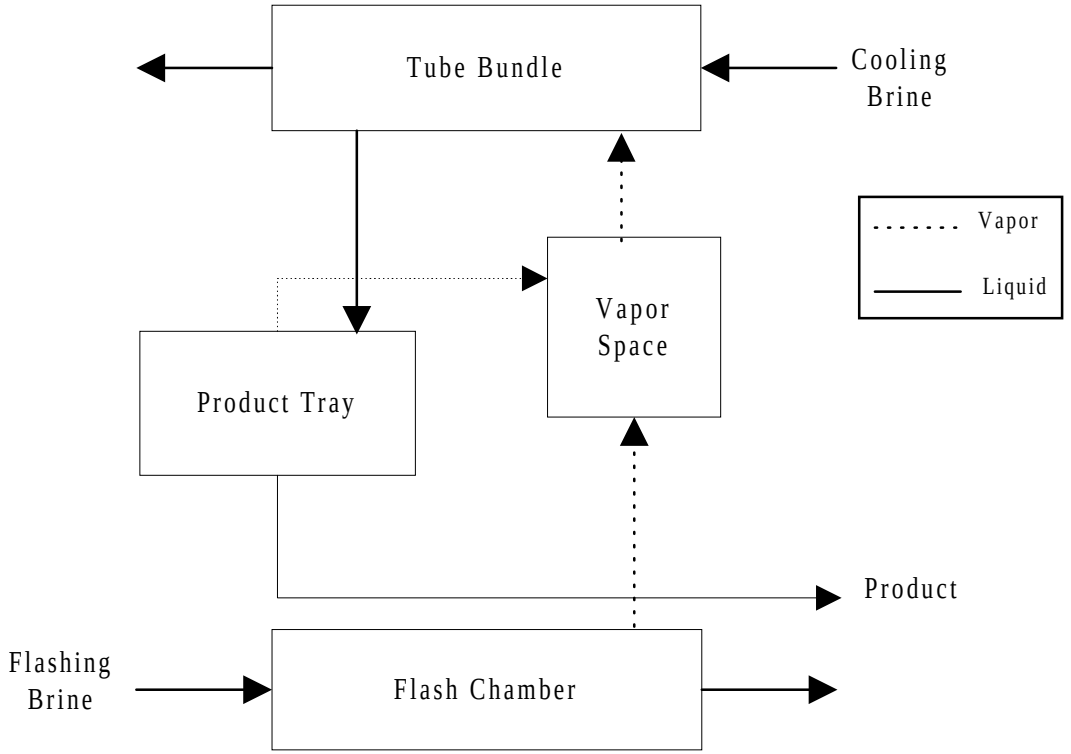

Figure 5.1: Representation of a single stage of the MSF plant.

With time derivatives included for the mass holdup, concentration, temperature and specific enthalpy in each of the compartment of the stage, we get an unsteady-state or dynamic model. With these derivatives put to zero, the model represents steady-state conditions.

Figure 5.2 illustrates schematically the MSF distillation plant. It consists of N stages divided into three main sections, the brine heater (BH), the heat-recovery section (HRS), and the heat-rejection section (HJS). The heat-recovery and heat-rejection sections in turn, consists of several flash stages (N). The first NR stages (1 to NR) constitute the heat-recovery section, where the recycle brine inside the condensing tubes recovers the latent heat of vaporization of the flashing brine. The remaining stages (NR+1 to N) represent the heat-rejection section which removes the heat added by the brine heater.

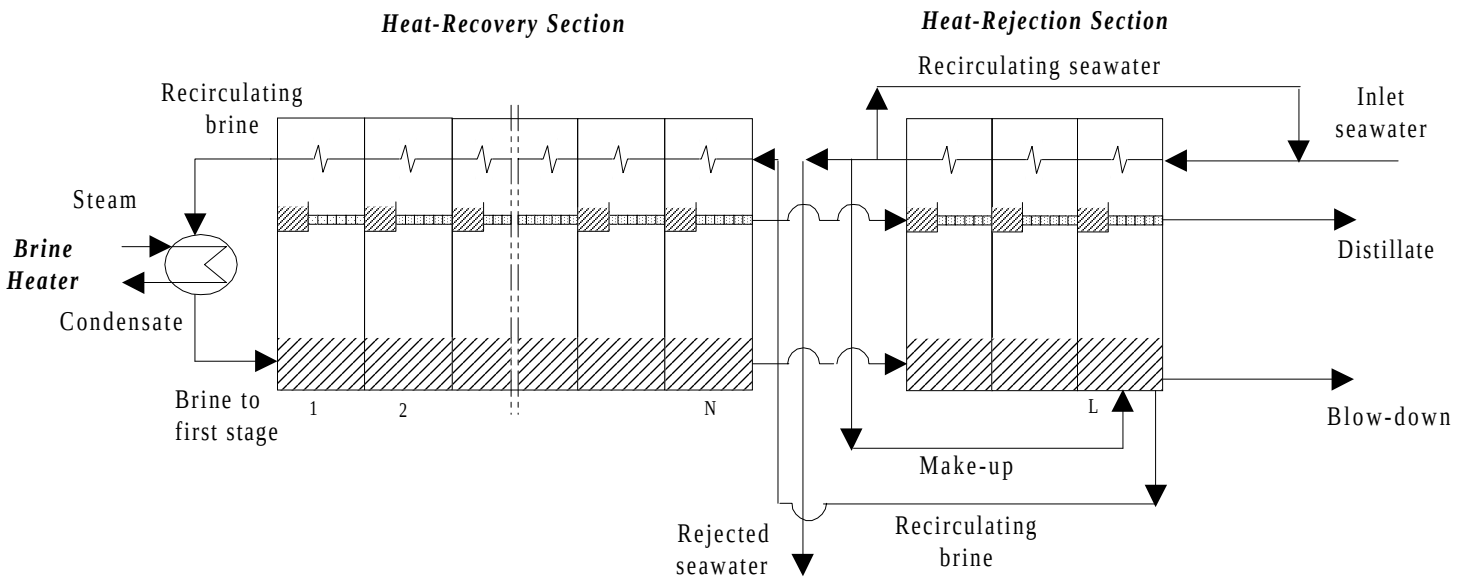

Figure 5.2: MSF desalination plant.

B. Design and Operational Data

Tables 5.2 and 5.3 show the dimensions and operational data of the AZ-ZOUR South desalination plant used throughout this study.

We make the following assumptions in the development of steady-state and dynamic models.

1. The distillate leaving any stage is salt-free.
2. The system is well-insulated so there is no heat loss to the surroundings.
3. The tube temperature is equal to the vapor temperature.
4. All liquid and vapor phases are well-mixed, so their temperatures, concentrations, and specific enthalpies are the same as those of the outlet brine from the flash chamber.
5. There is no entrainment of mist by the vapor flashed from the brine.
6. No subcooling of condendsate leaving the brine heater.
7. The low-pressure saturated steam is supplied to the brine heater.
8. Non-condensable gases have negligible effects on the efficiency of heat transfer since they are removed by the ejectors at particular stages in the plant.
9. The contractor’s total temperature loss is considered.

Table 5.2: Design and operational data of AZ-ZOUR South desalination plant.

Process variable	Units	Specification
Distillate produced	T/min	18.795
LP steam flowrate to the brine heater	T/min	2.3477
Recycle brine flowrate	T/min	238.1
Seawater rejected flowrate	T/min	160.48
Blowdown flowrate	T/min	29.96
Make-up flowrate	T/min	48.757
Top brine temperature	°C	90
Seawater inlet temperature to the heat-rejection section	°C	32.22
LP Steam temperature to the brine heater	°C	100

Table 5.3: Dimensional details of AZ-ZOUR South MSF desalination plant.

Dimension	Unit	Brine-Heater	Heat-Recovery section	Heat-Rejection Section
Stage length	m	-	3.998	3.998
stage width	m	-	17.66	17.66
stage height	m	-	8.34	8.34
Orifice width	m	-	16.92	16.92
No. of tubes		1367	1451	1588
Tube length	m	18.99	18.41	18.45
Tube inside diameter	mm	0.04258	0.04258	0.03298
Tube thickness	mm	1.219	1.219	1.219
Area of heat transfer	m^2	3544	3676.47	3148
Cross-sectional area of a flash chamber	m^2	-	70.605	70.605

5.3 Steady-State and Dynamic Simulations Using Advanced Commercial Software Tools

MSF process is a nonlinear recycle process with a closed-loop information flow. Solution methods recognizing these features must be used. One is the simultaneous (equation-solving) approach and the other is stage-by-stage (sequential or modular) approach.

The calculations involved for individual process units, along with the computation of different physical and thermodynamic properties, a library of numerical routines, convergence algorithms, etc. can be common to a variety of packages. This makes it attractive to apply commercial software tools for modeling or simulating any process plant of a given configuration. This research applies two advanced commercial software tools:

- ASPEN PLUS for steady-state simulations
- SPEEDUP for steady-state and dynamic simulations

A. Steady-State Simulation Using ASPEN PLUS

1. Description of ASPEN PLUS

ASPEN PLUS is an advanced commercial software that allows the user to build and run a steady-state simulation model for a chemical process. ASPEN PLUS provides a flexible and productive engineering environment designed to maximize the results of engineering efforts, such as;

- User Interface Mode Manager
- Quick Property Analysis
- Rigorous and Robust Flowsheet Modeling
- Interactive Architecture
- Powerful Model Analysis Tools
- Analysis and Communication of Results.

Therefore, ASPEN PLUS lets the user focus his/her energies on solving the engineering problems, not on how to use the software.

Process simulation, via ASPEN PLUS, enables the user to run many cases, conduct "what if" analyses, and perform sensitivity studies and optimization runs. Not only is ASPEN PLUS good for process simulation, it also allows the user to perform a wide range of other tasks such as estimating and regressing physical properties, generating custom graphical and tabular output results, data-fitting plant data to simulation models, costing the plant, optimizing the process, and interfacing results to spreadsheets.

2. Problem Description

A process consists of all the components that are manipulated thermodynamically by unit operations in a system. The components range from the unit operations, to the process streams that flow, to the chemical components contained in each. The development of a simulation model for a chemical process using ASPEN PLUS involves the following steps:

1. Define the process flowsheet configuration by specifying
    a. Unit operations

   b. Process streams flowing between the units
   c. Unit operation models to describe each unit operation

2. Specify the chemical components.
3. Choose a thermodynamic model to represent the physical properties of the components and mixtures in the process.
4. Specify the component flow rates and thermodynamic conditions (i.e. temperature, pressure, or phase condition) of the feed streams.
5. Specify the operating conditions for the unit operations.

Table 5.4 gives additional details of this developmental process.

Table 5.4: Developmental process for an ASPEN PLUS simulation model.

Step	Used to
Defining the flowsheet	Break down the desired process into its parts: feed streams, unit operations, and product streams.
Specifying stream properties and units	Calculate the temperature, pressure, vapor fraction, molecular weight, enthalpy, entropy and density for the simulation streams.
Entering components	From a databank that is full of common components.
Estimating property parameters	Property Constant Estimate System (PCES) can estimate many of the property parameters required by physical property models.
Specifying streams	Streams connect unit operation blocks in a flowsheet and carry material and energy flows from one block to another. For all process feed streams, we must specify flowrate, composition, and thermodynamic condition.
Unit operation blocks	We choose unit operation models for flowsheet blocks when we define our simulation flowsheet.

3. ASPEN PLUS MSF Model Formulation

Following the procedure described in the previous section, we develop a steady-state model for the MSF plant in ASPEN PLUS. The design of an MSF desalination plant consists of three section: brine heater, heat-recovery section and heat-rejection section.

a. Brine Heater

Figure 5.3 compares the actual plant flowsheet and the ASPEN PLUS model for the brine heater. Figure 5.4 shows the ASPEN PLUS simulation flowsheet in more detail.

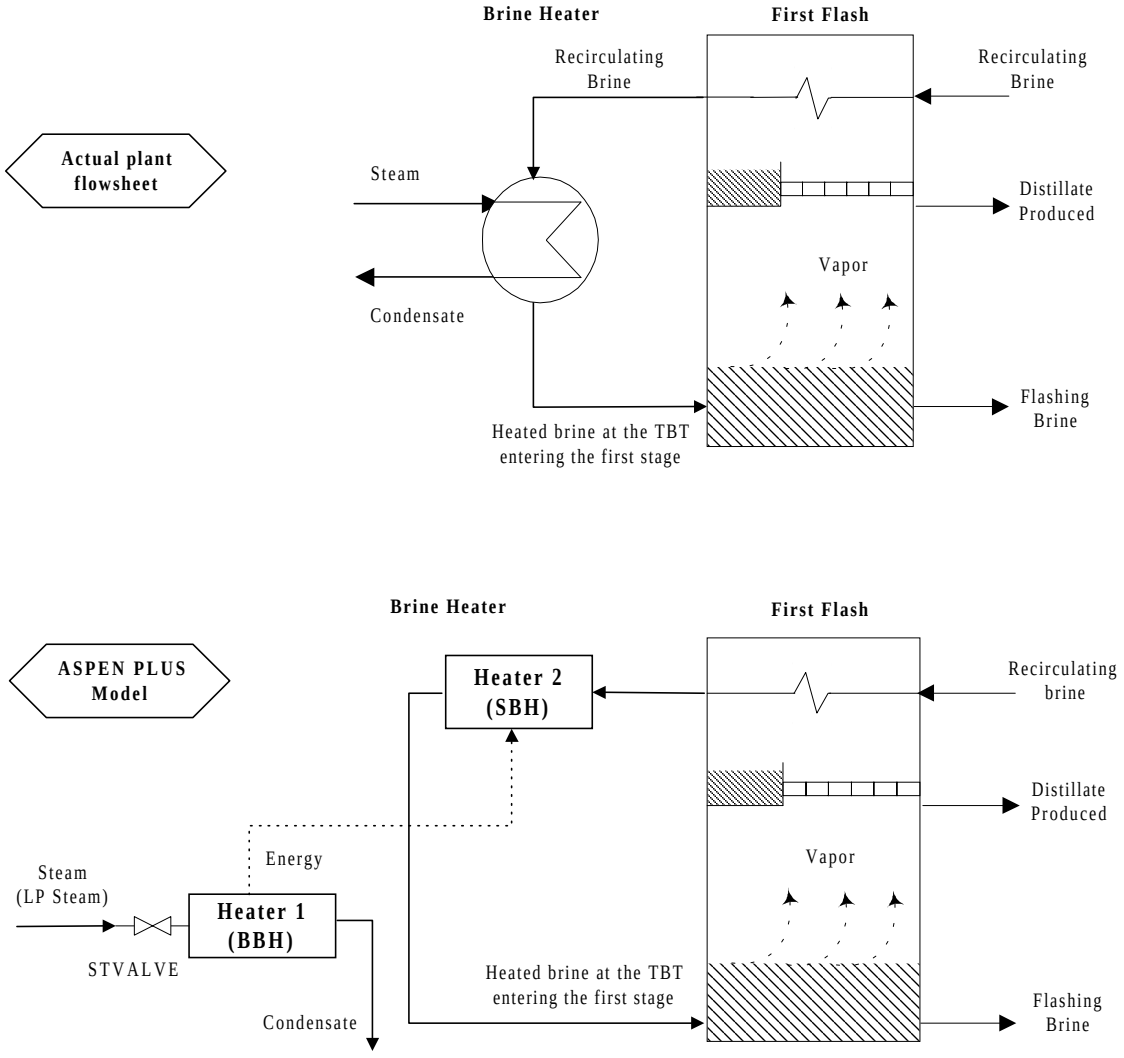

Figure 5.3: A comparison of the actual plant flowsheet and the ASPEN PLUS model for the brine heater.

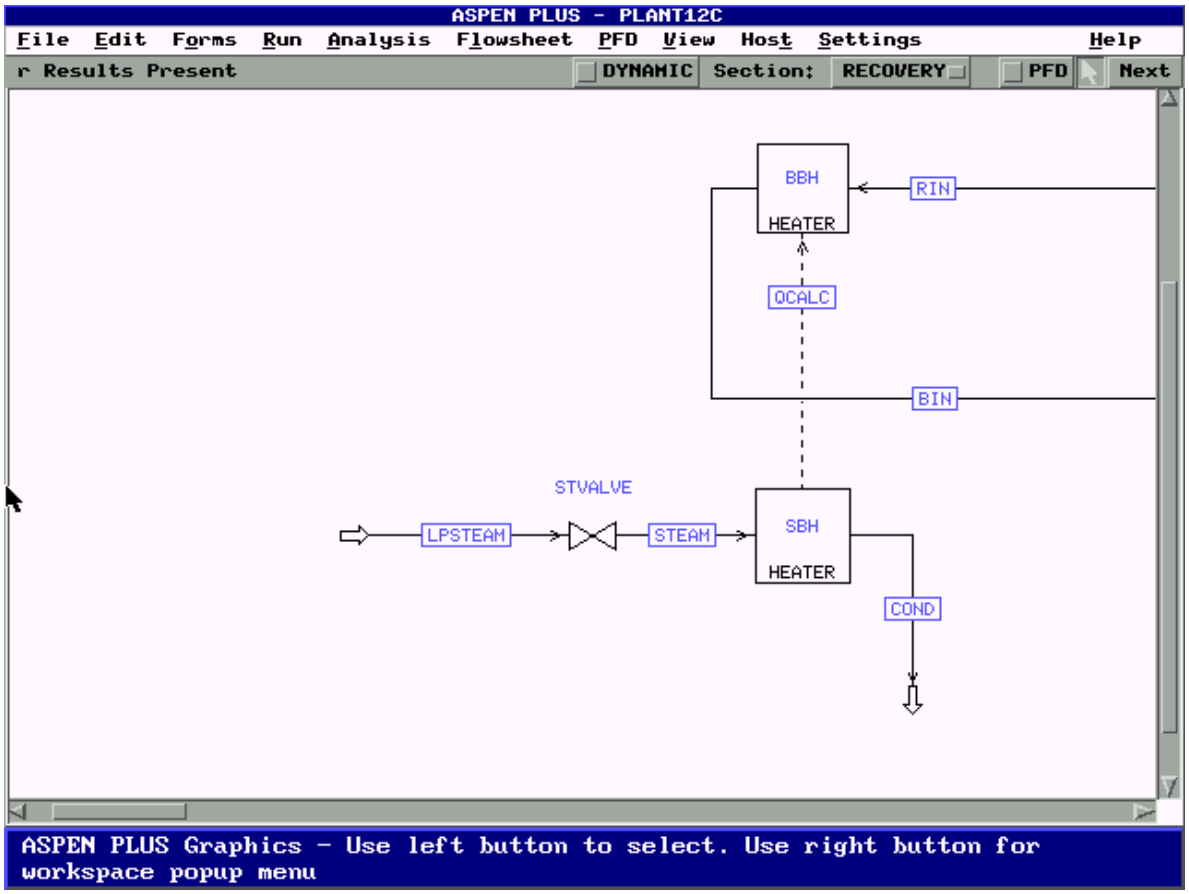

Figure 5.4: Brine heater ASPEN PLUS diagram.

The brine heater consists of two inlet streams and two outlet streams. One inlet stream is the recirculating brine ready to be heated to the desired temperature. The second inlet stream is the steam used to heat the recirculating brine. Both streams exit accordingly, without mixing.

ASPEN PLUS design software has the model type HEATER which is sufficient to represent the process of the brine heater. We use two heaters (Heater 1 and Heater 2) in ASPEN PLUS to simulate the brine heater model. Table 5.5 lists the brine-heater specification in the ASPEN PLUS model.

Table 5.5: Brine-heater specifications.

Block Name	**Specifications**
Heater 1 (BBH):	
Pressure	0.702 (Bar)
Heat input	Heat stream from Heater 2
Heater 2 (SBH):	
Temperature	100 (°C)
Vapor fraction	0
Steam valve (STVALVE):	
Temperature	100 (°C)
Vapor fraction	0
Steam inlet stream (LPSTEAM):	
Temperature	101.5 (°C)
Vapor fraction	0

b. <u>Flash and First Flash</u>

Figure 5.5 compares the actual plant flowsheet and ASPEN PLUS model for a single stage, and Figure 5.6 shows additional details for the ASPEN PLUS model.

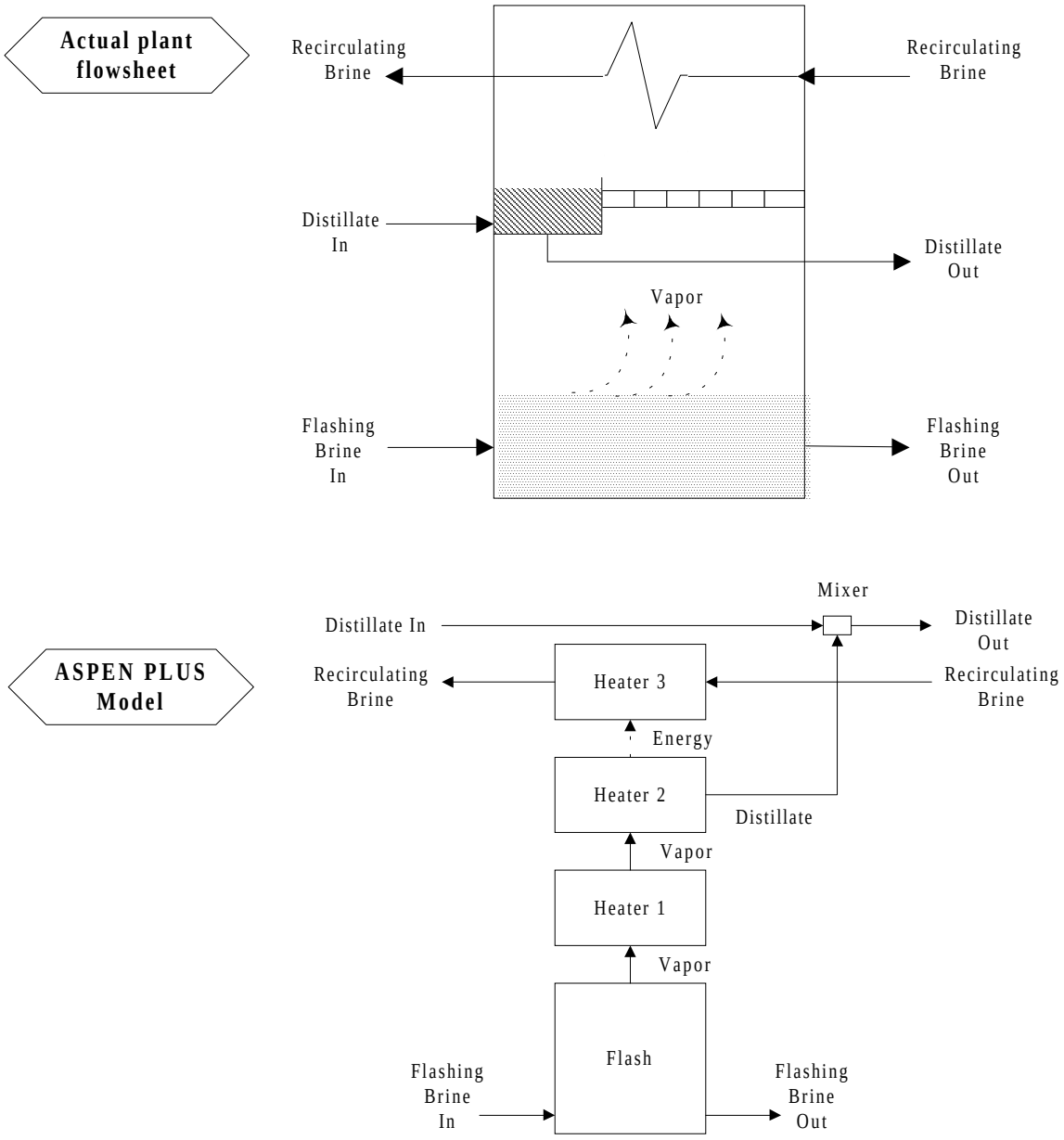

Figure 5.5: A comparison of the actual plant flowsheet and ASPEN PLUS model for a single stage.

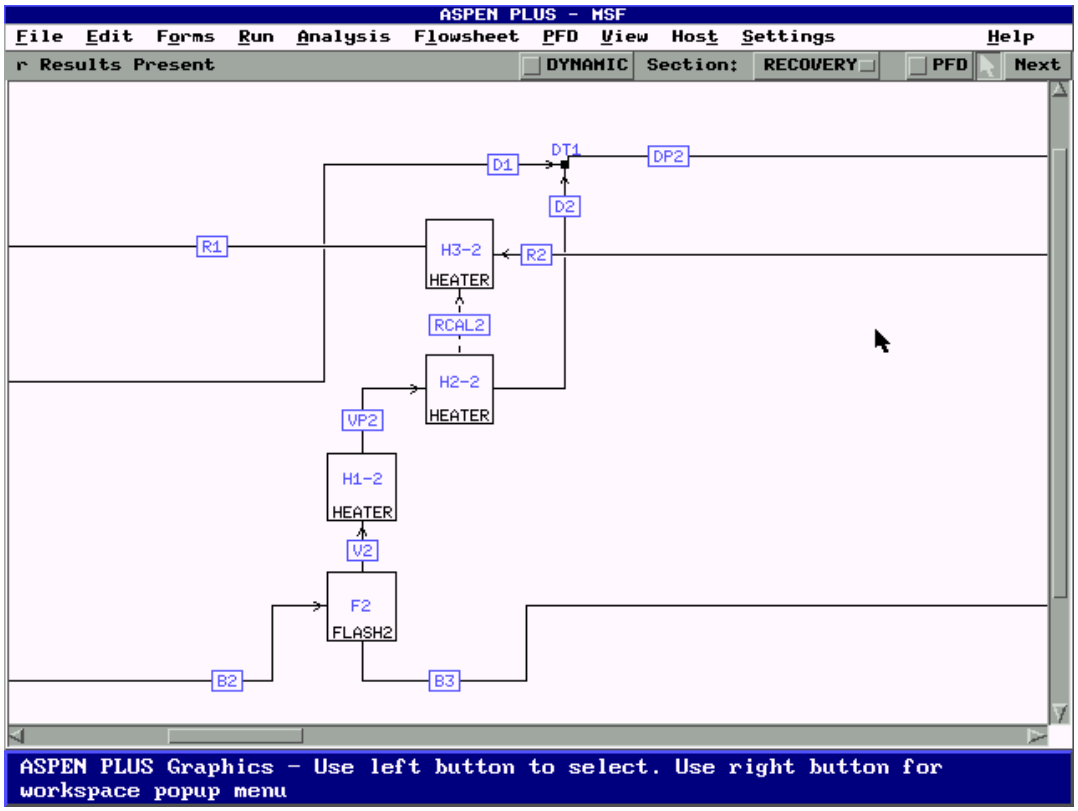

Figure 5.6: ASPEN PLUS simulation flowsheet for a single flash stage.

Table 5.6 gives the specification of the ASPEN PLUS model for the first flash stage. We briefly describe the flash simulation as follows.

Table 5.6: Specification of the ASPEN PLUS model for the first flash stage for summer operation.

Block name	Specifications
Flash:	
Temperature	88.9 9 (°C)
Pressure	0.6574 (Bar)
Heater 1:	
Temperature	87.9 (°C)
Vapor fraction	1
Heater 2:	
Temperature	87.7 (°C)
Vapor fraction	0
Heater 3:	
Pressure	0.75
Heat input	Heat stream from Heater 2
Mixer:	
Pressure	0
Nphase	1
Phase	Liquid

Referring to the ASPEN PLUS model of Figure 5.6, we see the flash stage is a block, Flash, which describes the flashing of the brine. As the brine flows into the stage, it becomes superheated and ultimately flashed off to give pure vapor as a result of pressure reduction. In the actual process, the vapor passes through the demisters where the salt carried with the vapor is removed. Due to the limitations of ASPEN PLUS, we cannot include demisters in the flash model and we assume the vapor to be salt-free. There

exists a temperature drop across the demisters due to pressure drop, as well as across the stage due to boiling-point elevation. To account for this temperature change, we include a block, Heater 1, in the ASPEN PLUS model of Figure 5.5.

As the vapor passes through the demisters, it condenses on the cooling tubes into a water box. The cooling tubes contain recirculating brine which uses the heat released by condensation to preheat the feed. In order to model this process, we include a block, Heater 2, to simulate the phase change from vapor to liquid. Here, the vapor enters the heater and condenses into a liquid, while generating heat. At the same time, the generated energy serves as heat stream and enters Heater 3 to simulate the pre-heating of the recirculating brine flowing through tubes that run across the top of the stage.

The condensed vapor is collected as distillate in the distillate tray inside the flashing stage. The distillate produced from one stage is combined from previous stages into a distillate duct. In order to model this, we use a block, MIXER, to combine the distillate produced from one stage with the distillate produced with all the successive stages.

c. Heat-Recovery Section

The heat-recovery section consists of a number of flash stages (21 stages) connected to one another. Figure 5.7 (in seven pages) shows the block diagram of the ASPEN PLUS simulation model, and Table 5.7 gives the ASPEN PLUS specification of all flash stages in the heat-recover section.

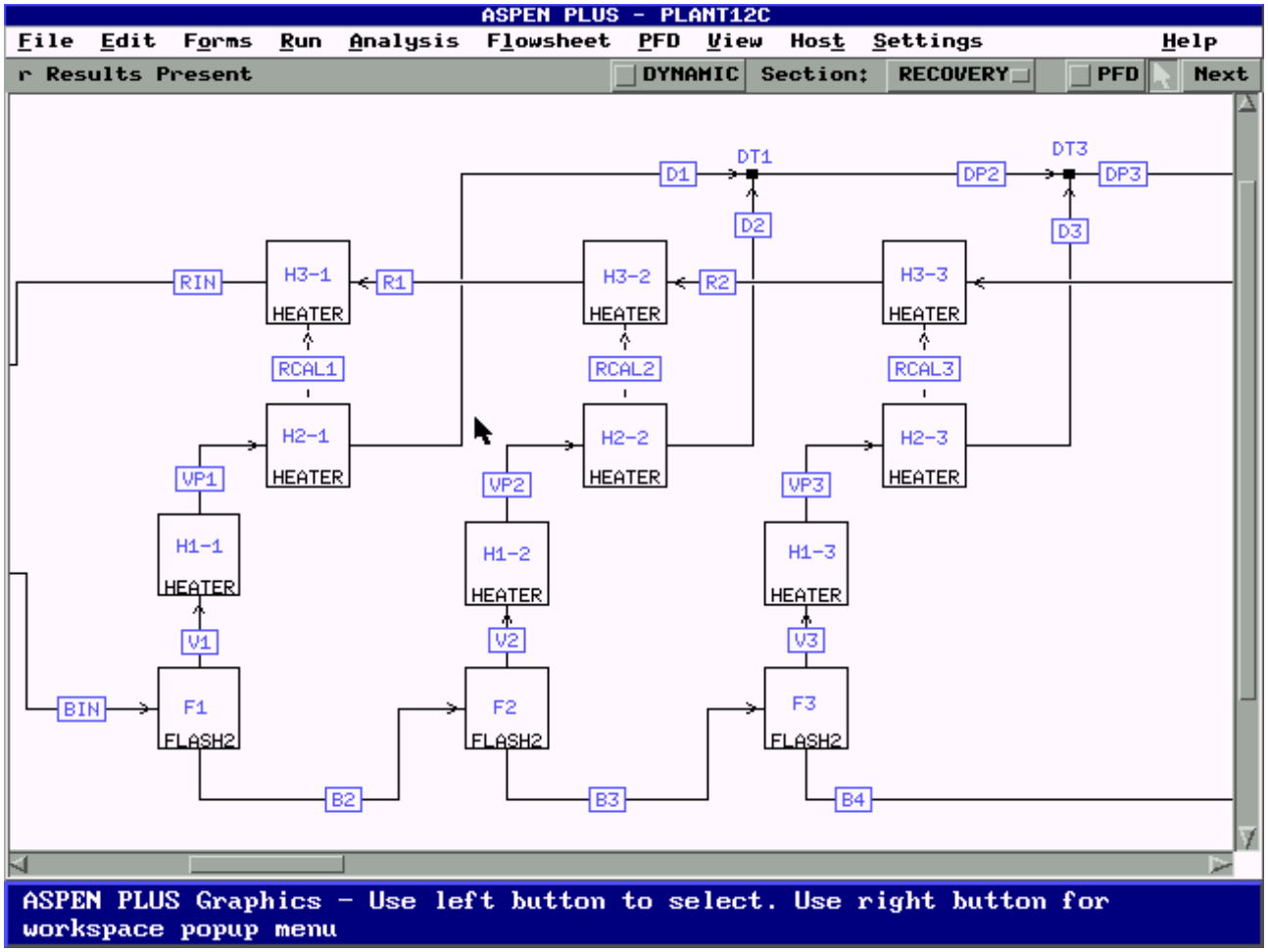

Figure 5.7: ASPEN PLUS simulation model for the heat-recovery section.

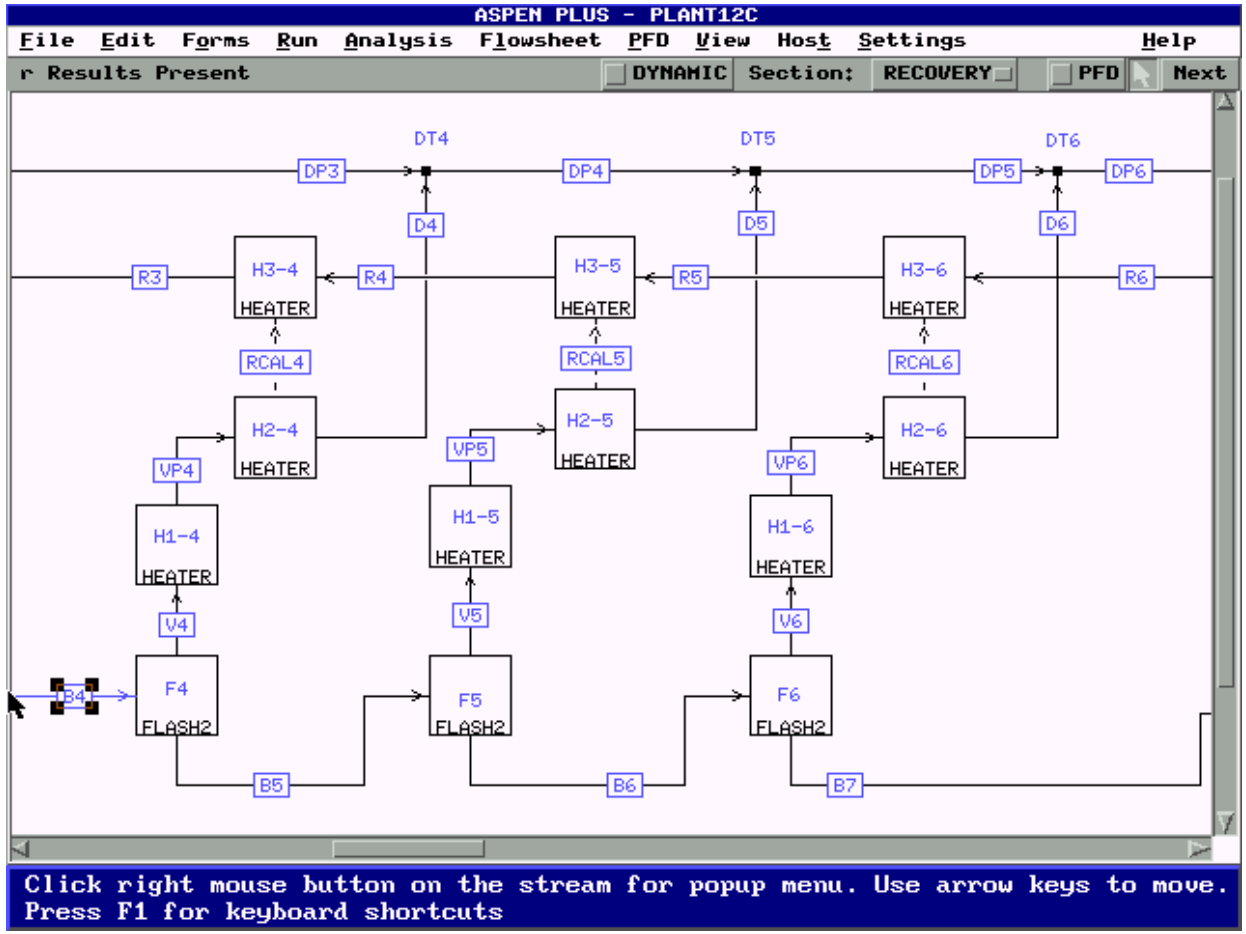

Figure 5.7: ASPEN PLUS simulation model for the heat-recovery section (continued).

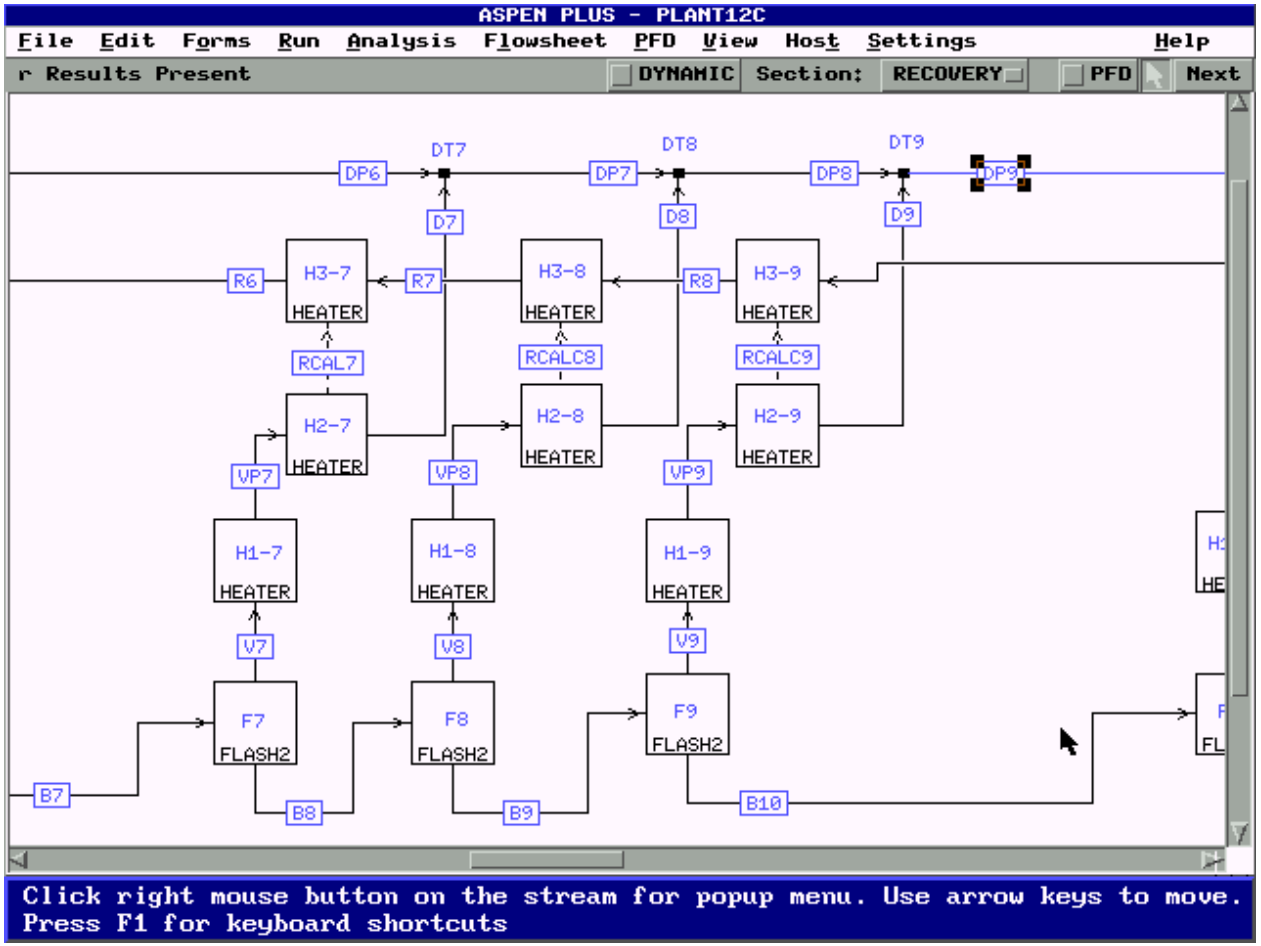

Figure 5.7: ASPEN PLUS simulation model for the heat-recovery section (continued).

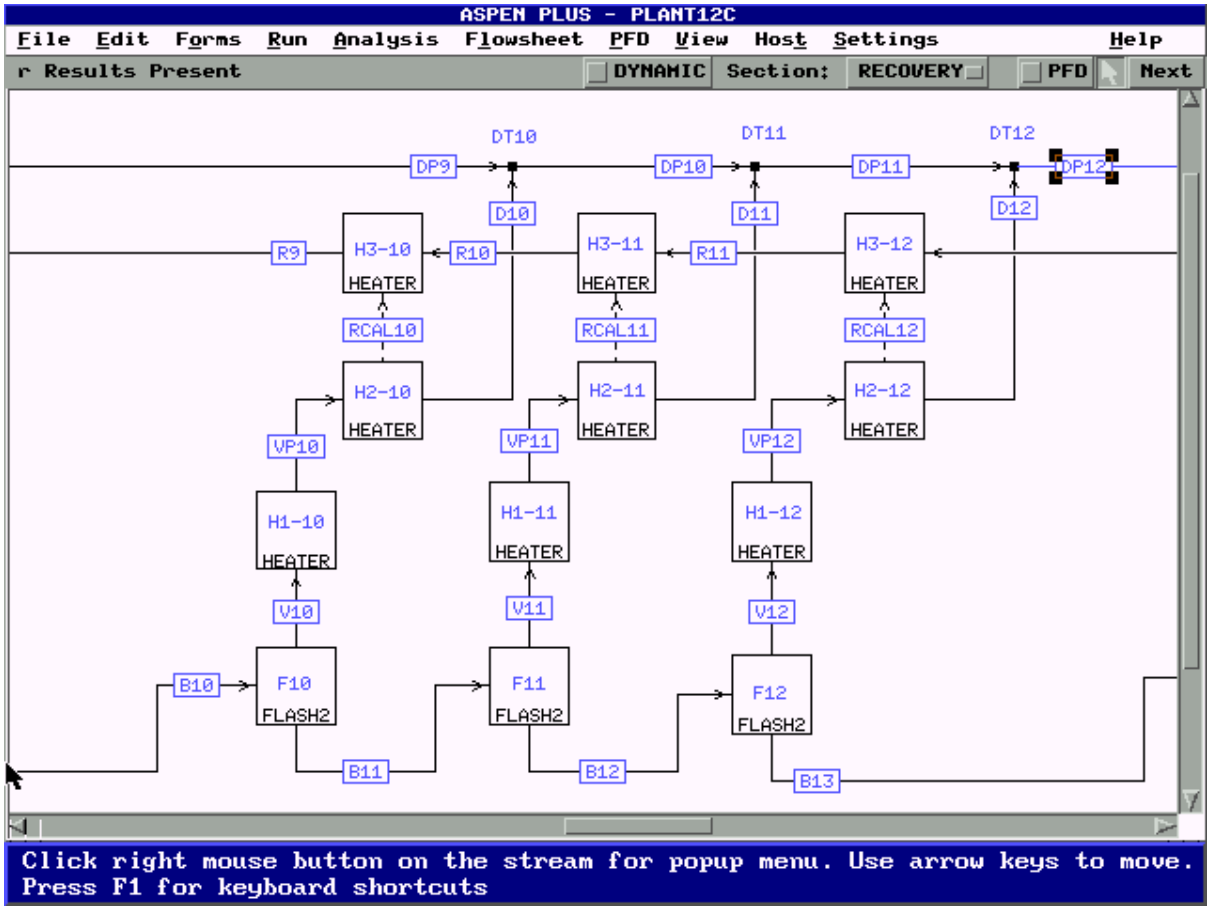

Figure 5.7: ASPEN PLUS simulation model for the heat-recovery section (continued).

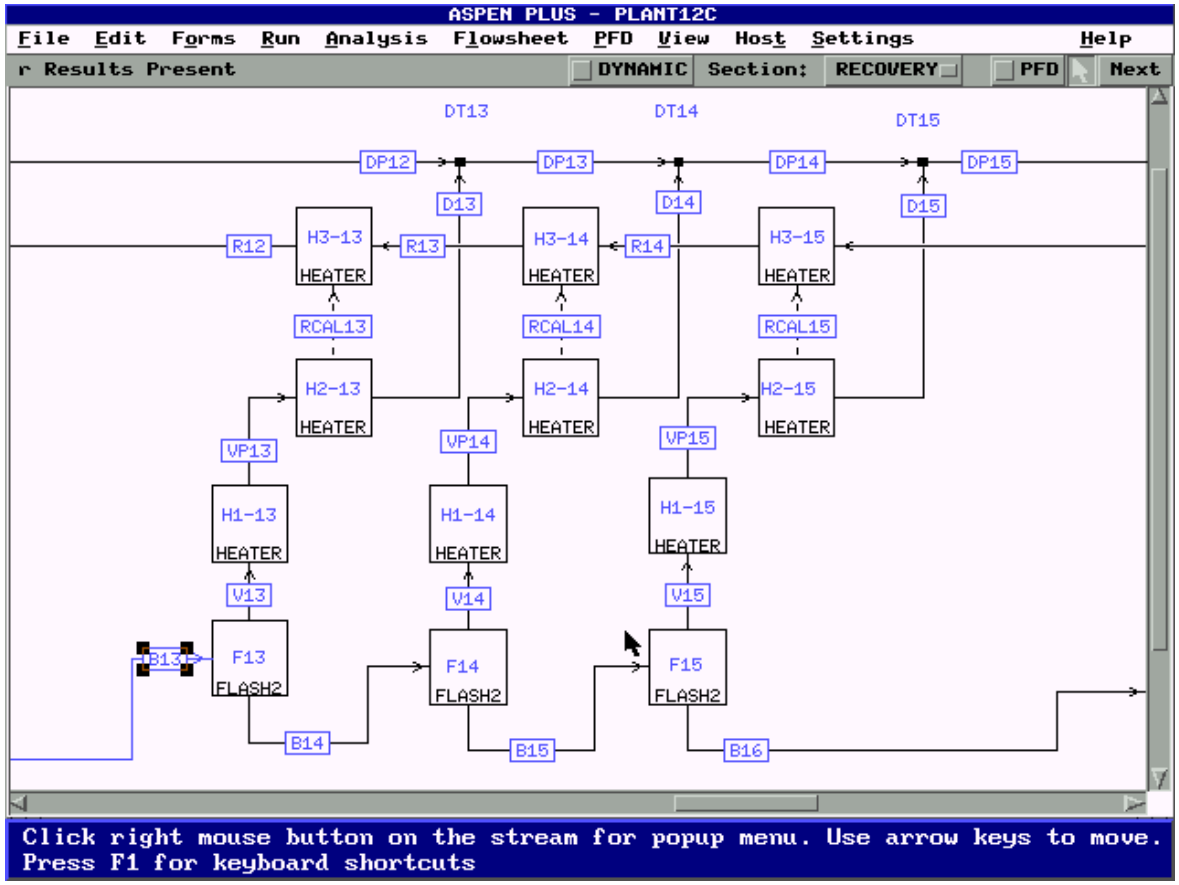

Figure 5.7: ASPEN PLUS simulation model for the heat-recovery section (continued).

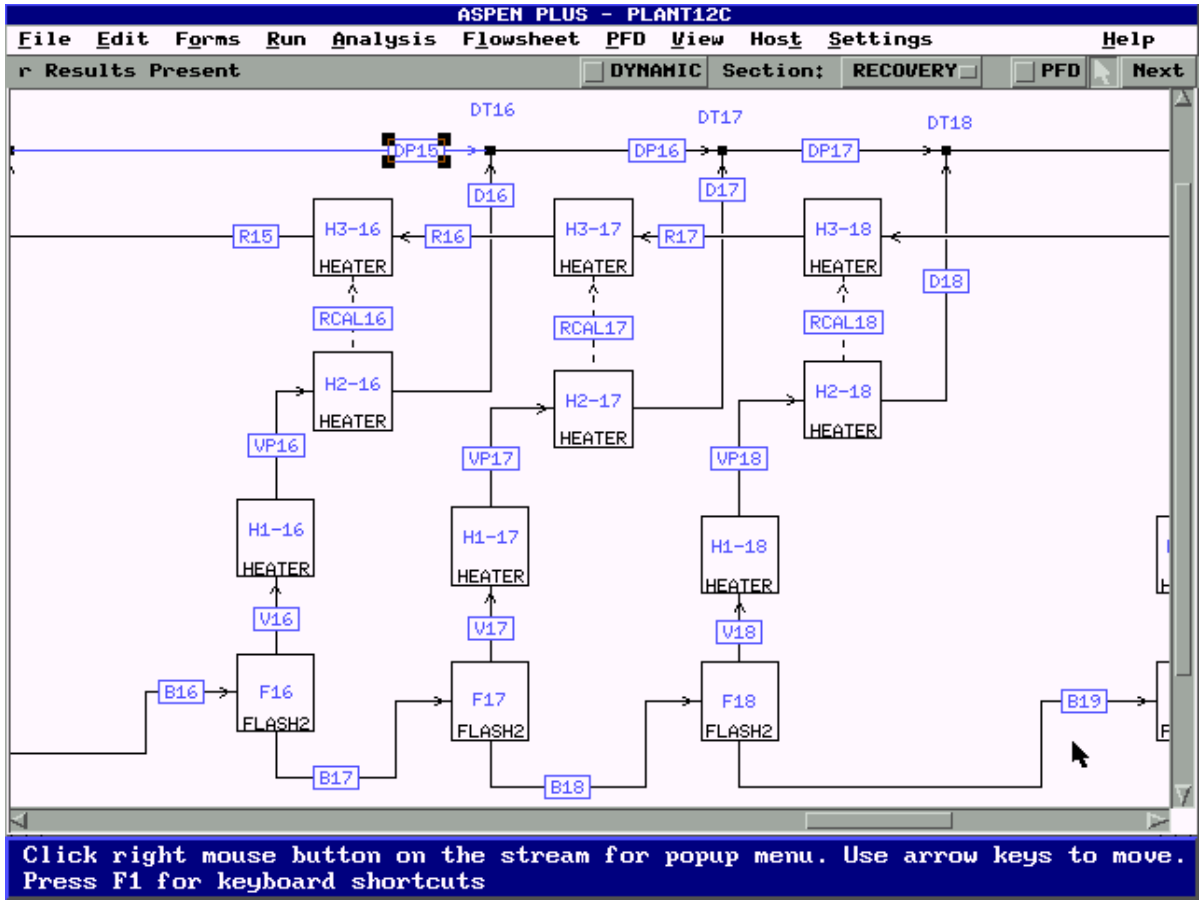

Figure 5.7: ASPEN PLUS simulation model for the heat-recovery section (continued).

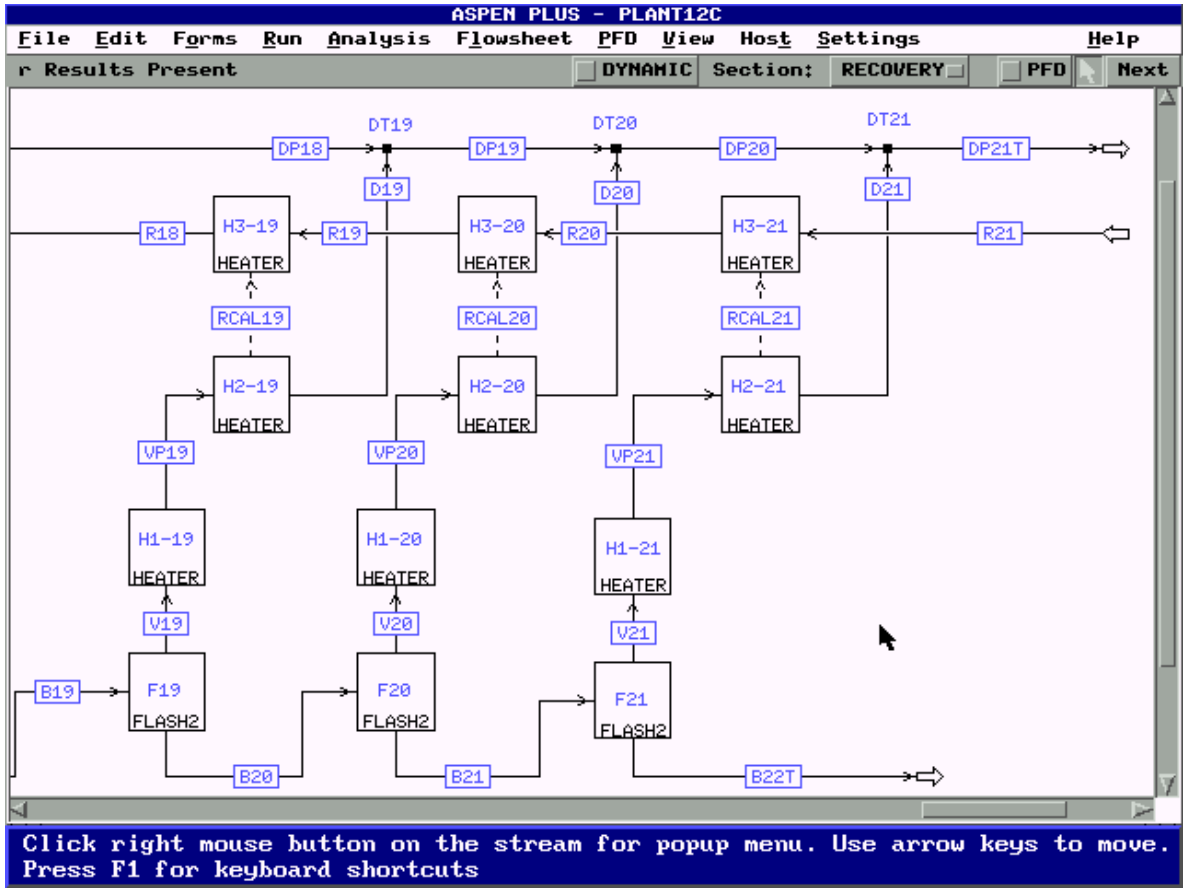

Figure 5.7: ASPEN PLUS simulation model for the heat-recovery section (continued).

Table 5.7: ASPEN PLUS specifications of all flash stages in the heat-recovery section for summer operation.

Block name	**Stage 1**	**Stage 2**	**Stage 3**	**Stage 4**	**Stage 5**	**Stage 6**	**Stage 7**
Flash:							
Temperature (°C)	88.9	86.7	84.4	82.0	79.6	77.3	75.0
Pressure (Bar)	0.65737	0.60396	0.55204	0.50191	0.45566	0.41474	0.37696
Heater 1:							
Temperature (°C)	87.9	85.7	83.4	81.0	78.6	76.3	69.5
Vapor fraction	1	1	1	1	1	1	1
Heater 2:							
Temperature (°C)	87.7	85.5	83.2	82.8	78.4	76.1	69.3
Vapor fraction	0	0	0	0	0	0	0
Heater 3:							
Pressure (Bar)	0.75	0.93	1.12	1.3	1.48	1.67	1.85
Heat input	Heat stream from Heater 2-1	Heat stream from Heater 2-2	Heat stream from Heater 2-3	Heat stream from Heater 2-4	Heat stream from Heater 2-5	Heat stream from Heater 2-6	Heat stream from Heater 2-7
Mixer:							
Pressure drop (Bar)	0	0	0	0	0	0	0
Nphase	1	1	1	1	1	1	1
Phase	Liquid	Liquid	Liquid	Liquid	Liquid	Liquid	Liquid

Table 5.7: ASPEN PLUS specifications of all flash stages in the heat-recovery section for summer operation (continued).

Block name	**Stage 8**	**Stage 9**	**Stage 10**	**Stage 11**	**Stage 12**	**Stage 13**	**Stage 14**
Flash:							
Temperature (°C)	72.7	70.5	68.3	66.2	64	61.9	59.8
Pressure (Bar)	0.34212	0.31138	0.28301	0.25800	0.23358	0.21221	0.19301
Heater 1:							
Temperature (°C)	71.7	69.5	67.3	65.2	63.0	60.8	58.7
Vapor fraction	1	1	1	1	1	1	1
Heater 2:							
Temperature (°C)	71.5	69.3	67.1	65.0	62.8	60.6	58.5
Vapor fraction	0	0	0	0	0	0	0
Heater 3:							
Pressure (Bar)	2.03	2.22	2.4	2.58	2.77	2.95	3.13
Heat input	Heat stream from Heater 2-8	Heat stream from Heater 2-9	Heat stream from Heater 2-10	Heat stream from Heater 2-11	Heat stream from Heater 2-12	Heat stream from Heater 2-13	Heat stream from Heater 2-14
Mixer:							
Pressure drop (Bar)	0	0	0	0	0	0	0
Nphase	1	1	1	1	1	1	1
Phase	Liquid	Liquid	Liquid	Liquid	Liquid	Liquid	Liquid

Table 5.7: ASPEN PLUS specifications of all flash stages in the heat-recovery section for summer operation (continued).

Block name	**Stage15**	**Stage 16**	**Stage 17**	**Stage 18**	**Stage 19**	**Stage 20**	**Stage 21**
Flash:							
Temperature (°C)	57.7	55.6	53.6	51.6	49.7	47.8	45.9
Pressure (Bar)	0.17498	0.15841	0.14390	0.13053	0.11884	0.10805	0.09116
Heater 1:							
Temperature (°C)	56.5	54.4	52.4	50.3	48.3	46.3	44.4
Vapor fraction	1	1	1	1	1	1	1
Heater 2:							
Temperature (°C)	56.3	54.2	52.2	50.1	48.1	46.1	44.2
Vapor fraction	0	0	0	0	0	0	0
Heater 3:							
Pressure (Bar)	3.32	3.5	3.68	3.87	4.05	4.23	4.42
Heat input	Heat stream from Heater 2-15	Heat stream from Heater 2-16	Heat stream from Heater 2-17	Heat stream from Heater 2-18	Heat stream from Heater 2-19	Heat stream from Heater 2-20	Heat stream from Heater 2-14
Mixer:							
Pressure drop (Bar)	0	0	0	0	0	0	0
Nphase	1	1	1	1	1	1	1
Phase	Liquid	Liquid	Liquid	Liquid	Liquid	Liquid	Liquid

d. Heat-Rejection Section

The heat-rejection section consists of three stages. We simulate all the stages in the heat-rejection section in the same manner as in the heat-recovery section except for the last stage. Figure 5.8 compares the actual plant flowsheet and ASPEN PLUS model for the last stage of the heat-rejection section.

In the last flash, there is one additional input (make-up seawater) and one more output stream (recirculating brine). The cooling water in the heat-rejection tubes is seawater and not brine as in the heat-recovery section. The feed seawater (make-up) and a large mass of the last-stage brine mix together to give the recirculating brine that circulates through the heat-recovery tubes. In the actual plant, this mixing takes place inside the last stage. However, since this is not possible with model FLASH2 in ASPEN PLUS, we assume outside mixing after rejecting part of the last-stage outlet brine (blowdown) back to the sea.

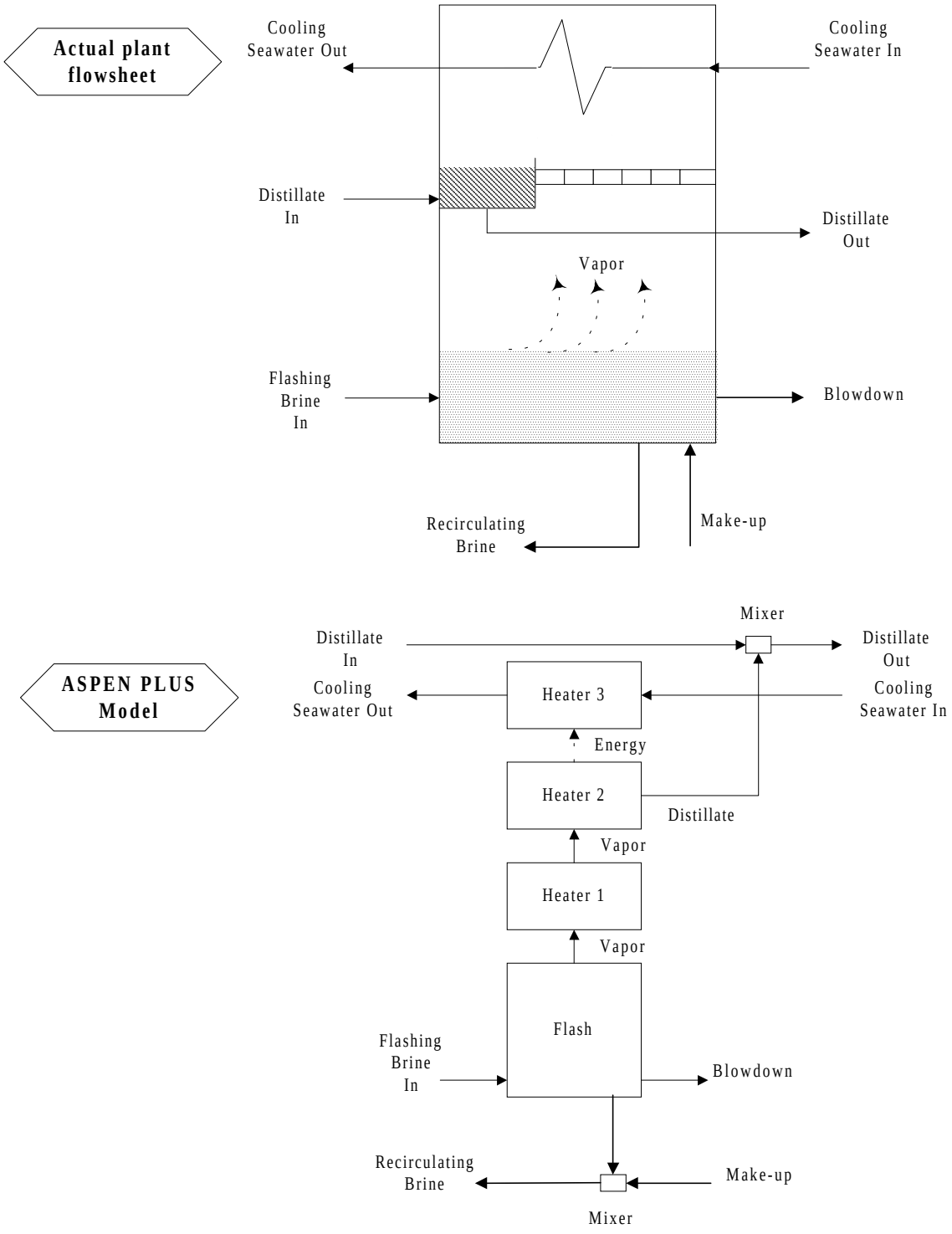

Figure 5.8: A comparison of the actual plant flowsheet and ASPEN PLUS model for the last stage of the heat-rejection section.

Figure 5.9 (in four pages) shows the block diagram of the ASPEN PLUS model for the heat-rejection section. Table 5.8 gives the specifications of all stages in the ASPEN PLUS model for the heat-rejection section.

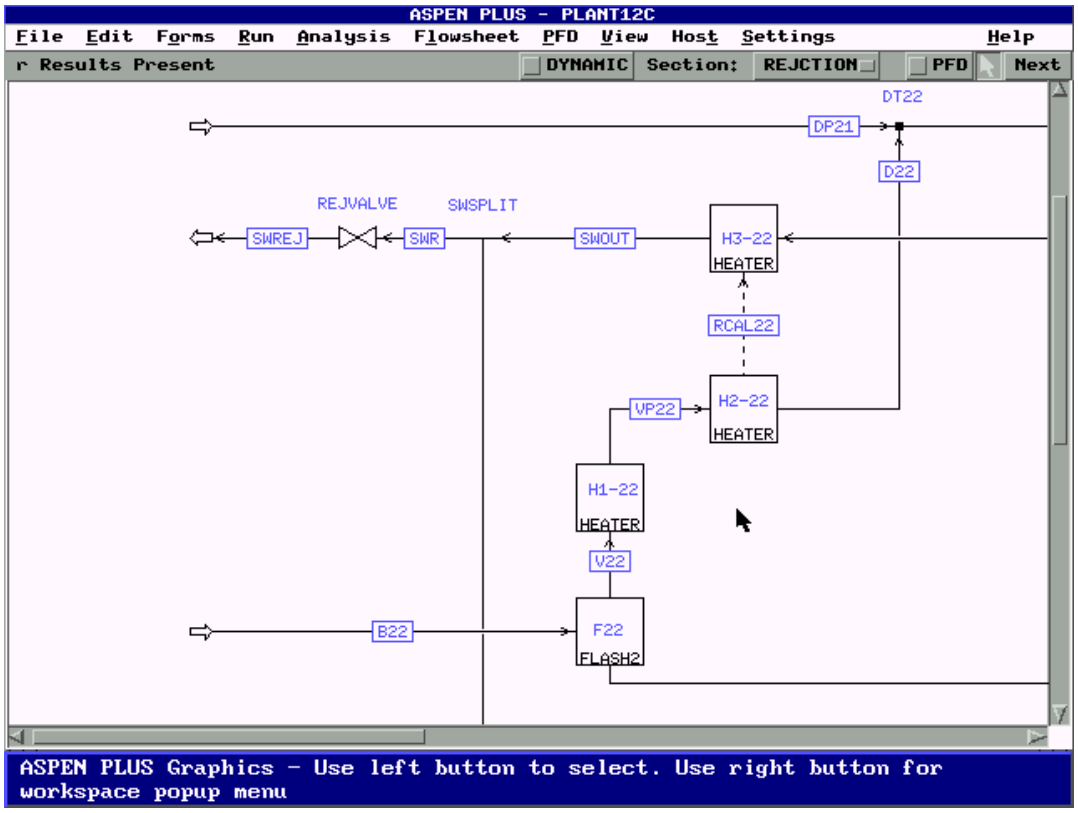

Figure 5.9: Block diagram of the ASPEN PLUS model for the heat-rejection section.

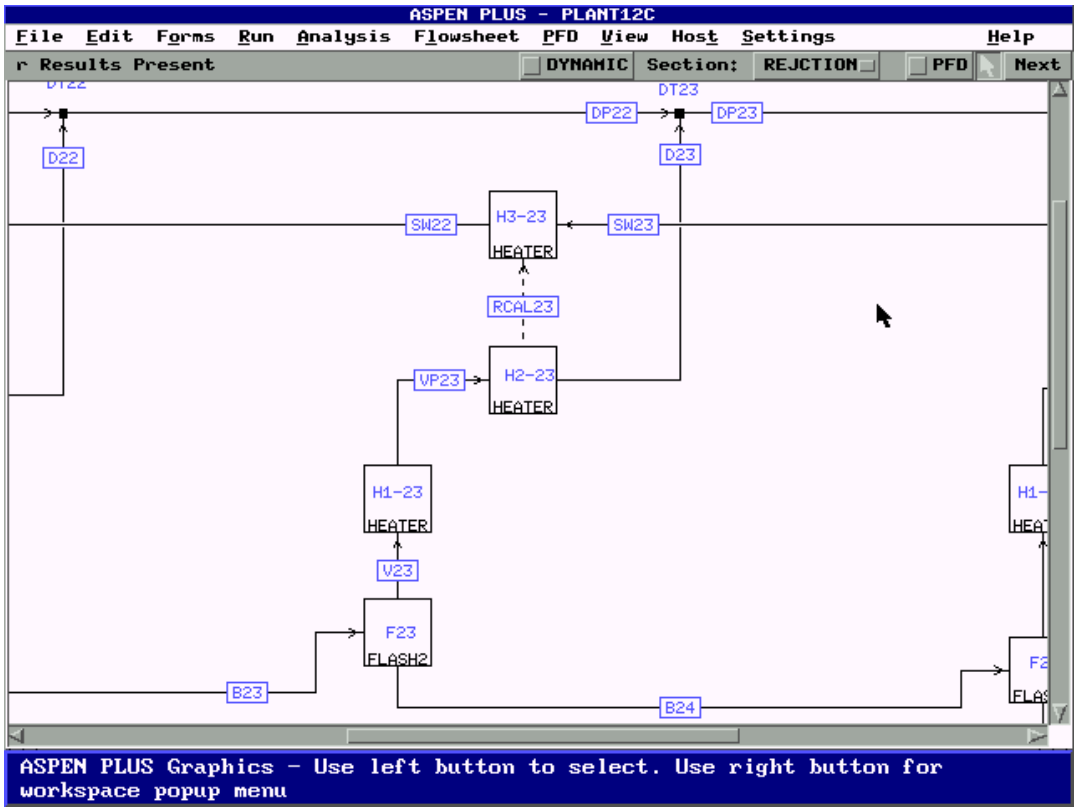

Figure 5.9: Block diagram of the ASPEN PLUS model for the heat-rejection section (continued).

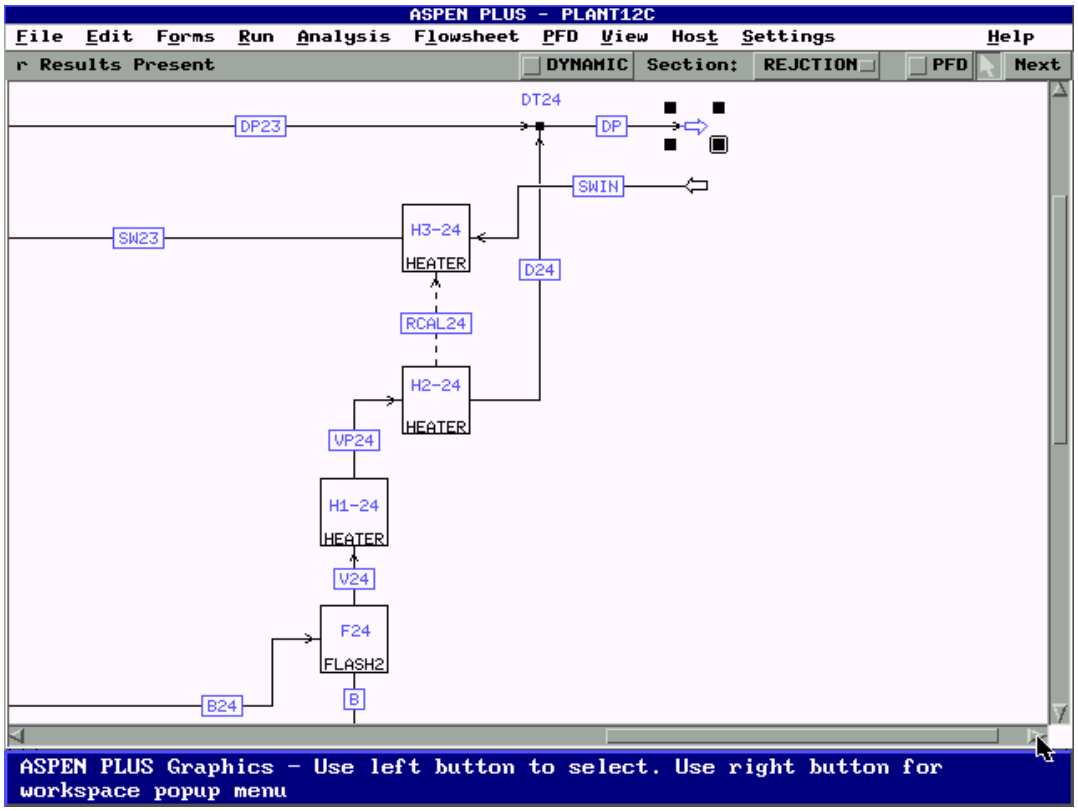

Figure 5.9: Block diagram of the ASPEN PLUS model for the heat-rejection section (continued).

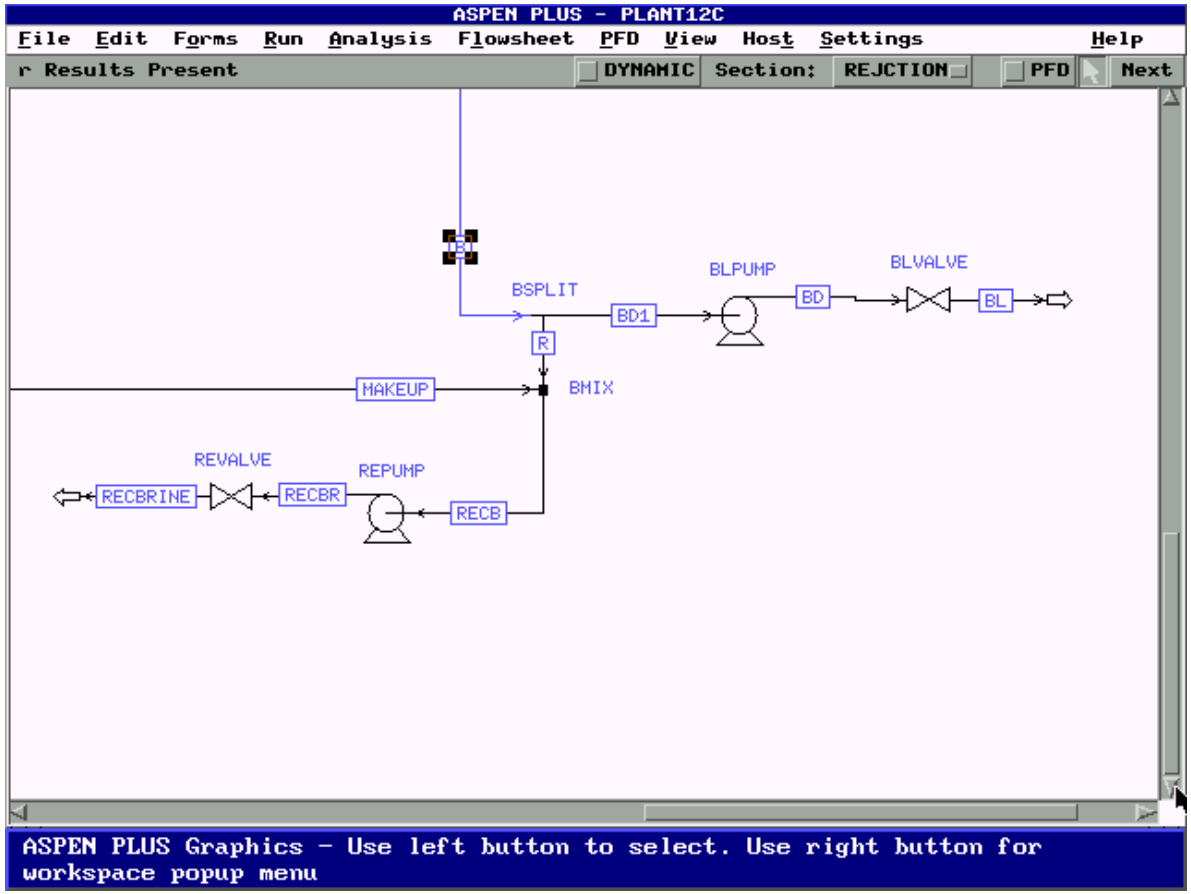

Figure 5.9: Block diagram of the ASPEN PLUS model for the heat-rejection section (continued).

Table 5.8: ASPEN PLUS specifications of all flash stages in the heat-rejection section for summer operation.

Block name		**Stage 22**	**Stage 23**	**Stage 24**	**Auxiliaries**
Flash:					
Temperature	(°C)	44.4	42.6	40.5	
Pressure	(Bar)	0.09084	0.08272	0.07405	
Heater 1:					
Temperature	(°C)	42.8	40.9	38.8	
Vapor fraction		1	1	1	
Heater 2:					
Temperature	(°C)	42.6	40.7	38.6	
Vapor fraction		0	0	0	
Heater 3:					
Pressure	(Bar)	2.5	2.83	2.67	
Heat input		Heat stream from Heater 2-22	Heat stream from Heater 2-23	Heat stream from Heater 2-24	
Mixer:					
Pressure drop	(Bar)	0	0	0	
Nphase		1	1	1	
Phase		Liquid	Liquid	Liquid	
Recirculating brine pump (REPUMP)					
Pressure	(Bar)				4.7

Table 5.8: ASPEN PLUS specifications of all flash stages and auxiliaries in the heat-rejection section for summer operation (continued).

Block name	Stage 22	Stage 23	Stage 24	Auxiliaries
Blowdown pump (BLPUMP)				
Pressure (Bar)				1.27
Recirculating brine valve (REVALVE)				
Pressure (Bar)				4.6
Blowdown valve (BLVALVE)				
Vapor fraction				0
Temperature drop (°C)				0
Seawater reject valve (SWVALVE)				
Vapor fraction				0
Temperature drop (°C)				0
Inlet cooling seawater (SWIN):				
Temperature (°C)				32.22
Pressure (Bar)				3
Flowrate (T/hr)				9629.3
Concentration				45,000
Make-up (MAKEUP):				
Flowrate (T/hr)				2925.4
Blowdown (BDI):				
Flowrate (T/hr)				1797.7

4. ASPEN PLUS Results and Discussion

a. Comparison of Simulation Results with Design and Operational Data

As a rule in process design and simulation, we should always include the final stream table. Appendix C gives the stream tables resulting from ASPEN PLUS simulation of summer operations.

Table 5.9 compares the simulated values, and design and operational data for two variables: (1) the temperature of recirculating brine entering each stage, TF_IN, (°C); (2) distillate produces by each stage (T/min). There is only a very minor difference between the TF_OUT values, and the D_OUT values are essentially identical.

Table 5.19: A comparison of simulated values with design and operational data for temperature of recirculating brine entering each flash stage, TF_IN (°C), and distillate produced from each stage, D_OUT (T/min).

Flash Stage No.	**TF_IN (°C)**		**D_OUT (T/min)**	
	ASPEN PLUS	**Design**	**ASPEN PLUS**	**Design**
1	82.00	83.20	0.70	0.69
2	79.90	81.10	0.87	0.87
3	77.60	78.80	0.93	0.93
4	75.30	76.40	0.95	0.95
5	73.00	74.00	0.94	0.94
6	70.70	71.70	0.91	0.91
7	68.50	69.40	0.88	0.88
8	66.30	67.10	0.86	0.86
9	64.20	64.80	0.85	0.85
10	62.00	62.70	0.83	0.83
11	59.90	60.50	0.82	0.82
12	57.80	58.30	0.81	0.81
13	55.80	56.20	0.80	0.80
14	53.70	54.10	0.78	0.78
15	51.70	52.00	0.77	0.77
16	49.80	49.90	0.75	0.75
17	47.80	47.90	0.73	0.73
18	45.90	45.90	0.72	0.72
19	44.00	44.00	0.70	0.70
20	42.20	42.10	0.68	0.68
21	40.40	40.34	0.66	0.65
22	37.50	38.00	0.55	0.55
23	35.00	35.30	0.63	0.63
24	32.22	32.22	0.70	0.70

Figure 5.10 compares the design specifications and simulated results of the outlet pressure from each stage, P_OUT (Bar) for summer operations.

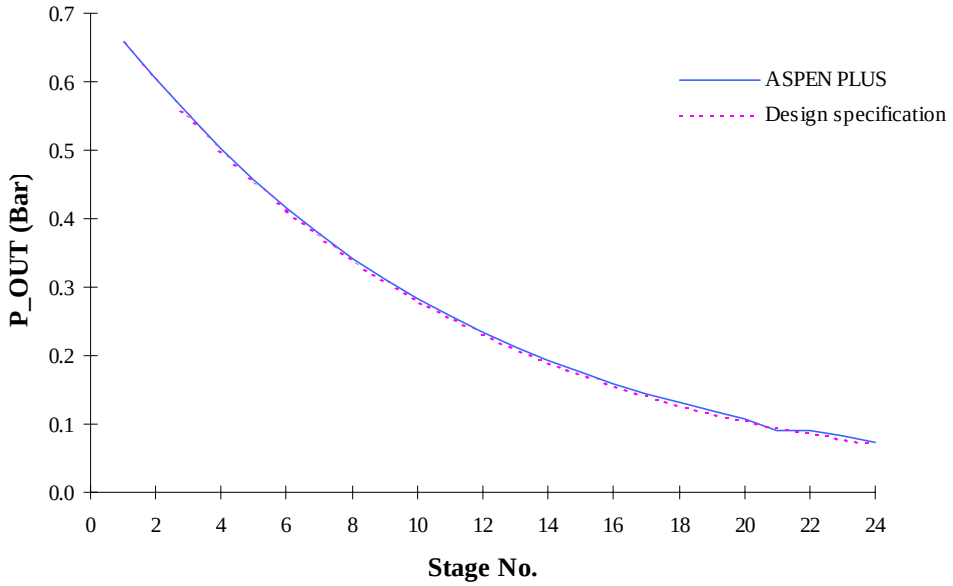

Figure 5.10: A comparison of simulated values and design specifications for the outlet pressure from each flash stage for summer operation.

Table 5.10 compares the simulated results and design specifications for three performance variables for summer operation. The MSF desalination plant can operate without a problem within ±5 °C of design top brine temperature. Therefore, a temperature difference of 1.46 °C between the simulated and design top brine temperature is not significant.

Table 5.10: A comparison of simulated values and design specifications of three key performance variables for summer operations.

Performance variable	**Unit**	**ASPEN PLUS**	**Design specification**
Top brine temperature	°C	89.1	90.56
Recycle brine flowrate	T/min	238.09	238.1
Distillate produced	T/min	18.816	18.795

It is evident from the proceeding comparison that the current ASPEN PLUS model is able to accurately duplicate the design and operational data of the MSF desalination plant for summer operations. In contrast to the two recent simulation studies cited in Table 5.1, *this study is the first steady-state simulation that successfully duplicates design and operational data from a large-scale commercial MSF desalination plant using ASPEN PLUS package.*

In the following, we illustrate the application of the ASPEN PLUS model to predict the performance of the MSF desalination plant under new operating conditions.

b. <u>Prediction of Desalination Performance under New Operating Conditions</u>.

In designing a single flash stage, we must specify the temperature and pressure of the flash operation. We choose the temperature based on actual plant data, and apply the ASPEN PLUS model to determine the outlet pressure of the flashing brine using a sensitivity analysis. For example, we wish to find the required outlet pressure to produce 41.1 T/hr of vapor from the first flash stage, when the inlet and outlet temperature of the flashing brine are 90.56 °C and 88.9 °C, respectively. Figure 5.11 shows the effect of the flash outlet pressure on the amount of vapor produced for the first flash stage. We see that the outlet pressure requires to produce 41.1 T/hr of vapor is 0.6574 Bar.

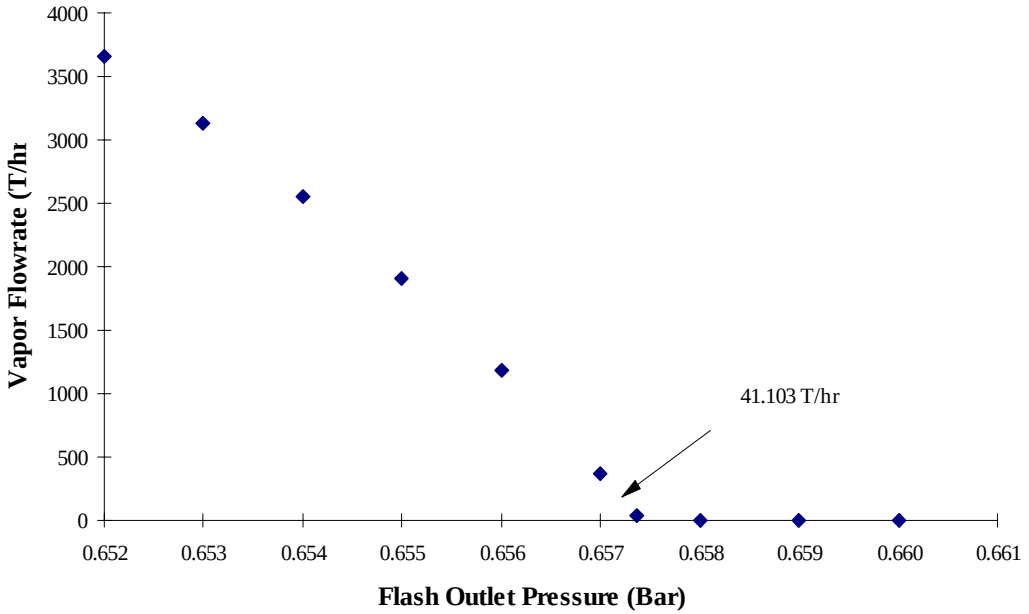

Figure 5.11: Effect of flash outlet pressure on the amount of vapor produced for the first flash stage.

As another application of ASPEN PLUS model, we investigate the effect of changing seawater temperature on the resulting top brine temperature, a key performance variable of a commercial desalination plant. The sensitivity analysis tool available in ASPEN PLUS allows us to simulate this effect easily. Figure 5.12 shows a resulting plot of the top brine temperature versus the seawater inlet temperature.

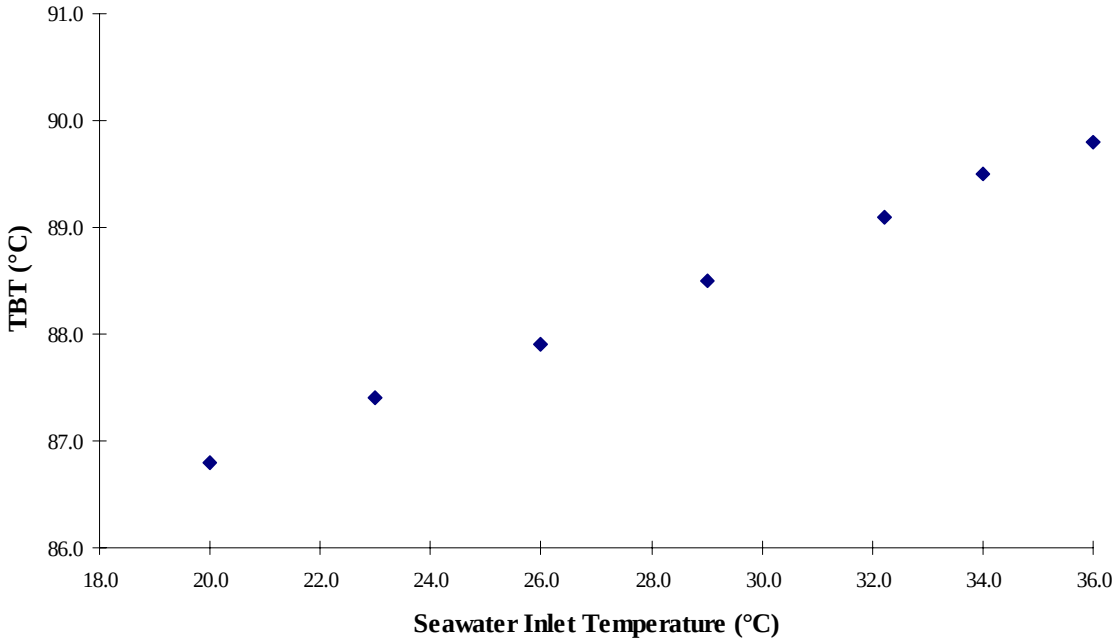

Figure 5.12: Effect of changing seawater inlet temperature on the top brine temperature.

In summary, the current ASPEN PLUS model is an effective tool to predict the performance of large-scale commercial MSF plants under new operating conditions.

B. Steady-State and Dynamic Simulations by SPEEDUP

SPEEDUP, by Aspen Technology, Cambridge, Massachusetts, is the most popular commercial flowsheeting package for solving the mass and energy balances equations, as well as process control relationship. We briefly describe its features below.

1. Description of SPEEDUP

SPEEDUP was originally developed at the Imperial College-London, and is being marketed by Aspen Tech. Figure 5.13 shows the structure of the SPEEDUP environment.

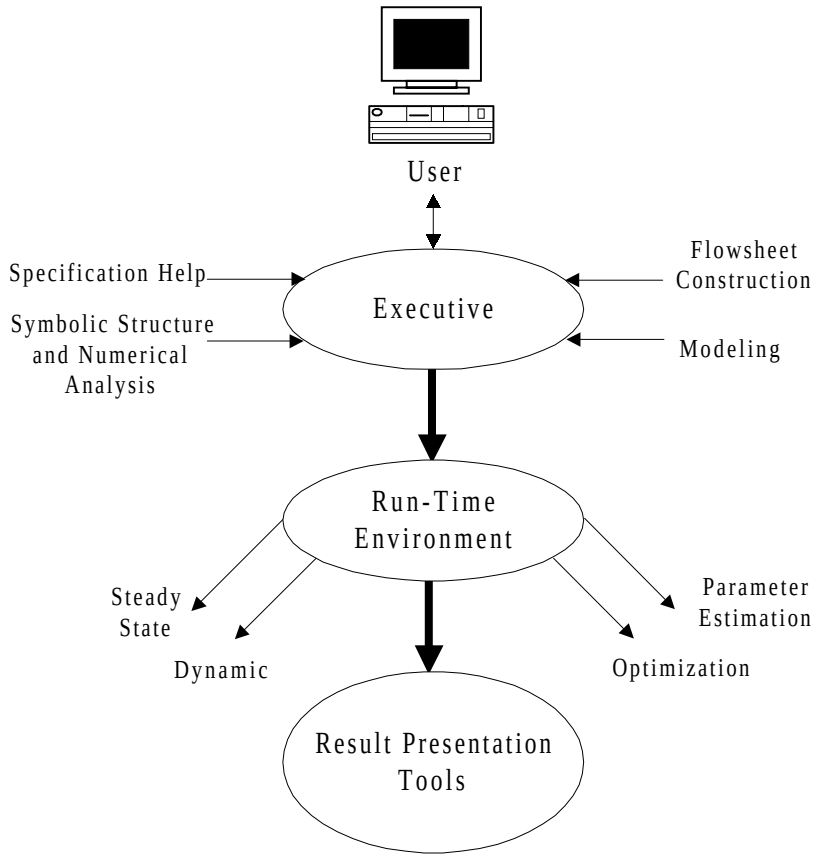

Figure 5.13: SPEEDUP environment

SPEEDUP is a comprehensive package designed for the following applications using the same software tool and the same program input:

- Solving steady-state simulation and design problems
- Optimizing steady-state solutions using an objective function and constraints supplied by the user.
- Simulating dynamic processes where dependent variables change with time.
- Modeling the dynamics of control systems for new designs or tuning existing control loops.
- Fitting model parameters to laboratory or plant data.
- Performing data-regression calculations to compare steady-state plant performance with that predicted by a model.
- Analyzing processes to produce manipulated input for control design software.

SPEEDUP is an equation-oriented flowsheet simulation and optimization tool for process engineering systems. When solving simulation problems, SPEEDUP attempts to iteratively solve a set of modeling equations.

SPEEDUP views a chemical process as a series of unit operations, chemical reactors and other equipment items interconnected by process streams. It represents these process equipment items in terms of algebraic and ordinary differential equations. Applying SPEEDUP involves two steps: (1) generation of an input file in SPEEDUP modeling language using a text editor, and (2) loading the input file into the data base for process simulation.

2. Problem Description

We represent the problem to be solved in the SPEEDUP input language consisting of a number of input sections, each of which describes some aspects of the problem. Table 5.11 summarizes the key features of SPEEDUP input sections.

Table 5.11: SPEEDUP problem input sections.

Input Section Name(s)	Used To
Sections required for all simulations	
Unit	Specify a model, such as FLASH or PUMP, for each unit in the flowsheet.
Flowsheet	Describe the topology of a flowsheet being modeled, and define all interconnections between the units within a problem.
Declare	Give initial values and allowable ranges of different variables, and define the stream structure used in the problem.
Operation	Specify operating data for the process being modeled.
Optional sections	
Options	Provide specification and estimation options for a particular run such as tolerance and printing option.
Title	Enter a title for the simulation to appear on the output.
Global	Define global relationships in the flowsheet.
Sections for optimization	
Estimation, Global, Conditions	Define aspects of particular run modes.
Sections for dynamic simulation	
Conditions	Print information and warnings, or terminate the calculation when certain conditions are met
Sections for defining user-written models	
Model	Write the model description.
Procedure	Give any FORTRAN subroutines which are to be interfaced to SPEEDUP.

SPEEDUP can store a complete simulation including input data, unit models and calculated results, on its database for later examination and further calculations. It also includes a library of simulation models for commonly occurring unit operations, chemical reactors and process controllers.

After checking all the input sections to ensure their accuracy, SPEEDUP solves a problem in a run-time environment.

For steady-state and initialization simulations, the equations are first broken down into as many independent blocks as possible. This approach minimizes the solution time and reduces the complexity of the problem to be solved. In all run modes, SPEEDUP processes the equations using a symbolic differentiation system. This produces analytical partial derivatives with respect to unknown variables. SPEEDUP compiles and links together the whole program with the numerical solution subroutines and any other subroutines that are required. These may include user-written subroutines and physical property correlations. The resulting executable is then run.

3. SPEEDUP MSF Model Formulation

a. International Center for Water and Energy Systems (ICWEC) SPEEDUP Model

The International Center for Water and Energy Systems (ICWES), Abu Dhabi, United Arab Emirates (UAE), has developed a SPEEDUP model for simulating the steady-state and dynamic behavior of a 18-stage MSF desalination plant located Abu Dhabi (Husain, et al., 1995).

We have adopted and modified this model for specifically applying it to the AZ-ZOUR South MSF desalination plant in Kuwait. This plant has 21 heat-recovery stages and 3 heat-rejection stages.

Figure 5.14 shows the components of the MSF desalination plant under consideration. In the following, we first describe each key component model, and then summarize our specific modifications to the ICWES model for our application.

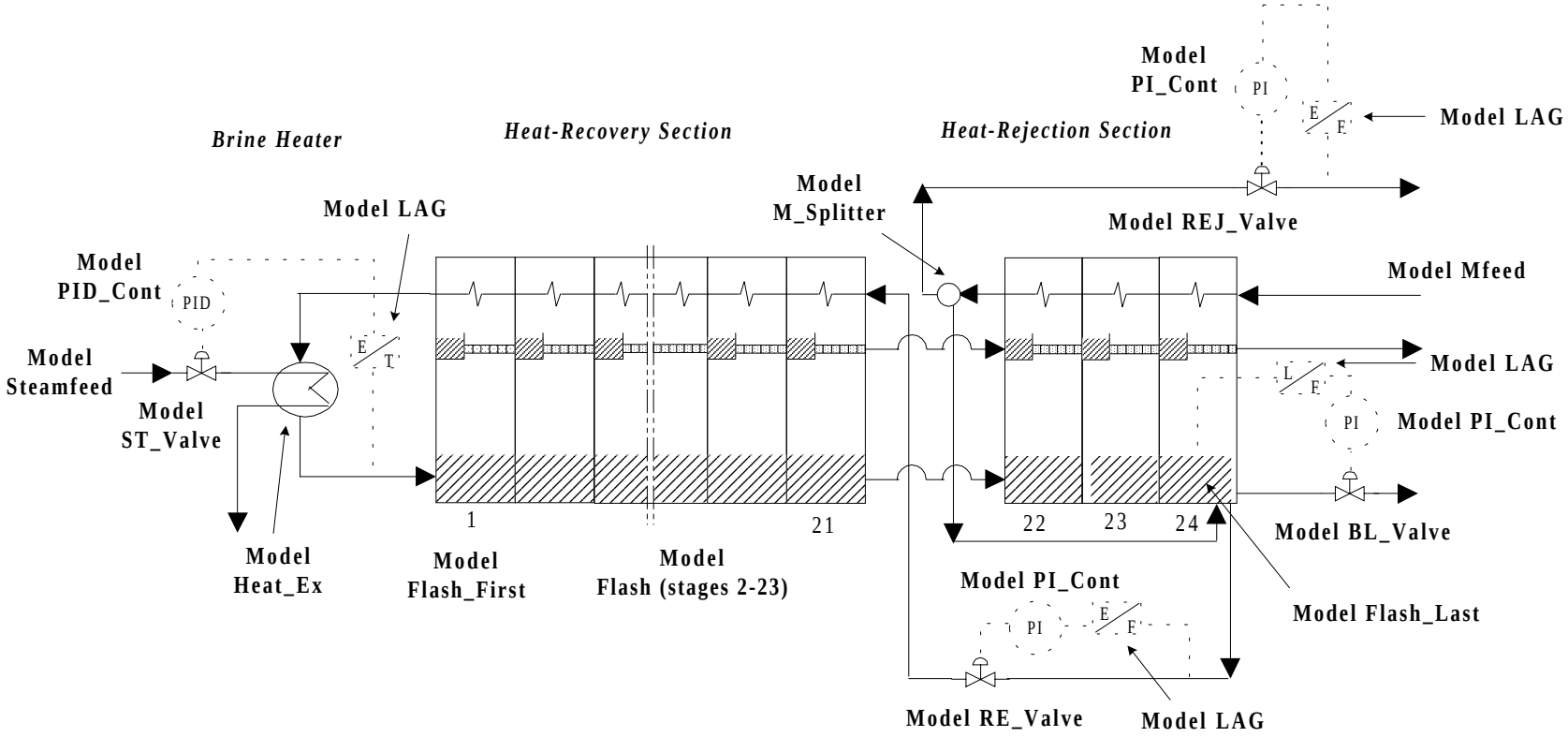

Figure 5.14: The components of the MSF desalination plant.

The MSF process model equations consist of mass and energy balances for all sections in the MSF plant together with the supplementary correlations for heat transfer and physical properties. Appendix A describes the mathematical model of a multistage flash desalination process. Appendix B lists all the physical property correlations used to develop a FORTRAN program to calculate the thermodynamic properties of different liquid and vapor streams. The SPEEDUP model developed by the International Center for Water and Energy Systems (ICWES) consists of the following sections.

1. Model Heat_Ex: Brine Heater

Model Heat_Ex is the brine heater model with streams in countercurrent flow. There are two inputs and two outputs. Figure 5.15 shows the input and output variables in these streams, and Table 5.12 lists the figure nomenclatures. The model equations consist of mass and energy balances, the latter including a dynamic change of temperature of brine inside the tubes.

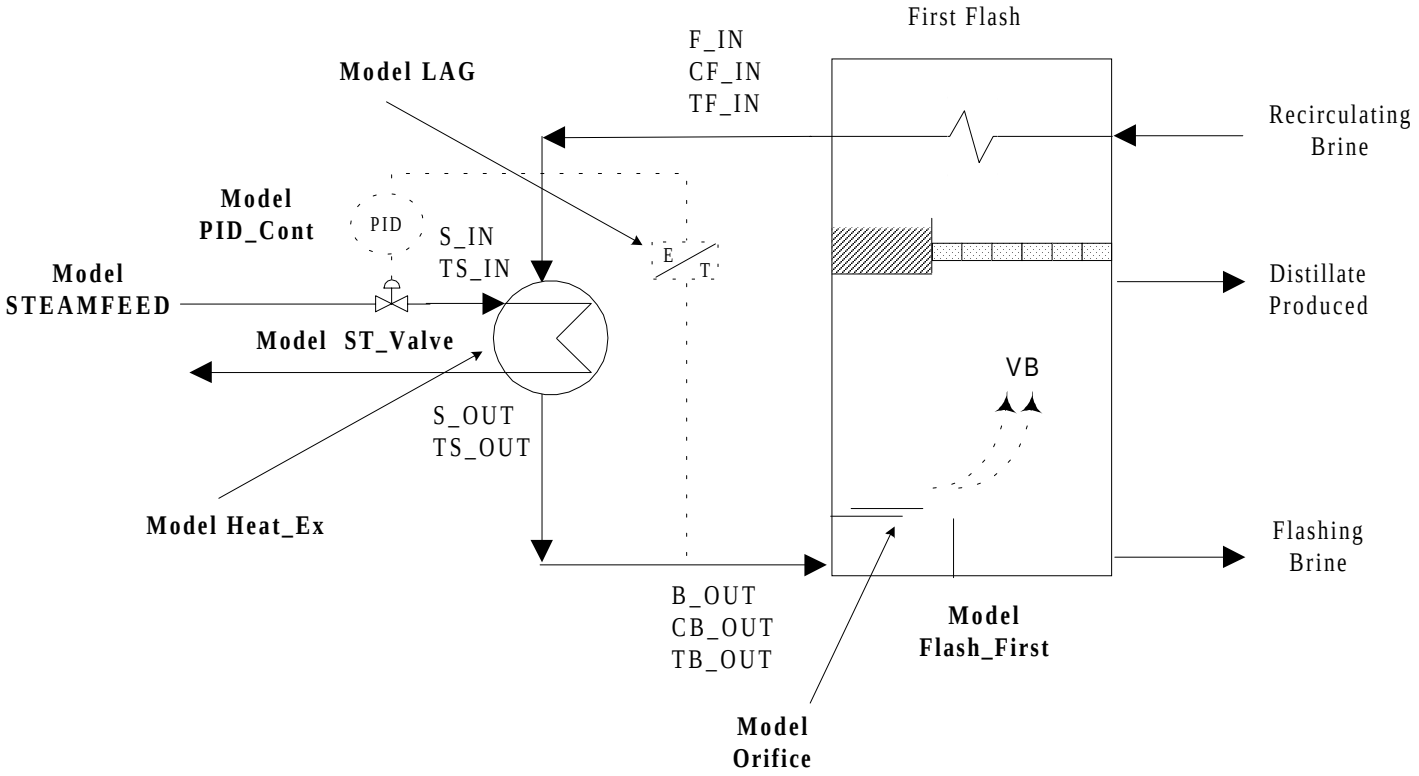

Figure 5.15: Brine-heater section variables.

Table 5.12: A list of variables for SPEEDUP model for the brine heater.

Nomenclature	Description	Unit
F	Recirculating brine flowrate	T/min
CF	Recirculating brine concentration	kg/kg
TF	Recirculating brine temperature	°C
B	Brine flowrate	T/min
CB	Brine concentration	kg/kg
TB	Brine temperature	°C
S	Steam flowrate	T/min
TS	Steam temperature	°C
Subscripts:		
IN	Inlet stream the brine heater	
OUT	Outlet stream from the brine heater	

2. Model Flash and Flash_First

Figure 5.16 shows a flash stage with its input and output variables, and Table 5.13 lists the figure nomenclatures. First flash does not have the input distillate stream. The model consists of the following parts:

Flash Chamber:

- Overall mass balance with dynamic change in mass holdup.
- Salt balance with dynamic change in brine concentration.
- Enthalpy balance with dynamic change in the brine specific enthalpy with brine temperature.

Distillate Tray:

- Overall mass balance.

- Temperature losses due to boiling-point elevation, non-equilibration, etc.

Tube Bundle:

- Overall mass and salt balance.
- Enthalpy balance with dynamic changes in cooled brine temperature.
- Heat-transfer equation between condensing vapor and cooling brine.

Auxiliary equations:

- Equations to calculate mass hold-up in the flash chamber and inside tube bundle, and several procedures for calculating various properties required and the pressure inside the flash chamber.

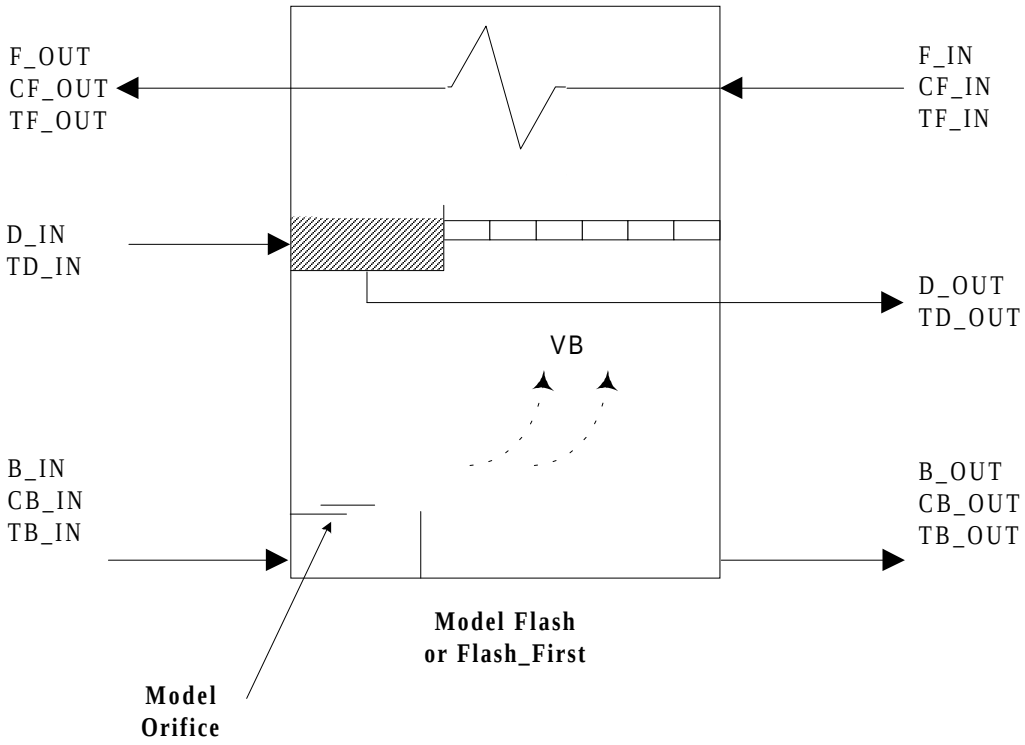

Figure 5.16: A general flash in an MSF desalination plant.

Table 5.13: A list of variables for SPEEDUP model for the flash stage.

Nomenclature	Description	Unit
F	Recirculating brine flowrate	T/min
CF	Recirculating brine concentration	kg/kg
TF	Recirculating brine temperature	°C
D	Distillate flowrate	T/min
TD	Distillate temperature	°C
B	Brine flowrate	T/min
CB	Brine concentration	kg/kg
TB	Brine temperature	°C
VB	Vapor flowrate	T/min
Subscripts:		
IN	Inlet stream to the flash stage	
OUT	Outlet stream from the flash stage	

3. Model Flash_Last

Figure 5.17 shows the input and output variables of the last flash stage, and Table 5.14 lists the figure nomenclatures. In the last flash, there is one additional input (make-up seawater) and one more output stream (recycle brine) which appear in the flash equations.

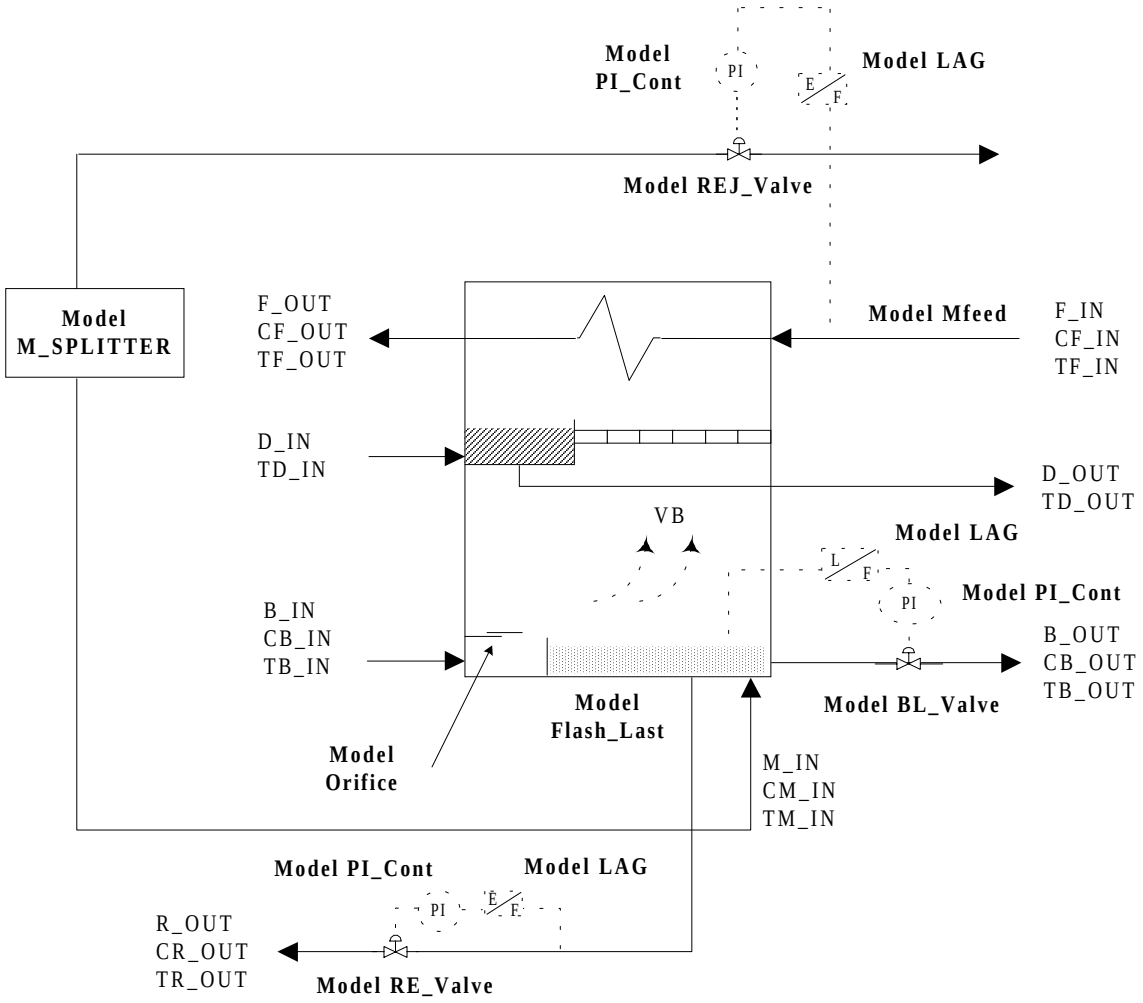

Figure 5.17: Last flash in a MSF desalination plant.

Table 5.14: A list of variables for SPEEDUP model for the last flash stage.

Nomenclature	Description	Unit
F	Seawater flowrate	T/min
CF	Seawater concentration	kg/kg
TF	Seawater temperature	°C
D	Distillate flowrate	T/min
TD	Distillate temperature	°C
B	Brine flowrate	T/min
CB	Brine concentration	kg/kg
TB	Brine temperature	°C
VB	Vapor flowrate	T/min
R	Recirculating brine flowrate	T/min
CR	Recirculating brine concentration	kg/kg
TR	Recirculating brine temperature	°C
M	Make-up flowrate	T/min
CM	Make-up concentration	kg/kg
TM	Make-up temperature	°C
Subscripts:		
IN	Inlet stream to the last stage	
OUT	Outlet stream from the last stage	

4. Model Orifice

Although orifice is part of the flash chamber, we write a separate model for it to aid our modeling. We include an orifice model following each flash model, except after the last flash. The interconnections are built in the FLOWSHEET section. The model consists of equations for calculating the pressure drop, orifice coefficient and the outlet (Homig, 1978). Figure 5.18 show the orifice configuration, and Table 5.15 lists the figure nomenclatures.

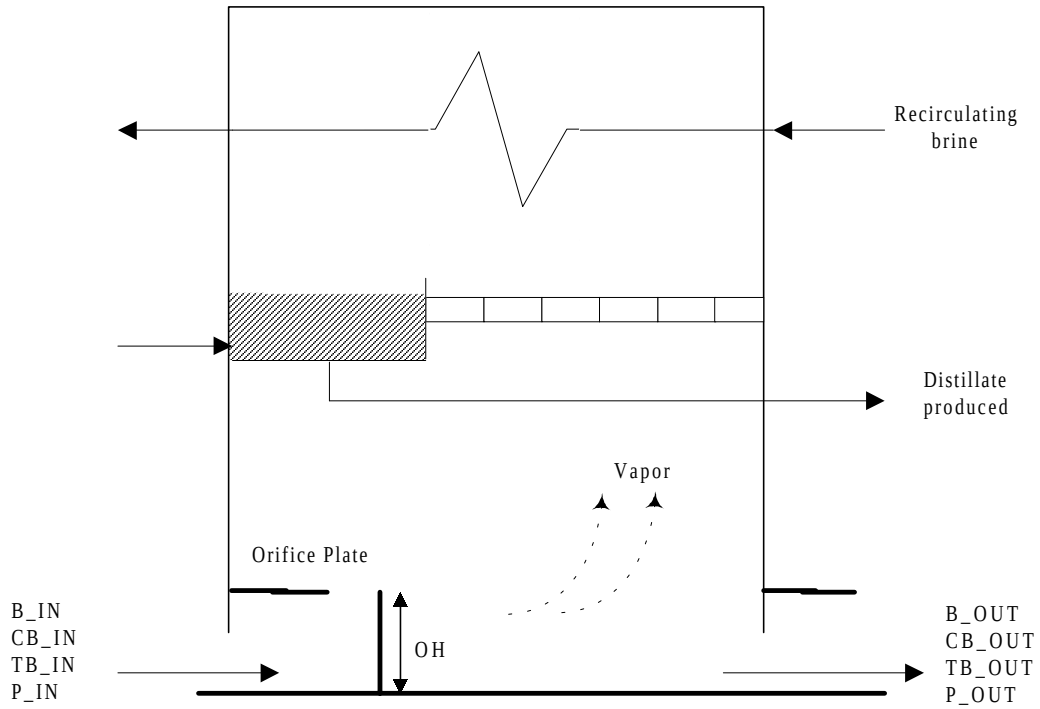

Figure 5.18: Orifice configuration in an MSF desalination plant

Table 5.15: A list of variables for SPEEDUP model for the orifice.

Nomenclature	Description	Unit
B	Brine flowrate	T/min
CB	Brine concentration	kg/kg
TB	Brine temperature	°C
P	Brine pressure	Bar
OH	Orifice height	m
Subscripts:		
IN	Inlet stream to the orifice	
OUT	Outlet stream from the orifice	

5. Model M_Splitter

Splitter divides the total seawater flow in the tube bundle of reject stages into makeup water and reject water according to the ratio specified. The model equation consists of mass balances. Figure 5.19 shows the splitter used to split the seawater outlet from the heat -rejection section cooling tubes into a make-up and seawater reject streams, and Table 5.16 lists the figure nomenclatures.

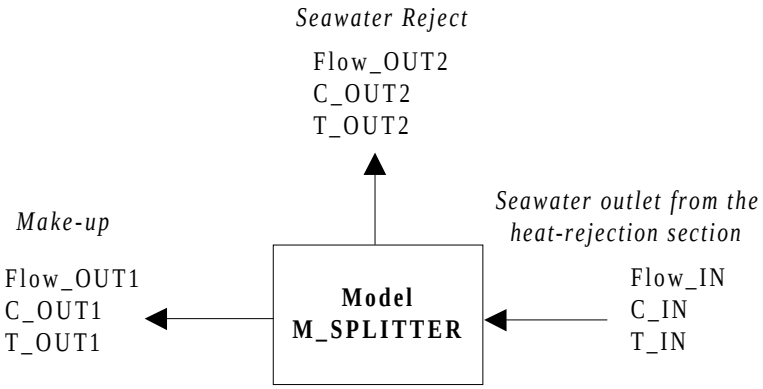

Figure 5.19: Splitter in a MSF desalination plant.

Table 5.16: A list of variables for SPEEDUP model for the splitter.

Nomenclature	**Description**	**Unit**
Flow_IN	Seawater flowrate leaving the heat-rejection section	T/min
C_IN	Concentration of seawater leaving the heat-rejection section	kg/kg
T_IN	Temperature of seawater leaving the heat-rejection section	°C
Flow_OUT1	Make-up flowrate	T/min
C_OUT1	Make-up concentration	kg/kg
T_OUT1	Make-up temperature	°C
Flow_OUT2	Seawater reject flowrate	T/min
C_OUT2	Seawater reject temperature	kg/kg
T_OUT2	Seawater reject concentration	°C

6. Model Controller: PID_Cont, PI_Cont, LAG

Commercial MSF desalination plants typically use a PID controller to control temperature and PI controllers for other variables. As shown in Figure 5.14, we include one PID controller to control the steam temperature entering the brine heater, and three PI controllers to control the rejected seawater, blowdown flowrate, and recycle brine flowrate. Model Lag, PI and PID are those from the SPEEDUP library of standard models, and we will not present their details here.

b. Modifications to the ICWES Model

Table 5.17 compares the plants specifications used in the ICWES SPEEDUP model and our SPEEDUP model. In order to adopt the ICWES model to our MSF desalination plant during summer operation, we have made the following modifications.

1. Changing initial values and allowable ranges of different variables in the Declare section. Unrealistic choice of initial guesses and bounds can cause serious convergence problems in SPEEDUP.
2. Modifying the interconnections between units within the problem in the Flowsheet section. The interconnections may be either process flows which are known as 'streams', or information flows which are known as 'connections'.
3. Changing the SET and PRESET variables in the Operation section. SET is used to set the values of problem variables to known values. Sufficient variables must be set so as to take up all the degrees of freedom in the problem. PRESET is used to enter individual estimates of the solution values for variables.
4. Adding the following sections:
    - Unit Flash; 19, 20, 21, 22, 23, and 24.
    - Unit Orifice; 18, 19, 20, 21, 22, and 23.
    - Control Design Interface (CDI) section to generate the state-space matrices A,B,C and D (see section 7.3). In producing these matrices, CDI eliminates all the algebraic variables from original SPEEDUP problem which do not appear in the linear model.
    - Three Report sections to define customized reports for displaying results.

Table 5.18 summarize the SPEEDUP input sections for the resulting model.

Table 5.17: A comparison of plant specifications used in the ICWES SPEEDUP model and our SPEEDUP model.

Plant specification	**ICWES model**	**Our model**
Total number of stages	18	24
Number of stages in heat-recovery section	15	21
Number of stages in heat-rejection section	3	3
Number of tubes:		
Brine heater	2895	1367
Heat-recovery section	3097	1451
Heat-rejection section	2940	1588
Tube length (m):		
Brine heater	17.5	18.99
Heat-recovery section	15.9	18.41
Heat-rejection section	15.9	18.41
Heat-transfer area (m^2):		
Brine heater	4664	3544
Heat-recovery section	4535.67	3676.47
Heat-rejection section	4306	3148
Inlet seawater:		
Flowrate (T/min)	241.66	160.488
Temperature (°C)	35	32.22
Concentration (mg/l)	50,000	45,000
Last-stage brine level (m)	0.6	0.6
Blowdown-valve outlet pressure (Bar)	0.0819	0.075
Recirculating brine flowrate (T/min)	241.83	238.1
Make-up flowrate (T/min)	91.88	48.757
Steam flowrate (T/min)	2.821	2.349
Top brine temperature (°C)	90	90.56
Steam temperature (°C)	105	100

Table 5.18: The SPEEDUP input sections for the resulting model.

Input section	Input section name	Input section	Input section name
Options		***Units:***	RE_Valve
			RE_Cont
Declare			RE_Valve_Act
			REJ_Valve
Models:	Heat_Ex		REJ_Cont
	Flash_First		REJ_Valve_Act
	Flash		ST_Valve
	Flash_Last		ST_Cont
	Mfeed		ST_Valve_Act
	M_Splitter		
	Orifice	***Flowsheet***	
	SteamFeed		
	BL_Valve	***Operation***	
	RE_Valve		
	REJ_Valve	***External***	
	ST_Valve		
	PID_Cont	***Report***	
	PI_Cont		
	LAG		
Units:	Brine_Heater		
	F1		
	F2		
	:		
	:		
	F23		
	F24		
	W1		
	W2		
	:		
	:		
	W22		
	W23		
	Feed1		
	Sfeed		
	Split2		
	BL_Valve		
	BL_Cont		
	BL_Valve_Act		

5. Model Validation with Design and Operational Data

a. Steady-State Model and Simulation Results

Table 5.19 compares the temperatures of the flashing brine (TB_OUT), distillate (TD_OUT), and recirculating brine (TF_IN) as well as the flash pressures (P_OUT) in 24 flash stages with actual plant data.

Table 5.19: Comparison of simulated values with actual plant data.

Flash Stage No.	TB_OUT (°C)		TD_OUT (°C)		TF_IN (°C)		P_OUT (Bar)	
	SPEEDUP	Design	SPEEDUP	Design	SPEEDUP	Design	SPEEDUP	Design
1	88.36	88.90	87.16	87.70	82.22	83.20	0.63	0.66
2	85.73	86.70	84.53	85.50	79.60	81.10	0.57	0.60
3	83.09	84.40	81.89	83.20	76.97	78.80	0.52	0.55
4	80.46	82.00	79.26	80.80	74.36	76.40	0.46	0.50
5	77.83	79.60	76.63	78.40	71.77	74.00	0.42	0.45
6	75.21	77.30	74.01	76.10	69.21	71.70	0.37	0.41
7	72.62	75.00	71.42	73.80	66.68	69.40	0.33	0.38
8	70.05	72.70	68.85	71.50	64.19	67.10	0.30	0.34
9	67.52	70.50	66.32	69.30	61.75	64.80	0.27	0.31
10	65.03	68.30	63.83	67.10	59.35	62.70	0.24	0.28
11	62.59	66.20	61.39	65.00	57.01	60.50	0.22	0.26
12	60.19	64.00	58.99	62.80	54.73	58.30	0.19	0.23
13	57.91	61.90	56.61	60.60	52.56	56.20	0.17	0.21
14	55.68	59.80	54.38	58.50	50.45	54.10	0.16	0.19
15	53.58	57.70	52.18	56.30	48.47	52.00	0.14	0.17
16	51.53	55.60	50.13	54.20	46.55	49.90	0.12	0.16
17	49.55	53.60	48.15	52.20	44.70	47.90	0.12	0.14
18	47.70	51.60	46.20	50.10	42.97	45.90	0.11	0.13
19	45.96	49.70	44.36	48.10	41.36	44.00	0.10	0.12
20	44.35	47.80	42.65	46.10	39.87	42.10	0.09	0.10
21	42.80	45.90	41.10	44.20	38.44	40.34	0.08	0.10
22	41.52	44.40	39.72	42.60	36.08	38.00	0.08	0.09
23	40.11	42.60	38.21	40.70	34.23	35.30	0.07	0.08
24	38.44	40.50	36.54	38.60	32.22	32.22	0.13	0.07

Table 5.20 compares actual and simulated values of the recirculating brine temperature entering the brine heater (TF), temperature of the final distillate produced (TD) and the top brine temperature (TB), as well as the flowrate of distillate produced (D), blowdown (B), and steam to brine heater (S). In addition, this table shows the simulated and actual performance ratio, which is the ratio of distillate produced to steam consumed.

Table 5.20: Comparison of simulated performance variables with design data.

Variables	**Unit**	**SPEEDUP**	**Design**
TF_IN	°C	84.43	84.89
TD_OUT	°C	36.54	38.60
TB_OUT	°C	38.44	40.50
D_OUT	T/min	19.33	18.80
B_OUT	T/min	29.43	29.96
S_OUT	T/min	2.50	2.35
Performance Ratio	Kg/540 Kcal	7.76	8.00

Figures 5.20 and 5.21 compare some operational variable profiles and the brine levels. It is clear that there is a very good agreement between the simulated and the actual and/or design data. Temperatures of all streams agree within ±3°C. Deviation in the outlet pressure is very small.

a. Flashing Brine Outlet Temperature TB_OUT (°C)

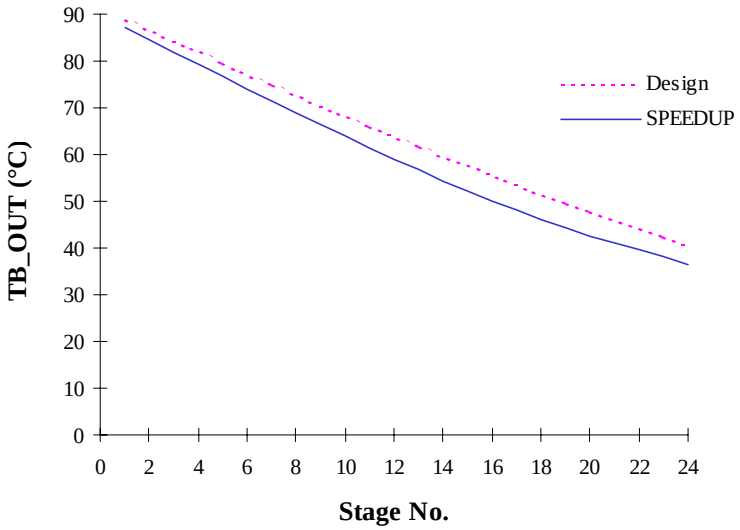

b. Distillate Temperature TD_OUT (°C)

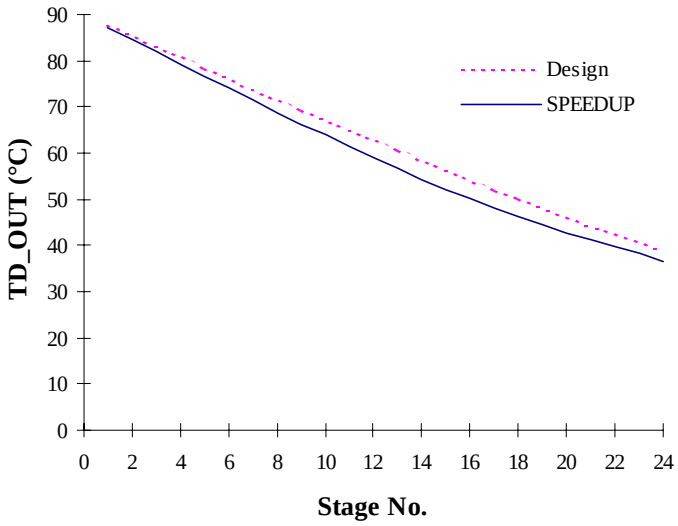

Figure 5.20: Simulated operational variables vs. design data: (a) flashing brine temperature (TB_OUT), (b) distillate produced temperature (TD_OUT), (c) recirculating brine temperature (TF_IN), and (d) flash pressures (P_OUT).

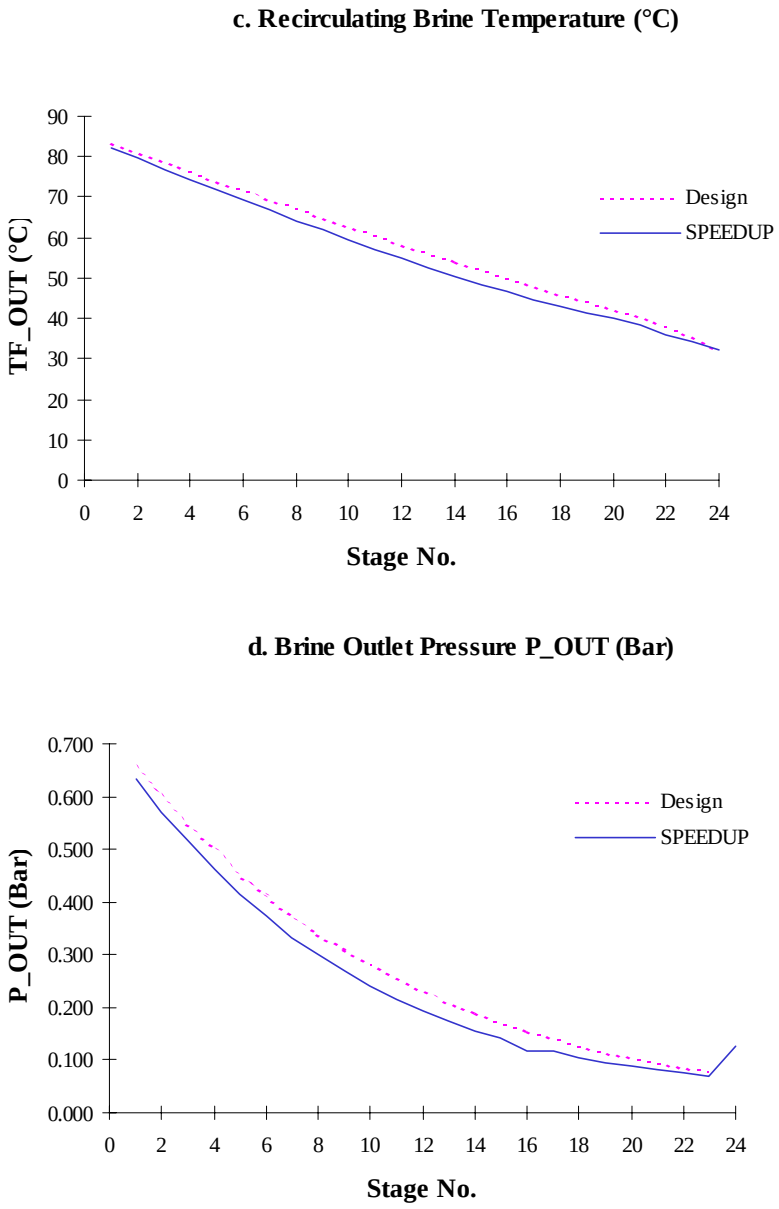

Figure 5.20: Simulated operational variables vs. design data: (a) flashing brine temperature (TB_OUT), (b) distillate produced temperature (TD_OUT), (c) recirculating brine temperature (TF_IN), and (d) flash pressures (P_OUT) (continued).

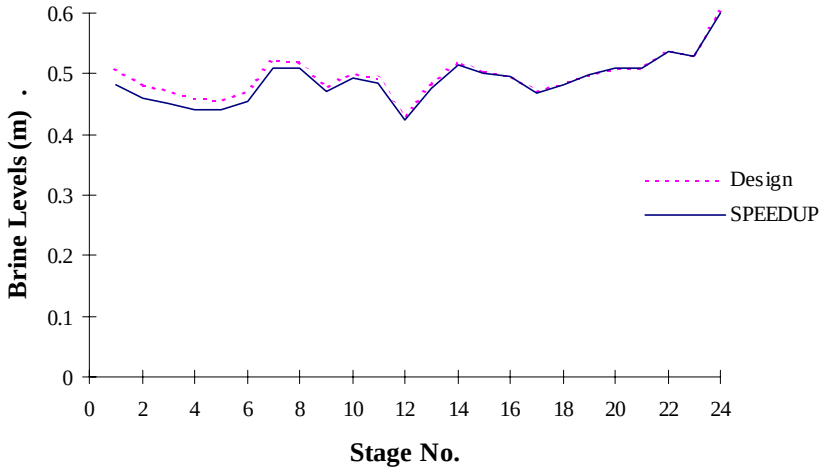

Figure 5.21: Simulated brine level versus design data.

b. Dynamic Model and Simulation Results

We apply the SPEEDUP model to carry out dynamic simulations of the MSF plant. After steady-state simulation presented in the previous section have converged, we use the steady-state solutions as initial conditions for system variables, and also include the controller and LAG models depicted previously in Figure 5.14. Table 5.21 lists the set-points for the four controllers.

Table 5.21: Control loops in dynamic simulation.

Control loop	**Nature**	**Set point**	**Controlled variables**	**Manipulated variables**
1	PID	90.56 (°C)	Top brine temperature	Steam valve position
2	PI	238.1 (T/min)	Recycle flowrate	Recycle brine valve position
3	PI	160.5 (T/min)	Seawater flowrate	Rejected seawater valve position
4	PI	0.6 (m)	Last-stage brine level	Blowdown valve position

Table 5.22 summarizes the step changes (increase or decrease) that we introduce in the key manipulated variables, such as the steam-valve opening, recycle-brine valve opening, and seawater temperature. Through SPEEDUP simulations, we monitor the dynamic response of top brine temperature, distillate produced and the brine level in stages 1,17, and 24 and control the last-stage brine level. We carry out the steady-state simulation for 1 minute before introducing step changes, followed by monitoring the dynamic response for 90 minutes.

Table 5.22: Dynamic simulation tests.

Case No.	Values
Step increase:	
1: 10% increase in the set point of steam-valve opening	2.74 T/min
2: 5% increase in the set point of the recirculating brine flowrate	250 T/min
3: 5°C increase in seawater temperature	37 °C
Step decrease:	
4: 20% decrease in the set point of steam-valve opening	1.996 T/min
5: 5% decrease in the set point of the recirculating brine flowrate	226.19 T/min
6: 7 °C decrease in seawater temperature	25 °C

Figures 5.22 to 5.27 plot some of the resulting top brine temperature (TBT, °C), distillate produced (D_OUT, T/min), and brine level (m) under different dynamic conditions mentioned above. Table 5.23 summarizes different dynamic tests results presented in Figures 5.22 to 5.27. It is clear from the figures that system reaches a stable operation after approximately 40 minutes. This long time is expected because of the size of the MSF desalination plant and the large number of variables involved. However, this can be improved by changing the controller settings.

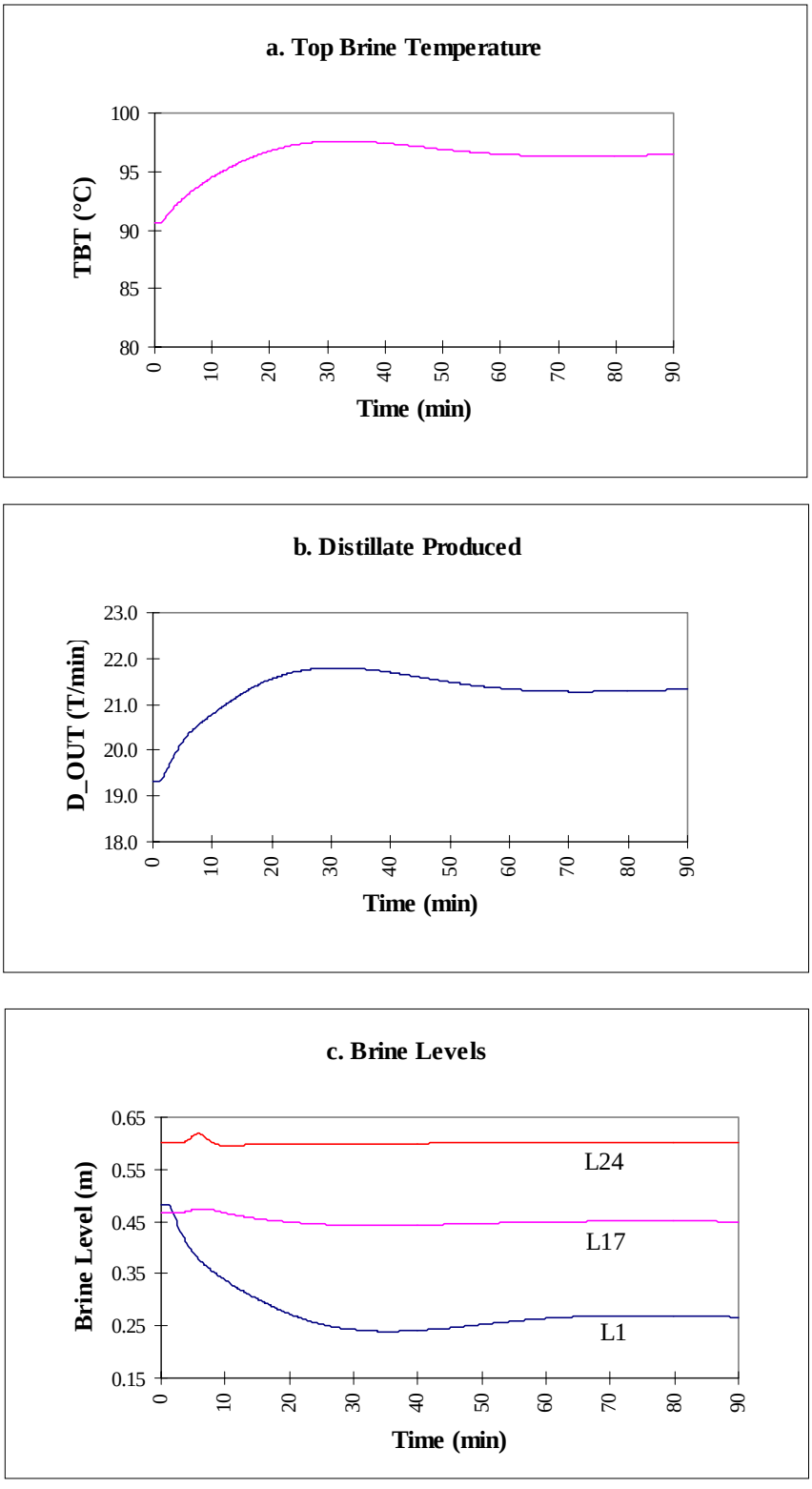

Figure 5.22: Dynamic responses of process variables for step increases of set point in steam-valve opening.

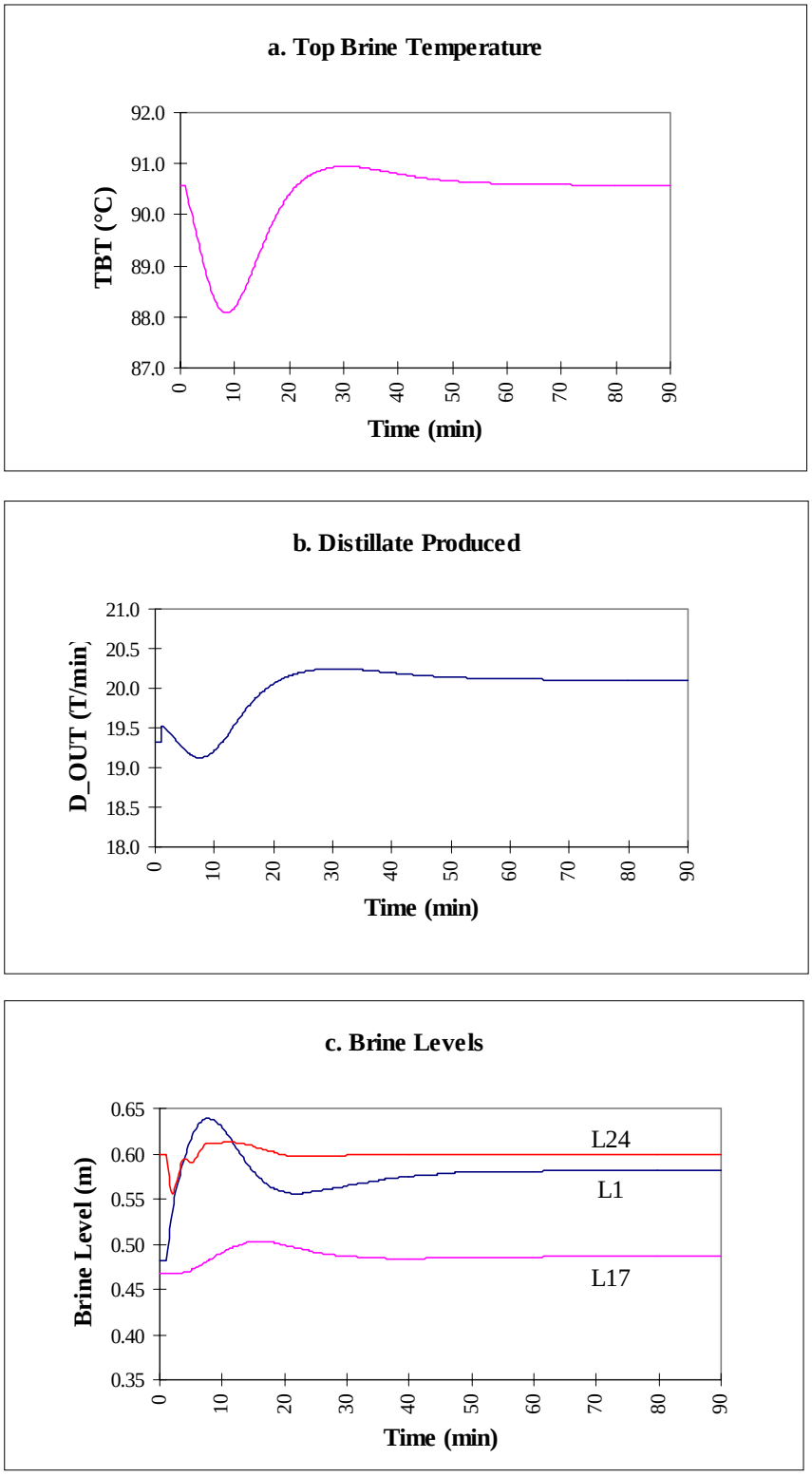

Figure 5.23: Dynamic responses of process variables for step increases of set point in recirculating brine flowrate.

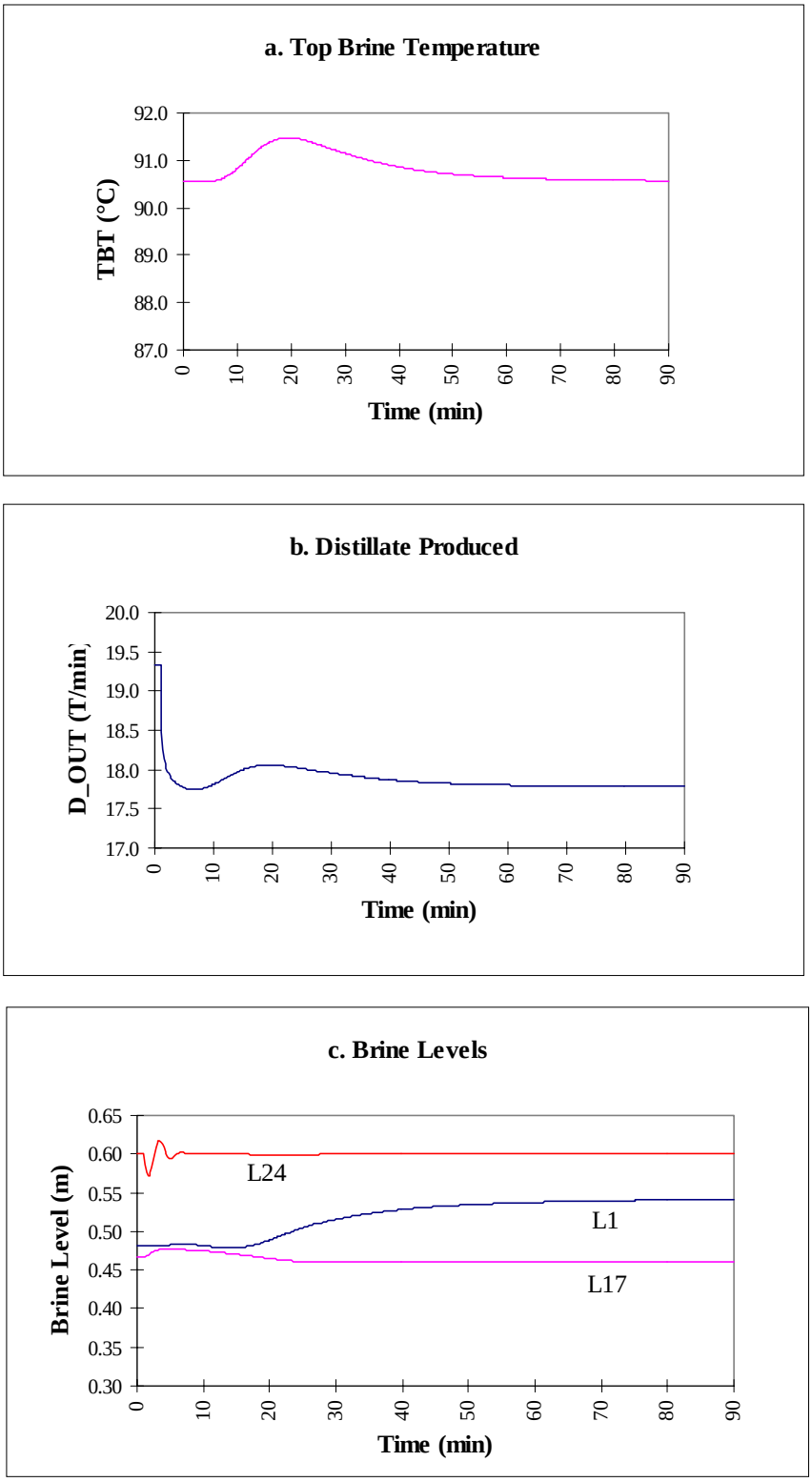

Figure 5.24: Dynamic responses of process variables for step increases of set point in seawater inlet temperature.

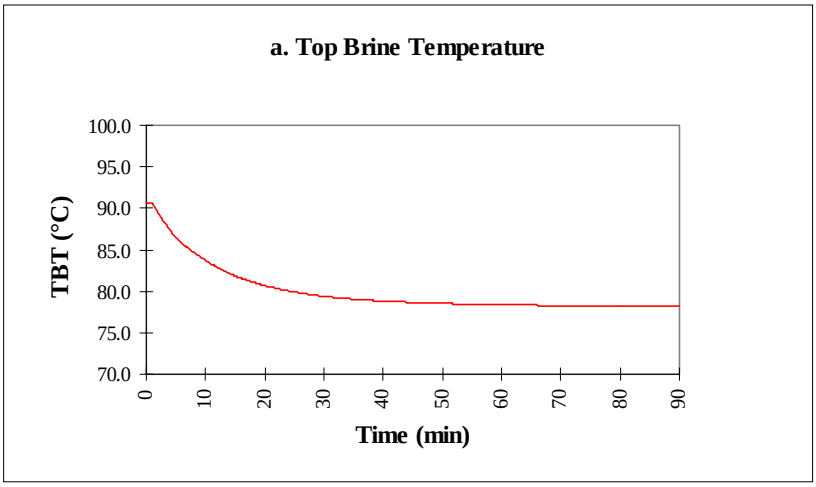

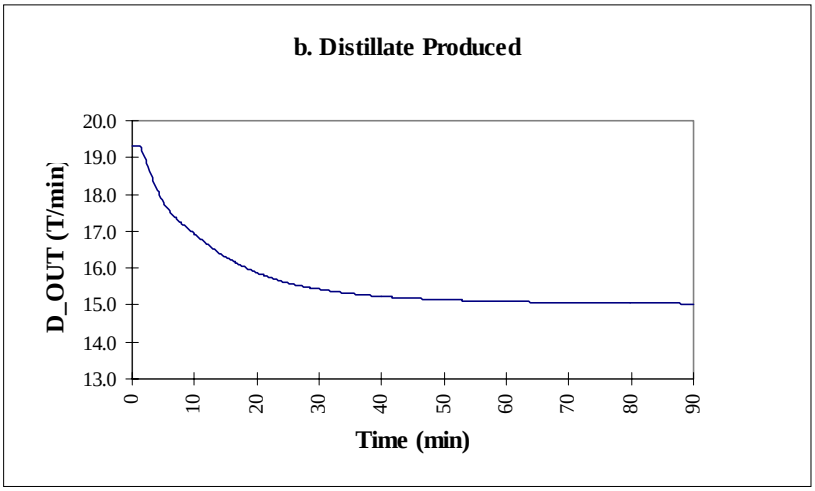

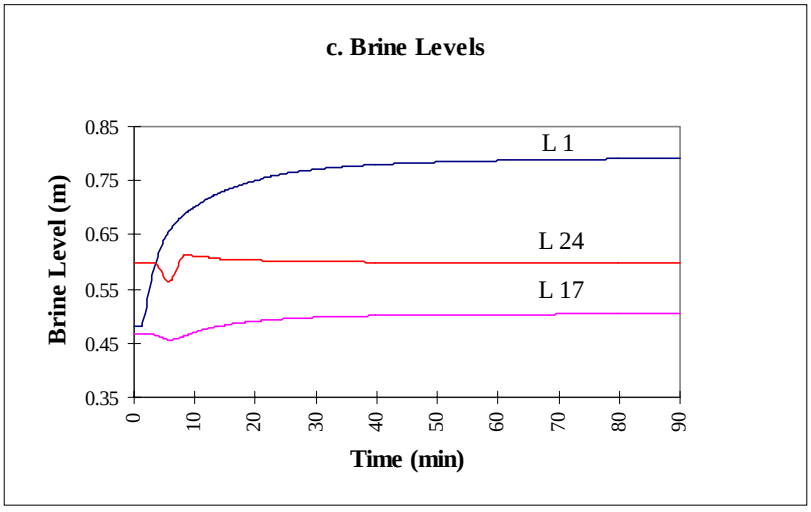

Figure 5.25: Dynamic responses of process variables for step decreases of set point in steam-valve opening.

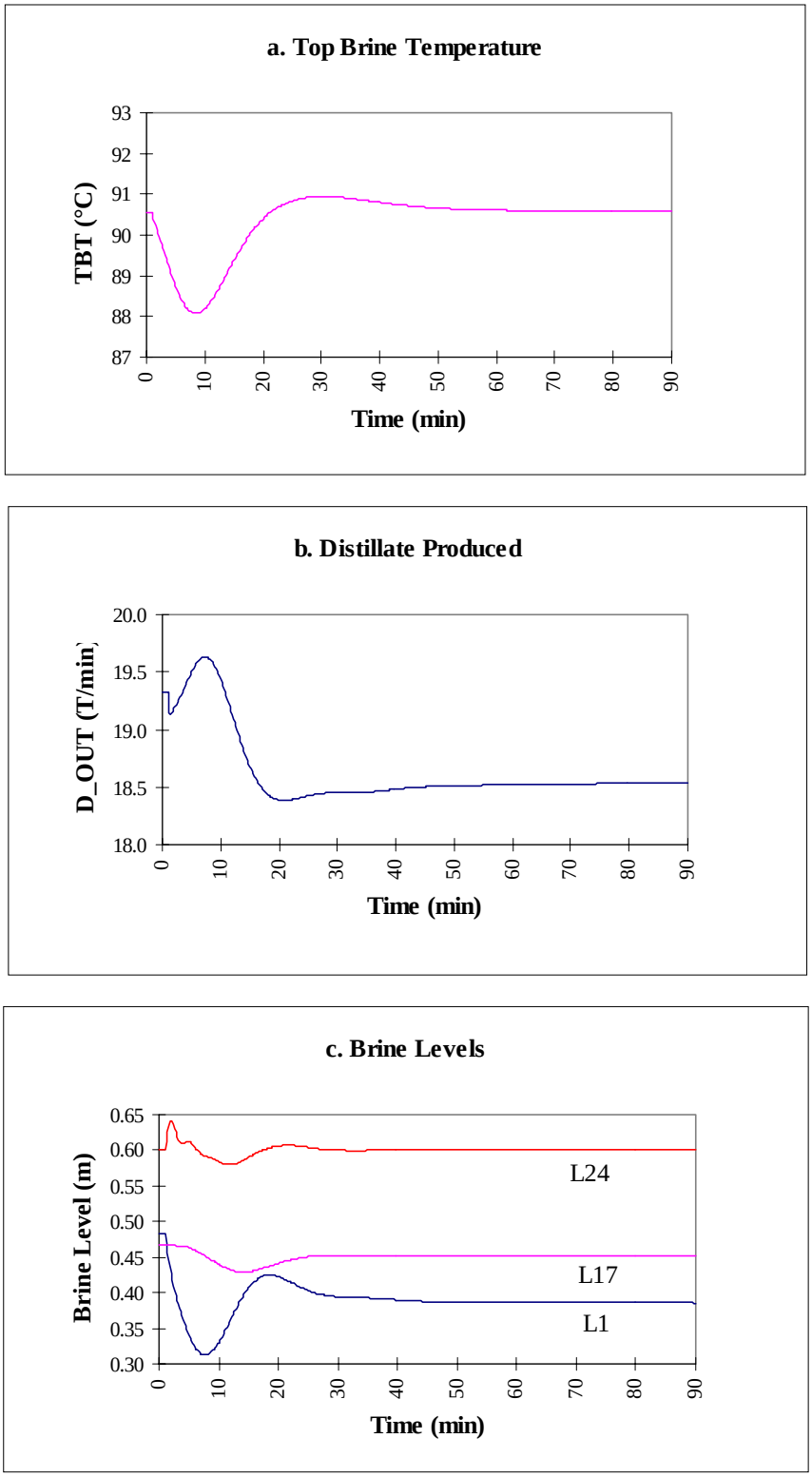

Figure 5.26: Dynamic responses of process variables for step decreases of step point in recirculating brine flowrate.

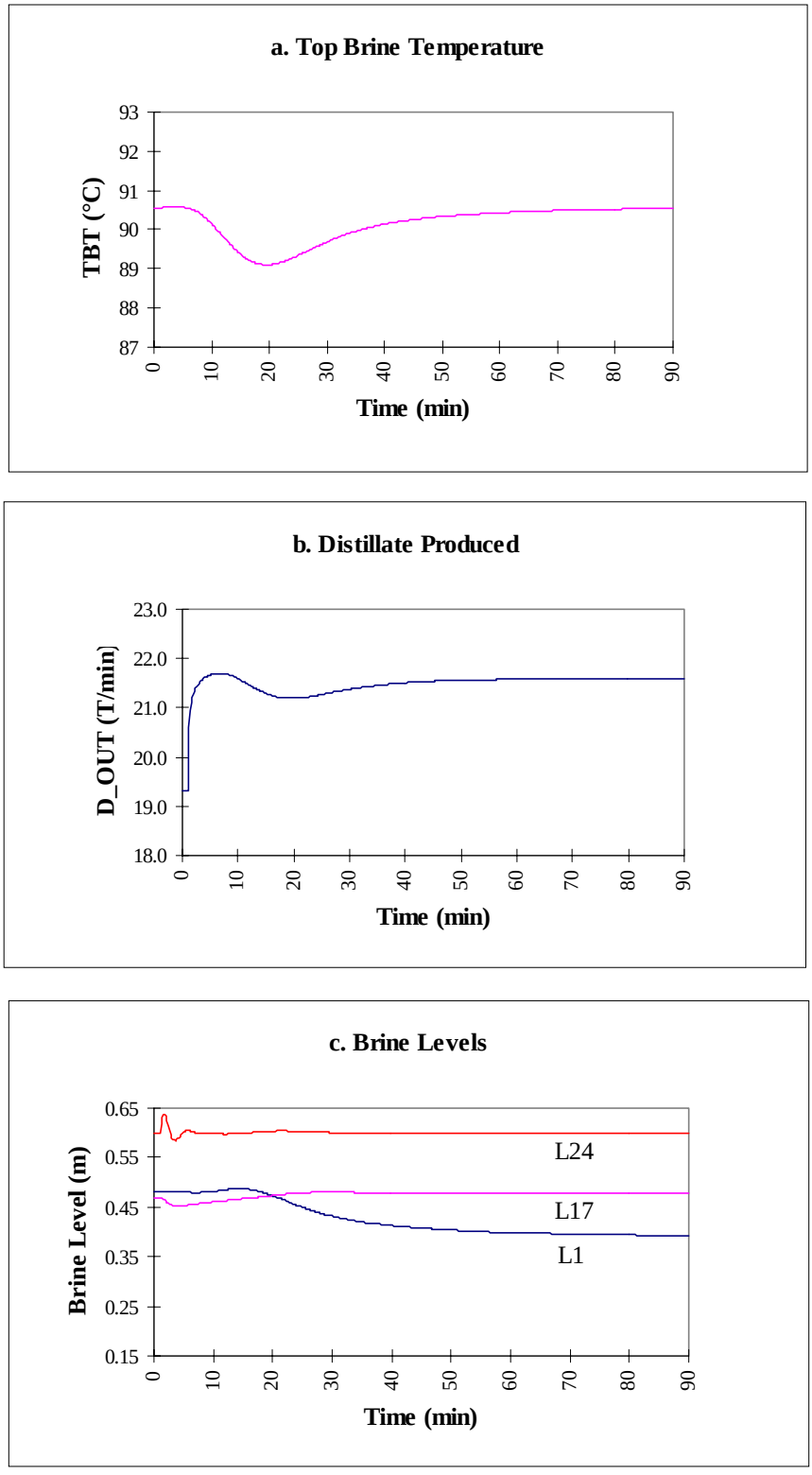

Figure 5.27: Dynamic responses of process variables for step decreases of set point in seawater inlet temperature.

Table 5.23: Dynamic response of process variables for step increases and decreases in set points on some key manipulated variables from Figures 5.22 to 5.27.

Key manipulated variables	**Design Values**	**Steam-valve opening**		**Recirculating brine flowrate**		**Seawater inlet temperature**	
		Increase	Decrease	Increase	Decrease	Increase	Decrease
Top brine temperature (TBT, °C)	90.56	96.439	78.167	90.57	90.553	90.57	90.539
Distillate produced (D_OUT, T/min)	18.795	21.328	15.037	20.097	18.536	17.786	21.597
Brine level (m) (maximum/minimum):							
First stage (L1)	0.482	0.482/0.239	0.792/0.482	0.639/0.482	0.482/0.313	0.53/0.479	0.487/0.393
Stage 17 (L17)	0.467	0.474/0.442	0.504/0.456	0.503/0.467	0.467/0.429	0.478/0.46	0.48/0.453
Last stage (L24)	0.6	0.618/0.595	0.613/0.563	0.613/0.556	0.642/0.58	0.617/0.571	0.638/0.584

Table 5.24 summarizes different dynamic tests carried out at different control loop conditions with a step change of 20% reduction in the steam flowrate to the brine heater. Figure 5.28 shows that inlet and outlet brine temperatures in the brine heater change almost simultaneously. Figure 5.29 illustrates that the brine level in the first stage immediately goes up, while other stages, such as stage 10, indicate a small inverse response before the brine level rises. This effect becomes more clear in Figure 5.30 when we do not control the last stage brine level. The inverse response of brine levels occurs because raising the brine level in the first stage causes a pressure change and hydrodynamic instability, which is transmitted to downstream stages. Therefore, the exit brine flow exceeds the inlet flow in each stage. This results in a decrease of flashing temperature (flash range), thus reducing vaporization and increasing brine level.

Table 5.24: Dynamic change in control loop conditions.

Test no.	**Control loops**	**Results**	**Remarks**
1	open 1 and 3 close 2 and 4	Figure 5.19: Brine-heater temperature profile Figure 5.20: Brine levels in stages 1, 10, and 24	Introducing step change in steam-valve opening (steam flowrate) introduced after reaching steady-state conditions for one minute
2	open 1 close 2-4	Same as above	Same as above
3	Open all loops (1-4)	Figure 5.21: Uncontrolled last-stage brine level	Same as above

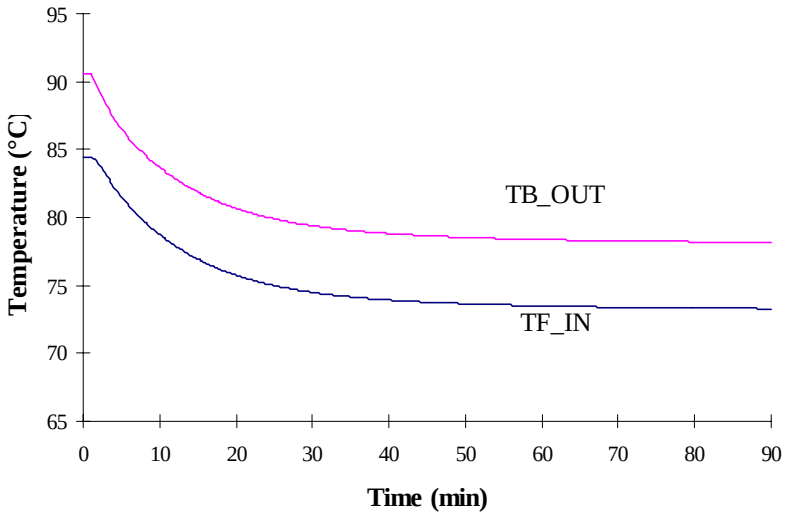

Figure 5.28: Brine-heater temperature profile (Test 1 in Table 5.24).

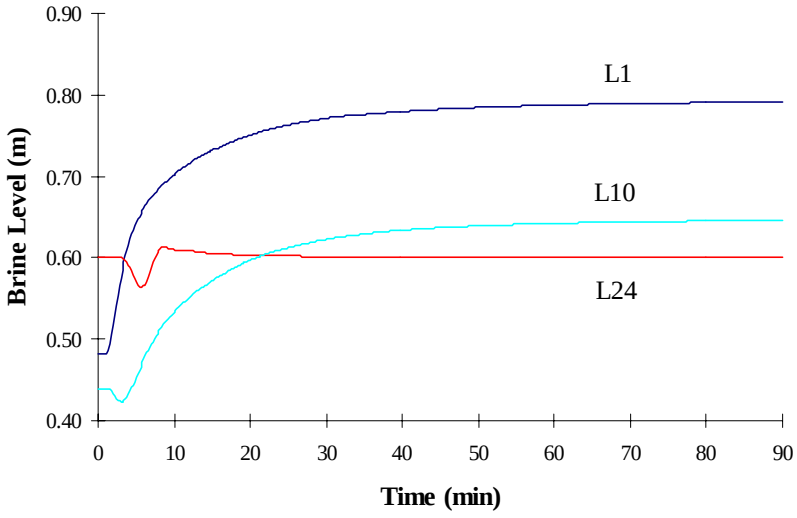

Figure 5.29: Brine levels in stages 1, 10, and 24 (Test 2 in Table 5.24).

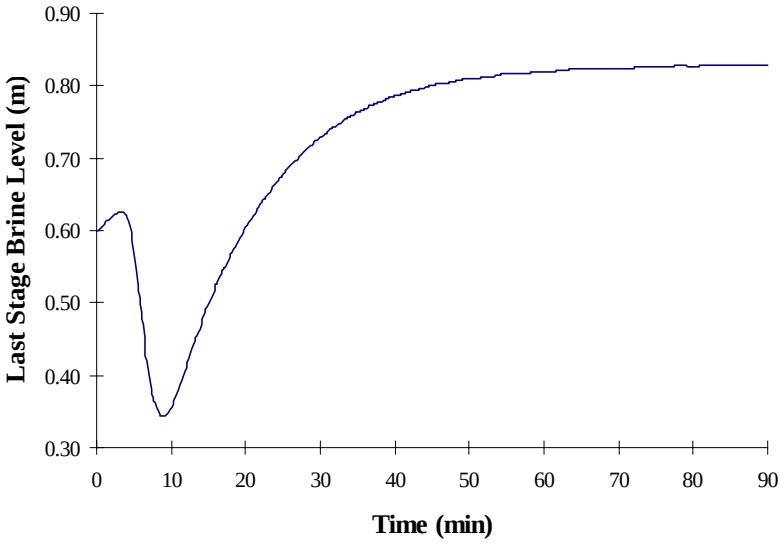

Figure 5.30: Last-stage brine level (Test 3 in Table 5.24).

5.4 Comparison of Neural Network, ASPEN PLUS, and SPEEDUP Simulation Results

When developing a simulation model for commercial MSF desalination plants, we have used two different approaches in order to predict the plant performance. As seen in Figure 5.31, the first approach is data-based using neural networks. The second approach is model-based applying a mathematical model derived from physical principles to describe the steady-state and dynamics behavior of an MSF plant. The second approach incorporates both a modular approach using ASPEN PLUS design software, as well as an equation-solving approach, using SPEEDUP. We compare the simulations results from all three cases below.

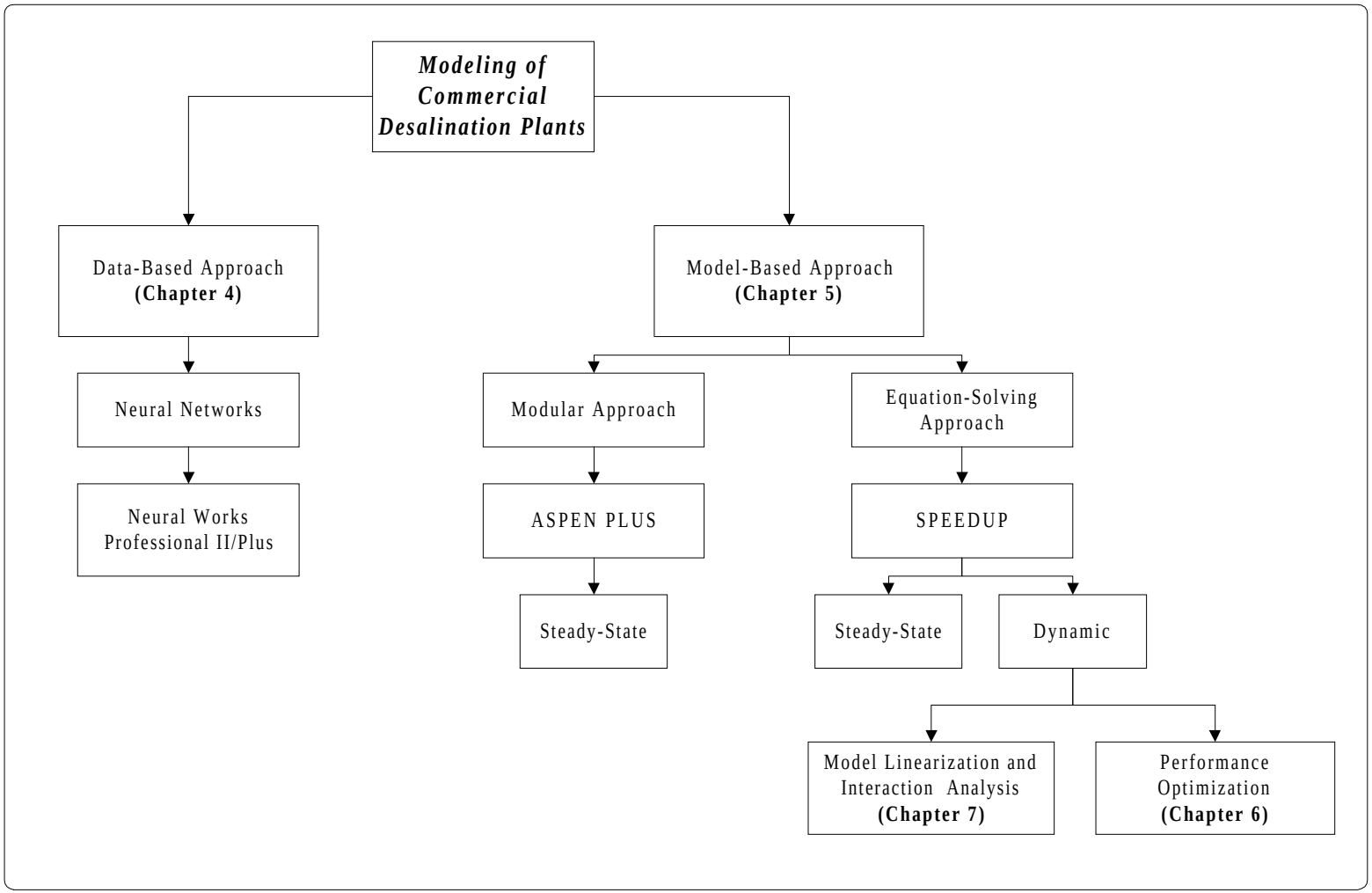

Figure 5.31: Data-based and model-based approaches to modeling.

Table 5.25 compares the distillate produced by each approach. All approaches are able to produce satisfactory results, with both ASPEN PLUS and SPEEDUP giving the closest values to the design specification.

Table 5.25: Distillate produced from the three modeling approaches

Modeling approach	**Distillate produced (T/min)**
Summer operation at a top brine temperature of 90.56°C	18.79
Neural Network	23.92
ASPEN PLUS	18.82
SPEEDUP	19.33

Neural networks may not seem at first to have produced favorable results, but this is due to the range of data with which a network is trained. As discussed in Chapter 4, neural network interpolates data very well, but it does not extrapolate. Therefore, the training set should be selected in such a way that it includes data from all regions of desired operation. Note that the prediction network for distillate produced as developed in Chapter 4, is trained with summer operation data operating at high-top brine temperature mode. The ranges of top brine temperatures and distillate product flowrates for the training set are 104°C-105.6°C (not at 90.56°C as in Table 5.25), and 21.85 T/hr-23.83 T/hr, respectively. Therefore, testing the network with the designed distillate product flowrate of 18.79 T/hr at a top brine temperature of 90.56°C is expected to predict a higher distillate flowrate. In order to produce favorable results, the network needs to be trained with a wider range of operating data.

To completely model in ASPEN PLUS, we need to enter the values of some manipulated variables into the software. Because of this, the model was created based on producing

the desired distillate flowrate. Therefore, the distillate product flowrate obtained by ASPEN PLUS is very close to the design value, as can be seen by the relative error of 0.14%.

SPEEDUP produces desired results because we accurately model the plant with mass and energy balances, as well as with physical property correlations. The accuracy of a model-based approach relies heavily on the quality of the model itself. In order to get more exact results, we need to improve several equations to make the model more representative, as will be discussed in Chapter 9.

5.5 Conclusions

This chapter presents an overview of modeling and simulation aspects of multistage flash desalination plant using modular and equation-solving approaches through the use of ASPEN PLUS and SPEEDDUP simulation packages marketed by Aspen Tech.

Both approaches, modular and equation-solving, have their advantages and disadvantages. The modular approach is conceptually easy to understand. Errors can be easily diagnosed and good initialization procedures developed by experience are available. A primary disadvantage of a modular approach is that it may be difficult to find satisfactory convergence schemes for large-scale complex chemical processes, such as commercial desalination plants.

Among the advantages of the equation-solving approach are that:

- easy to specify variables and constraints
- can handle highly integrated problems
- equally applicable for dynamic simulations as well as steady-state design calculations.

The major disadvantages of the equation-solving approach are:

- difficult to diagnose errors
- good initial estimates of all the variables are needed
- difficult to handle highly nonlinear and discontinuous relations

Steady-state simulations give an excellent agreement with the design data. The flowsheeting capabilities of ASPEN PLUS with Model Manager and SPEEDUP provide the process engineer with the flexibility to investigate systems at any level of complexity and to quickly create, adapt, or expand simulations of sub systems into full system simulations and ultimately complete plants.

However, a flowsheeting package like SPEEDUP may not be quite suitable for day-to-day plant simulations to be carried out for the purpose of process or set-point optimization. This follows for several reasons. The first is the licensing cost of the package for commercial use. Secondary, the input preparation for SPEEDUP takes a considerable amount of time. To handle a typical commercial MSF plant, SPEEDUP has to solve a total of 975 equations including 1362 variables and parameters, which are further grouped into 238 blocks. Consequently, convergence problems may often occur and it proves costly to re-do simulations for any small change in the input conditions.

Additionally, in the ASPEN PLUS modular approach, we need to take into account of constraints through additional iteration loops around the module, provided these

constraints involve stream variables associated with that module. However, if the constraints involve streams not presented in the module, we need to carry out iterations involving the entire flowsheet. This type of procedure is quit cumbersome and tedious. For that reason, the modular approach could not gain popularity for simulation in the design mode of commercial MSF desalination plants.

5.6 References

Al-Gobaisi, M., "A Quarter-century of Seawater Desalination by Large Multistage Flash Plants in Abu-Dahbi", *Desalination*, **99**, 483 (1994).

Al-Gobaisi, M., A., Husain, G., Rao, A., Sattar, A., Woldai, and R., Borsani, "Toward Improved Automation for Desalination Processes, Part I: Advanced Control", *Desalination*, **97**, 469 (1994).

Al-Gobaisi, M., "An Overview of Modern Control Strategies for Optimizing Thermal Desalination Plants", *Desalination*, **84**, 3-43, 1991.

Al-Shayji, K., "Simulation of MSF Desalination Plant AZ-Zour South Station", *MS Thesis*, University of Glasgow, Glasgow, UK (1993).

Helal, A., M. Medani, and M. Soliman, "A Tridiagonal Matrix Model for Multistage Flash Desalination Plants", *Comp. Chem. Eng*., **10**, No. 4, 327-342, 1986.

Homig, H.E., *Fichtner-Handbook, Seawater and Seawater Distillation*, Vulkan-Verlag. Essen, Germany (1978).

Husain, A., *Chemical Process Simulation*, Wiley Eastern Limited, New Delhi, India (1986).

Husain, A., A. Hassan, M. Al-Gobaisi, A. Al-Radif, A. Woldai, and C. Sommariva, "Modeling , Simulation, Optimization, and Control of Multistage Flashing (MSF) Desalination Plants Part I: Modeling and Simulation", *Desalination*, **92**, 21 (1993).

Husain, A., A. Woldai, A. Al-Radif, A. Kesou, R. Borsani, H. Sultan, and P. Deshpandey, "Modeling and Simulation of a Multistage Flash (MSF) Desalination Plant", *Desalination*, **97**, 555 (1994).

Husain, A., K.V., Reddy, A. Woldai, and S.M., Al-Gobaisi, "*Modeling, Simulation and Optimization of an MSF Desalination Plant", Eurotherm Seminar No. 40*, Thessaloniki, Greece, (1994).

Khan, A.H., *Desalination and Water Purification: 1. Desalination Processes and Multistage Flash Distillation Practice*, Elsevier, New York, N. Y. (1986).

Lior, N., *Desalination and Water purification: 2. Measurements and Control in Water Desalination*, Elsevier, New York, N. Y. (1986).

Maniar, V., and P. Deshpande, "Advanced Control for Multi-Stage Flash (MSF) Desalination Plant Optimization", *J. Proc. Cont.*, **6**, 1, 49 (1996).

Rahbar, M., "Improvement of the Design and Operation of Desalination Plants by Computer Modeling and Simulation", *Desalination*, 92, 253 (1993).

Reddy, K.V., A. Husain, A. Woldai, and M. Al-Gobaisi, "Dynamic Modeling of the MSF Desalination Process", *Proceedings of the IDA World Congress on Desalination and Water Sciences*, Abu Dhabi Publishing Co., Abu Dhabi, UAE, **Vol. IV**, 227 (1995).

Seborg, D.E., T.F., Edgar, and D.A., Mellichamp, *Process Dynamic and Control*, John Wily and Sons, New York, N. Y. (1989).

CHAPTER 6

PERFORMANCE OPTIMIZATION OF A LARGE-SCALE COMMERCIAL MULTISTAGE FLASH DESALINATION PLANT

Chapter 6 deals with the steady-state optimization of the operation of an existing MSF desalination plant. It begins with a discussion of the most important process variables and constraints, that directly affect the production and performance ratio of the plant. Next, we develop the optimal operating conditions for achieving a stable plant operation using the SPEEDUP model for the steady-state simulation developed in Chapter 5.

6.1 Introduction

Optimization can improve a chemical process at various stages of its life cycle, spanning various phases of conceptualization, design, construction, operation and control of a plant.

For MSF desalination plants, optimization can be quite useful at the planning, design, and operation phases. Optimization of planning and design phases is well established, while optimization in the operation phase has not received much attention (Hornburg and Watson, 1993). The goals of MSF process optimization are to :

- minimize energy consumption: this means high performance ratio, which is defined as the ratio of distillate production rate to the steam condensate rate.
- achieve stable operation: this means reasonable brine levels in flashing stages.
- avoid equipment fouling: which limit the top brine temperature and tube side velocities.

- reduce chemical consumptions (e.g., for antiscaling and antifoaming in process operation).

This chapter illustrates our results of steady-state performance optimization of a large-scale commercial MSF desalination plant to maximize the production rate and improve the process efficiency. Specifically, we shall consider the following two optimization cases.

- In the summer season, demand for the water increases. In this situation, the plant has to maximize distillate product flowrate at any performance ratio.
- In another situation, the distillate product flowrate may be limited due to available storage capacity. Here, the objective is to maximize performance ratio at the desired target production rate.

We apply the SPEEDUP model for these optimization studies.

6.2 Process Variables

To maximize performance ratio and ensure stable operation, we can optimize the following process variables:

- Top brine temperature
- Recirculating brine flowrate
- Make-up flowrate

The top brine temperature (TBT) plays a crucial role in the performance of the MSF plant. By increasing TBT, both the production rate and performance ratio increase. The production rate goes up because of an increase in the flashing range. The performance ratio increases due to a decrease in the latent heat of vaporization of water at a higher temperature. At the same time, higher TBT leads to an increased scale formation. Our experience in simulation runs indicates that both the production rate and performance

Increasing the recirculating brine flowrate (R) increases the distillate product flowrate, but it adversely affects the performance ratio. An increase in the distillate production is due to a drop in the flashing brine temperature from stage to stage. The maximum flowrate for the recirculating brine is limited by the maximum allowable velocity in the cooling tubes, as higher velocities may cause erosion of the tube material. A upper velocity limit is about 2.0 m/s. On the other hand, the minimum permissible velocity is 1.8 m/s, since a lower velocities will reduce the heat-transfer coefficient and enhance the sedimentation of solids on the heat-transfer surface.

A high make-up flowrate results in a lower salt concentration in the blowdown stream for a specified production rate. It also causes a decrease in the brine specific gravity, boiling-point elevation and other thermodynamic penalities. By contrast, a larger make-up flowrate requires more anti-scaling chemicals.

6.3 Process Constraints

Based on the discussion in the preceding section, we note the following process constraints:

- Upper limit of TBT to avoid any scaling
- Upper and lower limits of the flow velocity inside the tubes
- The make-up feed temperature should be close enough to the flashing temperature in the last stage.
- Upper limit of the salt concentration in the blowdown stream.

6.4 Process Efficiency

Performance ratio (PR) is a measure of the process efficiency, which is the ratio of the distillate product rate to the steam condensate rate. More precisely, it is defined as kgs. of distillate produced per 540 Kcal heat supplied by the steam.

6.5 Development of Optimal Operational Conditions ('Operating Envelopes')

From the above description, it is clear that both the top brine temperature and recirculating brine flowrate can significantly affect the performance ratio and production rate. Therefore, we shall vary these two process variables, while fixing the make-up flowrate at a value that gives a salt concentration in the blowdown stream within the permissible limit. Additionally, we fix the seawater flowrate at a value such that the flow velocity within cooling tubes in the heat-rejection section is between 1.8 and 2.0 m/s.

By applying the SPEEDUP model, we develop the optimal operating conditions. We assume a seawater temperature at 32.22 °C, a make-up flowrate of 48.76 T/min, and a brine level of 0.6 m for the last flash stage. Figure 6.1 shows an operating envelope in which the solid lines refer to a constant recirculatinmg brine flowrate (R), decreasing from maximum (Rmax) to minimum (Rmin) values (256.4-230.8 T/min). The latter correspond to the allowable limits of flow velocities through cooling tubes (1.8-2.0 m/s). The dashed lines in the figure represent constant top brine temperatures between minimum (TBTmin) and maximum (TBTmax) values (86.03-95.08°C). Table 6.1 gives the specific operating conditions for points labeled 1 to 22 in Figure 6.1.

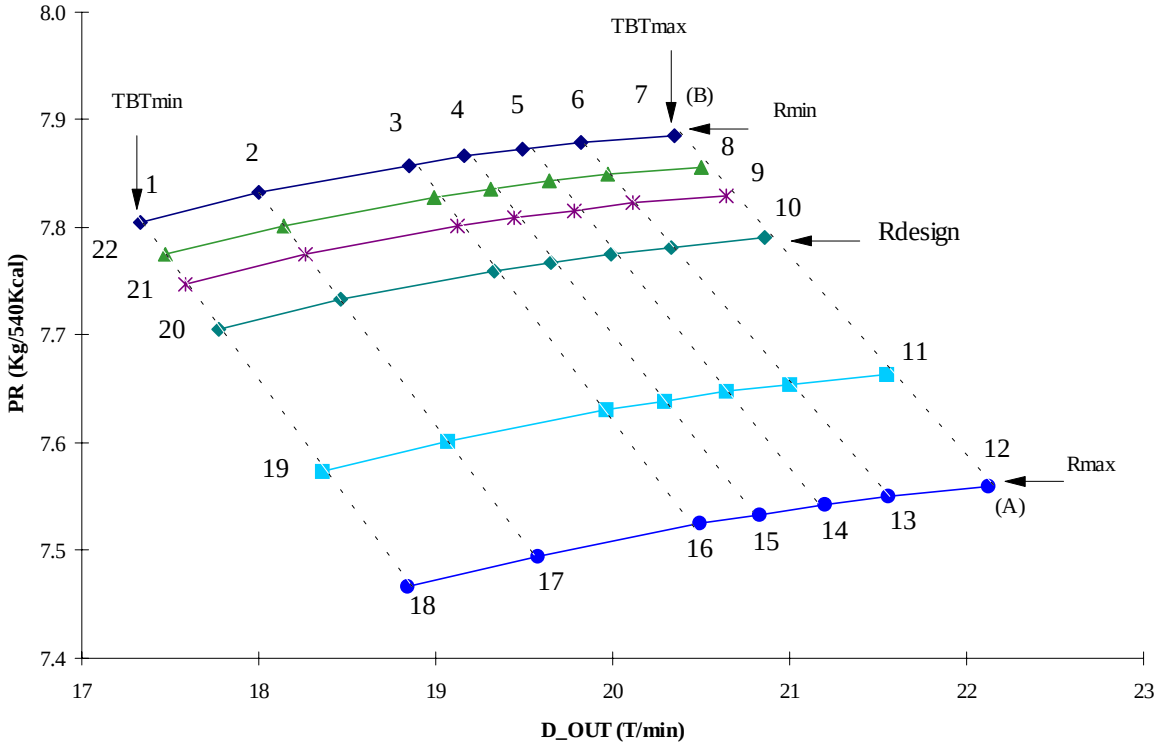

Figure 6.1: Optimal operating conditions for distillate produced (D_OUT) and performance ration (PR).

See Table 6.1 for conditions for points 1 to 22.

Table 6.1: Boundary points of the operating envelop shown in Figure 1.

Points	**Operating conditions**
1-7	Recirculating brine flowrate constant at a minimum of 230.8 T/min at increasing TBT (86.03, 88.03, 90.56, 91.5, 92.5, 93.5,95.08°C).
8-12	TBT constant at a maximum of 95.08°C and at increasing recirculating brine flowrate (233, 235, 238.1, 248, 256.4 T/min).
13-18	Recirculating brine flowrate constant at a maximum of 256.4 T/min and at decreasing TBT (93.5, 92.5, 91.5, 90.56, 88.03, 86.03 °C)
19-22	TBT constant at a minimum of 86.03°C and at decreasing recirculating brine flowrate (248, 238.1, 235, 233 T/min) .

Point A in Figure 6.1 indicates the conditions to attain the maximum production rate at lower performance ratios. Point B represents the operating conditions to attain the maximum performance ratio with a certain loss of production capacity. In principle, we can operate at any point on the borders or within the envelope.

Figure 6.2 plots the brine levels for various flash stages at increasing recirculating brine flowrate (R, T/min) and orifice height. Tests 1-7 represent tests at different TBT values of 86.03, 88.03, 90.56, 91.5, 92.5, 93.5, and 95.08 °C.

This figure shows that at some test conditions, a blowthrough of vapor into subsequent flash stages occurs. Vapor blowthrough may results in various consequences such as energy loss due to vapor leakage to the lower temperature stages, and drop of pressure in the flash chamber. The later, in turn, will result in an increase in the pressure difference.

Therefore, for practical operations, we must reduce the size of the operating envelope to maintain reasonable brine levels in all stages and to prevent vapor blowthrough. Figure 6.3 shows a revised operating envelope after eliminating those operating conditions for which vapor blowthrough could occur.

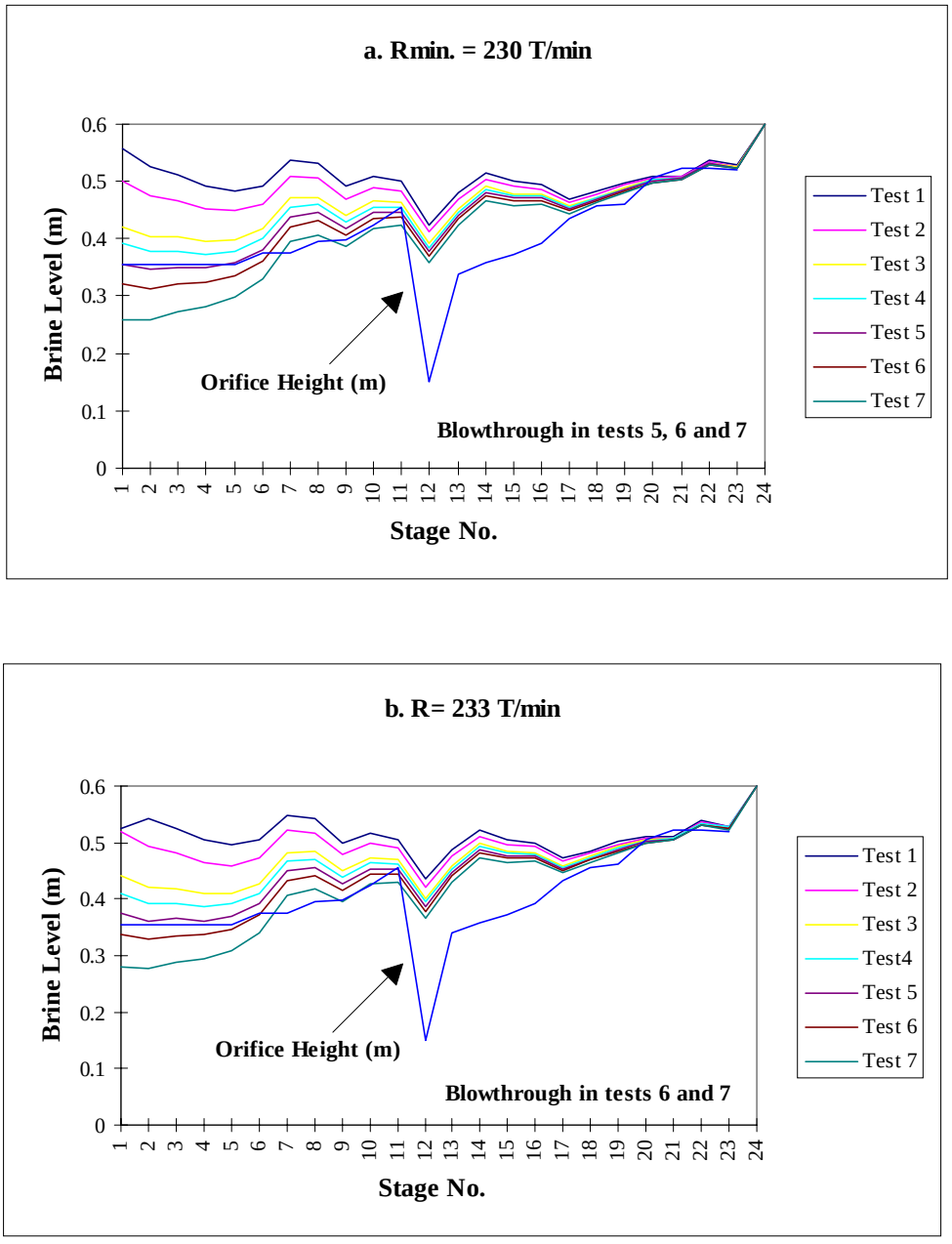

Figure 6.2: Brine levels and orifice heights for various flash stages at increasing recirculating brine flowrate and top brine temperature.

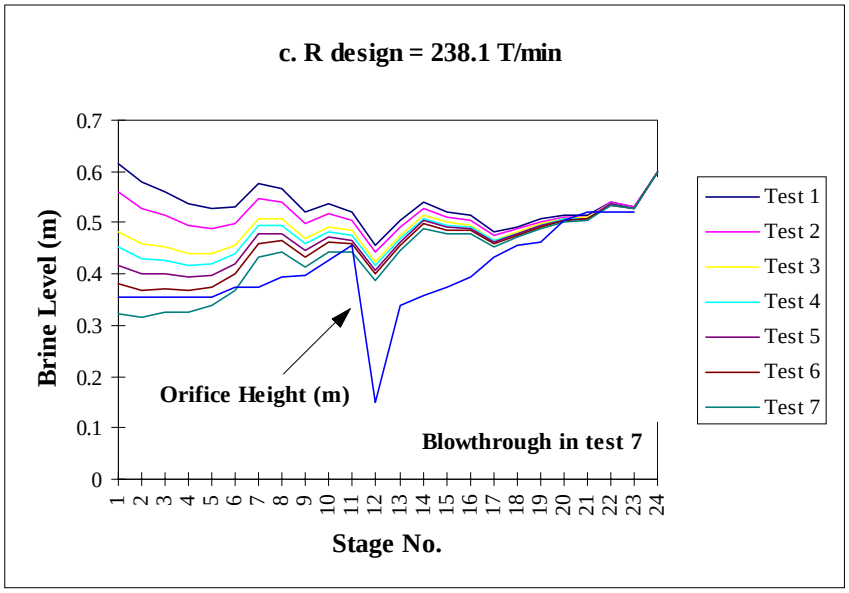

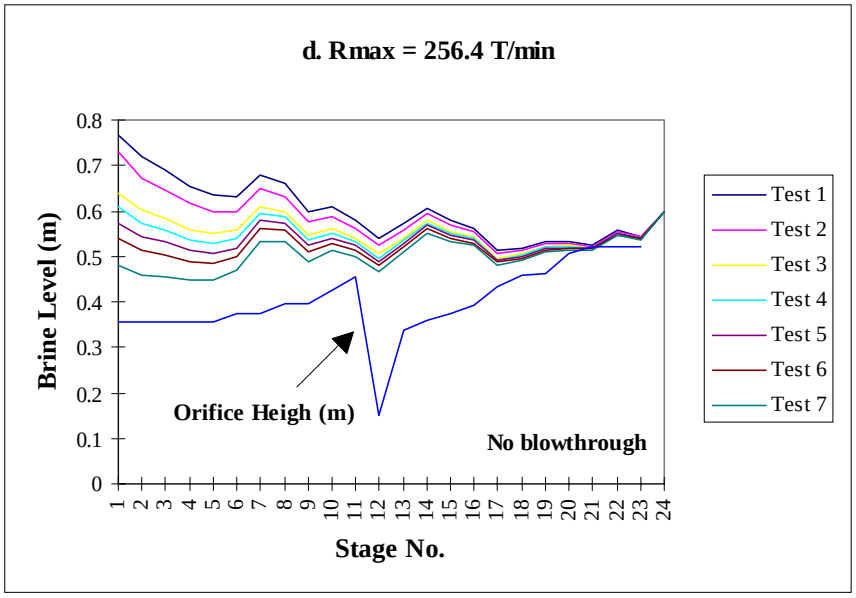

Figure 6.2: Brine levels and orifice heights for various flash stages at increasing recirculating brine flowrate and top brine temperature (continued).

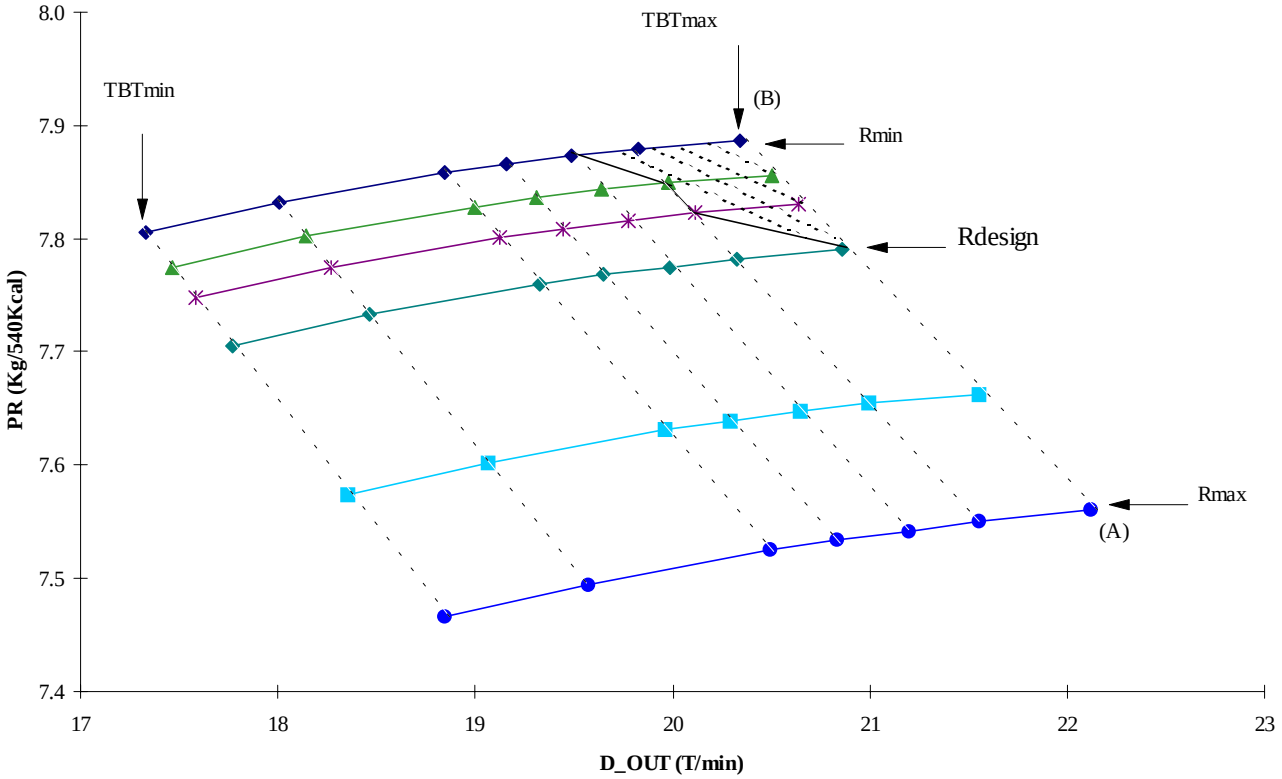

Figure 6.3: Revised optimal operating conditions for distillate produced (D_OUT) and performance ration (PR) after eliminating conditions leading to vapor blowthrough.

6.6 Conclusions

An optimal operating envelope generated by a SPEEDUP model helps in finding the stable operation region for a commercial MSF desalination plant.

Stable operation of the plant should lead to good distillate quality, avoiding mechanical and corrosion damage, and minimizing energy consumption by lowering thermodynamic losses. Additionally, the interstage brine transfer through orifices devices plays a very important role. Instability in operation arises because of high or low brine levels due to improper settings in the transfer orifices. An under-sized orifice causes high brine levels upstream of the orifice, while an over-sized orifice can lead to vapor blowthrough into the subsequent stages. Therefore, we should maintain the brine levels in all stages at reasonable levels to prevent vapor blowthrough or brine carryover.

6.7 References

Al-Gobaisi, D.M., A quarter-century of seawater desalination by large multistage flash plants in Abu Dhabi, *Desalination*, **99**, 483 (1994).

Beveridge, G., and R., Schechter, *Optimization: Theory and Practice*, McGraw-Hill Book Company, New York, N. Y. (1970).

Hornburg, C.D., and B.M., Watson, "Operation Optimization of MSF systems", *Desalination* **92**, 333 (1993).

Husain, A., *Chemical Process Simulation*, Wiley Eastern Limited, New Delhi, India (1986).

Husain, A., A., Woldai, A., Al-Radif, A., Kesou, R., Borsani, H., Sultan, and P.B., Deshpandey, "Modeling and Simulation of a Multistage Flash (MSF) Desalination Plant", *Desalination*, **97**, 555 (1994).

CHAPTER 7

MODEL LINEARIZATION AND INTERACTION ANALYSIS OF A COMMERCIAL MULTISTAGE FLASH DESALINATION PLANT.

This chapter briefly introduces model linearization of a commercial MSF plant using dynamic run and invoking the tool of Control Design Interface (CDI) available in SPEEDUP. Then, we focus on the use of Bristol's interaction analysis based on the concept of a relative gain array to find the best paring of manipulated and controlled variables in commercial MSF desalination plants.

7.1 Introduction

The open-loop process characteristics are the basis for control-system design. In Chapter 5, we developed a SPEEDUP model for a commercial MSF desalination plant that involves nonlinear algebraic and ordinary differential equations. For controller design, it is a frequent practice to linearize these nonlinear equations about the nominal operating conditions. This chapter investigates the use of a linearized SPEEDUP model to find the best pairing of controlled and manipulated variables aid in the development of the control structure of a commercial MSF desalination process.

7.2 Control System for MSF Desalination Plants

The MSF process is a multi-input and multi-output process from the point of view of control. Therefore, the control system should understand the process behavior. Commercial MSF desalination plants typically use a PID controller to control the top

brine temperature and PI controllers for the rest of variables. There are several shortcomings in the conventional control systems of MSF plants. The following are some of the deficiencies in the current operating systems (Al-Gobaisi, et al., 1994):

- Poor methods for the suppression of disturbances.
- Lack of robust stability.
- Narrow range of conditions for reliable operation.
- Slow response to changes in process load and ambient conditions.
- Non-optimal utilization, and poor optimization of available resources and energy.
- Propagation of disturbances leading to instability.
- Near-optimal design, but unsatisfactory control strategy.

Although the number of control loops in MSF desalination plants is not too large, and there are considerable nonlinearity and non-stationary behavior, errors and uncertainties, loop interaction, disturbances, etc.

There are about twenty control loops in a large-scale commercial MSF desalination plant. Some of the most influential controlled variables affect the distillate quantity and quality, and need to be well-tuned in order to achieve stable operations. They are listed as follows.

1. Top brine temperature
2. Low-pressure steam temperature to the brine heater
3. Recirculating brine flowrate

4. Seawater flowrate entering the last rejection section
5. Seawater inlet temperature to the heat rejection section
6. Make-up flowrate
7. Last-stage brine level
8. Last-stage distillate level
9. Brine-heater condensate level

It is necessary to define some of the process variables used in the control system.

Controlled variables: the process variables that must be maintained or controlled at some desired values (set points).

Input variables: the variables that indicate the effect of the surrounding on the process system, and can thereby induce change in the internal conditions of the process.

Manipulated variables: those input variables that can be freely adjusted in their values by a human operator or a “control mechanism”.

Disturbances: those input variables that are not subjected to adjustment by an operator or “control mechanism”.

Output variables: the variables that indicate the effect of the process system on its surroundings.

The selection of the controlled and manipulated variables plays an important role in control-system design.

7.3 Model Linearization

The mathematical models for chemical process control often utilize nonlinear algebraic and ordinary differential equations. The design of control systems for nonlinear chemical processes typically involves specifications in a regulatory mode rather than in the tracking mode. We start by assuming that the process works normally at fixed or nominal operating conditions. By linearizing the nonlinear process model around the close neighborhood of nominal operating conditions, we can then develop relevant controllers based on the well established linear control methodology.

Consider a general set of nonlinear algebraic and ordinary differential equations used to model a process. The state equation is:

$$\mathbf{x}(t) = \mathbf{f}\left[\mathbf{x}(t)\,,\mathbf{u}(t)\right] \tag{7.1}$$

The output equation is:

$$\mathbf{y}(t) = \mathbf{g}\left[\mathbf{x}(t)\,,\ \mathbf{u}(t)\right] \tag{7.2}$$

In these equations, the vector variables are:

$$\mathbf{x}(t) = \left[\mathbf{x}_1(t) \quad \mathbf{x}_2(t) \quad \ldots \quad \mathbf{x}_n(t)\right]^T \tag{7.3}$$

$$\mathbf{y}(t) = \left[\mathbf{y}_1(t) \quad \mathbf{y}_2(t) \quad \ldots \quad \mathbf{y}_n(t)\right]^T \tag{7.4}$$

$$\mathbf{u}(t) = \left[\mathbf{u}_1(t) \quad \mathbf{u}_2(t) \quad \ldots \quad \mathbf{u}_n(t)\right]^T \tag{7.5}$$

where $\mathbf{f}$ and $\mathbf{g}$ are *n*-and *m*- dimensional, vector-valued functions of the state vector $\mathbf{x}(t)$ and the input vector $\mathbf{u}(t)$, and $\mathbf{y}(t)$ is an m-dimensional output vector.

Consider the steady-state operating condition, ($\bar{\mathbf{x}}$, $\bar{\mathbf{u}}$) and let the process be perturbed by small deviations $\mathbf{x}^*(t)$ and $\mathbf{u}^*(t)$ around the steady-state such that:

$$\begin{aligned} \mathbf{x}(t) &= \bar{\mathbf{x}} + \mathbf{x}^*(t) \\ \mathbf{u}(t) &= \bar{\mathbf{u}} + \mathbf{u}^*(t) \end{aligned} \tag{7.6}$$

We linearize Equation (7.1) to obtain the following equation for the deviation variables:

$$\mathbf{x}^*(t) = A\mathbf{x}^*(t) + B\mathbf{u}^*(t) \tag{7.7}$$

where

$$A = \left[\begin{array}{ccc} \dfrac{\partial f_1}{\partial x_1} & \cdots & \dfrac{\partial f_1}{\partial x_n} \\ \cdot & \cdot & \cdot \\ \cdot & \cdot & \cdot \\ \dfrac{\partial f_n}{\partial x_1} & \cdots & \dfrac{\partial f_n}{\partial x_n} \end{array}\right]_{\substack{x=\bar{x} \\ u=\bar{u}}} \tag{7.8}$$

and

$$B = \left[\begin{array}{ccc} \frac{\partial f_1}{\partial u_1} & \cdots & \frac{\partial f_1}{\partial u_r} \\ \cdot & \cdot & \cdot \\ \cdot & \cdot & \cdot \\ \frac{\partial f_n}{\partial u_1} & \cdots & \frac{\partial f_n}{\partial u_r} \end{array}\right]_{\substack{x=\bar{x} \\ u=\bar{u}}} \tag{7.9}$$

Similarly, we linearize Equation (7.2) to give the following deviation equation for the output vector:

$$\mathbf{y}^*(t) = C\mathbf{x}^*(t) + D\mathbf{u}^*(t) \tag{7.10}$$

where

$$C = \left[\begin{array}{ccc} \frac{\partial g_1}{\partial x_1} & \cdots & \frac{\partial g_1}{\partial x_n} \\ \cdot & \cdot & \cdot \\ \cdot & \cdot & \cdot \\ \frac{\partial g_m}{\partial x_1} & \cdots & \frac{\partial g_m}{\partial x_n} \end{array}\right]_{\substack{x=\bar{x} \\ u=\bar{u}}} \tag{7.11}$$

and

$$D = \left[\begin{array}{ccc} \frac{\partial g_1}{\partial u_1} & \cdots & \frac{\partial g_1}{\partial u_r} \\ \cdot & \cdot & \cdot \\ \cdot & \cdot & \cdot \\ \frac{\partial g_m}{\partial u_1} & \cdots & \frac{\partial g_m}{\partial u_r} \end{array}\right]_{\substack{x=\bar{x} \\ u=\bar{u}}} \tag{7.12}$$

Equations (7.7) to (7.12) are the linearized state-space equations for the deviation variables ($\mathbf{x}^*$, $\mathbf{u}^*$) around the nominal operating conditions, ($\bar{\mathbf{x}}$, $\bar{\mathbf{u}}$). The linear model

and the related controller are valid in the close neighborhood of the nominal operating point ($\bar{\mathbf{x}}$, $\bar{\mathbf{u}}$) .

Taking the Laplace transform on both sides of Equations (7.7) and (7.10), we write

$$\mathrm{SI}\,\mathbf{x}^*(s) - \mathbf{x}(0) \;=\; A\mathbf{x}^*(s) + B\mathbf{u}^*(s) \tag{7.13}$$

$$\mathbf{y}^*(s) \;=\; C\mathbf{x}^*(s) + D\mathbf{u}^*(s) \tag{7.14}$$

Rearranging Equation (7.13) and substituting the resulting expression for $\mathbf{x}^*(s)$ into Equation (7.14) gives

$$\mathbf{x}^*(s)\,[\mathrm{SI} - A] \;= \mathbf{x}_0 + B\mathbf{u}^*(s)$$

$$\mathbf{x}^*(s) = \;[\mathrm{SI} - A]^{-1}\;\mathbf{x}_0 \;+\; [\mathrm{SI} - A]^{-1}\;B\mathbf{u}^*(s)$$

$$\mathbf{y}^*(s) = \;C[\mathrm{SI} - A]^{-1}\;\mathbf{x}_0 \;+\; C[\mathrm{SI} - A]^{-1}\;B\mathbf{u}^*(s) \;+\; D\mathbf{u}^*(s)$$

Assuming that the initial state vector $\mathbf{x}_0$ represents the nominal operating conditions, $\mathbf{x}_0 = \mathbf{0}$, we simplify the last equation to give

$$\mathbf{y}^*(s) = \;\left\{C[\mathrm{SI} - A]^{-1}\;B \;+\; D\right\}\mathbf{u}^*(s)$$

Defining a gain matrix,

$$G(s) = C[\mathrm{SI} - A]^{-1} B + D \qquad (7.15)$$

we write the following relationship between the deviation in the input vector $\mathbf{u}^*(s)$ (manipulated variables) and output vector $\mathbf{y}^*(s)$ (controlled variables):

$$\mathbf{y}^*(s) = G(s)\,\mathbf{u}^*(s) \qquad (7.16)$$

For an open-loop, uncontrolled situation, D of Equation (7.12) is a zero matrix. We find the steady-state gain G(0) from Equation (7.15) when s=0

$$G(0) = -CA^{-1} B \qquad (7.17)$$

7.4 Linearized Model of a Commercial MSF Desalination Plant:

In Chapter 5, we developed a SPEEDUP model for a 24-stage, commercial MSF desalination process. We consider linearizing the model around the following nominal operating conditions of Table 7.1:

Table 7.1: Nominal operating conditions for developing the linearized model.

Variable	Set point	Maximum/Minimum
Steam flow-valve position	2.349 T/min	4.698/0
Recycle flow-valve position	238.1 T/min	476.2/0
Reject flow-valve position	160.488 T/min	223.5/0

SPEEDUP software provides a useful tool, called control design interface (CDI), that allows us to develop the matrices A, B, C, and D of the linearized model, i.e., Equations (7.8), (7.9), (7.11) and (7.14), corresponding to given nominal operating conditions.

Applying the tools of CDI gives a linearized model with 104 state variables (4 state variables in each flash stage for a total of 24 stages, plus 8 state variables for the brine heater and controllers). Appendix D gives the state variables of the resulting linear model.

Next, the model of the present MSF desalination plant is set up in a SPEEDUP flowsheet simulator. We linearize the model at operating conditions of top brine temperature of 90.56°C, and recirculating brine flowrate of 238.1 T/min and invoke the control design interface (CDI) of SPEEDUP with the following three input variables (manipulated variables) and three output variables (controlled variables):

(1) Manipulated variables (inputs):

u1 : Steam flow-valve position

u2 : Recycle flow-valve position

u3 : Reject flow-valve position

(2) Controlled variables (outputs):

y1 : Top brine temperature (TBT) of the brine heater

y2 : Recirculating brine flowrate (R)

y3 : Seawater reject flowrate

CDI generates the matrices A, B, C, and D of the state space and compute the steady - state gain matrix G(0). Specifically, we evaluate the deviations from nominal operating conditions following Table 7.2 and using the tool of CDI:

Table 7.2: Operating conditions for the SPEEDUP control-design-interface (CDI) test.

Case no.	Conditions
A step change in the steam flowrate is introduced after 1-minute run on the steady-state conditions.	The step decrease and increase in the steam-valve opening, respectively, cause
a. 20% decrease in the steam-valve opening	1: a decrease in top brine temperature to a value of 78.167 °C
b. 10% increase in the steam-valve opening	2: an increase in top brine temperature to a value of 96.439 °C

Applying Equation (7.17) together with values of state-space matrices A, B, C, and D, we find the following gain matrix for the deviations specified in Table 7.2:

$$G(o)=\begin{bmatrix} 114.18 & -146.70 & -5.43 \\ 0 & 476.2 & 0 \\ 0 & 0 & 223.46 \end{bmatrix}$$

The steady-state gain between an input and an output is obtained by introducing a step change in the input and recording the new steady-state value of the output, and calculated the difference between the final and initial steady-state values of the output divided by the magnitude of the step change.

7.5 Interaction Analysis: Relative Gain Array (RGA)

Bristol (1966) propose a simple and effective approach to analyzing the interactions between manipulated and controlled variables (i.e., input and output variables) of a multivariable process. His approach requires only steady-state information and provides two important items of information:

- a measure of process interaction, called relative gain array (RGA);
- a recommendation concerning the most effective pairing of controlled and manipulated variables.

The relative gain array (RGA) is a square matrix (for equal number of manipulated and controlled variables) whose columns refer to manipulated variables and the rows to controlled variables:

$$\text{RGA or } \Lambda \quad = \quad \begin{bmatrix} \lambda_{11} & \lambda_{12} & \cdots & \lambda_{1n} \\ \lambda_{21} & \lambda_{22} & \cdots & \lambda_{2n} \\ \cdot & \cdot & \cdot & \cdot \\ \cdot & \cdot & \cdot & \cdot \\ \cdot & \cdot & \cdot & \cdot \\ \lambda_{n1} & \lambda_{n2} & \cdots & \lambda_{nn} \end{bmatrix} \tag{7.18}$$

The RGA has two important properties:

- It is normalized since the sum of the elements in each row or column is one.

$$\sum_{i=1}^{n} \lambda_{ij} = 1 \quad \text{, for j = 1,2,…,n}$$

- The relative gains are dimensionless and are independent of the choice of units or scaling of variables.

A relative gain λ_{ij} close to or equal to one indicates that closing or opening other loops does not affect on the control loop involving a manipulated variable u_j and an output variable y_i which, in this case, is preferred pairing. A relative gain λ_{ij} close to zero indicates that the manipulated variables u_j only has a negligible effect on output variable y_i, implying that such a pairing cannot achieve good control. For $0 < \lambda_{ij} < 1$, the open-loop gain is lower than the closed-loop gain, suggesting, a definite interaction between the manipulated variable u_j and the output variable y_i (maximal interaction at $\lambda_{ij} = 0.5$). The same holds for λ_{ij} values greater than one. Pairing with negative λ_{ij} values should be avoided, since they imply that the open-loop effect of a manipulated variable on an output is reversed if other loops are operated. Thus, in case of failure of one of the loops, a control scheme involving negative relative gains could become unstable. If we arrange the input and output variables in the order of their pairing, we should attempt to achieve a relative gain array as close to an identity matrix as possible.

Consider again the three inputs and three outputs and by giving the deviations specifies in Table 7.2. The steady-state gain matrix $G_{TBT,R}(0) = G_{90.56,238.1}(0)$ for 3×3 system is:

$$\begin{bmatrix} y_1 \\ y_2 \\ y_3 \end{bmatrix} = \begin{bmatrix} 114.18 & -146.70 & -5.43 \\ 0 & 476.2 & 0 \\ 0 & 0 & 223.46 \end{bmatrix} \begin{bmatrix} u_1 \\ u_2 \\ u_3 \end{bmatrix}$$

We calculate RGA by the following expression

$$\lambda_{ij} = \frac{(\partial y_i / \partial u_j)_{u_{1 \neq j}}}{(\partial y_i / \partial u_j)_{y_{1 \neq i}}} = g_{ij}[G^{-1}]_{ij} \tag{7.19}$$

In all the cases here

$$\Lambda = \begin{bmatrix} 1 & 0 & 0 \\ 0 & 1 & 0 \\ 0 & 0 & 1 \end{bmatrix}$$

clearly suggesting the pairings of ($u_1 \rightarrow y_1$), ($u_2 \rightarrow y_2$) and ($u_3 \rightarrow y_3$). Thus, we can tune these control loops independently using the conventional single-loop tuning methods.

Since the RGA analysis in all cases here indicates a very clear pairing strategy, we do not need to carry out further stability tests.

7.6 Application of the Present Model

We first use the linearized model matrices A, B, C, and D to compute the steady-state gain matrix G(0), which gives the basis to calculate the RGA. The step response of the original plant model is obtained by using the route STEP of MATLAB at a different time until the response approaches a steady state.

Figure 7.1 shows the step response of the TBT (°C) control loop versus time (minutes). Since TBT is critical for the plant performance, its control is important in MSF desalination processes. This is controlled by manipulating the steam flow into the brine heater.

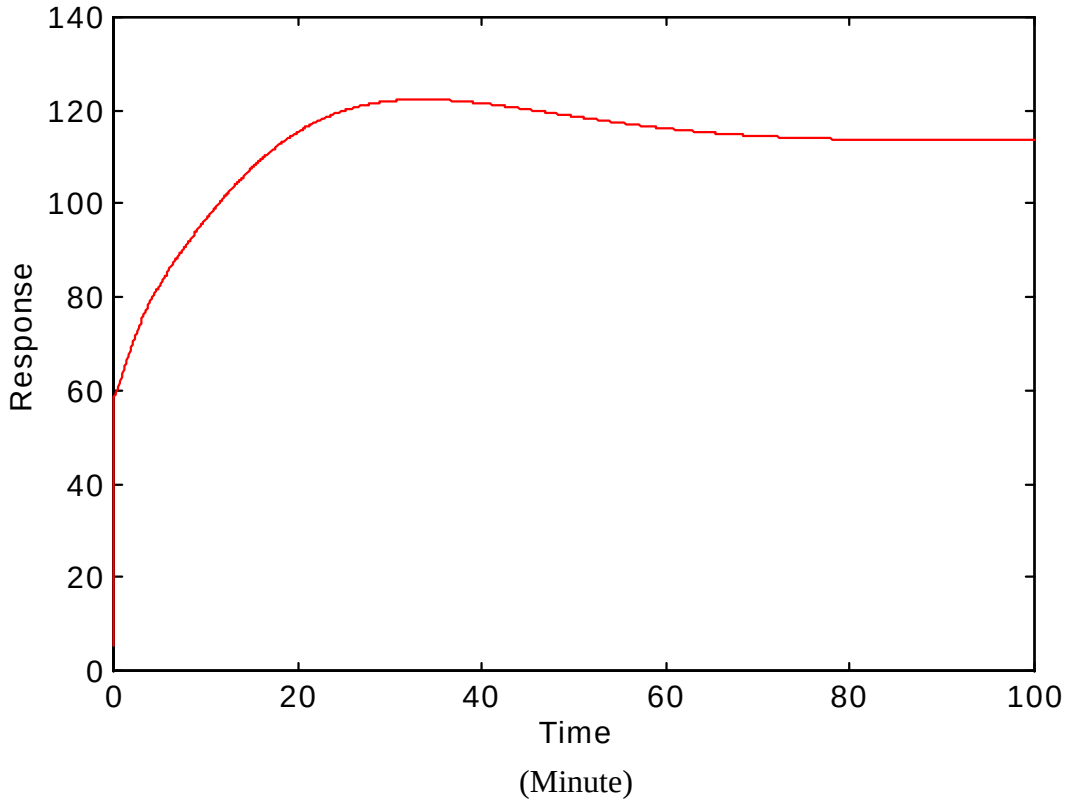

Figure 7.1 Step response of the TBT (°C) control loop.

7.7 Conclusion

Relative gain array (RGA) interaction analysis is a simple and effective approach to analyzing the interactions between manipulated and controlled variables of a commercial MSF desalination plant. The selection of the controlled and manipulated variables plays an important role in control-system design.

7.8 References

Al-Gobaisi, M., A., Hassan, G., Rao, A., Sattar, A., Woldai, and R., Borsani, "Toward Improved Automation for Desalination Processes, Part I: Advanced Control", *Desalination*, **97**, 469 (1994).

Bristol, E.M., "On a new measure of interaction for multivariable process control", *IEEE Trans. Automatic Control*, **11**, 133 (1966).

Luyben, W.L., *Process Modeling , Simulation and Control for Chemical Engineers*, McGraw-Hill Publishing Company, New York, N. Y. (1990).

Ogunnaike, B.A., and W.H., Ray, *Process Dynamics, Modeling and Control*, Oxford University Press, New York, N. Y. (1994).

Seborg, D.E., T.F., Edgar, and D.A., Mellichamp, *Process Dynamic and Control*, John Wily and Sons, New York, N. Y. (1989).

Woldai, A., D.M., Al-Gobaisi, R.W., Dunn, A., Kurdali, and G.P., Rao, " An Adaptive Scheme with an Optimally Tuned PID Controller for A Large MSF Desalination Plant", *Control Eng. Practice*, **4**, 721 (1996).

CHAPTER 8

EVALUATION OF A COMMERCIAL SOFTWARE FOR COMBINED STEADY-STATE AND DYNAMIC SIMULATIONS OF A COMMERCIAL MSF DESALINATION PLANT.

This chapter describes our experience in applying a commercial software, called DynaPLUS, for combined steady-state and dynamic simulations of a commercial MSF desalination plant.

8.1 Description of DynaPLUS

DynaPLUS is a layered product that provides close integration between ASPEN PLUS and SPEEDUP. DynaPLUS enables the user to generate complete SPEEDUP dynamic simulations from new or existing ASPEN PLUS steady-state simulations. In addition, DynaPLUS Control Manager provides a graphical environment that enables the user to perform the following tasks in DynaPLUS-generated SPEEDUP input files:

- Easily add and remove control elements
- Conveniently change control element properties
- Select input and output variables from selected lists
- Easily configure cascade control loops
- Automatically update SPEEDUP input files
- Import control structures from other SPEEDUP input files
- Add new types of control elements.

8.2 DynaPLUS MSF Dynamic Model

To produce a DynaPLUS dynamic simulation, we must start with an existing ASPEN PLUS steady-state simulation. However, some models require additional information for dynamic simulations.

We use the ASPEN PLUS MSF model generated for the AZ-ZOUR South desalination plant in Chapter 5 to accomplish this work. Model FLASH2 used in the MSF ASPEN PLUS steady-state model requires additional data for dynamic simulation as described below.

We apply the FLASH2 Dynamic Form in ASPEN PLUS to add the specifications for dynamic simulation. We can use FLASH2 to represent either an instantaneous flash, with no dynamic effects, or vertical or horizontal flash vessels. For vertical or horizontal vessels, we must specify vessel geometry and liquid fraction, and choose a method of calculating the heat transfer within the vessel. We assume all vessels to be cylindrical. We can specify the length, diameter, orientation, and head type. Figure 8.1 shows the different orientations and head types of flash vessels.

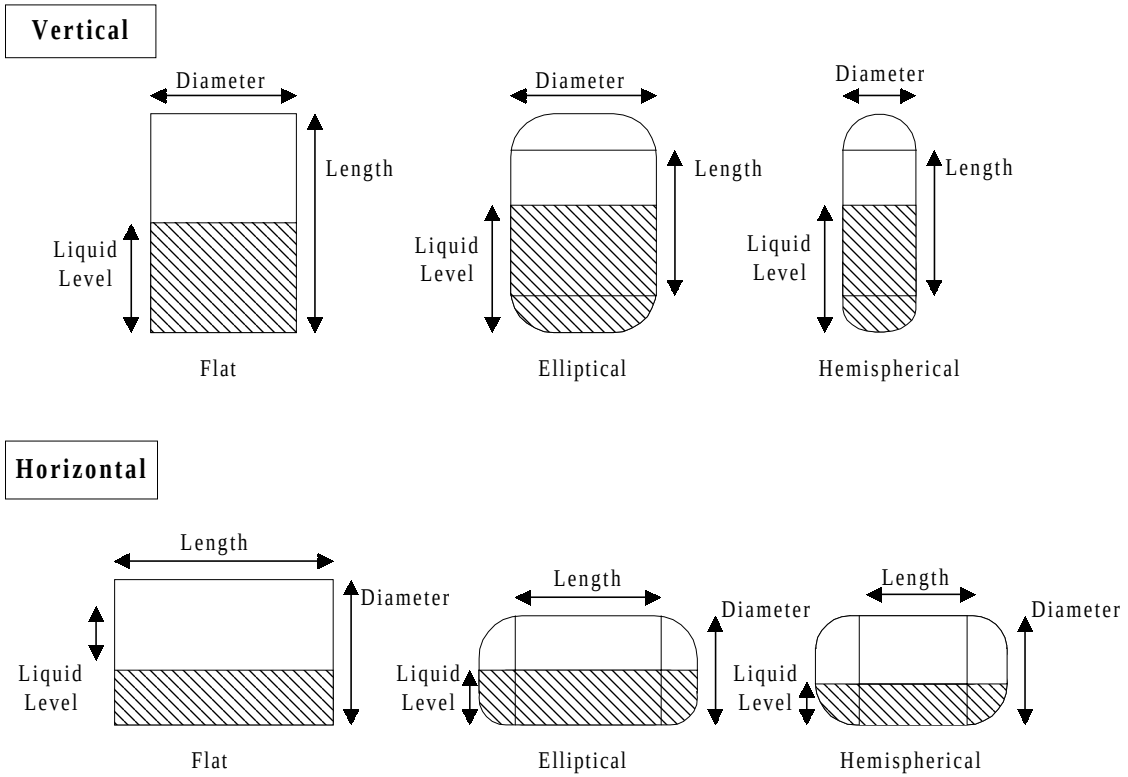

Figure 8.1: Vessel geometries in ASPEN PLUS dynamic flash model.

None of the vessel orientations in Figure 8.1 represents the actual flash stage in the MSF desalination plant. However, we use the flat-head vertical vessel as a test. Table 8.1 illustrates the ASPEN PLUS FLASH2 dynamic specifications.

Table 8.1: ASPEN PLUS FLASH2 dynamic specifications.

Variable	**Value**
Length	8.34 (m)
Diameter	3.98 (m)
Heat transfer calculating method	CONST-DUTY
Liquid fraction of stage number:	
1	0.9971
2	0.9963
3	0.9960
4	0.9959
5	0.9960
6	0.9961
7	0.9962
8	0.9963
9	0.9963
10	0.9964
11	0.9964
12	0.9965
13	0.9965
14	0.9966
15	0.9966
16	0.9967
17	0.9967
18	0.9968
19	0.9969
20	0.9969
21	0.9970
22	0.9975
23	0.9971
24	0.9968

CONST-DUTY means a specified heat duty. Initially, the heat duty is equal to the steady-state value, but we can manipulate it during the simulation either manually or using a controller.

The following steps generate the SPEEDUP dynamic model from a steady-state ASPEN PLUS model within the DynaPLUS environment:

1. Start with the ASPEN PLUS steady-state simulation.
2. Enter the dynamic data required for FLASH2 model, as discussed in the previous section.
3. Export the dynamic simulation from the file menu in ASPEN PLUS. Select SPEEDUP file (.SPE) and Input Summary (.INP). Dynamic simulation requires both files.
4. Run the dynamic simulation when the linking is complete. SPEEDUP starts the Run-Time Environment, which enables the user to monitor the progress of the dynamic simulation, introduce disturbances, and plot selected input variables.

8.3 Results and Discussions

On completion of translation, SPEEDUP performs a number of tasks to analyze, structure, and compile the input description ready for execution. A number of messages are executed after translation describing the compiling procedures, block decomposition, linking, etc. Table 8.2 compares the block decomposition, system size, and number of variables/equations of the SPEEDUP model generated by DynaPLUS with the SPEEDUP model developed in Chapter 5.

Table 8.2: Run-Time information for the SPEEDUP model generated by DynaPLUS and SPEEDUP developed in Chapter 5.

Run-Time information	SPEEDUP model generated by DynaPLUS	SPEEDUP model developed from equations (Chapter 5)
Block decomposition:		
System size (variables/equations)	8207	975
Number of blocks	4412	230
Maximum block size	3187	738
Total system size (knowns + unknowns)	9474	1362
Number of nonlinear blocks	51	11
Number of variables SET in operation	1046	283
Number of variables PRESET in operation	3318	1079

SPEEDUP performs the block-decomposition analysis for steady-state simulations. This analysis performs checks for structural singularities and the ability to reduce the main solution matrix into sub-matrices for quicker solution. The system size is the number of equations (or unknown variables), the number of blocks is the number of sub-matrices that SPEEDUP has broken the problem down into, and the maximum block size is the number of equations(or unknown variables) in the largest sub-matrix. The total system size is the number of declared variables in the entire problem. The number of variables are set and preset variables in the OPERATION section in SPEEDUP.

Table 8.2 shows that the SPEEDUP model generated by DynaPLUS is a very large model when compared with that developed from mass and energy balance equations in Chapter

5. DynaPLUS generates many files during the exporting process (step 3), taking a lot of memory space in the computer.

Furthermore, during the SPEEDUP exporting step from ASPEN PLUS (step 3), the SPEEDUP model executes an error message which indicates flooding in the vessels. This proves that the flat-head vertical vessel tested is the wrong vessel geometry for dynamic MSF flashing stage.

8.4 Conclusion

DynaPLUS is not applicable for use in modeling MSF desalination plants. However, DynaPLUS may be recommended to be used for processes with more simple models in ASPEN PLUS. This will help in converting a steady-state model into a computationally manageable dynamic model. DynaPLUS Control Manager has capabilities which are worth studying.

8.5 Reference

Aspen Technology, *DynaPLUS Installation and User Manual*, Aspen Technology, Cambridge, MA (1997).

CHAPTER 9

SUGGESTED DIRECTIONS FOR FURTHER WORK

The dependency on desalination plants to produce fresh water from the sea is increasing throughout the world. This has created considerable interest in investigating ways to improve the design and optimize the operation of desalination plants. Desalination processes control is an area wherein the application of advanced techniques will help develop much needed world water resources.

There are several aspects of desalination plants in general and MSF in particular that need further investigations.

Neural Networks

Artificial intelligence techniques (i.e., expert systems, neural networks, and fuzzy-logic systems) could be involved in the design, operation, control, and performance optimization of desalination plants. The following application of artificial intelligent are worth studying:

- Plant classification: fault detection, alarm processing and feature categorization
- Load forecasting.
- An intelligent system for supervision and optimization of a control system: data monitoring, selection of objective function for optimization, and set-point optimization.

- The use of expert system or neural networks in tuning of feedback control loop of top brine temperature in combination with an adaptive controller.
- Study and investigate the various forms of corrosion damage suffered by different components in the desalination plants.
- Advanced control system for the reverse osmosis plant.
- Membrane fouling prediction and prevention in a reverse osmosis plant.

Modeling, Simulation and Optimization of MSF Desalination Plants

Any results which are based on modeling rely heavily on the quality of the model itself. The phenomenological model of the MSF desalination process described in Chapter 5 is sufficiently representative when compared with the design data of the plant in our study. However, further work is needed to improve the performance of the dynamic simulation. Several supporting equations are needed to make the model more representative:

- Fouling, vapor and heat losses, and venting phenomena from the individual stages plus brine heater have to be incorporated in the model.
- Evaporation from the distillate tray.
- Maintaining proper hydrodynamics in a flash stage which can be achieved by modification in the interstage orifice and internal wires.
- Proper evaluation of the effect of non-condensable gases on the rate of heat transfer.
- Evaluation of the total temperature losses due to boiling-point elevation, non-equilibration, and pressure drop across the demisters.
- Heat-transfer coefficient.
- Start-up, shut-down, and load change of the plant.

Fitting of simulation facilities into the framework of the overall system for the purpose of process studies and operator training is necessary.

Since MSF plants are usually coupled with a power station, optimization of the entire system could be preferred. In addition, maintenance management optimization is also worth studying.

In conclusion, it should be recognized that the efforts of single individuals can hardly suffice to tackle the large and complex modeling problem with several issues of concern. Coherent and well-coordinated team work is the only approach to the solution of the several problems in MSF desalination process control. The nature of the problem is interdisciplinary. The MSF desalination process, which supports life in many parts of the world, deserves much research attention and I hope that it will receive its due in the future. It is also hoped that this work will contribute to motivating research and application of artificial intelligence to desalination plant operation.

APPENDIX A

DYNAMIC MODEL OF A MULTISTAGE FLASH (MSF) DESALINATION PROCESS

The MSF process models equations consist of mass and energy balance equations for all sections in the MSF plant together with the supplementary correlations for heat transfer and physical properties. Each process stream has four attributes defining the stream, namely, flowrate, temperature, concentration, and enthalpy. Table A.1 lists the nomenclatures used throughout the MSF plant mathematical modeling.

A. Brine Heater

The model equations consist of mass and energy balances, the latter including a dynamic change of temperature of brine inside the heat-transfer tubes.

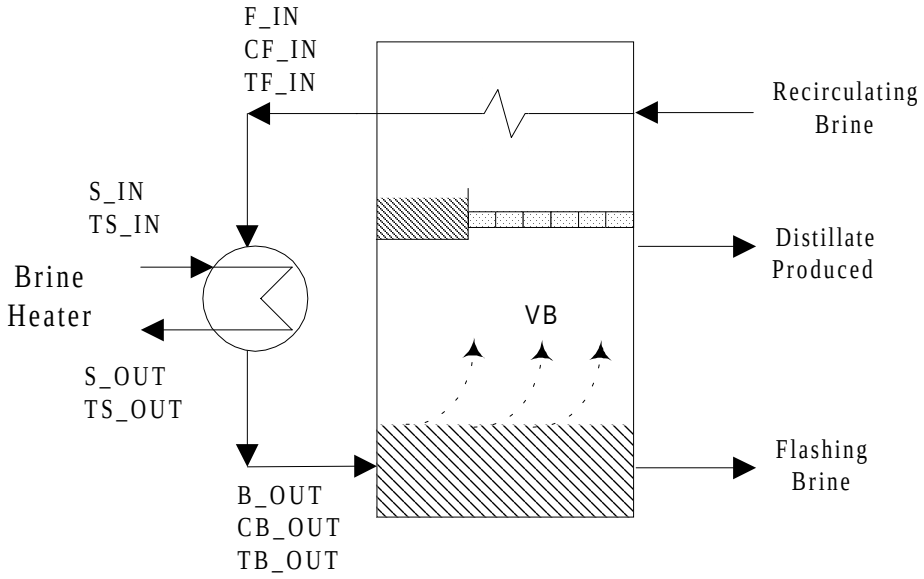

Figure A.1: Brine heater section.

Mass and salt balances on tube side:

$$B\_OUT = F\_IN \quad (A.1)$$

$$CB\_OUT = CF\_IN \quad (A.2)$$

Mass balance on shell side:

$$S\_IN = S\_OUT \quad (A.3)$$

$$TS\_IN = TS\_OUT \tag{A.4}$$

Energy balance:

$$F\_IN * (HB\_OUT - HF\_IN) = Q - \left(MWB\_OUT * CPB\_OUT * \frac{dTB\_OUT}{dt}\right) \tag{A.5}$$

where

$$Q = S\_IN * (HS\_IN - HS\_OUT) \tag{A.6}$$

Tube holdup:

$$MW = \rho B * VT * NT \tag{A.7}$$

$$VT = AT * LT \tag{A.8}$$

Thermodynamic Properties:

HS_OUT = f (TS_OUT)

HS_IN = f (TS_IN)

HB_OUT = f (TB_OUT,CB_OUT)

HF_IN = f (TF_IN,CF_IN)

CPB_OUT = f (TB_OUT, CB_OUT)

ρB = f (TB_OUT, CB_OUT)

B. First Flash

The descriptive equations for the single stage are developed from fundamental mass and energy balances on the four divisions of the stage. The model equations consist of the following:

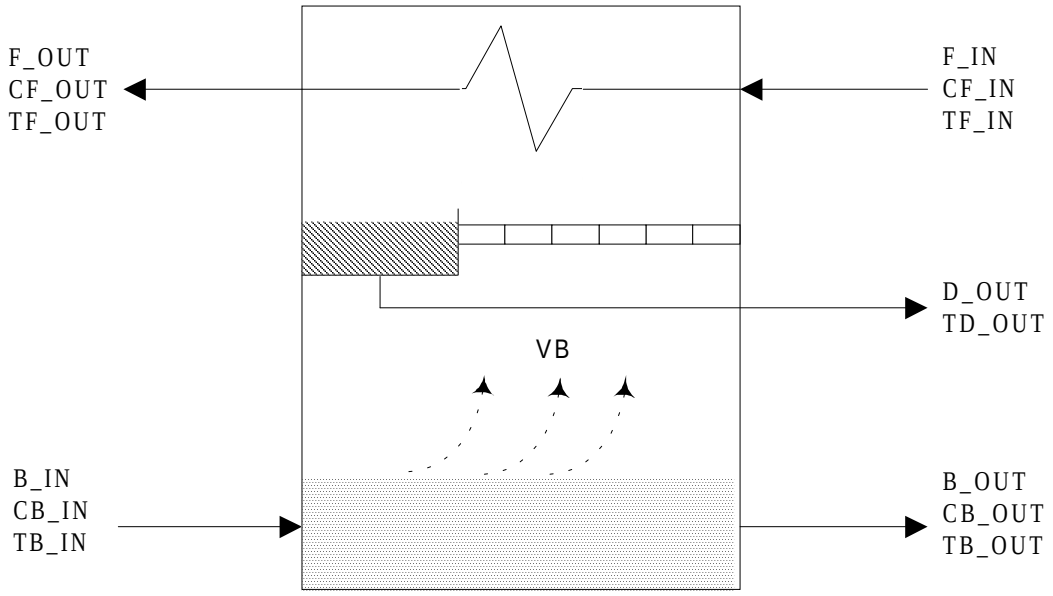

Figure A.2: First flash chamber.

1. Flash Chamber

Mass and salt balances:

$$\frac{dM_1}{dt} = (B\_IN \text{ - } B\_OUT \text{ - } VB) \qquad (A.9)$$

Salt balance:

$$\frac{d(M * CB\_OUT)}{dt} = (B\_IN * CB\_IN - B\_OUT * CB\_OUT) \quad \text{(A.10)}$$

Enthalpy Balance:

$$\frac{d(M * HB\_OUT)}{dt} = (B\_IN * HB\_IN - B\_OUT * HB\_OUT - VB * HVB) \quad \text{(A.11)}$$

$$M = rB * AF * LB / 1000 \quad \text{(A.12)}$$

Pressure balance for the brine:

$$PB\_IN = PB\_OUT = PB_{vap} \quad \text{(A.13)}$$

2. Product (Distillate) Tray

$$D\_OUT = VB \quad \text{(A.14)}$$

$$TD\_OUT + T_{Loss} = TB\_OUT \quad \text{(A.15)}$$

3. Tube Bundle

Mass balance:

$$F\_IN = F\_OUT \quad \text{(A.16)}$$

Salt balance:

$$CF\_IN = CF\_OUT \tag{A.17}$$

Enthalpy balance:

Recirculating brine,

$$1000 * F\_IN * (HF\_IN - HF\_IN) = \left(MW * CPF * \frac{dTF\_OUT}{dt} \right) - U_o * AH * (TD\_OUT - TF_{Ave}) \tag{A.18}$$

Vapor and distillate,

$$1000 * VB * (HVB - HD\_OUT) = U_o * AH * (TD\_OUT - TF_{Ave}) \tag{A.19}$$

$$TF_{Ave} = \frac{TF\_IN + TF\_OUT}{2} \tag{A.20}$$

Tube Holdup:

$$MW = \rho F * VT * NT \tag{A.21}$$

$$VT = AT * LT \tag{A.22}$$

Thermodynamic Properties:

$$HD\_OUT = f(TD\_OUT)$$

HVB = f (TB_OUT)

HF_OUT = f (TF_OUT, CF_OUT)

HB_OUT = f (TB_OUT, CB_OUT)

CPF = f (TF_IN, CF_IN)

ρB = f (TB_OUT, CB_OUT)

ρF = f (TF_OUT, CF_OUT)

PB_{vap} = f (TB_OUT, CB_OUT)

C. Flash j (j= 2 to L-1, any stage except the first and last)

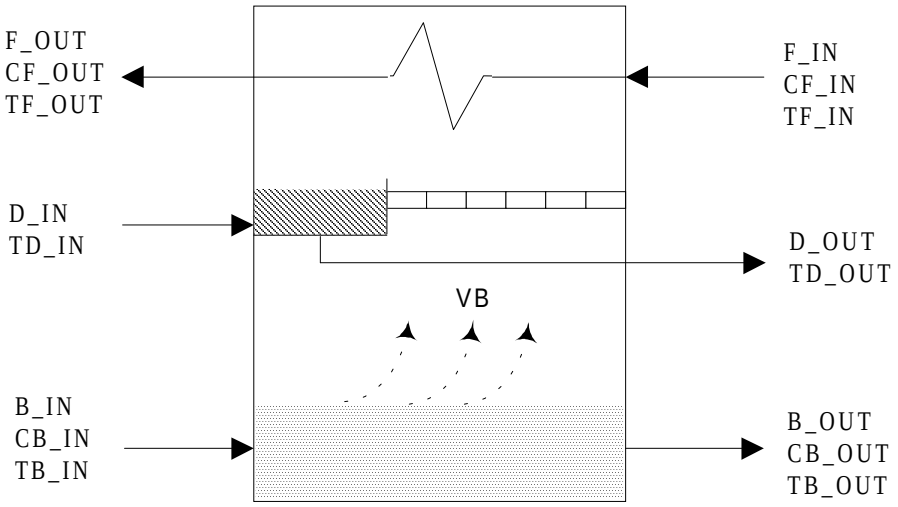

Figure A.3: A general stage in a MSF plant.

1. Flash Chamber

Mass balance:

$$\frac{dM}{dt} = (B\_IN - B\_OUT - VB) \qquad A.23)$$

Salt balance:

$$\frac{d(M * CB\_OUT)}{dt} = (B\_IN * CB\_IN - B\_OUT * CB\_OUT) \qquad (A.24)$$

Enthalpy Balance:

$$\frac{d(M * HB\_OUT)}{dt} = (B\_IN * HB\_IN - B\_OUT * HB\_OUT - VB * HVB) \qquad (A.25)$$

$$M = rB * AF * LB/1000 \qquad (A.26)$$

Pressure balance for the brine:

$$PB\_IN = PB\_OUT = PB_{vap} \qquad (A.27)$$

2. Product (Distillate) Tray

$$D\_OUT = VB + D\_IN \qquad (A.28)$$

$$TD\_OUT + T_{Loss} = TB\_OUT \qquad (A.29)$$

3. Tube Bundle

Mass balance:

$$F\_IN = F\_OUT \tag{A.30}$$

Salt balance:

$$CF\_IN = CF\_OUT \tag{A.31}$$

Enthalpy balance:

Recirculating brine,

$$1000 * F\_IN * \left(HF\_IN - HF\_OUT\right) = \left(MW * CPF * \frac{dTF\_OUT}{dt}\right) - U_o * AH * \left(TD\_OUT - TF_{Ave}\right) \tag{A.32}$$

Vapor and distillate,

$$1000 * VB * \left(HVB - HD\_OUT\right) = Uo * AH * \left(TD\_OUT - TF_{Ave}\right) \tag{A.33}$$

$$TF_{Ave} = \frac{TF\_IN + TF\_OUT}{2} \tag{A.34}$$

Tube Holdup:

$$MW = \rho_F * VT * NT \tag{A.35}$$

$$VT = AT * LT \tag{A.36}$$

Thermodynamic Properties:

HD_OUT = f (TD_OUT)

HVB = f (TB_OUT)

HF_OUT = f (TF_OUT, CF_OUT)

HB_OUT = f (TB_OUT, CB_OUT)

CPF = f (TF_IN, CF_IN)

ρB = f (TB_OUT, CB_OUT)

ρF = f (TF_OUT, CF_OUT)

PB_{vap} = f (TB_OUT, CB_OUT)

D. Last Flash (L)

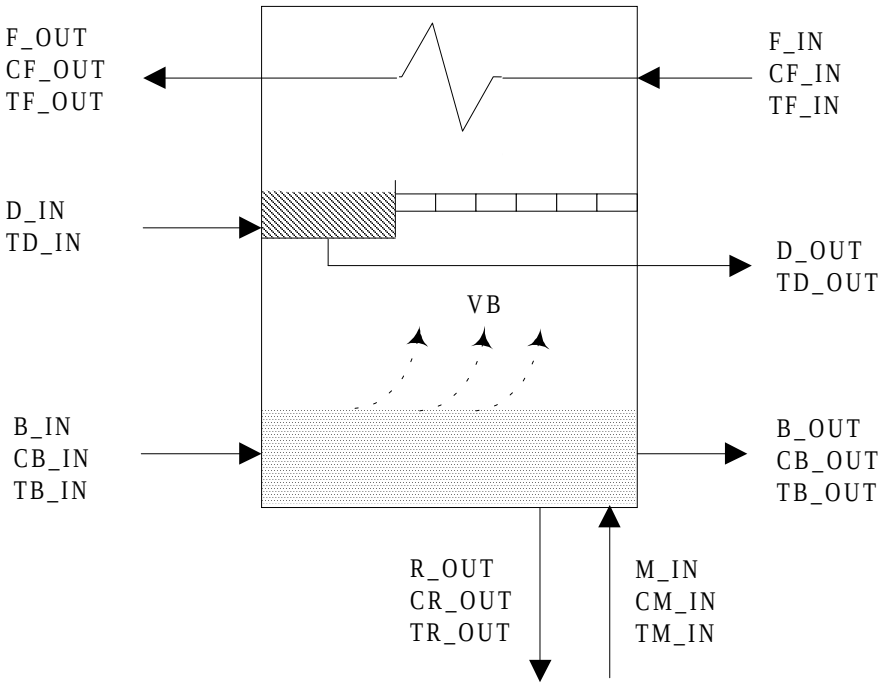

Figure A.4: Last stage in a MSF plant

1. Flash Chamber

Mass balance:

$$\frac{dM}{dt} = (B\_IN - B\_OUT - VB - R\_OUT + M\_IN) \quad \text{(A.37)}$$

Salt balance:

$$\frac{d(M * CB\_OUT)}{dt} = (B\_IN * CB\_IN - (B\_OUT + R\_OUT) * CB\_OUT + M\_IN * CM\_IN) \quad \text{(A.38)}$$

Enthalpy Balance:

$$\frac{d(M * HB\_OUT)}{dt} = (B\_IN * HB\_IN - (B\_OUT + R\_OUT) * HB\_OUT - VB * HVB + M\_IN * HM\_IN) \quad \text{(A.39)}$$

$$M = r_B * AF * LB / 1000 \quad \text{(A.40)}$$

Pressure balance for the brine:

$$PB\_IN = PB_{vap} \quad \text{(A.41)}$$

$$PB\_OUT = PB\_IN + (\rho_B * L * G * 1E-5) \quad \text{(A.42)}$$

2. Product (Distillate) Tray

$$D\_OUT = VB + D\_IN \tag{A.43}$$

$$TD\_OUT + T_{Loss} = TB\_OUT \tag{A.44}$$

3. Tube Bundle

Mass balance:

$$F\_IN = F\_OUT \tag{A.45}$$

Salt balance:

$$CF\_IN = CF\_OUT \tag{A.46}$$

Enthalpy balance:

Recirculating brine,

$$1000 * F\_IN * \left(HF\_IN - HF\_OUT\right) = \left(MW * CPF * \frac{dTF\_OUT}{dt}\right) - U_o * AH * \left(TD\_OUT - TF_{Ave}\right) \tag{A.47}$$

Vapor and distillate,

$$1000 * VB * \left(HVB - HD\_OUT\right) = U_o * AH * \left(TD\_OUT - TF_{Ave}\right) \tag{A.48}$$

$$TF_{Ave} = \frac{TF_{IN} + TF_{OUT}}{2} \quad (A.49)$$

Tube Holdup:

$$MW = \rho F * VT * NT \quad (A.50)$$

$$VT = AT * LT \quad (A.51)$$

Thermodynamic Properties:

HD_OUT = f (TD_OUT)

HVB = f (TB_OUT)

HF_OUT = f (TF_OUT, CF_OUT)

HB_OUT = f (TB_OUT, CB_OUT)

HM_IN = f (TM_IN, CM_IN)

CPF = f (TF_IN, CF_IN)

ρB = f (TB_OUT, CB_OUT)

ρF = f (TF_OUT, CF_OUT)

PB_{vap} = f (TB_OUT, CB_OUT)

E. Splitters and Mixer

Splitter divides the total seawater flow in the tube bundle of reject stages into makeup water and reject water, according to the ratio specified. The model equation consists of mass balance.

1. Summer Operation

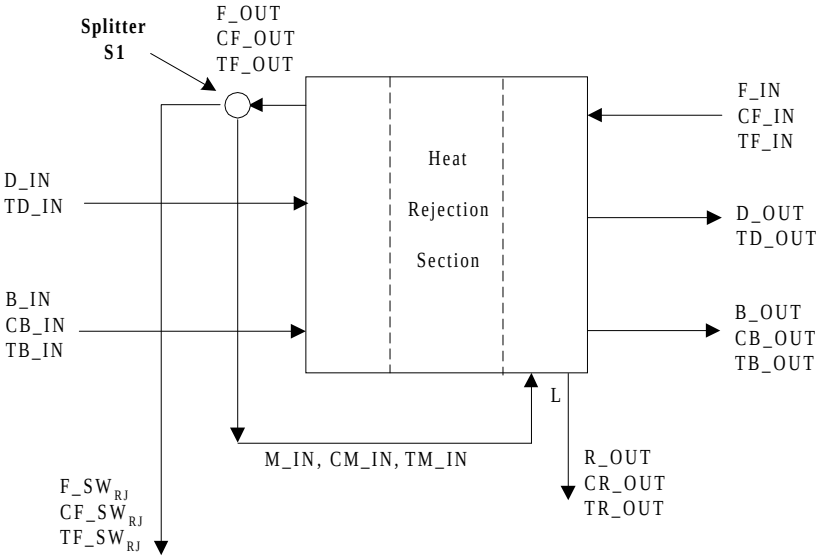

Figure A.5: Splitting point in a MSF desalination plant (summer operation).

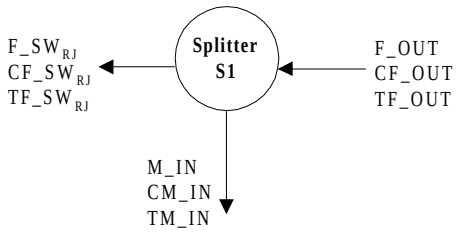

Figure A.6: Splitter

Splitter (S1)

Mass and salt balance:

$$F\_OUT = M\_IN + F\_SW_{RJ} \quad \text{(A.53)}$$

$$F\_SW_{RJ} = Ratio * F\_OUT \quad \text{(A.54)}$$

Concentration equality:

$$CF\_OUT = CM\_IN = CF\_SW_{RJ} \quad \text{(A.55)}$$

Temperature equality:

$$TF\_OUT = TM\_IN = TF\_SW_{RJ} \quad \text{(A.56)}$$

Enthalpy equality:

$$HF\_OUT = HM\_IN = HF\_SW_{RJ} \quad \text{(A.57)}$$

2. Winter Operation

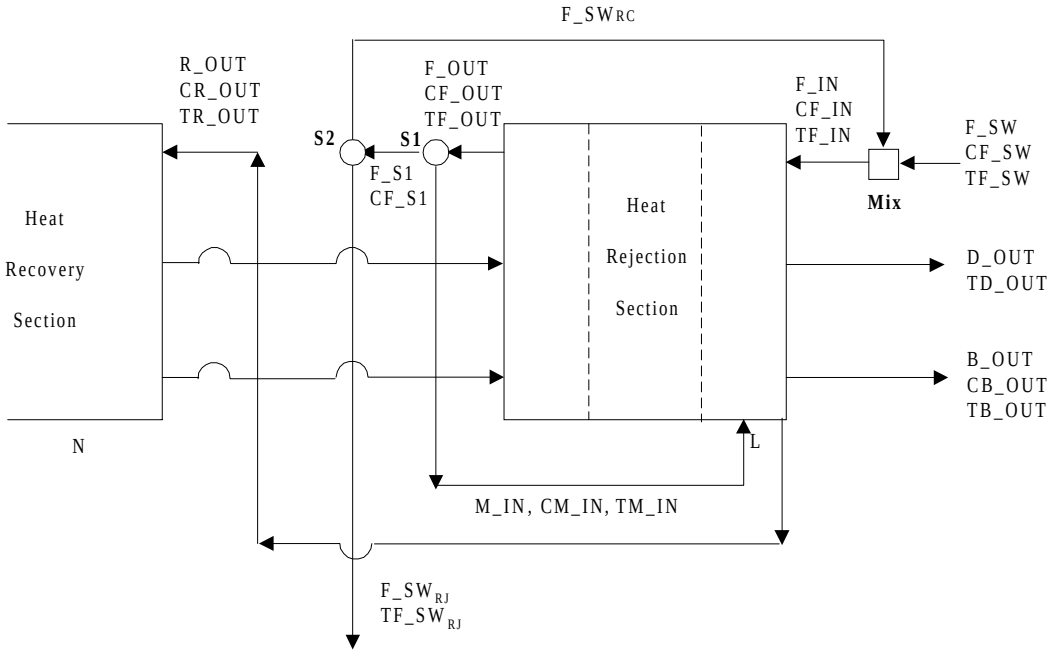

Figure A.7: Splitting and mixing points in a MSF desalination plant (winter operation).

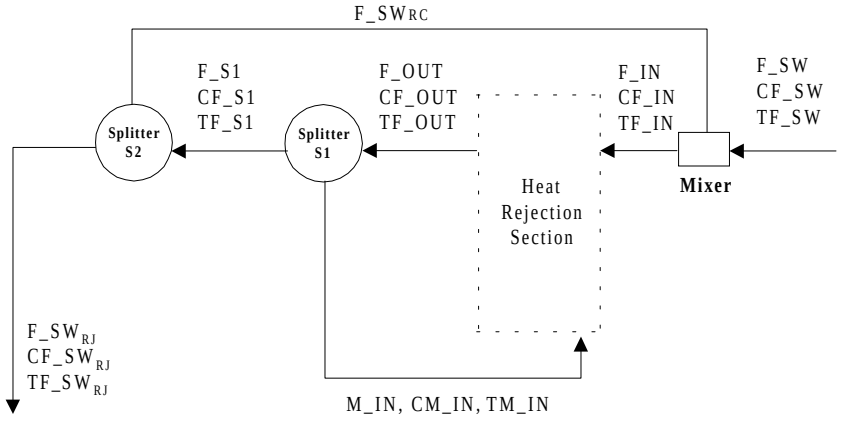

Figure A.8: Splitters and mixer in a MSF desalination plant (winter operation)

Splitter (S_1)

Mass balance:

$$F\_OUT = M\_IN + F\_S1 \quad \text{(A.58)}$$

Concentration equality:

$$CF\_OUT = CM\_IN = CF\_S1 \quad \text{(A.59)}$$

Temperature equality:

$$TF\_OUT = TM\_IN = TF\_S1 \quad \text{(A.60)}$$

Enthalpy equality:

$$HF\_OUT = HM\_IN = HF\_S1 \quad \text{(A.61)}$$

Splitter (S_2)

Mass balance:

$$F\_S1 = F\_SW_{RJ} + F\_SW_{RC} \quad \text{(A.62)}$$

Salt balance:

$$CF\_S1 = CF\_SW_{RJ} = CF\_SW_{RC} \quad \text{(A.63)}$$

Temperature equality:

$$TF\_S1 = TF\_SW_{RJ} = TF\_SW_{RC} \quad \text{(A.64)}$$

Enthalpy balance:

$$HF\_S1 = HF\_SW_{RJ} = HF\_SW_{RC} \quad \text{(A.65)}$$

Mixer (mix)

Mass balance:

$$F\_IN = F\_SW_{RC} + F\_SW \quad \text{(A.66)}$$

Salt balance:

$$F\_IN * CF\_IN = F\_SW_{RC} * CF\_SW_{RC} + F\_SW * CF\_SW \quad \text{(A.67)}$$

Enthalpy balance:

$$F\_IN * HF\_IN = F\_SW_{RC} * HF\_SW_{RC} + F\_SW * HF\_SW \quad \text{(A.68)}$$

Thermodynamic Properties:

HF_SW = f (TF_SW, CF_SW)

HF_IN = f (TF_IN, CF_IN)

HF_OUT = f (TF_OUT, CF_OUT)

F. Orifice

Although orifice is part of the flash chamber but a separate model is written for it for convenience in modeling. An orifice model follows each flash model, but there is no orifice after the last flash. The interconnections are built in the FLOWSHEET section. The model consist of equations for calculating the pressure drop, orifice coefficient and the outlet flow.

$$B\_IN = B\_OUT \tag{A.69}$$

$$TB\_IN = TB\_OUT \tag{A.70}$$

$$CB\_IN = CB\_OUT \tag{A.71}$$

$$HB\_IN = HB\_OUT \tag{A.72}$$

$$DelP = (PB\_IN - PB\_OUT) + 0.098 * (Level - C * OH) \tag{A.73}$$

$$C + 0.058 * X^2 = 0.061 + 0.18 * X + 0.7 * X^3 \tag{A.74}$$

$$G * \rho B / 1000 * OH = X * 100 * (PB\_IN - PB\_OUT) + X * G * \rho B / 1000 * L \tag{A.75}$$

$$1.96E-5 * B\_OUT * 60 = K * \sqrt{(DelP * \rho B / 1000)} * W * OH \tag{A.76}$$

Thermodynamic Properties:

$$\rho B = f(TB\_OUT, CB\_OUT)$$

G. Controllers

Commercial MSF desalination plants typically use a PID controller to control temperature and PI controllers for the rest of variables. One PID controller is used to control the steam temperature entering the brine heater and three PI controllers are used to control the rejected seawater, blow-down flowrate, and recirculating brine flowrate. Model Lag, PI and PID are those from the SPEEDUP library of standard models.

Table A.1: Nomenclatures for MSF model.

Symbol	Description	Unit
AF	Cross sectional area of the flash chamber	m^2
B	Brine flow rate	T/min
C	Orifice contraction coefficient	---
CB	Brine concentration	kg/kg
CF	Recirculating cooling water brine concentration	kg/kg
CF_SW	Seawater concentration entering the mixer	kg/kg
CM	Make-up concentration	kg/kg
CpB	Specific heat of brine	kcal/kg °C
CpD	Specific heat of water	kcal/kg °C
CpF	Specific heat of recirculating cooling water	kcal/kg °C
CpM	Specific heat of make-up seawater	kcal/kg °C
D	Distillate flow rate	T/min
Delp	Pressure drop	bar
F_SW	Seawater recycle flow	T/min
F_SW_{RJ}	Seawater reject flow	T/min
g	Gravitational constant	m/s^2
HB	Enthalpy of brine	kcal/kg
HD	Enthalpy of distillate	kcal/kg
HF	Enthalpy of recirculating cooling water	kcal/kg
HS	Enthalpy of steam entering the brine heater	kcal/kg
HVB	Enthalpy of vapor	kcal/kg
ID_{BH}	Inner diameter of brine heater	in
ID_{RC}	Inner diameter of a stage in the recovery section	in
ID_{RJ}	Inner diameter of a stage in the rejection section	in
K	Orifice discharge coefficient	---
L	Total number of stages	---
LB	Brine level	m
M	Mass of brine	kg
M_IN	Make-up flow rate	T/min
MW	Mass of the brine in brine heater tubes	kg
N	Number of stages in the recovery section	---
NJ	Number of stages in the rejection stages	---
OH	Orifice Height	m

Table A.1: Nomenclatures for MSF model (continued).

Symbol	Description	Unit
PB	Pressure in the flash chamber	Bar
PV_{vap}	Vapor pressure of the brine	Bar
R_OUT	Recirculating cooling water flow rate	T/min
S_IN	Steam flow rate entering the brine heater	T/min
S_OUT	Steam condensate flow rate	T/min
TB	Brine temperature	°C
TD	Distillate temperature	°C
TF	Recirculating cooling water temperature	°C
T_{loss}	Total temperature loss due to BPE, NE, and ΔT	°C
TM	Make-up seawater temperature	°C
TR	Recirculating cooling water temperature	°C
TS	Temperature of the steam entering the brine heater	°C
Tx	Reference temperature	°C
ρB	Brine density	kg/m^3
ρF	Recirculating cooling water density	kg/m^3
Uo	Overall heat transfer coefficient	kcal/min °C m^2
VB	Vapor flow rate	T/min
W	Orifice width	m

Subscripts

B :Brine
BH :Brine heater
IN :Inlet stream
j :jth stage
L :Last stage
Mix :Mixer
M :Make-up
N :Stage N
OUT :Outlet stream
R :Recirculating brine
RC :Recovery
RJ :Reject
S1 :Splitter 1
S2 :Splitter 2
SW :Seawater

APPENDIX B

PROPERTY CORRELATIONS FOR STEAM, WATER, AND BRINE SOLUTIONS

A FORTRAN program is developed to calculate the thermodynamic properties of different liquid and vapor streams from their highly nonlinear governing correlations. The FORTRAN program is linked to SPEEDUP package used in this work.
In the following sections, we present the relevant physical properties correlations.

Brine Density (Ro)

The following equation is valid for the range of 0-26% concentration and 40-300°F. Density of pure water is calculated from the same equation by putting $C_B = 0$.

$$Ro = 62.707172 + 49.364088\, C_B - 0.43955304 \times 10^{-2}\, T^B - 0.032554667\, C_B\, T_B - 0.46076921 \times 10^{-4}\, T_B^2 + 0.63240299E\text{-}4\, C_B\, T_B^2 \qquad (B.1)$$

where

C_B = brine concentration [=] mass fraction [=] g/g

T_B = brine temperature [=] °F

Ro = brine density [=] lb / ft^3

Brine Density (RHO)

$$RHO = \tfrac{1}{2} A_0 + A_1 Y + A_2 (2Y^2 - 1) + A_3 (4Y^3 - 3Y) \qquad (B.2)$$

where

$$S = 1000\ C_B \quad \text{(B.3)}$$

$$Y = (2\ T_B - 200) / 160 \quad \text{(B.4)}$$

$$\sigma = (2\ S_B - 150) / 150 \quad \text{(B.5)}$$

$$A_0 = 2.016110 + 0.115313\ \sigma + 0.000326\ (2\sigma^2 - 1) \quad \text{(B.6)}$$

$$A_1 = -0.0541 + 0.001571\ \sigma - 0.000423\ (2\sigma^2 - 1) \quad \text{(B.7)}$$

$$A_2 = -0.006124 + 0.001740\ \sigma - 9.0 \times 10^{-6}\ (2\sigma^2 - 1) \quad \text{(B.8)}$$

$$A_3 = 0.000346 + 8.7 \times 10^{-5}\ \sigma - 5.3 \times 10^{-5}\ (2\sigma^2 - 1) \quad \text{(B.9)}$$

C_B = brine concentration [=] g / g

S = brine concentration [=] g / kg

T_B = brine temperature [=] °C

RHO = brine density [=] g / cm^3 [=] kg / L

Heat Capacity of Water ($C_{p,w}$)

The following equation is valid for a temperature range of 50-300°F.

$$C_{p,w} = 1.0011833 - 6.1666652 \times 10^{-5}\ T_w + 1.3999989 \times 10^{-7}\ T_w^2 + 1.3333336 \times 10^{-9}\ T_w^3 \quad \text{(B.10)}$$

where

T_w = boiling temperature of water [=] °F

$C_{p,w}$ = specific heat capacity of water [=] BTU / lb °F

Heat Capacity of Brine ($C_{p,B}$)

It is obtained by multiplying the heat capacity of pure water by a factor dependent upon the brine concentration and temperature.

$$C_{p,B} = (1 - S_B (0.011311 - 1.146 \times 10^{-5} T_B)) C_{p,w} \qquad (B.11)$$

where

S_B = brine concentration percentage

T_B = brine temperature [=] °F

$C_{p,w}$ = specific heat capacity of water [=] BTU / lb °F

$C_{p,B}$ = specific heat capacity of brine [=] BTU / lb °F

Specific Enthalpy of Saturated Water (h_W)

The specific enthalpy of saturated water is obtained by integrating the heat-capacity correlation of water between a reference temperature T^* and Tw.

$$h_w = -31.92 + 1.0011833\ Tw - 3.0833326 \times 10^{-5} T_w^2 + 4.666663 \times 10^{-8} T_w^3 + 3.333334 \times 10^{-10} T_w^4 \qquad (B.12)$$

where

T_w = boiling temperature of water [=] °F

h_w = specific enthalpy of water at the boiling temperature [=] BTU / lb

Specific Enthalpy of Brine (h_B)

The specific enthalpy of brine is obtained by integrating the heat capacity of brine equation between a reference temperature T^* and T_B.

$$h_B = \frac{AT_B - 1/2\, BT_B^2 + 1/3\, LT_B^3}{4.1868} \qquad \text{(B.13)}$$

where

$$A = 4.185 - 5.381 \times 10^{-3} S + 6.260 \times 10^{-6} S^2 \qquad \text{(B.14)}$$

$$B = 3.055 \times 10^{-5} + 2.774 \times 10^{-6} S - 4.318 \times 10^{-8} S^2 \qquad \text{(B.15)}$$

$$L = 8.844 \times 10^{-7} + 6.527 \times 10^{-8} S - 4.003 \times 10^{-10} S^2 \qquad \text{(B.16)}$$

S = brine concentration [=] g / kg

T_B = brine temperature [=] °C

h_B = brine enthalpy [=] Kcal / kg

Specific Enthalpy of Saturated Steam (hs)

$$hs = \frac{(2499.15 + 1.955\, Ts - 1.927 \times 10^{-3}\, Ts^2)}{4.1868} \qquad \text{(B.17)}$$

where

Ts = steam temperature [=] °C

hs = enthalpy of steam [=] Kcal / kg

Boiling Point Elevation (BPE)

Water molecules cannot evaporate from salt solution as easily as they can from pure water. Hence, the boiling point of water is raised in proportion to the concentration of dissolved ionic substance. The importance of this phenomenon is that the magnitude of the BPE defines the minimum temperature difference between the evaporation and condensation process at constant pressure and, thereby, the minimum energy of separation for a distillation process. The BPE is a function of the brine concentration and temperature, and it is usually of the order of 1°C or less.

$$BPE = \left[\left(\frac{565.757}{T_B} - 9.81559 + 1.54739 \ln T_B \right) - \left(\frac{337.178}{T_B} - 6.41981 + 0.922753 \ln T_B \right) \cdot \bar{C} + \left(\frac{32.681}{T_B} - 0.55368 + 0.079022 \ln T_B \right) \cdot \bar{C}^2 \right] * \left(\frac{\bar{C}}{\frac{266919.6}{T_B^2} - \frac{379.669}{T_B} + 0.334169} \right) \quad \text{(B.18)}$$

where

$$\bar{C} = \frac{19.819\, C_B}{(1 - C_B)} \quad \text{(B.19)}$$

C_B = brine concentration [=] g / g

T_B = brine temperature [=] K

BPE = boiling point elevation [=] °C

Non-Equilibration Allowance (δ)

When the flashing brine enters a stage through the flashing device, it undergoes a reduction in pressure, that causes flashing. The brine does not have time to cool down or equilibrate fully before going on to the next stage. The degree of equilibrium achieved is usually expressed in terms of the fraction of equilibrium defined as:

$$\beta = \frac{\text{Actual flash drop in stage}}{\text{Flash drop for full equilibrium}} = \frac{\Delta T_B}{\Delta T_B + \delta} \qquad \text{(B.20)}$$

$$\delta = \frac{1-\beta}{\beta} \Delta T_B \qquad \text{(B.21)}$$

β is a function of temperature, flash drop, brine flow, stage length, brine depth, and stage geometry. There is no universal exact formula that successfully predicts β for various stage geometries. Helal (1986) suggests the following equation for the non-equilibration allowance.

$$\delta = (352\, H_{B,j})^{1.1} \; (\Delta T_B)^{-0.25} \, (\omega_j \times 10^{-3})^{0.5} \, (T_{D,j})^{-2.5} \qquad \text{(B.22)}$$

where

$$\Delta T_B = T_{B,j-1} - T_{B,j} \qquad \text{(B.23)}$$

$$\omega_j = \frac{W}{w_j} \qquad \text{(B.24)}$$

The chamber load (ω_j), which is defined as the flow rate of the circulated stream per unit width of the flash chamber, must be monitored in order to control the brine level in the flash chamber and to minimize the non-equilibration losses

$T_{B,j-1}$ = brine temperature in stage j-1 [=] °F

$T_{B,j}$ = brine temperature in stage j [=] °F

$\Delta T_{B,j}$ = flash down in stage j [=] °F

W = total mass circulated in the system [=] lb / hr

w_j = width of stage [=] ft

ω_j = chamber load [=] lb / hr ft

$H_{B,j}$ = brine level in stage j [=] inches

$T_{D,j}$ = saturation temperature in stage j [=] °F

δ = non-equilibration allowance [=] °F

Temperature Loss Across the Demister and Condenser Tubes (Δt)

Reduction of the pressure, due to friction, results as vapor passes though the demisters to remove any entrained salt droplets. This causes a decrease of the saturation temperature to which the vapor must be cooled before condensation takes place. In a similar manner to the loss of pressure incurred in passing through the demisters, the vapor also suffers a pressure loss on passing through the condenser-tube bundle.

The temperature loss accompanying the pressure drop through the demister and condenser tubes together is calculated from the following equation:

$$\Delta t_p = \exp [1.885 - 0.02063\ T_{D,j}] \qquad \text{(B.25)}$$

where

$T_{D,j}$ = saturation temperature in stage j [=] °F

Δt_p = temperature loss [=] °F

Overall Heat Transfer Coefficient (Uo)

The summation of the various thermal resistances in series, between the condensing saturated vapor and cooling-brine stream, gives the overall heat-transfer coefficient. It can be expressed as:

$$Uo = \frac{U}{1 + U \cdot FF} \qquad \text{(B.26)}$$

where

$$z = 0.1024768 \times 10^{-2} - 0.7473939 \times 10^{-5}\, T_{D,j} + 0.999077 \times 10^{-7}\, T_{D,j}^{2} - 0.430046 \times 10^{-9}\, T_{D,j}^{3} + 0.6206744 \times 10^{-12}\, T_{D,j}^{4} \qquad \text{(B.27)}$$

$$y = \frac{(V_j\, ID_j)^{0.2}}{(160 + 1.92\, T_{R,j})\, V_j} \qquad \text{(B.28)}$$

$$U = \frac{1}{z + y} \qquad \text{(B.29)}$$

z = sum of vapor-side resistances: (steam-side condensing, steam-side fouling, tube wall, brine-side fouling)

y = brine-side film resistance

$T_{D,j}$ = saturation temperature in stage j [=] °F

V_j = linear velocity of brine [=] ft / s

ID_j = inner diameter of tube [=] inches

$T_{R,j}$ = temperature of brine at exit from the condenser [=] °F

U = overall heat-transfer coefficient [=] BTU / hr ft^2 °F

FF = fouling factor [=] hr ft^2 °F / BTU

Uo = overall heat-transfer coefficient [=] BTU / hr ft^2 °F (including fouling factor)

Vapor Pressure (P_v)

$$\ln \frac{P_w}{Pc} = \frac{Tc}{T_B} \sum_{i=1}^{8} b_i \left(1 - \frac{T_B}{Tc}\right)^{\frac{(i+1)}{2}} \qquad \text{(B.30)}$$

$$P_v = P_w (1 - 0.537\, C_B) \qquad \text{(B.31)}$$

where

Pc = critical pressure = 220.93 bar

Tc = critical temperature = 647.25 K

b_i = [-7.8889166, 2.5514255, -6.7161690, 33.239495, -105.38479, 174.35319, -148.39348, 48.631602]

i = 1 to 8

P_w = vapor pressure of pure water [=] bar

T_B = temperature of brine [=] K

C_B = brine concentration [=] g / g

P_v = vapor pressure of brine [=] bar

References

Helal, A.M., M.S. Medani, M.A. Soliman, and J.R. Flower, "A TDM Model for MSF Desalination Plants", *Comp. Chem. Eng.* **10**, 327 (1986).

Husain, A., A. Woldai, A. Al-Radif, A. Kesou, R. Borsani, H. Sultan, and P. Deshpandey, "Modeling and Simulation of a Multistage Flash (MSF) Desalination Plant", *Desalination*, **97**, 555 (1994).

APPENDIX C

STREAM TABLES RESULTING FROM ASPEN PLUS SIMULATION OF MSF DESALINATION PLANT UNDER SUMMER OPERATION

Streams	LPSTEAM	STEAM	COND	BIN	B2	B3	B4	B5	B6
From		STVALVE	SBH	BBH	F1	F2	F3	F4	F5
To	STVALVE	SBH		F1	F2	F3	F4	F5	F6
Phase	VAPOR	VAPOR	LIQUID	LIQUID	LIQUID	LIQUID	LIQUID	LIQUID	LIQUID
Temperature C	102.0	101.0	100.0	89.1	88.9	86.7	84.4	82.0	79.6
Pressure BAR	1.09	1.05	1.01	0.70	0.66	0.60	0.55	0.50	0.46
Vapor Frac	1.00	1.00	0.00	0.00	0.00	0.00	0.00	0.00	0.00
Mole Flow KMOL/HR	7824	7824	7824	755973	753639	750751	747641	744476	741348
Mass Flow TONNE/HR	141	141	141	14286	14244	14192	14136	14079	14023
Volume Flow CUM/HR	222828	230277	154	14261	14214	14135	14050	13964	13879
Enthalpy KCAL/HR	-4.5E+08	-4.5E+08	-5.2E+08	-5.1E+10	-5.1E+10	-5.1E+10	-5.1E+10	-5.0E+10	-5.0E+10
Mass Flow TONNE/HR									
H2O	141	141	141	13322	13280	13228	13172	13115	13058
NACL	0	0	0	964	964	964	964	964	964
Mole Flow KMOL/HR									
H2O	7824	7824	7824	739475	737141	734253	731144	727979	724850
NACL	0	0	0	16497	16497	16497	16497	16497	16497

Streams	B7	B8	B9	B10	B11	B12	B13	B14	B15
From	F6	F7	F8	F9	F10	F11	F12	F13	F14
To	F7	F8	F9	F10	F11	F12	F13	F14	F15
Phase	LIQUID	LIQUID	LIQUID	LIQUID	LIQUID	LIQUID	LIQUID	LIQUID	LIQUID
Temperature C	77.3	75.0	72.7	70.5	68.3	66.2	64.0	61.9	59.8
Pressure BAR	0.42	0.38	0.34	0.31	0.28	0.26	0.23	0.21	0.19
Vapor Frac	0.00	0.00	0.00	0.00	0.00	0.00	0.00	0.00	0.00
Mole Flow KMOL/HR	738311	735372	732502	729676	726901	724170	721472	718824	716220
Mass Flow TONNE/HR	13968	13915	13863	13812	13762	13713	13664	13617	13570
Volume Flow CUM/HR	13797	13717	13640	13564	13489	13417	13345	13275	13206
Enthalpy KCAL/HR	-5.0E+10	-5.0E+10	-5.0E+10	-4.9E+10	-4.9E+10	-4.9E+10	-4.9E+10	-4.9E+10	-4.9E+10
Mass Flow TONNE/HR									
H2O	13004	12951	12899	12848	12798	12749	12700	12653	12606
NACL	964	964	964	964	964	964	964	964	964
Mole Flow KMOL/HR									
H2O	721814	718875	716005	713179	710404	707672	704975	702327	699723
NACL	16497	16497	16497	16497	16497	16497	16497	16497	16497

Streams	B16	B17	B18	B19	B20	B21	B22	B23	B24
From	F15	F16	F17	F18	F19	F20		F22	F23
To	F16	F17	F18	F19	F20	F21	F22	F23	F24
Phase	LIQUID	LIQUID	LIQUID	LIQUID	LIQUID	LIQUID	LIQUID	LIQUID	LIQUID
Temperature C	57.7	55.6	53.6	51.6	49.7	47.8	45.9	44.4	42.6
Pressure BAR	0.18	0.16	0.14	0.13	0.12	0.11	0.10	0.09	0.08
Vapor Frac	0.00	0.00	0.00	0.00	0.00	0.00	0.00	0.00	0.00
Mole Flow KMOL/HR	713657	711159	708716	706329	704009	701755	699573	697753	695643
Mass Flow TONNE/HR	13524	13479	13435	13392	13350	13309	13270	13237	13199
Volume Flow CUM/HR	13138	13071	13007	12944	12884	12825	12767	12720	12665
Enthalpy KCAL/HR	-4.9E+10	-4.8E+10	-4.8E+10	-4.8E+10	-4.8E+10	-4.8E+10	-4.8E+10	-4.8E+10	-4.8E+10
Mass Flow TONNE/HR									
H2O	12560	12515	12471	12428	12386	12345	12306	12273	12235
NACL	964	964	964	964	964	964	964	964	964
Mole Flow KMOL/HR									
H2O	697159	694661	692219	689832	687512	685257	683076	681255	679146
NACL	16497	16497	16497	16497	16497	16497	16497	16497	16497

Streams	B	BD1	BD	BL	R	MAKEUP	RECB	RECBR	RECBRINE
From	F24	BSPLIT	BLPUMP	BLVALVE	BSPLIT	SWSPLIT	BMIX	REPUMP	REVALVE
To	BSPLIT	BLPUMP	BLVALVE		BMIX	BMIX	REPUMP	REVALVE	
Phase	LIQUID	LIQUID	LIQUID	LIQUID	LIQUID	LIQUID	LIQUID	LIQUID	LIQUID
Temperature C	40.5	40.5	40.5	40.5	40.5	39.7	40.3	40.4	40.4
Pressure BAR	0.07	0.07	1.27	0.07	0.07	2.50	0.07	4.70	4.60
Vapor Frac	0.00	0.00	0.00	0.00	0.00	0.00	0.00	0.00	0.00
Mole Flow KMOL/HR	693306	94663	94663	94663	598643	157330	755973	755973	755973
Mass Flow TONNE/HR	13157	1796	1796	1796	11361	2925	14286	14286	14286
Volume Flow CUM/HR	12604	1721	1721	1721	10883	2863	13743	13743	13743
Enthalpy KCAL/HR	-4.7E+10	-6.5E+09	-6.5E+09	-6.5E+09	-4.1E+10	-1.1E+10	-5.2E+10	-5.2E+10	-5.2E+10
Mass Flow TONNE/HR									
H2O	12193	1665	1665	1665	10528	2794	13322	13322	13322
NACL	964	132	132	132	833	132	964	964	964
Mole Flow KMOL/HR									
H2O	676809	92411	92411	92411	584398	155077	739475	739475	739475
NACL	16497	2253	2253	2253	14245	2253	16497	16497	16497

Streams	R21	R20	R19	R18	R17	R16	R15	R14	R13
From		H3-21	H3-20	H3-19	H3-18	H3-17	H3-16	H3-15	H3-14
To	H3-21	H3-20	H3-19	H3-18	H3-17	H3-16	H3-15	H3-14	H3-13
Phase	LIQUID	LIQUID	LIQUID	LIQUID	LIQUID	LIQUID	LIQUID	LIQUID	LIQUID
Temperature C	40.4	42.2	44.0	45.9	47.8	49.7	51.7	53.7	55.7
Pressure BAR	4.60	4.42	4.23	4.05	3.87	3.68	3.50	3.32	3.13
Vapor Frac	0.00	0.00	0.00	0.00	0.00	0.00	0.00	0.00	0.00
Mole Flow KMOL/HR	755973	755973	755973	755973	755973	755973	755973	755973	755973
Mass Flow TONNE/HR	14286	14286	14286	14286	14286	14286	14286	14286	14286
Volume Flow CUM/HR	13743	13761	13779	13798	13818	13838	13858	13879	13900
Enthalpy KCAL/HR	-5.2E+10	-5.2E+10	-5.2E+10	-5.2E+10	-5.2E+10	-5.2E+10	-5.2E+10	-5.1E+10	-5.1E+10
Mass Flow TONNE/HR									
H2O	13322	13322	13322	13322	13322	13322	13322	13322	13322
NACL	964	964	964	964	964	964	964	964	964
Mole Flow KMOL/HR									
H2O	739475	739475	739475	739475	739475	739475	739475	739475	739475
NACL	16497	16497	16497	16497	16497	16497	16497	16497	16497

Streams	R12	R11	R10	R9	R8	R7	R6	R5	R4
From	H3-13	H3-12	H3-11	H3-10	H3-9	H3-8	H3-7	H3-6	H3-5
To	H3-12	H3-11	H3-10	H3-9	H3-8	H3-7	H3-6	H3-5	H3-4
Phase	LIQUID	LIQUID	LIQUID	LIQUID	LIQUID	LIQUID	LIQUID	LIQUID	LIQUID
Temperature C	57.8	59.9	62.0	64.1	66.3	68.5	70.7	72.9	75.3
Pressure BAR	2.95	2.77	2.58	2.40	2.22	2.03	1.85	1.67	1.48
Vapor Frac	0.00	0.00	0.00	0.00	0.00	0.00	0.00	0.00	0.00
Mole Flow KMOL/HR	755973	755973	755973	755973	755973	755973	755973	755973	755973
Mass Flow TONNE/HR	14286	14286	14286	14286	14286	14286	14286	14286	14286
Volume Flow CUM/HR	13922	13944	13966	13988	14011	14034	14058	14083	14108
Enthalpy KCAL/HR	-5.1E+10	-5.1E+10	-5.1E+10	-5.1E+10	-5.1E+10	-5.1E+10	-5.1E+10	-5.1E+10	-5.1E+10
Mass Flow TONNE/HR									
H2O	13322	13322	13322	13322	13322	13322	13322	13322	13322
NACL	964	964	964	964	964	964	964	964	964
Mole Flow KMOL/HR									
H2O	739475	739475	739475	739475	739475	739475	739475	739475	739475
NACL	16497	16497	16497	16497	16497	16497	16497	16497	16497

Streams	R3	R2	R1	RIN	SWIN	SW23	SW22	SWOUT	SWR
From	H3-4	H3-3	H3-2	H3-1		H3-24	H3-23	H3-22	SWSPLIT
To	H3-3	H3-2	H3-1	BBH	H3-24	H3-23	H3-22	SWSPLIT	REJVALVE
Phase	LIQUID	LIQUID	LIQUID	LIQUID	LIQUID	LIQUID	LIQUID	LIQUID	LIQUID
Temperature C	77.6	79.9	82.0	83.7	32.2	35.0	37.5	39.7	39.7
Pressure BAR	1.30	1.12	0.93	0.75	3.00	2.83	2.67	2.50	2.50
Vapor Frac	0.00	0.00	0.00	0.00	0.00	0.00	0.00	0.00	0.00
Mole Flow KMOL/HR	755973	755973	755973	755973	517869	517869	517869	517869	360539
Mass Flow TONNE/HR	14286	14286	14286	14286	9629	9629	9629	9629	6704
Volume Flow CUM/HR	14133	14158	14182	14200	9368	9389	9408	9425	6562
Enthalpy KCAL/HR	-5.1E+10	-5.1E+10	-5.1E+10	-5.1E+10	-3.5E+10	-3.5E+10	-3.5E+10	-3.5E+10	-2.5E+10
Mass Flow TONNE/HR									
H2O	13322	13322	13322	13322	9196	9196	9196	9196	6402
NACL	964	964	964	964	433	433	433	433	302
Mole Flow KMOL/HR									
H2O	739475	739475	739475	739475	510455	510455	510455	510455	355377
NACL	16497	16497	16497	16497	7414	7414	7414	7414	5162

Streams	SWREJ	V1	V2	V3	V4	V5	V6	V7	V8
From	REJVALVE	F1	F2	F3	F4	F5	F6	F7	F8
To		H1-1	H1-2	H1-3	H1-4	H1-5	H1-6	H1-7	H1-8
Phase	LIQUID	VAPOR	VAPOR	VAPOR	VAPOR	VAPOR	VAPOR	VAPOR	VAPOR
Temperature C	39.7	88.9	86.7	84.4	82.0	79.6	77.3	75.0	72.7
Pressure BAR	0.07	0.66	0.60	0.55	0.50	0.46	0.42	0.38	0.34
Vapor Frac	0.00	1.00	1.00	1.00	1.00	1.00	1.00	1.00	1.00
Mole Flow KMOL/HR	360539	2334	2888	3109	3165	3128	3037	2939	2870
Mass Flow TONNE/HR	6704	42	52	56	57	56	55	53	52
Volume Flow CUM/HR	6562	106345	142407	166718	185459	200619	212606	224953	240513
Enthalpy KCAL/HR	-2.5E+10	-1.3E+08	-1.7E+08	-1.8E+08	-1.8E+08	-1.8E+08	-1.7E+08	-1.7E+08	-1.6E+08
Mass Flow TONNE/HR									
H2O	6402	42	52	56	57	56	55	53	52
NACL	302	0	0	0	0	0	0	0	0
Mole Flow KMOL/HR									
H2O	355377	2334	2888	3109	3165	3128	3037	2939	2870
NACL	5162	0	0	0	0	0	0	0	0

Streams	V9	V10	V11	V12	V13	V14	V15	V16	V17
From	F9	F10	F11	F12	F13	F14	F15	F16	F17
To	H1-9	H1-10	H1-11	H1-12	H1-13	H1-14	H1-15	H1-16	H1-17
Phase	VAPOR	VAPOR	VAPOR	VAPOR	VAPOR	VAPOR	VAPOR	VAPOR	VAPOR
Temperature C	70.5	68.3	66.2	64.0	61.9	59.8	57.7	55.6	53.6
Pressure BAR	0.31	0.28	0.26	0.23	0.21	0.19	0.18	0.16	0.14
Vapor Frac	1.00	1.00	1.00	1.00	1.00	1.00	1.00	1.00	1.00
Mole Flow KMOL/HR	2826	2775	2731	2698	2648	2603	2564	2498	2442
Mass Flow TONNE/HR	51	50	49	49	48	47	46	45	44
Volume Flow CUM/HR	258597	277694	297980	322692	346341	372718	402365	430340	460428
Enthalpy KCAL/HR	-1.6E+08	-1.6E+08	-1.6E+08	-1.5E+08	-1.5E+08	-1.5E+08	-1.5E+08	-1.4E+08	-1.4E+08
Mass Flow TONNE/HR									
H2O	51	50	49	49	48	47	46	45	44
NACL	0	0	0	0	0	0	0	0	0
Mole Flow KMOL/HR									
H2O	2826	2775	2731	2698	2648	2603	2564	2498	2442
NACL	0	0	0	0	0	0	0	0	0

Streams	V18	V19	V20	V21	V22	V23	V24	VP1	VP2
From	F18	F19	F20	F21	F22	F23	F24	H1-1	H1-2
To	H1-18	H1-19	H1-20	H1-21	H1-22	H1-23	H1-24	H2-1	H2-2
Phase	VAPOR	VAPOR	VAPOR	VAPOR	VAPOR	VAPOR	VAPOR	VAPOR	VAPOR
Temperature C	51.6	49.7	47.8	45.9	44.4	42.6	40.5	87.9	85.7
Pressure BAR	0.13	0.12	0.11	0.10	0.09	0.08	0.07	0.65	0.59
Vapor Frac	1.00	1.00	1.00	1.00	1.00	1.00	1.00	1.00	1.00
Mole Flow KMOL/HR	2387	2320	2254	2181	1821	2109	2337	2334	2888
Mass Flow TONNE/HR	43	42	41	39	33	38	42	42	52
Volume Flow CUM/HR	493133	523469	556128	589164	528674	668811	822308	107776	144386
Enthalpy KCAL/HR	-1.4E+08	-1.3E+08	-1.3E+08	-1.3E+08	-1.0E+08	-1.2E+08	-1.3E+08	-1.3E+08	-1.7E+08
Mass Flow TONNE/HR									
H2O	43	42	41	39	33	38	42	42	52
NACL	0	0	0	0	0	0	0	0	0
Mole Flow KMOL/HR									
H2O	2387	2320	2254	2181	1821	2109	2337	2334	2888
NACL	0	0	0	0	0	0	0	0	0

Streams	VP3	VP4	VP5	VP6	VP7	VP8	VP9	VP10	VP11
From	H1-3	H1-4	H1-5	H1-6	H1-7	H1-8	H1-9	H1-10	H1-11
To	H2-3	H2-4	H2-5	H2-6	H2-7	H2-8	H2-9	H2-10	H2-11
Phase	VAPOR	VAPOR	VAPOR	VAPOR	VAPOR	VAPOR	VAPOR	VAPOR	VAPOR
Temperature C	83.4	81.0	78.6	76.3	74.0	71.7	69.5	67.3	65.2
Pressure BAR	0.54	0.49	0.45	0.41	0.37	0.34	0.31	0.28	0.25
Vapor Frac	1.00	1.00	1.00	1.00	1.00	1.00	1.00	1.00	1.00
Mole Flow KMOL/HR	3109	3165	3128	3037	2939	2870	2826	2775	2731
Mass Flow TONNE/HR	56	57	56	55	53	52	51	50	49
Volume Flow CUM/HR	169114	188220	203713	215993	228658	244606	263135	282720	303532
Enthalpy KCAL/HR	-1.8E+08	-1.8E+08	-1.8E+08	-1.7E+08	-1.7E+08	-1.6E+08	-1.6E+08	-1.6E+08	-1.6E+08
Mass Flow TONNE/HR									
H2O	56	57	56	55	53	52	51	50	49
NACL	0	0	0	0	0	0	0	0	0
Mole Flow KMOL/HR									
H2O	3109	3165	3128	3037	2939	2870	2826	2775	2731
NACL	0	0	0	0	0	0	0	0	0

Streams	VP12	VP13	VP14	VP15	VP16	VP17	VP18	VP19	VP20
From	H1-12	H1-13	H1-14	H1-15	H1-16	H1-17	H1-18	H1-19	H1-20
To	H2-12	H2-13	H2-14	H2-15	H2-16	H2-17	H2-18	H2-19	H2-20
Phase	VAPOR	VAPOR	VAPOR	VAPOR	VAPOR	VAPOR	VAPOR	VAPOR	VAPOR
Temperature C	63.0	60.8	58.7	56.5	54.4	52.4	50.3	48.3	46.3
Pressure BAR	0.23	0.21	0.19	0.17	0.15	0.14	0.13	0.11	0.10
Vapor Frac	1.00	1.00	1.00	1.00	1.00	1.00	1.00	1.00	1.00
Mole Flow KMOL/HR	2698	2648	2603	2564	2498	2442	2387	2320	2254
Mass Flow TONNE/HR	49	48	47	46	45	44	43	42	41
Volume Flow CUM/HR	328891	354712	381968	414452	443591	474941	511415	545859	583192
Enthalpy KCAL/HR	-1.5E+08	-1.5E+08	-1.5E+08	-1.5E+08	-1.4E+08	-1.4E+08	-1.4E+08	-1.3E+08	-1.3E+08
Mass Flow TONNE/HR									
H2O	49	48	47	46	45	44	43	42	41
NACL	0	0	0	0	0	0	0	0	0
Mole Flow KMOL/HR									
H2O	2698	2648	2603	2564	2498	2442	2387	2320	2254
NACL	0	0	0	0	0	0	0	0	0

Streams	VP21	VP22	VP23	VP24	D1	D2	D3	D4	D5
From	H1-21	H1-22	H1-23	H1-24	H2-1	H2-2	H2-3	H2-4	H2-5
To	H2-21	H2-22	H2-23	H2-24	DT1	DT1	DT3	DT4	DT5
Phase	VAPOR	VAPOR	VAPOR	VAPOR	LIQUID	LIQUID	LIQUID	LIQUID	LIQUID
Temperature C	44.4	42.8	40.9	38.8	87.7	85.5	83.2	80.8	78.4
Pressure BAR	0.09	0.09	0.08	0.07	0.64	0.59	0.54	0.49	0.44
Vapor Frac	1.00	1.00	1.00	1.00	0.00	0.00	0.00	0.00	0.00
Mole Flow KMOL/HR	2181	1821	2109	2337	2334	2888	3109	3165	3128
Mass Flow TONNE/HR	39	33	38	42	42	52	56	57	56
Volume Flow CUM/HR	618416	558073	710229	874334	45	56	60	61	60
Enthalpy KCAL/HR	-1.3E+08	-1.0E+08	-1.2E+08	-1.3E+08	-1.6E+08	-1.9E+08	-2.1E+08	-2.1E+08	-2.1E+08
Mass Flow TONNE/HR									
H2O	39	33	38	42	42	52	56	57	56
NACL	0	0	0	0	0	0	0	0	0
Mole Flow KMOL/HR									
H2O	2181	1821	2109	2337	2334	2888	3109	3165	3128
NACL	0	0	0	0	0	0	0	0	0

Streams	D6	D7	D8	D9	D10	D11	D12	D13	D14
From	H2-6	H2-7	H2-8	H2-9	H2-10	H2-11	H2-12	H2-13	H2-14
To	DT6	DT7	DT8	DT9	DT10	DT11	DT12	DT13	DT14
Phase	LIQUID	LIQUID	LIQUID	LIQUID	LIQUID	LIQUID	LIQUID	LIQUID	LIQUID
Temperature C	76.1	73.8	71.5	69.3	67.1	65.0	62.8	60.6	58.5
Pressure BAR	0.40	0.37	0.33	0.30	0.28	0.25	0.23	0.21	0.19
Vapor Frac	0.00	0.00	0.00	0.00	0.00	0.00	0.00	0.00	0.00
Mole Flow KMOL/HR	3037	2939	2870	2826	2775	2731	2698	2648	2603
Mass Flow TONNE/HR	55	53	52	51	50	49	49	48	47
Volume Flow CUM/HR	58	56	55	54	53	52	51	50	49
Enthalpy KCAL/HR	-2.0E+08	-2.0E+08	-1.9E+08	-1.9E+08	-1.9E+08	-1.8E+08	-1.8E+08	-1.8E+08	-1.8E+08
Mass Flow TONNE/HR									
H2O	55	53	52	51	50	49	49	48	47
NACL	0	0	0	0	0	0	0	0	0
Mole Flow KMOL/HR									
H2O	3037	2939	2870	2826	2775	2731	2698	2648	2603
NACL	0	0	0	0	0	0	0	0	0

Streams	D15	D16	D17	D18	D19	D20	D21	D22	D23
From	H2-15	H2-16	H2-17	H2-18	H2-19	H2-20	H2-21	H2-22	H2-23
To	DT15	DT16	DT17	DT18	DT19	DT20	DT21	DT22	DT23
Phase	LIQUID	LIQUID	LIQUID	LIQUID	LIQUID	LIQUID	LIQUID	LIQUID	LIQUID
Temperature C	56.3	54.2	52.2	50.1	48.1	46.1	44.2	42.6	40.7
Pressure BAR	0.17	0.15	0.14	0.12	0.11	0.10	0.09	0.09	0.08
Vapor Frac	0.00	0.00	0.00	0.00	0.00	0.00	0.00	0.00	0.00
Mole Flow KMOL/HR	2564	2498	2442	2387	2320	2254	2181	1821	2109
Mass Flow TONNE/HR	46	45	44	43	42	41	39	33	38
Volume Flow CUM/HR	48	47	46	44	43	42	40	34	39
Enthalpy KCAL/HR	-1.7E+08	-1.7E+08	-1.7E+08	-1.6E+08	-1.6E+08	-1.5E+08	-1.5E+08	-1.2E+08	-1.4E+08
Mass Flow TONNE/HR									
H2O	46	45	44	43	42	41	39	33	38
NACL	0	0	0	0	0	0	0	0	0
Mole Flow KMOL/HR									
H2O	2564	2498	2442	2387	2320	2254	2181	1821	2109
NACL	0	0	0	0	0	0	0	0	0

Streams	D24	DP2	DP3	DP4	DP5	DP6	DP7	DP8	DP9
From	H2-24	DT1	DT3	DT4	DT5	DT6	DT7	DT8	DT9
To	DT24	DT3	DT4	DT5	DT6	DT7	DT8	DT9	DT10
Phase	LIQUID	LIQUID	LIQUID	LIQUID	LIQUID	LIQUID	LIQUID	LIQUID	LIQUID
Temperature C	38.6	86.5	85.3	84.0	82.8	81.7	80.6	79.5	78.4
Pressure BAR	0.07	0.59	0.54	0.49	0.44	0.40	0.37	0.33	0.30
Vapor Frac	0.00	0.00	0.00	0.00	0.00	0.00	0.00	0.00	0.00
Mole Flow KMOL/HR	2337	5222	8332	11497	14625	17662	20601	23471	26297
Mass Flow TONNE/HR	42	94	150	207	263	318	371	423	474
Volume Flow CUM/HR	43	101	161	222	282	340	396	450	504
Enthalpy KCAL/HR	-1.6E+08	-3.5E+08	-5.6E+08	-7.7E+08	-9.8E+08	-1.2E+09	-1.4E+09	-1.6E+09	-1.8E+09
Mass Flow TONNE/HR									
H2O	42	94	150	207	263	318	371	423	474
NACL	0	0	0	0	0	0	0	0	0
Mole Flow KMOL/HR									
H2O	2337	5222	8332	11497	14625	17662	20601	23471	26297
NACL	0	0	0	0	0	0	0	0	0

Streams	DP10	DP11	DP12	DP13	DP14	DP15	DP16	DP17	DP18
From	DT10	DT11	DT12	DT13	DT14	DT15	DT16	DT17	DT18
To	DT11	DT12	DT13	DT14	DT15	DT16	DT17	DT18	DT19
Phase	LIQUID	LIQUID	LIQUID	LIQUID	LIQUID	LIQUID	LIQUID	LIQUID	LIQUID
Temperature C	77.3	76.3	75.2	74.2	73.2	72.2	71.2	70.2	69.3
Pressure BAR	0.28	0.25	0.23	0.21	0.19	0.17	0.15	0.14	0.12
Vapor Frac	0.00	0.00	0.00	0.00	0.00	0.00	0.00	0.00	0.00
Mole Flow KMOL/HR	29072	31803	34501	37149	39752	42316	44814	47256	49643
Mass Flow TONNE/HR	524	573	622	669	716	762	807	851	894
Volume Flow CUM/HR	556	608	659	708	757	805	852	897	942
Enthalpy KCAL/HR	-2.0E+09	-2.1E+09	-2.3E+09	-2.5E+09	-2.7E+09	-2.9E+09	-3.0E+09	-3.2E+09	-3.3E+09
Mass Flow TONNE/HR									
H2O	524	573	622	669	716	762	807	851	894
NACL	0	0	0	0	0	0	0	0	0
Mole Flow KMOL/HR									
H2O	29072	31803	34501	37149	39752	42316	44814	47256	49643
NACL	0	0	0	0	0	0	0	0	0

Streams	DP19	DP20	DP21	DP22	DP23	DP
From	DT19	DT20		DT22	DT23	DT24
To	DT20	DT21	DT22	DT23	DT24	
Phase	LIQUID	LIQUID	LIQUID	LIQUID	LIQUID	LIQUID
Temperature C	68.3	67.4	66.6	65.8	65.0	64.0
Pressure BAR	0.11	0.10	0.09	0.09	0.08	0.07
Vapor Frac	0.00	0.00	0.00	0.00	0.00	0.00
Mole Flow KMOL/HR	51964	54218	56400	58220	60330	62666
Mass Flow TONNE/HR	936	977	1016	1049	1087	1129
Volume Flow CUM/HR	985	1026	1067	1100	1139	1182
Enthalpy KCAL/HR	-3.5E+09	-3.7E+09	-3.8E+09	-3.9E+09	-4.1E+09	-4.2E+09
Mass Flow TONNE/HR						
H2O	936	977	1016	1049	1087	1129
NACL	0	0	0	0	0	0
Mole Flow KMOL/HR						
H2O	51964	54218	56400	58220	60330	62666
NACL	0	0	0	0	0	0

Streams **From** **To**	**QCALC** **SBH** **BBH**	**RCAL1** **H2-1** **H3-1**	**RCAL2** **H2-2** **H3-2**	**RCAL3** **H2-3** **H3-3**	**RCAL4** **H2-4** **H3-4**	**RCAL5** **H2-5** **H3-5**	**RCAL6** **H2-6** **H3-6**
HeatFlow KCAL/HR	7.6E+07	2.3E+07	2.9E+07	3.1E+07	3.2E+07	3.1E+07	3.0E+07

Streams **From** **To**	**RCAL7** **H2-7** **H3-7**	**RCALC8** **H2-8** **H3-8**	**RCALC9** **H2-9** **H3-9**	**RCAL10** **H2-10** **H3-10**	**RCAL11** **H2-11** **H3-11**	**RCAL12** **H2-12** **H3-12**	**RCAL13** **H2-13** **H3-13**
HeatFlow KCAL/HR	2.9E+07	2.9E+07	2.8E+07	2.8E+07	2.8E+07	2.7E+07	2.7E+07

Streams **From** **To**	**RCAL14** **H2-14** **H3-14**	**RCAL15** **H2-15** **H3-15**	**RCAL16** **H2-16** **H3-16**	**RCAL17** **H2-17** **H3-17**	**RCAL18** **H2-18** **H3-18**	**RCAL19** **H2-19** **H3-19**	**RCAL20** **H2-20** **H3-20**
HeatFlow KCAL/HR	2.6E+07	2.6E+07	2.6E+07	2.5E+07	2.4E+07	2.4E+07	2.3E+07

Streams **From** **To**	**RCAL21** **H2-21** **H3-21**	**RCAL22** **H2-22** **H3-22**	**RCAL23** **H2-23** **H3-23**	**RCAL24** **H2-24** **H3-24**
HeatFlow KCAL/HR	2.2E+07	1.9E+07	2.2E+07	2.4E+07

APPENDIX D

STATE VARIABLES OF THE MSF SPEEDUP MODEL

Number of state variables = 104
Number of input variables = 3
Number of output variables = 3

State Variables:

Variable Number	Variable Name
1	8	BL_CONT.I_ERROR
2	29	BL_VALVE_ACT.I
3	50	BRINE_HEATER.TF
4	74	F1.H
5	78	F1.M
6	85	F1.TF
7	89	F1.CB
8	126	F10.H
9	130	F10.M
10	137	F10.TF
11	141	F10.CB
12	171	F11.H
13	175	F11.M
14	182	F11.TF
15	186	F11.CB
16	216	F12.H
17	220	F12.M
18	227	F12.TF
19	231	F12.CB
20	261	F13.H
21	265	F13.M
22	272	F13.TF
23	276	F13.CB
24	306	F14.H
25	310	F14.M
26	317	F14.TF
27	321	F14.CB

28	351	F15.H
29	355	F15.M
30	362	F15.TF
31	366	F15.CB
32	396	F16.H
33	400	F16.M
34	407	F16.TF
35	411	F16.CB
36	441	F17.H
37	445	F17.M
38	452	F17.TF
39	456	F17.CB
40	486	F18.H
41	490	F18.M
42	497	F18.TF
43	501	F18.CB
44	531	F19.H
45	535	F19.M
46	542	F19.TF
47	546	F19.CB
48	576	F2.H
49	580	F2.M
50	587	F2.TF
51	591	F2.CB
52	621	F20.H
53	625	F20.M
54	632	F20.TF
55	636	F20.CB
56	666	F21.H
57	670	F21.M
58	677	F21.TF
59	681	F21.CB
60	715	F22.H
61	719	F22.M
62	726	F22.TF
63	730	F22.CB
64	760	F23.H
65	764	F23.M
66	771	F23.TF
67	775	F23.CB
68	808	F24.H
69	812	F24.M
70	819	F24.TF
71	823	F24.CB
72	853	F3.H

73	857	F3.M
74	864	F3.TF
75	868	F3.CB
76	898	F4.H
77	902	F4.M
78	909	F4.TF
79	913	F4.CB
80	943	F5.H
81	947	F5.M
82	954	F5.TF
83	958	F5.CB
84	988	F6.H
85	992	F6.M
86	999	F6.TF
87	1003	F6.CB
88	1033	F7.H
89	1037	F7.M
90	1044	F7.TF
91	1048	F7.CB
92	1078	F8.H
93	1082	F8.M
94	1089	F8.TF
95	1093	F8.CB
96	1116	F9.H
97	1120	F9.M
98	1127	F9.TF
99	1131	F9.CB
100	1146	REJ_CONT.I_ERROR
101	1168	RE_CONT.I_ERROR
102	1185	ST_CONT.DUMMY
103	1188	ST_CONT.I_ERROR
104	1198	ST_VALVE_ACT.I

APPENDIX E

DATA FILES AND LOCATION of DEPOSIT

Reference	***File name***
Figure 4.3	*Outlier.nna*
Figure 4.6 and Figure 4.7	*E and F TBT.nna, E and F DP.nna, E and F STF.nna*
Figure 4.8 and Figure 4.9	*50TBT.nna, 100TBT.nna, 150TBT.nna, 200TBT.nna, 250TBT.nna*
Table 4.12, and Figures 4.10, 4.11, 4.12, 4.13, 4.14 and 4.15	*WTBT.nna*
Tables 4.14 and 4.15, Figures 4.16 and 4.18	*WMIMO.nna, WTBT.nna, WDP.nna, WSTF.nna*
Table 4.16, Table 4.17, and Figure 4.19	*SMIMO.nna, STBT.nna, SDP.nna, SSTF.nna*
Table 4.23, Table 4.24, and Figure 4.26	*ROMIMO.nna, ROPF.nna, ROPC.nna*
Table 4.21, Table 4.22, and Figure 4.23	*E and F PF.nna, E and F PC.nna, T.nna*
Table 4.25, Figure 4.29, and Figure 4.30	*K.nna, L.nna, M.nna, N.nna, O.nna, P.nna, Q.nna, R.nna, S.nna, T.nna*
Chapter 5 section 5.3.A Tables and Figure	*MSF.bkp*
Chapter 5 section 5.3.B Tables and Figure	*MSF.spe*

* A complete set of PC diskettes for these files is deposited in the office of Professor Y.A. Liu, 136 Randolph Hall, Virginia Tech.

VITA

Khawla A. Al-Shayji was born in Kuwait, on October 19, 1964. After graduating from Kuwait University, Kuwait, in June 1987 with a Bachelor of Engineering in Chemical Engineering, she worked for the Ministry of Electricity and Water in Kuwait from 1987 to 1992. In 1992, she received a scholarship from Kuwait University. She was awarded the degree of Master of Science in Desalination Technology from the Mechanical Engineering at the University of Glasgow in Scotland in the United Kingdom, in October 1993. In January 1994, she enrolled as a Ph.D. student in the Department of Chemical Engineering at Virginia Polytechnic Institute and State University. Upon receiving her doctoral degree, she will continuously work as a professor at the Chemical Engineering Department at Kuwait University, Kuwait.